

Final Report

**Evaluation of the Proposed New European Methodology
for Determination of Particle Number Emissions
and its Potential in California for In-Use Screening**

**Prepared for:
Dr. Jorn Herner
California Air Resources Board
1001 "I" Street
P.O. Box 2815
Sacramento, CA 95812**

August 2008

**Submitted by:
Dr. Thomas D. Durbin
Dr. Heejung Jung
Dr. David R. Cocker
Mr. Kent Johnson
Mr. Ajay Chaudhary
University of California
CE-CERT
Riverside, CA 92521
951-781-5791
951-781-5790 (fax)**

Disclaimer

The statements and conclusions in this report are those of the contractor and not necessarily those of California Air Resources Board. The mention of commercial products, their source, or their use in connection with material reported herein is not to be construed as actual or implied endorsement of such products.

Acknowledgments

The authors thank the following organizations and individuals for their valuable contributions to this project.

The authors acknowledge Drs. Jorn Herner, Bill Robertson, Tao Huai, and Alberto Ayala of the California Air Resources Board (CARB) for their assistance in developing the test plan procedures, in carrying out the experiments, and in analysis of the data. The authors also acknowledge other CARB staff that assisted in setting up and carrying out the experiments including Mr. Keshev Sahay, Mr. John Karim, Mr. Ralph Rodas, and Mr. George Gatt.

The authors acknowledge Dr. David Kittelson of the University of Minnesota, Dr. Marcus Kasper of Matter Engineering Inc., Mr. Jon Andersson of Ricardo, and Mr. Andreas Mayer for their assistance in developing the test plan procedures, in carrying out the experiments, and in analysis of the data.

We acknowledge funding from the California Air Resources Board (CARB) under contract No. 05-320.

We acknowledge Mr. Donald Pacocha, University of California, Riverside for his contribution in setting up and executing this field project, the data collection and quality control.

Table of Contents

Disclaimer	ii
Acknowledgments	ii
Table of Contents	iii
Table of Figures	vi
Abstract	viii
Acronyms and Abbreviations	x
Executive Summary	xii
1.0 Background	1
2.0 Experimental Procedures for Chassis Dynamometer Laboratory Tests	2
2.1 Overview of Experimental Approach	2
2.2 Test Vehicle and Fuel	2
2.3 Test Cycles and Other Test Parameters	2
2.4 Emissions and Other Measurements	3
3.0 Experimental Procedures for On-Road Testing	11
3.1 Overview of Experimental Approach	11
3.2 Test Vehicle and Fuel	11
3.3 Test Cycles and Other Test Parameters	11
3.4 Emissions and Other Measurements	14
4.0 Emissions Results for Chassis Dynamometer Laboratory Testing	22
4.1 Gas-Phase Emissions	22
4.2 PM Mass Results	24
4.3 PMP and other Particle Number Results	26
4.4 Particle Size Distributions	30
4.5 Real Time CPC, EAD, EEPS, and PAS Results	31
5.0 On-Road Emissions Results	40
5.1 Gas-Phase Emissions	40
5.2 PM Mass Results	43
5.3 Particle Size Distributions	47
5.4 PMP and other Particle Number Results	49
5.5 Real Time PM Number Results	59
5.6 Intercomparisons Between CPCs and the PMP Dilution Systems	69
6.0 Summary	71
7.0 Discussion and Implications	75
8.0 References	78
Appendix A – Test Cycle	A-1
Appendix B – Time Response Experiments with PMP System	B-1
Appendix C – Background Information on UCR’s Mobile Emission Lab	C-1
Appendix D – Operation of the Dekati DMM	D-1
Appendix E – Quality Assurance/Quality Control	E-1
Appendix F – CPC Chamber Calibration Experiment and Pseudo Span Results from the On-Road Testing	F-1
Appendix G – Additional Test Data for the Chassis Dynamometer Testing Portion of the Study	G-1

Appendix H – Supplemental Gas-Phase Test Results for the On-Road Testing	H-1
Appendix I – On-Road Test Route Repeatability for Gas-Phase Measurements	I-1
Appendix J – Supplemental Integrated PM Mass and Number Information for the On-Road Testing	J-1
Appendix K – Supplemental Real-Time PM Number Measurements for the On-Road Testing	K-1

Table of Tables

Table 2-1. Sample Collection Test Matrix for Chassis Dynamometer Testing	4
Table 3-1. Sample Collection Test Matrix for On-Road Testing	14
Table 3-2 PMP designs comparisons between the MEL and MD-19 systems.	18
Table 5-1. THC, CH ₄ , and CO Concentration Measurements.	41
Table 5-2. Number of Tests for Each Cycle Grouped by Direction	49

Table of Figures

Figure 2-1. Schematic of the Sampling layout for the Test Program	5
Figure 2-2. Schematic of PMP System from European PMP Literature.	6
Figure 2-3. Overall picture of Sampling Set-Up with PMP System	7
Figure 2-4. Close-up Picture of MD-19 Rotating Disk Dilutor	8
Figure 3-1. Schematic Map of Road Section Used for On-Road Cycles (except the Cruise)	13
Figure 3-2. Schematic of PM Sampling System for On-Road Testing (not to scale)	15
Figure 3-3. Partial flow dilution system with single venturi, concentration measurement and fractional sampling method [modified from ISO 8178-1:1996]	18
Figure 3-4. Sampling Set-up for PMP Systems.	19
Figure 4-1. NO _x Emissions Results.	22
Figure 4-2. THC Emissions Results	23
Figure 4-3. CO Emissions Results	24
Figure 4-4. PM Emissions Results	25
Figure 4-5. PM Filter Masses	25
Figure 4-6. Particle Number Counts for different CPCs for the UDDS and the Cruise, including all Test Runs.	26
Figure 4-7. Particle Number Counts for different CPCs for the UDDS and the CPC, excluding the Test with the Highest Particle Concentration for each Cycle. * Note this outlier criteria is typically used in the PMP protocol for PM mass, not particle number.	27
Figure 4-8. Particle Number Counts for Individual Test Runs for the UDDS.	28
Figure 4-9. Particle Number Counts for Individual Test Runs for the Cruise.	28
Figure 4-10. Correlation between two 3025A systems.	29
Figure 4-11. Coefficients of Variation for Various Instruments. * Note this outlier criteria is typically used in the PMP protocol for PM mass, not particle number.	30
Figure 4-12. Average Size Distribution for UDDS tests (dN/dLogDp).	31
Figure 4-13. Average Size Distributions for Cruise Tests (dN/dLogDp).	31
Figure 4-14. Real-Time Particle Number Counts for Various Instruments for the UDDS 2x	32
Figure 4-15. EEPS data for UDDS 2x Cycle	33
Figure 4-16. Real-Time CPC data for outlier UDDS conducted on 6/1/07 Run 1	34
Figure 4-17. CPC 3025A data runs from 5/25/07 over the 50 mph cruise.	35
Figure 4-18. CPC 3790 data runs from 5/25/07 over the 50 cruise.	35
Figure 4-19. EEPS data for a 50 mph Cruise with the Corresponding Warm-up	36
Figure 4-20. CPC 3025A data for two outlier test runs over the 50 mph cruise.	37
Figure 4-21. CPC and EAD measurements during Idle Testing	38
Figure 4-22. Real-Time Particle Counts for Various Instruments for a 50 mph Cruise.	39
Figure 5-1. NO _x Emissions Results on a g/mi basis.	41
Figure 5-2. NMHC Emissions Results on a g/mi basis	42
Figure 5-3. CO Emissions Results on a g/mi basis	43
Figure 5-4. Particulate matter results on a g/mi basis	44
Figure 5-5. Particulate matter results on a mg/bhp-hr basis	45
Figure 5-6. Particulate matter results on a filter weight basis (mg/filter).	46
Figure 5-7. Average Size Distribution for ETC Cruise Cycle using the f-SMPS.	48
Figure 5-8. Average Size Distribution for ETC Urban Cycle using the f-SMPS.	48
Figure 5-9. Average Size Distribution for CARB Creep Cycle using the f-SMPS.	49

Figure 5-10. Particle number rate (#/mi) for all CPC's on driving cycles grouped by direction and flow-of-traffic tests (Note log scale y-axis)	50
Figure 5-11. Particle number rate (#/mi) on driving cycles not grouped by direction and flow-of-traffic tests (Note log scale y-axis)	50
Figure 5-12. Particle number rate (#/mi) for similar cut point CPC's (3760A and 3790) for driving cycles grouped by direction	52
Figure 5-13. Particle number rate (#/mi) for similar cut point CPC's (3760A and 3790) for driving cycles grouped by direction and flow-of-traffic tests (log scale).	53
Figure 5-14. Particle number rate (#/mi) for similar cut point CPC's (3025A and 3022) for driving cycles grouped by direction (log scale).	54
Figure 5-15. Particle number rate (#/mi) for similar cut point CPC's (3025A and 3022) for driving cycles not grouped by direction and for flow-of-traffic tests (log scale).	54
Figure 5-16. Particle number rate (#/mi) for the UDDS cycle over four separate days and two different driving directions to show day to day trends for similar cut point CPC's (3760A and 3790)	56
Figure 5-17. Particle number rate (#/mi) for the UDDS cycle over four separate days and two different driving directions to show day to day trends for similar cut point CPC's (3025A and 3022) Note y-axis log scale.	56
Figure 5-18. Coefficient of Variation for all CPC's and selected regulated measurements for on-road driving cycles grouped by direction	57
Figure 5-19. Coefficient of Variation for all CPC's and selected regulated measurements for on-road driving cycles not grouped by direction	58
Figure 5-20. Real-time particle rate (#/cc) for the 3025A and 3022 CPCs on the ETC cruise cycle	60
Figure 5-21 f-SMPS size distribution for the westbound ETC cruise cycle $dN/d\log(D_p)$	61
Figure 5-22. Real-time particle rate (#/cc) for the 3025A and 3022 CPCs on the UDDS cycle	62
Figure 5-23 Detail C. Real-time particle rate (#/cc) for the 3025A and 3022 CPCs on the UDDS cycle	62
Figure 5-24. Real-time particle rate (#/cc) for CPCs 3790 and 3760 on the UDDS cycle	63
Figure 5-25. f-SMPS size distribution over a typical 20 minute UDDS cycle $dN/d\log(D_p)$	64
Figure 5-26. Real-time particle rate (#/cc) for CPCs 3025A on the creep and urban cycles	65
Figure 5-27. Real-time particle rate (#/cc) for CPCs 3790 and 3760 on the creep and urban cycles	66
Figure 5-28. Real-time particle rate (#/cc) for similar cuts point CPCs (3790 and 3760) with Dekati DMM mass concentration ($\mu\text{g}/\text{m}^3$) for the flow-of-traffic Indio to Riverside run	67
Figure 5-29. EEPS size distribution for Riverside to Indio flow-of-traffic Run $dN/d\log(D_p)$	68
Figure 5-30. CPC 3760A correlation full data set and reduced data set with flow-of-traffic data removed	70
Figure 5-31. CPC 3025A correlation full data set and reduced data set	70

Abstract

The European countries have developed new methodologies for the measurement of “solid” particle number above a size cut threshold of 23 nanometers (nm) to compliment gravimetric measurements at low particle levels typically found with engines and vehicles equipped with diesel particle filters (DPFs). This methodology provides significant improvements in measurement sensitivity, but should be fully understood in terms of the representativeness of the particles, which are only solid and >23 nm in size, their adverse health effects, and the repeatability of the measurement. The California Air Resources Board (CARB) sought to enhance the understanding of the PMP methodology and to develop well-informed opinions regarding its application. The specific objective of this study was to critically evaluate the proposed PMP method for determining “solid” particle number emissions from heavy-duty vehicles in the laboratory and during over-the-road driving. For this program, testing was conducted on the chassis dynamometer at the CARB heavy-duty vehicle emissions laboratory in Los Angeles and over the road with the CE-CERT mobile emissions laboratory (MEL). One or two PMP dilutions systems for measuring solid particle number were tested and compared directly with filter-based PM measurements on two heavy-duty trucks equipped with a DPF. These PMP dilution systems met the latest specifications and design criteria for setting up the PMP system, but were not characterized for the calibration criteria incorporated into the final PMP methodology. As such, they can not be considered to be fully compliant with the most recent PMP requirements. A full suite of other particle measurements and instruments were also used in conjunction with this testing including a TSI EEPS, a Cambustion DMS, and TSI CPCs with lower size cuts ranging from 3 to 23 nm, a Dekati DMM, and a DustTrak. The test cycles included a 50 mph cruise, UDDS, idle, and some European driving schedules. This program was conducted in collaboration with other particle emission experts from Europe and the United States (US), including European counterparts who have direct, hands on experience with the PMP protocol.

Particle number offers the potential to more readily characterize emissions from DPF-equipped engines and vehicles. The emission level and variability between the different PMP particle number counts and the PM mass depended on the cycle, sampling location and time, the specific test instrument, and other experimental conditions. The advantages of particle number measurements in these respects was clearly seen for the on-road testing, but were less clear for the laboratory measurements, where longer tests produced higher/quantifiable PM mass levels and particle number outliers were found. Outlier tests were observed in the laboratory tests that appear to be real events that may be masked in the mass measurement. Thus, statistical techniques for the removal of outlier tests for particle number should be considered to provide for the most consistent and repeatable measurements. The particle number measurements provided the greatest advantages at typical emission levels for current wall-flow DPFs, which are often only a small percentage of the certification value. At these levels, the mass measurements typically show greater scatter, are usually below the quantification limit, and can be impacted heavily by artifact formation. At higher mass levels, such as levels closer to the actual limit of the 2007 standard for heavy-duty engines, the quantification accuracy and repeatability of the gravimetric PM measurements improve, so the advantages of the PMP system would not be as significant. Nucleation particles were found to form under a variety of testing conditions when

the temperature of the aftertreatment device exceeded a 'critical' temperature, which was typically in excess of 300°C. Sulfate was an important portion of the chemical make-up of the nucleation particles, suggesting that SO₂ to SO₃ conversion over the catalyst played an important role in their formation. The level of nucleation increased significantly under the most aggressive, on-road testing conditions. In order to better characterize the PMP system, further study is suggested to understand the chemical composition and nature of the particles measured below the PMP, the potential impacts of utilizing a smaller size cut for counting particles below the PMP, and the impacts of the different design elements of the PMP. Testing should also be expanded to include a wider range of vehicles and aftertreatment systems.

Acronyms and Abbreviations

ARB	Air Resources Board
CARB	California Air Resources Board
CE-CERT	College of Engineering-Center for Environmental Research and Technology (University of California, Riverside)
CFR	Code of Federal Regulations
CPC	condensation particle counter
CRT	Johnson Matthey Continuously Regenerating Technology® diesel particulate filter
CO	carbon monoxide
COV	coefficient of variation
CO ₂	carbon dioxide
CVS	constant volume sampling
DC	diffusion charger
DMM	Dekati Mass Monitor
DMS	differential mobility sizer
DPF	diesel particulate filter
DR	dilution ratio
EAD	electrical aerosol detector
ECE-GRPE	United Nation's Economic Commission for Europe – Group of Experts on Pollution and Energy
ECM	engine control module
EEPS	engine exhaust particle sizer
ET	evaporation tube
fA	fermtoamp
f-SMPS	fast-scan scanning mobility particle sampler
FTP	Federal Test Procedure
g/mi	grams per mile
g/bhp-hr	grams per brake horsepower hour
GVWR	gross vehicle weight rating
HDDT	Heavy-Duty Diesel Truck
HDETL	CARB's Heavy-Duty Emissions Testing Laboratory
HDV	heavy-duty vehicle
HEPA	high efficiency particle filter
id	inner diameter
LDV	light-duty vehicle
lpm	liters per minute
MD-19	rotating disk diluter from Matter Engineering AG
MDL	minimum detection limit
MEL	CE-CERT's Mobile Emissions Laboratory
nm	nanometers
NMHC	non-methane hydrocarbons
NO _x	nitrogen oxides
NO ₂	nitrogen dioxide
PAHs	poly aromatic hydrocarbons

PAS	photoelectric aerosol sensor
PM.....	particulate matter
PMP.....	Particle Measurement Program
PND1.....	first stage of dilution
PND2.....	second stage of dilution
QA.....	quality assurance
QC.....	quality control
scfm.....	standard cubic feet per minute
SMPS	scanning mobility particle sampler
THC.....	total hydrocarbons
UDDS.....	Urban Dynamometer Driving Schedule
ULSD	ultralow sulfur diesel
VPR.....	volatile particle remover

Executive Summary

With regulatory limits in California and the US for 2007 for newer heavy-duty diesel engines being met with the use of diesel particle filters (DPFs), there are considerable ongoing efforts to improve methods for the measurement of particulate matter (PM) at very low levels. Improvements to the gravimetric method have been issued by the US EPA and in Europe for emission certification. While the new gravimetric methods are adequate for measurements near the certification limit, accuracy will continue to be a problem at the much lower emission levels that current wall-flow DPFs typically produce. One methodology that has shown promise for making PM measurements at these low levels is the measurement of particle number. This methodology has been studied and developed through Europe's Particle Measurement Program (PMP), and has been shown to be 20 times more sensitive than gravimetric particle mass measurements at the very low emissions levels seen with wall flow DPFs. The European PMP program also includes important provisions in that it focuses on the measurement of "solid" particle number and only particles that are above a size cut threshold of 23 nanometers (nm). These provisions allow for a more repeatable measurement since it largely eliminates nucleation particles that are smaller in size, typically volatile in nature, and less predictable than larger particles. Important factors to consider in evaluating the PMP methodology include understanding the representativeness of the particles, which are only solid and >23 nm in size, their adverse health effects, and the repeatability of the measurement.

The PMP particle sampling system is designed to measure the number concentration of solid, non-volatile particles. The PMP-recommended suite of instruments consists of a Condensation Particle Counter (CPC), coupled with a thermal conditioning unit with stages of dilution for volatile specie control known as the volatile particle remover (VPR), and a pre-classifier for sampling directly from the Constant Volume Sampling (CVS) full-exhaust dilution tunnel. A schematic of the PMP system is provided in Figure ES-1. The PMP system is designed to measure "solid" particles that are operationally defined as ones having a diameter between 23 nm and 2.5 μm and of sufficiently low volatility to survive a residence time of 0.2 seconds at 300°C. The VPR includes a hot dilution stage where the mass concentration of volatiles is reduced to help prevent the subsequent nucleation of particles, a heated tube where volatiles are evaporated, followed by a second diluter that cools and dilutes particles to a point where no nucleation will occur. The particles are counted using a CPC. The TSI 3790 is the CPC currently approved for the PMP system. The size cut for this instrument is 23 nm. The PMP dilution systems used in this program met the latest specifications and design criteria for setting up the PMP system, but were not characterized for the calibration criteria incorporated into the final PMP methodology [Andersson et al., 2007]. As such, they can not be considered to be fully compliant with the most recent PMP requirements. The PMP system was initially applied to light-duty applications in Europe, but is now being evaluated for use with European heavy-duty regulations.

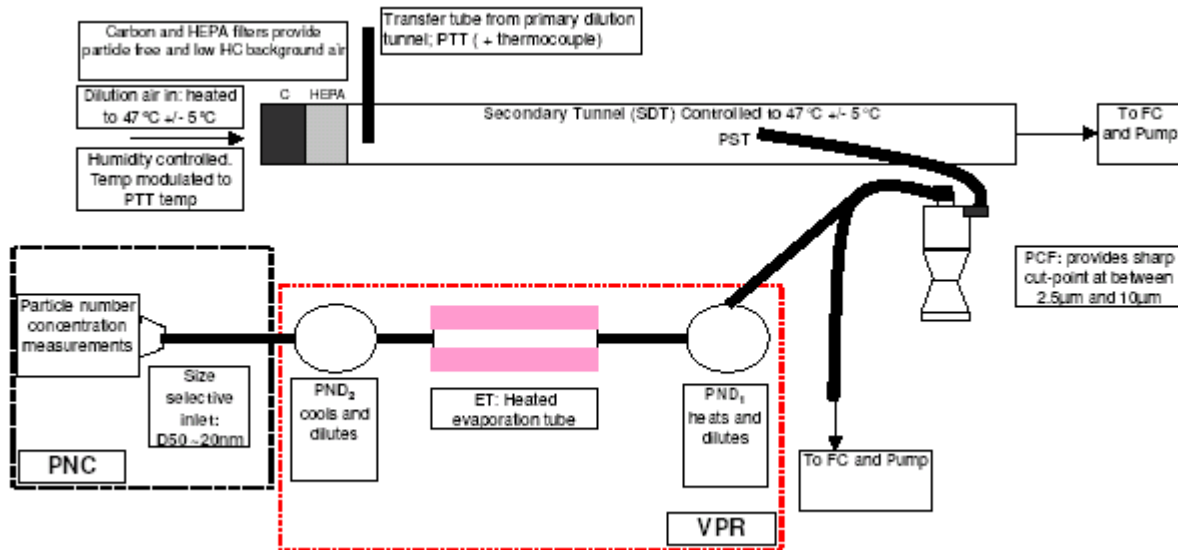


Figure ES-1. Schematic of PMP System from European PMP Literature.

This study was designed to evaluate the performance of the European PMP metrology for the measurement of solid particle number under laboratory and on-road conditions. The laboratory testing was conducted over a series of test cycle conditions at the California Air Resources Board's (CARB's) heavy-duty vehicle emissions laboratory in Los Angeles. The laboratory is equipped with a chassis dynamometer for heavy-duty vehicles. The laboratory was equipped with a PMP dilution sampling system and a range of instruments for characterizing particle number and size. Testing was performed using a 1999 International 4900 truck equipped with an 7.6 liter International DT466E engine with a retrofit DPF. The truck was tested over multiple iterations of an Urban Dynamometer Driving Schedule (UDDS) cycle, a 50 mph cruise, and an idle. These cycles were designed to provide a range of three different operating/load conditions.

The on-road testing was conducted using the University of California at Riverside's College of Engineering – Center for Environmental Research and Technology's (CE-CERT's) Mobile Emissions Laboratory (MEL). The MEL contains a CVS dilution tunnel and associated instruments that are fully compliant with regulatory requirements. The CVS is housed in a 53' trailer that can be utilized on-road for in-use emissions measurements. The MEL was equipped with two systems capable of measuring solid particles utilizing the European PMP metrology, including a system using a rotating disk dilutor and a second system based on a modified ISO 8178 partial flow single venturi fractional flow sampler. In addition to standard PM mass measurements, a number of instruments for characterizing particle number and size were used in conjunction with these systems. Testing was performed on-road using a 2000 Freightliner equipped Caterpillar C-15 engine with a retrofit DPF. The truck was tested over a series of standard cycles such as the UDDS, the urban and motorway segments of the European Transient Cycle (ETC), and the CARB creep cycle, as well as under typical on-road highway conditions. These cycles provide a range of operating conditions, including cycles/operation that can provide comparisons with the laboratory work above and with European efforts. This allowed comparison of the accuracy and repeatability of the PMP and other particle measurements under

conditions where variables of real-world measurements such as vibration, field deployment, ambient conditions, etc. were incorporated.

The laboratory and on-road testing incorporated a range of different instruments and sampling systems that are discussed briefly here to provide a better context for understanding the results and conclusions below. Both PMP systems sampled directly from the primary CVS. PM sampling for the other instruments was performed at three main locations: directly from the primary CVS, below the PMP system, and from the secondary dilution system for the traditional PM mass measurements. By sampling directly from the primary CVS as well as below the PMP, information is obtained about the nature of the PM before and after it is subjected to the PMP sampling conditions. CPCs with a range of different size cuts were also used to provide information not only about the particles typically measured above the 23 nm PMP cut point, but also those particles with lower size cuts that are not measured using the PMP methodology. Duplicate CPCs were also used below the different PMP systems to evaluate the repeatability/reproducibility within a particular PMP system and the comparability between different PMP systems. Other particle measurement instruments used to characterize particle number, size, or both included a TSI Engine Exhaust Particle Sizer (EEPS), a Cambustion Differential Mobility Spectrometer (DMS), an electrical aerosol detector (EAD), a photoelectric aerosol sensor (PAS), a fast scanning mobility particle sizer (f-SMPS), Dekati Mass Monitor (DMM), and a DustTrak. The various PM instruments used, size cut, and sampling location are provided in Table ES-2.

Instrument	Sampling Location	Size Cutoff (d50)	Measurement	Laboratory	On-Road
PM Mass	Secondary dilution tunnel		Mass	X	X
CPC 3790	MD-19 PMP system	23 nm	Particle #	X ¹	X
CPC 3025A	MD-19 PMP system	3 nm	Particle #	X	X
CPC 3760A	MD-19 PMP system	~11 nm	Particle #		X
CPC 3025A_dup	MD-19 PMP system	3 nm	Particle #	X	
CPC 3025A	MEL PMP system	3 nm	Particle #		X
CPC 3760A	MEL PMP system	~11 nm	Particle #		X
CPC 3022	Primary CVS tunnel	7 nm	Particle #	X ²	X
EEPS	Primary CVS tunnel	5.6 nm	Particle #/size	X	X
DMS	Primary CVS tunnel	5.6 nm	Particle #/size	X	
PAS	Primary CVS tunnel		Black carbon	X	
EAD	Primary CVS tunnel	10 nm	PM surface area	X	
f-SMPS	Primary CVS tunnel	10-190 nm	Particle #		X
DMM	Primary CVS tunnel		PM Mass/size		X
DustTrak	Primary CVS tunnel		PM Mass		X

1 PMP compliant CPC; 2 only for the idle test; MD-19 PMP system utilizes rotating disk dilutor; MEL PMP utilizes partial flow venturi

Table ES-2. Sample Collection Test Matrix for On-Road Testing

Laboratory Testing Results

The UDDS and 50 mph cruise cycles provided different distributions of particles for measurement in the laboratory testing. Both cycles showed a significant contribution of nucleation particles in the size distributions. The nucleation mode was typically observed once a critical temperature was reached on the post emission control device exhaust. For the UDDS cycles, elevated particle counts and nucleation occurred during the highest speed driving portions of the cycle. For the 50 mph cruise, nucleation was initiated once a critical exhaust/DPF temperature was reached and it continued for the remainder of the cycle. For this DPF device configuration, the critical temperature for nucleation mode formation was $\sim 310^{\circ}\text{C}$. It appears that the nucleation mode particles may be attributed to the conversion of SO_2 to SO_3 , which is likely aided by a Pt-catalytic coating on the DPF. This is consistent with previous studies that have shown sulfate makes an important contribution to nucleation particles downstream of an aftertreatment system [Kittelson et al., 2006; Grose et al., 2006].

The particle number results, with and without outliers removed, along with the PM mass results are provided in Figure ES-2. The particle number counts for the 3790 were below the European standard for light-duty vehicles (8×10^{11} particles/mi) for both the UDDS and cruise cycles, noting that the scale for the 3790 is multiplied by 10. The coefficient of variability (COV) of the 3790 measurements was comparable to that of PM mass for the cruise, but greater than that of PM mass for the UDDS at $\sim 120\%$. The COVs of the lower cut point 3025As were all greater than that of the PM mass and ranged from 110 to 270%. The high variability was primarily due to outlier tests for both the cruise and the UDDS cycles with significantly higher counts than the others in the sets. The removal of outliers improved the repeatability of measurements for the PMP-compliant 3790 and the 3025As, with the impact of outliers being greater for the 3025As. The presence of outliers suggests that the application of statistical methods may be useful or needed to get consistently repeatable particle number measurements.

It is significant to note that the outlier events are believed to represent real differences in particle number emissions that can be seen with the PMP but may be masked in the mass measurement. The real-time results provided insight for the outlier tests. During some of the outlier tests, the 3025A CPCs exhibited several spikes up to the 40,000 to 100,000 particles/cc level at conditions where the PMP was providing a 300 to 1 dilution from the primary tunnel. It should be noted that unusually large spikes in total particle counts have been observed by some other researchers downstream of an aftertreatment system (Kittelson, 2008). For one test, there was also a consistently high particle count level that trended downward throughout the test.

A test was also conducted where the evaporation tube temperature in the PMP system was gradually reduced and the instrument response monitored. As the temperature decline reached a temperature of 160°C , the lower cut point 3025A CPCs measured a significant increase in particle count, indicating that at this temperature more volatile particles were either passing straight through the PMP system or getting through due to incomplete evaporation or evaporation and renucleation after the evaporation tube. These tests also showed the 3790 is barely affected by turning off the evaporation tube, indicating that most of these more volatile particles are in the size range below 23 nm.

Laboratory Particle Number Emissions

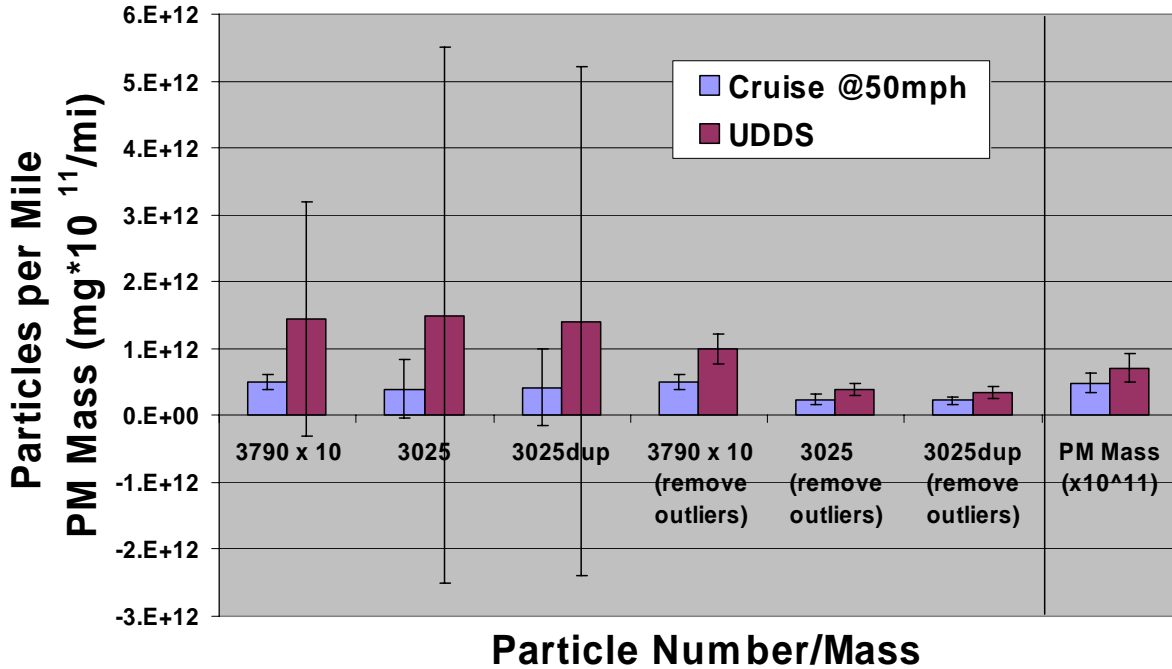


Figure ES-2. Particle Number and PM Mass for the Laboratory Tests.

***The number of outliers ranged from 0 to 2 depending on the instrument and cycle.**

PM mass emissions levels were on the order of 5-10 mg/mi, consistent with the levels of reduction expected for a DPF. PM mass levels were approximately 40 to 120 μg per filter, which is sufficiently above the tunnel blank and detection levels to allow accurate measurements. The coefficients of variation (COVs) for the PM mass measurements were comparable to those for the particle measurements using the PMP-compliant 3790 CPC for the cruise and better than those for the 3790 for the UDDS. It should be noted that the tests were conducted over testing periods of approximately 35 to 45 minutes, which is approximately twice as long as the typical certification test over the Federal Test Procedure (FTP). Hence, certification test filter mass levels would likely be less than those measured in the laboratory portion of this work. On the other hand, current wall-flow DPFs typically reduce PM to well below the 2007 PM standard, so PM mass levels for devices performing near the certification levels should be more readily measurable.

For NO_x emissions, the truck emission rates were on the order of 10 g/mi for the UDDS and 7 g/mi for the cruise. The percentage of NO_2 as a function of total NO_x varied depending on the test cycle, with highest percentage of NO_2 seen for the cruise cycle and the lowest seen for the idle. THC emissions were very low, and were either near or below the instrument detection limits. CO emissions were measurable for the UDDS and idle, but were still well below NO_x levels.

On-Road Testing Results

Particle number counts varied depending on the cycle, operating mode, measurement instrument, and sampling methodology/location for the on-road testing. The particle number measurements for each instrument and test cycle are provided in Figure ES-3, along with the PM mass $\times 10^{12}$. Note the PM mass was negative for the ETC Urban and no PM mass was available for the on-road flat testing. Comparisons of particle number counts for CPCs with different size cuts showed that the instruments with the lower size cuts (3022 and 3025A) showed consistently higher counts than those with the higher size cut points (3790 and 3760). The 3022 CPC, which was connected to the primary tunnel, also showed higher counts than the other CPCs below the PMP system when volatile nucleation particles formed.

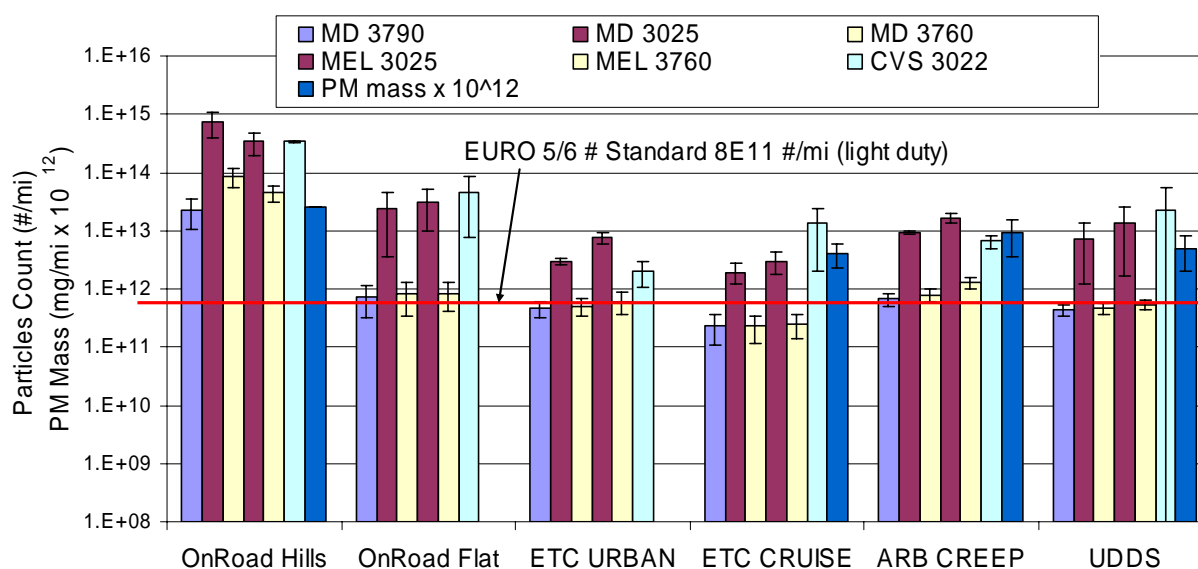


Figure ES-3. Particle Number Rate (#/mi) and PM Mass on On-Road Driving Cycles and Flow-of-Traffic Tests

Particle counts were highest for the higher load on-road driving conditions, denoted OnRoad Hills. Under these conditions PM emissions and concentrations for all types of particles increased significantly, including solid and nucleation particles. The high particle counts under these conditions were seen for both 3022 in the primary tunnel and the high and low cut point CPCs below the PMP. In fact, for the OnRoad Hills tests, the 3022 and the low cut point CPCs all saturated at the maximum count rate, thus the values reported represent absolute lower bounds. For the OnRoad Hills tests, the high cut point 3760s also reached concentrations above 10^4 #/cc, which is above the maximum stated range for the instruments and in a region where coincidence effects become significant. For the high cut point CPCs (3790 and 3760) below the PMP, the creep cycle showed the highest particle counts on a per mile basis for the standard cycles due to its transient, stop and go nature. The particle counts for the higher size cut CPCs for the ETC Urban and UDDS were lower, with the ETC cruise being the lowest. The particle counts for the 3790 for the standard cycles were generally below the European particle number standard for light-duty vehicles, with the exception of some creep cycles. For the low cut point

CPCs, there were less consistent trends between the cycles. The 3022 did measure higher particle numbers than the 3025A for some cruise cycles where a strong nucleation event was observed.

For some standard cycles, nucleation particles were formed. A nucleation event is observed near the beginning of the ETC cruise. Nucleation was also observed at the highest load in the UDDS cycle. Nucleation particles were not found for the creep or the ETC Urban cycles. The nucleation particles were generally formed during portions of the cycles when elevated exhaust temperatures were measured. The nucleation particles showed a strong response with the CPCs in the primary tunnel, but a much weaker response for the instruments below the PMP systems. This indicates the nucleation particles formed during the standard cycles are more volatile particles by nature.

The OnRoad Hills test runs representing steep hill climbing or a combination of hills and down hill driving showed significant nucleation throughout the test runs. These driving conditions were characterized by higher engine loads and exhaust temperatures consistently above 300°C or more. The nucleation particles for these driving conditions showed a much stronger response in the CPCs located below the PMP systems than for the standard cycles. A filter collected during one of these test runs showed a significant contribution from sulfate and associated water mass (~45%), suggesting that SO₂ to SO₃ conversion in the catalyst played an important role in these nucleation events. Previous studies have also shown a prevalence of sulfate in nucleation particles formed following aftertreatment systems, and that the level of nucleation increased with increasing exhaust temperature [Kittelson et al., 2006; Grose et al., 2006]. This could indicate the PMP sampling train has some inefficiencies in removing nucleation mode particles at such high levels or that there is a some breakthrough of volatiles through the PMP due to incomplete evaporation, evaporation and renucleation after the evaporation tube, or pyrolysis.

PM mass measurements for the standard cycles were on the order of 10 mg/mi or 4 mg/bhp-hr or less, consistent with the low levels measured in previous studies. PM filter mass measurements were near or below detection limits for most driving cycles. The filter masses for the standard cycles were generally below the three standard deviation detection limit of 7.5 µg per filter. The COV for the PM filter mass measurements was higher than that for the particle number measurements below the PMP for nearly all cycle/CPC combinations, especially where grouped by direction of travel, as shown in Figure ES-4. The COVs for the low cut point 3022 that sampled directly from the CVS were higher than those for the CPCs below the PMP system for cycles when nucleation occurred. This can be attributed to variability in nucleation and or other volatile particles eliminated by the PMP. Although nucleation events did contribute to higher variability and outliers in the measurements directly from the dilution tunnel, these outliers did not impact the repeatability of the 3790 measurements below the PMP, unlike in some of the laboratory measurements. There were no consistent differences between COVs the high and low cut point CPCs below the PMP.

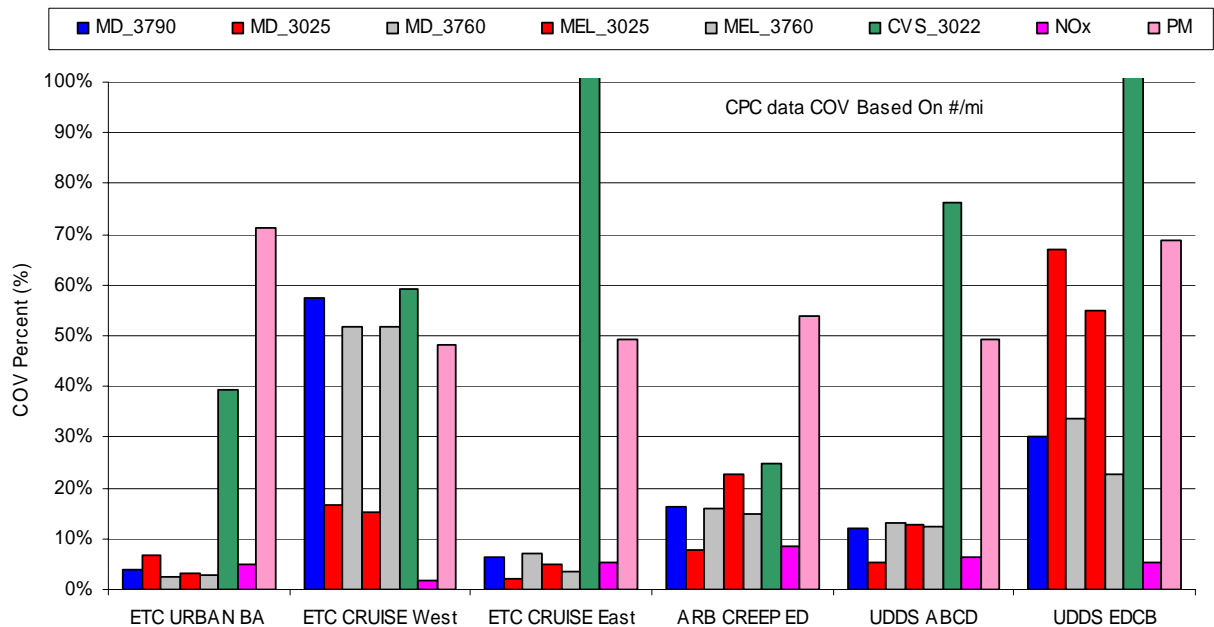


Figure ES-4. Coefficient of Variation for all CPC's and selected regulated measurements for on-road driving cycles grouped by direction

The rotating disk PMP system (denoted MD-19) and the ISO 8178 partial flow PMP system (denoted MEL) showed good agreement for the 3760A and 3790 CPCs with the higher size cuts. Good agreement is found for both the integrated and the real-time results. Good agreement for the 3760s was found on most cycles with the exception of the creep cycle. Comparisons between the MD-19 and the MEL PMP systems for the 3025As showed greater differences between the systems, including a faster response time for the MEL system. The MEL and MD-19 systems also showed biases relative to one another, with the MEL higher than the MD-19 for the standard cycles and the MD-19 system being higher than the MEL for the higher load on-road driving conditions. Additional analysis and measurements are needed to better understand the nature of these biases.

NO_x emissions ranged from 13 to ~22 g/mi for the ETC Urban, ETC cruise, and UDDS cycles, with NO_x emissions for the ETC cruise generally being the lowest. NO_x emissions for the creep cycle were considerably higher than those for the other cycles, and were on the order of 50 g/mi. The higher NO_x emissions for the creep cycle are due to its transient nature over a shorter distance. THC and CO emissions were very low and near the instrument detection limits.

General Observations and Implications

Particle number offers the potential to more readily characterize emissions at the low levels currently exhibited by DPFs, which are often only a small percentage of the certification value. The advantages of particle number measurements in these respects was clearly seen for the on-road testing, but were less clear for the laboratory measurements, where longer tests produced higher/quantifiable PM mass levels and particle number outliers were found. It should be noted that recent studies have suggested that PM mass loadings at levels close to the current US 2007

standards are adequate to get a precise mass measurement, as opposed to the actual tailpipe PM emissions levels for current wall-flow DPF-equipped engines. The role of artifacts was not explored here, but can also play an important role for low level mass measurements.

The variability between the different PMP particle number counts and the PM mass depended on the cycle, sampling location and time, the specific test instrument, and other experimental conditions. For the on-road testing, the variability of the particle number measurements below the PMP systems was lower than that of PM mass for nearly all test cycles. For some tests during the laboratory testing, however, significant outlier events were identified using the PMP system. It does appear that the outlier events represent real differences in particle number emissions that can be seen with the PMP, but may be masked in the mass measurement. The nature of these outlier events, whether they are sulfate derived, due to evaporation and renucleation in the PMP, or from regeneration-like events in the DPF should be further explored. Note that such outliers below the PMP, especially for the 3790, were not observed in the on-road testing or in CARB's previous PMP work.

The overall combined laboratory and on-road results seem to indicate that particle number can provide a more repeatable measurement for current wall-flow DPFs with particle emission levels well below the 2007 US PM mass standard, but not necessarily at PM levels near the standards. Additionally, the PMP methodology provides a new metric with which to better understand PM emissions. The development of statistical techniques for the removal of outlier tests for particle number should be considered. These statistical outlier criteria are not currently incorporated into the PMP protocols. Also, while the PM mass measurements have a lot of scatter at current wall-flow DPF tailpipe levels, the particle number measurements have outliers that can be removed using statistics.

The particle number measurements for the low cut point CPCs below the PMP system were approximately an order of magnitude higher than those for the PMP-compliant CPC and the other high cut point CPCs below the PMP system. This means that a significant fraction of particles are not being counted using the current 23 nm cut size either due to size and/or volatility. This has the advantage of removing nucleation particles that can contribute to variability, but also removes the ability to characterize these same small particles. The negative impacts of greater system variability were seen for the lower cut point CPCs in the laboratory testing, but not the on-road testing.

Significantly higher particle number counts were measured below the PMP when sulfate-based nucleation particles were formed during the on-road driving conditions with the highest engine loads and exhaust temperatures consistently above 300°C. This suggests that particle number counts and the robustness of the PMP system under these conditions should be investigated, although these conditions are more aggressive than those for typical certification. Other methods for the removal of sulfate-based nucleation particles, such as a catalytic stripper that combines a sulfur-trap that eliminates sulfur compounds and an oxidation catalyst that eliminates hydrocarbons, could also be investigated.

The comparison of two PMP compliant systems during the on-road testing showed biases and differences that should be further investigated to ensure consistency in the solid particle

measurements. This could include systematic evaluations of different designs and different parameters with the PMP system operation, such as different temperatures, dilution ratios, or residence time for the sampling system or CPCs with different cut points.

These results also suggest that additional information on the chemistry of the particles would be of value to determine specifically what types of particles are being measured below the PMP system. This could include elemental and organic carbon, sulfuric products, hydrocarbons, poly aromatic hydrocarbons (PAHs), water, trace elements/metals, and metal oxides from lube oils or wear.

The effectiveness of the PMP system should be evaluated in California over a wider range of vehicles and aftertreatment technology applications, similar to what has been accomplished in Europe. This could include vehicles/engines with active traps, DPF + NO_x aftertreatment systems and other vehicle/engine/aftertreatment systems.

1.0 Background

Particulate matter (PM) is one of the most important emissions components to control from diesel engines and its association with adverse health effects has been documented in numerous studies. The stringent PM regulations that have been implemented for new on-road heavy-duty engines have forced significant reductions in PM, and essentially require the use of diesel particulate filters (DPF). With the significant reduction in PM levels, it is anticipated that the current gravimetric methods used for the legal determination of emissions will have difficulty accurately quantifying PM mass emissions. Improvements to the gravimetric method have been issued by the US EPA and in Europe for emission certification. While the new gravimetric methods are adequate for measurements near the certification limit, accuracy will continue to be a problem at the much lower emission levels that DPFs typically produce [Khalek, 2005].

In Europe, greater emphasis has been placed on particle number measurement as a method to improve the accuracy and repeatability of PM measurements at low levels. Particle number methodologies have been developed as part of Europe's Particle Measurement Program (PMP) under the auspices of the United Nation's Economic Commission for Europe – Group of Experts on Pollution and Energy (ECE-GRPE) program. This program has put forth a new metrology that emphasizes the measurement of “solid” particles, including instrument specifications and sampling protocols. Studies conducted under this program have shown that these “solid” particle measurements are 20 times more sensitive than gravimetric methods [Andersson et al., 2007]. Particle number may also be a indicator metric for adverse health effects than particle mass [Brook et al., 2002; Oberdorster, 2001; Peters et al., 1997; Pope et al., 2002]. There are still important questions to be answered in the application of this particle number methodology, however. In counting only solid particles, this protocol may not be sufficiently representative of real diesel emissions. Total particle number (i.e., not just solid particle number) may be more related to adverse health effects than merely “solid” particle number. While counting only solid particles is problematic and may not be indicative of diesel PM health effects, this still represents a significant advancement, as it is currently the only methodology with low enough detection limits to produce precise measurements from DPF-equipped engines.

The objective of this project was to conduct a critical evaluation of the proposed PMP method for determining particle emissions from heavy-duty diesels and its potential in California for PM measurement and in-use screening. For this program, comparisons between particle mass and solid particle number (using the PMP protocols) and total particle number were made under both laboratory and in-use conditions. Testing was conducted on DPF-equipped engines to test the limitations of both PM mass and particle number measurements at these low levels. The goal of the on-road testing portion of this program is to specifically evaluate the effectiveness of the European PMP methodology under conditions encountered outside the laboratory under real-world operating conditions. The study aim to answer the following question: “*can the PMP protocol (with current instruments and methods) be applied for real-world over-the-road testing and achieve equal measurement precision and accuracy to laboratory testing.*” Several instruments for the measurement of real-time size distributions were also utilized in this evaluation in parallel with the PMP instrumentation. This program was conducted in collaboration with other particle emission experts from Europe and the United States (US), including European counterparts who have direct, hands-on experience with the PMP protocol.

2.0 Experimental Procedures for Chassis Dynamometer Laboratory Tests

2.1 Overview of Experimental Approach

The laboratory portion of the project was conducted at CARB's heavy-duty vehicle laboratory (HDV lab) located in Los Angeles, CA. The goal of this portion of the program was to provide a comparison between the current gravimetric method and the PMP method under more controlled conditions. Testing was conducted under three different operating conditions, including a 50 mph cruise, a Urban Dynamometer Driving Schedule (UDDS), and idle. Testing included a series of different real-time PM instruments operating in conjunction with and separate from the PMP system.

2.2 Test Vehicle and Fuel

Test Vehicle

The test vehicle was a 1999 International 4900 equipped with a 7.6 liter International DT466E. The vehicle was obtained from Caltrans, had a mileage of 40,000 miles, and was equipped with an Engelhard DPX diesel particle filter (DPF). The DPF was installed when the vehicle had seen 10,000 miles of service. The vehicle had a gross vehicle weight rating (GVWR) of 27,000 lbs and was tested at 20,920 lbs. The test vehicle was inspected for safety as well as for proper engine/vehicle operation prior to testing.

Test Fuel/Lubricant

The test vehicle was fueled with ultra-low sulfur diesel fuel (ULSD) donated in-kind by British Petroleum (BP), which is expected to have a fuel sulfur level < 15 ppm. A single batch of fuel was utilized for all chassis dynamometer testing. This fuel was utilized for CARB's extensive Phase II research program on the investigation of the toxicity of emissions from heavy-duty vehicles, which this project was run in conjunction with. The oil that the vehicle arrived with was used for testing. The sulfur content in the fuel and lubrication oil was measured to be 6 ppm and 0.383% by wt., respectively.

2.3 Test Cycles and Other Test Parameters

Test cycles

The chassis dynamometer tests for this program were run in conjunction with the CARB Phase II program, and hence both programs utilized the same basic testing sequence. The test cycles/operating conditions included an Urban Dynamometer Driving Schedule (UDDS), a cruise at 50 mph, and idle. It should be noted that the PMP sampling system was not available for the idle testing, and hence only a subset of measurements were made for this operating condition. Sampling at the test conditions was performed over a period of 35-45 minutes. Sampling for longer periods was initially considered, but preliminary testing indicated that the filter loadings over the long test periods may not be representative, due to potential effects on the filter of long exposure at high sampling temperatures or exposure to NO₂.

Cruise at 50 mph

The first portion of the testing was a cruise at 50 mph. Testing over the cruise cycle was conducted in continuous periods of 45 minutes. The 45 minute cruise cycle was repeated 16 times over a period of 3 days, with 5 or 6 test runs per day.

UDDS

The Federal heavy-duty vehicle UDDS is a transient test cycle with a short cruise section, and hence exercises both the test vehicle and the PMP system over a fairly wide range of operation. This cycle covers a distance of 5.55 miles with an average speed of 18.8 mph and maximum speed of 58 mph over 1060 seconds. The UDDS test cycle for this program was composed of 2 iterations of the UDDS cycle to provide a 35 minute test time, comparable to that for the other test conditions. This cycle was run 18 times over a 3 day period, with the cycle being run 5-7 times per day. The cycle is described in greater detail in Appendix A.

Idle

For the idle test condition, the vehicle was run at idle for a period of 45 minutes. A total of 3 separate idle tests were conducted.

Preconditioning

The engine was warmed up for 30 minutes at 50 mph prior to running the first cruise cycle each day and over a single UDDS prior to running the first double UDDS each day. The vehicle was turned off for 20 minutes and “hot soaked” in between tests throughout the remainder of the day. If there was a break in the test sequence of longer than 30 minutes, i.e., for lunch or repairs, the preconditioning using either the 30 minutes at 50 mph or the single UDDS was performed again prior to restarting testing.

Chassis Dynamometer Test Facility

Emissions testing was conducted at CARB’s Heavy-Duty Emissions Testing Laboratory (HDETL), located in downtown Los Angeles. This facility has a Schenck-Pegasus chassis dynamometer with a single 72 inch diameter roller. The dynamometer is driven by a direct current 675 hp motor that can absorb up to 660 hp. The dynamometer has a range of simulated inertial weights from 5,000 to 100,000 lbs. This facility is described in greater detail in Ayala et al. [2002].

2.4 Emissions and Other Measurements

The emissions sampling included regulated emissions, filter-based PM mass, the PMP system, additional real-time PM sizers, and organic and elemental carbon (OC/EC) measurements. A summary of the emissions measurements for this portion of the program is provided in Table 2-1. A schematic of the test set-up is also provided below in Figure 2-1. It should be noted that for the idle, 50 mph cruise, and UDDS, additional samples were collected as part of the CARB Phase II program, including PAHs, ions, trace elements, Ames assay, carbonyls, volatile organic compounds (VOCs) and toxics.

Analyte	Collection media	Lower Size Cut (d50)	Sample Location	Notes
THC	Bag			
NMHC	Bag			
NO _x , NO ₂ , CO, CO ₂	Bags			
PM Mass	Teflon 47mm (Teflo)		From secondary dilution tunnel	
CPC 3790		23 nm	Below PMP system	Not available for Idle testing
CPC 3025A		3 nm	Below PMP system	Not available for Idle testing
CPC 3025A		3 nm	From primary CVS tunnel	Not available for Idle testing
EEPS		5.6 nm	From primary CVS tunnel	Not available for Idle testing
CPC 3022		7 nm	From primary CVS tunnel	Utilized only for Idle testing
DMS		5.6 nm	From primary CVS tunnel	
PAS, DC			From primary CVS tunnel	
EAD		10 nm	From primary CVS tunnel	

Table 2-1. Sample Collection Test Matrix for Chassis Dynamometer Testing

Regulated Emissions

Standard emissions measurements were made for the regulated emissions (NO_x, NO₂, THC, NMHC, CO) and CO₂. NO_x and NO₂ were measured over a heated sampling path. Emissions measurements were made using the standard laboratory instruments at the CARB chassis dynamometer facility in Los Angeles, CA. For each test cycle, for gaseous emissions, both modal (second-by-second) as well as bag data were collected.

Filter-based PM Emissions

Filter-based PM mass measurements were collected for all tests. Over the double iterations of the UDDS, and over each of the segments of sampling for the cruise and idle tests, PM mass samples were collected cumulatively.

Samples were collected from a secondary dilution tunnel off the primary CVS. Samples were collected using 47 mm diameter, 2.0 um pore Gelman Teflon membrane filters and the sampling conditions specified in the 2007 regulations. This includes collection of PM samples at the appropriate 47°C±5°C and with the appropriate filter face velocities. The dilution was set such that a total dilution ratio (primary + secondary) of approximately 20 to 1 for the PM mass was achieved under fully loaded vehicle test conditions. Pre- and post-filter mass measurements were made using a Mettler Toledo UMX2 microbalance with a static neutralizer in a 2007 compliant glove box.

DRAFT

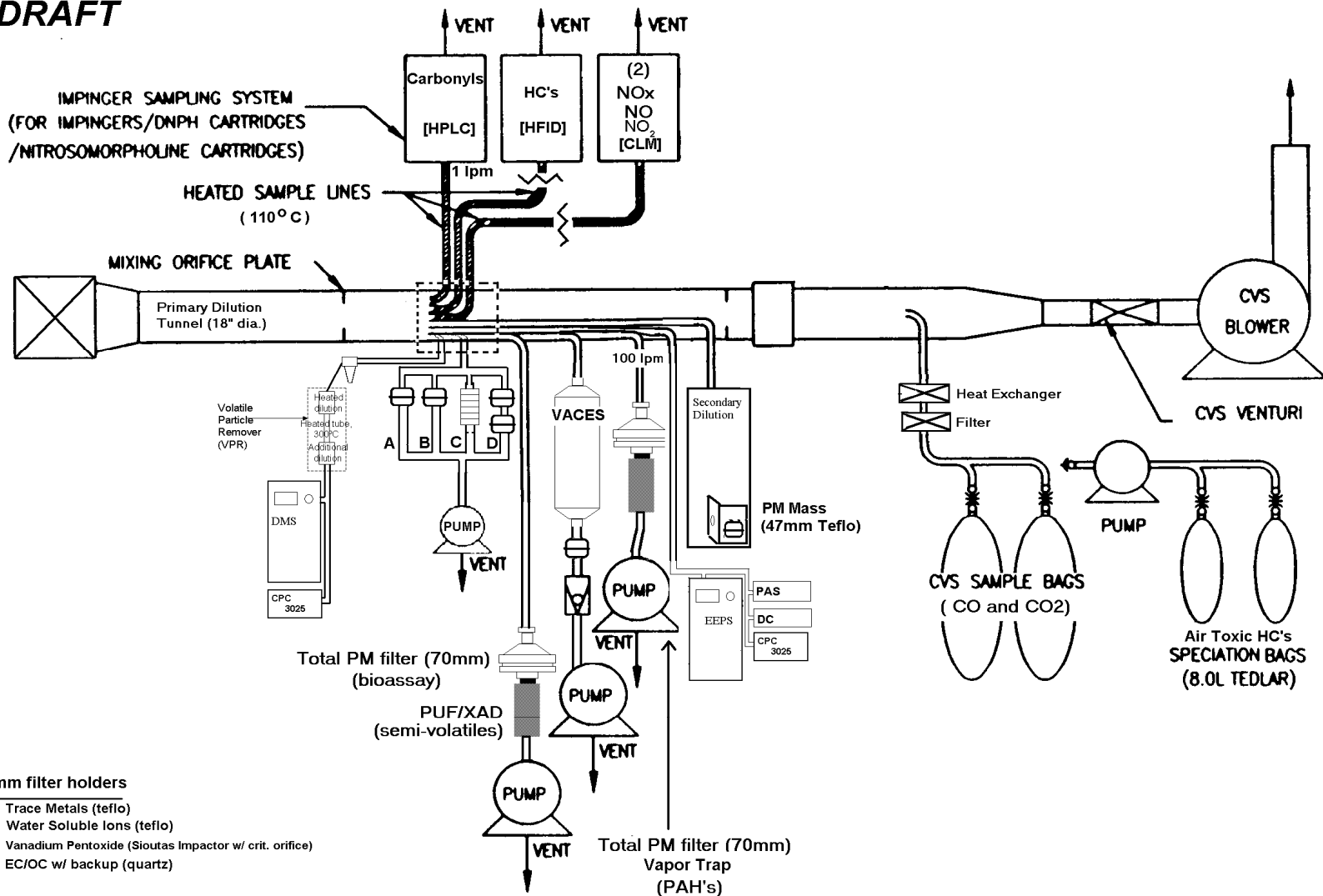


Figure 2-1. Schematic of the Sampling layout for the Test Program

PMP Measurement System

The PMP instrument is a particle sampling system designed to measure the number concentration of solid, non-volatile particles. This system was initially applied for light-duty vehicles, and is now being examined for heavy-duty applications. The PMP-recommended suite of instruments consists of a Condensation Particle Counter (CPC), coupled with a thermal conditioning unit for volatile specie control, known as the volatile particle remover (VPR), with two stages of dilution with the first being a rotating-disk diluter and a pre-classifier for sampling directly from the Constant Volume Sampling (CVS) full-exhaust dilution tunnel [Kasper, 2004; Andersson et al., 2007]. A Matter Engineering MD-19 rotating disk diluter was used for the primary PMP dilution at 150°C and a Dekati ejector diluter was used for secondary dilution in the VPR. The two stages of dilution are connected by an evaporation tube (ET) heated to 300°C. The thermal conditioning unit is used for elimination of the volatile fraction of the PM emissions so that the method can determine solid particle number emissions in a precise manner. This system is designed to include a hot dilution where the mass concentration of volatiles is reduced to help eliminate the subsequent nucleation of particles, a heated tube where volatiles are evaporated, followed by a second diluter that cools and dilutes particles to a point where no nucleation will occur. The particles are then counted using a CPC. The TSI 3790 is the CPC currently approved for the PMP system. The size cut for this instrument is 23 nm. It should be noted that the latest specifications for the PMP system including calibration criteria, as well as parameters for setting up the PMP system [Andersson et al., 2007]. Since this system was not characterized for these calibration criteria, it can not be considered to be fully compliant with the most recent PMP requirements.

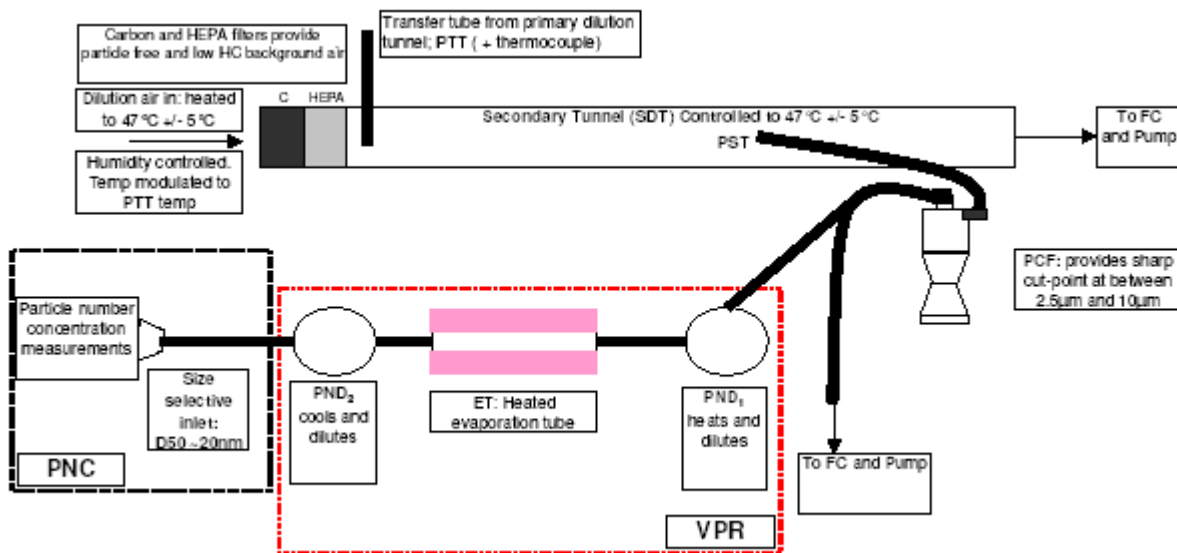


Figure 2-2. Schematic of PMP System from European PMP Literature.

Photographs of the in-use system along with some of the other PM instruments are shown below.



Figure 2-3. Overall picture of Sampling Set-Up with PMP System



Figure 2-4. Close-up Picture of MD-19 Rotating Disk Dilutor

The term “solid” applied to the particles measured by the PMP system is an operational definition based on parameters utilized in the design of the PMP system. Specifically, these “solid” particles are defined as ones having a diameter between 23 nm and 2.5 μm and of sufficiently low volatility to survive a residence time of 0.2 seconds at 300°C. Tests were conducted using evaporated tetracontane ($\text{C}_{40}\text{H}_{82}$) to evaluate the volatile particle removal efficiency of the PMP system (Kasper 2004). These tests showed that using a heating temperature of 300°C, the rotating disk PMP system was able to completely evaporate a number concentration of 5×10^6 particles/cubic centimeters (cc) with a mean diameter of 95 nm. Other tests by Kasper (2004) also indicated efficiencies of between 90-98% of volatile nucleation particles from a heavy-duty diesel engine equipped with a DPF. It is known that some fraction of volatile or organic carbon will be present at temperatures above 300°C. In thermal/optical reflectance, for example, organic carbon is operationally defined as carbon that evolves at temperatures up to 550°C in a He atmosphere (Chow et al. 1993).

Some experiments were conducted to evaluate the time response of the CARB-designed PMP system as part of this program. These results showed that while some broadening of the real-time signal occurred due to the PMP system, this did not affect the integrated average particle count values. These tests and results are discussed in greater detail in Appendix B.

Additional Condensation Particle Counters

One issue with the European PMP sampling system in its current configuration is the size range for the CPC is limited to particles greater than 23 nm in diameter. CARB has conducted some

preliminary testing to examine the magnitude of the effect of particles smaller than 23 nm on the measurements. In this preliminary testing, other particle counters including the following were used: a TSI 3786 (2.5 nm), a TSI 3025A (3 nm), and a TSI 3022A (7 nm). The use of these additional instruments showed that, dependent on engine operation, between 25-75% of the solid particles can have sizes smaller than 23 nm [Herner et al., 2007], so the ability to measure the smaller size particles is likely to be important. For this program, a TSI 3790 was used with the European PMP dilution system. An additional TSI 3025A was used down stream of the PMP dilution system to allow comparisons between the size ranges. A second TSI 3025A was used in two locations. The second TSI 3025A was downstream of the PMP system for most of the tests, to provide comparison and duplicate measurements with the other 3025. For one test run on the 50 cruise cycle, the second 3025A was used to sample directly from the dilution tunnel. The direct 3025A CVS measurements showed that the tunnel particle count levels were over range for the maximum particle count level for the CPC, so no further direct CVS measurements were made. Finally, a TSI 3022 was utilized for particle count measurements directly from the tunnel during the idle tests, since many of the other instruments were not available at that time.

Real-time Particle Size Classification Instruments

Two different particle sizers that utilize differential electrical mobility were used for the laboratory testing. This includes a TSI Model 3090 Engine Exhaust Particle Sizer (EEPS) [Johnson et al., 2004] and a Cambustion DMS500 [Reavell et al., 2002; Kittelson et al., 2004]. CARB has previously used the EEPS for measuring transient ultrafine particle emissions for a trap equipped diesel truck [Ayala and Herner, 2005]. Originally, CARB investigators had envisioned the EEPS as a potentially key instrument capable of providing not only total particle counts, but also size distribution with the necessary precision and accuracy. Recent experiments published by CARB investigators suggest that while the EEPS may not count total particle as accurately as a CPC during steady-state vehicle operation, the instrument is robust and adequate for measuring transient emissions [Herner et al., 2007].

Other Real-time PM instruments

An electrical aerosol detector (EAD) and a photoelectric aerosol sensor (PAS) were also used for the laboratory testing. These instruments use a corona discharge and photoelectric charging, respectively, to charge particles for subsequent measurement. The EAD signal is primarily a measure of the particle surface area and it does not depend on surface composition. The EAD has a size cut of 10 nm. The PAS uses an Excimer lamp as a narrow band source of UV radiation that is selected to ionize PAH coated aerosols while gas molecules and non-carbon aerosols remain neutral. The PAS is known to have a strong response to elemental carbon as well as particle bound PAHs [Matter et al., 1999].

These units were used for sampling directly from the CVS for most of the test program. For a small subset of tests, the EAD and PAS were moved to sample downstream of the PMP system to provide a direct measure of solid particles. For the tests below the PMP, no substantial signal was registered for either instrument. The PAS was set up to sample every 2 seconds during the UDDS cycle, and thus provide a more real-time indication of the concentration level. For the 50 mph cruise and the idle testing, the PAS was set up with a 4 second lamp on time and a 1:5 duty cycle for the lamp “on” to “off” time. Thus, the PAS would sample for 4 seconds with the light on and then the light would turn off for 20 seconds and no sampling would be done. This time

sequence for the cruise and idle tests was set up to help preserve the lamp lifetime, and since emissions were expected to be largely steady state for these cycles.

Quality Assurance/Quality Control

CARB has existing QA/QC procedures for the measurement of all regulated gaseous emissions and PM mass. These QA/QC procedures were applied to this program in their current form. The real-time PM instruments, including the EEPS, DMS, and CPCs, were checked for the zero value each morning by comparing the counts of the test cell air to counts when the air is filtered with a HEPA filter. The zero values were compared to reasonable estimates for the conditions and between the different instruments. A tunnel blank was also conducted each morning with all the real-time instruments in the typical locations and the PMP system warmed to its typical operating temperature. Laboratory CPC blanks averaged 0.33 #/cc for the 3790 and 0.71 #/cc for the 3025As. CPC tunnel blanks were not subtracted from the sampled values when calculating emissions, as prescribed by the PMP (Andersson et al. 2007). As discussed above, the PMP system was also not evaluated against the PMP calibration criteria [Andersson et al., 2007]. Also, an external particle generator calibration source was not available for this test program.

3.0 Experimental Procedures for On-Road Testing

3.1 Overview of Experimental Approach

The on-road testing was conducted using CE-CERT's Mobile Emissions Laboratory (MEL). MEL was equipped with two systems capable of measuring solid particles utilizing the European specifications. This allowed a direct comparison of the two PMP systems with filter-based mass measurements. Various other PM instruments were also used to provide additional insight into the nature of the PM. Testing was performed on-road using a series of standard cycles such as the Urban Dynamometer Driving Schedule (UDDS), the European ETC cycle, and the CARB creep cycle, as well as measurements in real-world, flow-of-traffic behavior. The standard cycles allowed comparison of the accuracy and repeatability of the PMP measurements under conditions where the variables of real-world measurements, such as vibration, field deployment, ambient conditions, etc., could be incorporated and the flow-of-traffic conditions allowed an evaluation under real world, off-cycle conditions that can be encountered.

3.2 Test Vehicle and Fuel

Test Vehicle

The test vehicle was CE-CERT's in-house, 2000 Caterpillar C-15 14.6 liter engine equipped, Freightliner Class 8 Truck retrofitted with a DPF. This vehicle is certified to EPA 2000 model year standards, with a NO_x certification level of 3.7 g/bhp-hr and a PM certification level of 0.08 g/bhp-hr without a DPF. The DPF used with this project was a Johnson Matthey CRT sized for engine displacements between 6 liters and 15 liters. It is recognized that this DPF is currently not verified for use in California, but this DPF represented a practical selection for this experiment. The DPF was installed on the truck by CE-CERT personnel at a location approximately equivalent to that of the existing muffler. The DPF was degreened using a 14.7 liter CAT 3406C generator operated at steady state loads for 45 hours with CARB ULSD as part of another program prior to installation. The MEL trailer itself provided the load for the on-road testing. The weight of the trailer including all emissions equipment is 65,000 lbs. The CE-CERT truck has a mileage of approximately 18,000 miles.

Test Fuel/Lubricant

The truck was tested with commercially available CARB ULSD fuel, which should have a sulfur level of < 15 ppm. The engine uses typical on-highway lubricating oil from a local service center. The oil trade name is CAT DELO SAE 15W-40 with a sulfated ash content of 1.35 wt. %. The engine has an oil consumption rate of approximately 1 gallon per 10,000 miles.

3.3 Test Cycles and Other Test Parameters

Test cycles

The on-road measurements were made using standard cycles that can provide repeatable measurements of PM. A total of four cycles were utilized for this testing, the UDDS, the CARB creep cycle, and the urban and the motorway or cruise portions of the European ETC cycle. The UDDS and cruise cycles are designed to provide conditions similar to the corresponding chassis

dynamometer testing. The European ETC cycle provides a link to European test procedures. These cycles are described briefly below with additional information provided in Appendix A. Each morning, the truck was driven to the test site, which provided a warm-up of the engine before testing. In between cycles, the truck was typically idled while the instruments and filters were prepared for the next test. No other special preconditioning was utilized before the different test cycles.

UDDS

The UDDS cycle was used to provide a direct comparison with the chassis dynamometer portion of this project, as discussed above

European ETC test cycle

The ETC test cycle (also known as the FIGE transient cycle) was introduced, together with the [ESC](#) (European Stationary Cycle), for emission certification of heavy-duty diesel engines in Europe starting in the year 2000 [*Directive [1999/96/EC](#) of December 13, 1999*]. The ETC cycle consists of three segments representing urban, rural and highway cruise driving. The Urban segment represents city driving with a maximum speed of 50 km/hr (31 mph), frequent starts, stops, and idling. The highway cruise (or motorway) cycle is higher speed and more steady state, with an average speed of 88 km/hr (55 mph). It is denoted as the “cruise” cycle throughout the remainder of this report.

The highway cruise portion of the cycle, has an average speed of approximately 55 mph and was expected to provide a good comparison point with the 50 mph cruise testing that is being done as part of the chassis dynamometer portion of this program. The rural driving schedule was not included because extensive surveys of the roads in the nearby Riverside area did not produce any roads where part 2 could be completed. This is because the stretches of road that were over 7 miles long had either stoplights or rolling hills. The rural driving cycle also was not considered representative of driving in California.

ARB Creep Cycle

The ARB Heavy Heavy-Duty Diesel Truck (HDDT) Schedule was developed by CARB for chassis dynamometer testing based on on-road activity measurements. This cycle includes four segments that include idle, creep, transient, and cruise. For this program, only the creep section of the cycle was utilized, since most of the other segments of the cycle are represented by other cycles discussed above. This cycle covers a distance of 0.12 miles over a period of 253 seconds with an average speed of 1.8 mph.

Flow-of-traffic

CE-CERT also recorded real-world, flow-of-traffic data from Riverside, CA to Indio, CA, Thermal, CA to Indio, CA and on a hill climb towards Blythe, CA east of Indio on the Interstate I-10. The Thermal to Indio trip was repeated four times, while the other flow-of-traffic routes were only done once. The flow-of-traffic tests provide conditions of real-world, on-road behavior and potential off-cycle emissions that are not captured in the predefined driving cycles.

Test Iterations

Each test cycle was conducted at least 7 times to provide a measure of the accuracy and repeatability of the measurement. A separate PM mass filter was collected for each of the individual test iterations. Some additional test iterations were also conducted under different operating conditions including utilizing the PMP dilution systems at higher temperatures and at different dilution ratios. These additional tests were conducted over only the UDDS cycle.

Test Location

A general description of the locations where all the cycles were conducted is provided in Appendix D. The testing for the lower speed, shorter distance cycles (ETC Urban, CARB Creep, UDDS) was conducted on a section of a farm road near Thermal, CA in the Palm Springs/eastern Coachella Valley area. The section of road is located at an elevation near sea level and has relatively long stretches of road with limited stopping needed for traffic signals and sparse traffic. Although the road provides significant advantages, the length of the road is still too short for the duration of an entire test cycle. As such, sampling was split into separate testing sections that are integrated to get the total mass emission rates for the modal data. The bag data were started and stopped automatically for each segment until the cycle was complete.

Figure 2-1 shows the basic layout for the tests in Thermal, CA and all start and stop points based on physical stop signs that were encountered. Typically, in past studies, CE-CERT had performed all the tests in the direction from A to B and then C to D to E and back to A1. A new stop sign was installed at A, however, and thus there was a change in direction of test from ABCDE (clockwise) to EDCBA (counter clockwise) for purposes of safety after completing some of the ETC and creep cycles. The impacts of these direction changes on emissions are discussed further in the results section and associated appendices.

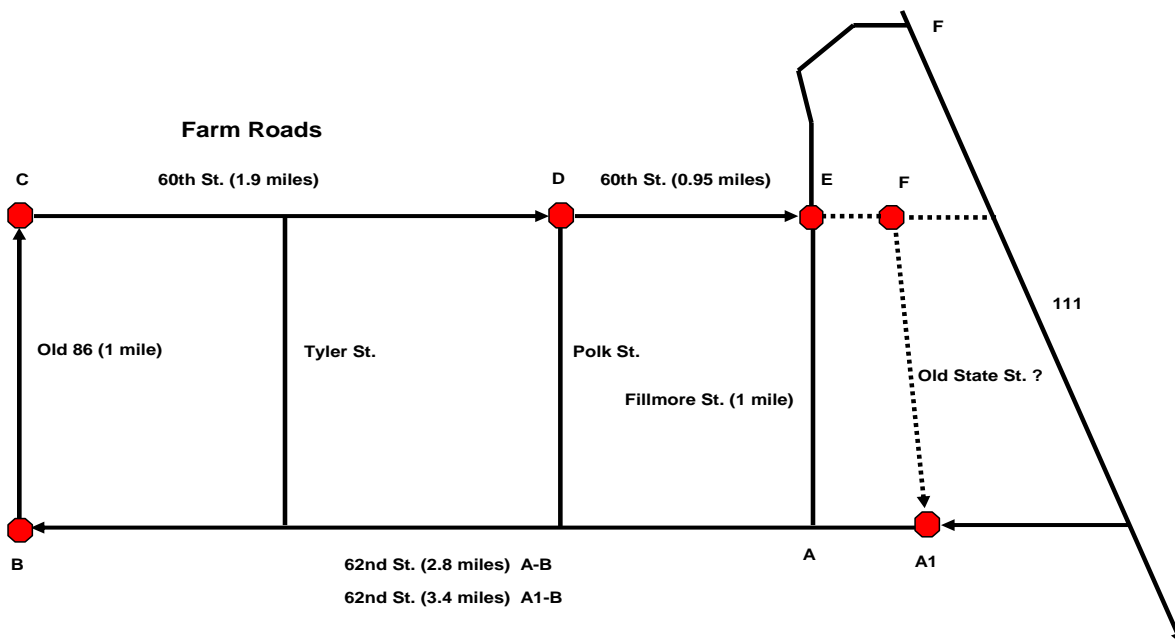


Figure 3-1. Schematic Map of Road Section Used for On-Road Cycles (except the Cruise)

The highway cruise portion of the ETC cycle was conducted on a segment of the I-10 freeway going back and forth between Palm Springs and Indio, CA. As there are different headwind and elevation conditions between the eastbound and westbound segments of the freeway, the back and forth trips needed to be counted as separate trips from one another. A total of 7 full ETC cruise cycles were conducted, with 3 in the eastbound direction and 4 in the westbound direction.

3.4 Emissions and Other Measurements

The following section discusses the gaseous and PM emissions measurements used for this study. A schematic of the experimental set-up for the PM measurements is provided in Figure 3-2. Table 3-1 provides a summary of the emissions measurements made and the instruments used.

Analyte/Instrument	Sampling Location	Low Size Cut (d50)	Maximum range (#/cc)
THC NMHC NO _x , NO ₂ , CO, CO ₂ PM Mass	From secondary dilution tunnel		
CPC 3790 _ MD	Below MD-19 PMP system	23 nm	1 x 10 ⁴
CPC 3025A _ MD	Below MD-19 PMP system	3 nm	1 x 10 ⁵
CPC 3760A _ MD	Below MD-19 PMP system	~11 nm	1 x 10 ⁴
CPC 3025A _ MEL	Below MEL PMP system	3 nm	1 x 10 ⁵
CPC 3760A _ MEL	Below MEL PMP system	~11 nm	1 x 10 ⁴
CPC 3022	From primary CVS tunnel	7 nm	1 x 10 ⁴
EEPS	From primary CVS tunnel	5.6 nm	
f-SMPS	From primary CVS tunnel	10-190 nm	
DMM	From primary CVS tunnel		
DustTrak	From primary CVS tunnel		

Table 3-1. Sample Collection Test Matrix for On-Road Testing

Gas-Phase Emissions

Standard emissions measurements were made for the regulated gaseous emissions (NO_x, NO₂, THC, NMHC, CO) and CO₂. For specific test cycles such as the UDDS, etc., both bag and modal gas-phase measurements were made. Gas-phase emissions measurements were made using the standard laboratory instruments in the CE-CERT MEL, as discussed in Appendix C and Cocker et al. [2004a].

Filter-based PM Emissions

Filter-based PM mass measurements were collected for all tests over a standardized cycle. Samples were collected from a secondary dilution tunnel off the primary CVS. These measurements were in compliance with the most recent modifications to the CFR, promulgated by the US EPA as Part 1065, for sampling temperature (47°C±5°C) and face velocities (50 cc/sec), but not for weighing conditions and the specified filter holder requirements [Cocker et al., 2004b]. The secondary dilution was set to provide a minimum total dilution ratio (primary + secondary) of between 4:1 to 6:1 at the highest load point for any given cycle. A discussion of

potential improvements in weighing accuracy compared to the methods used prior to the implementation the Part 1065 compliant systems is provided later in the PM mass results section.

A routine tunnel blank for PM mass measurements was collected on the first day of testing and the following week after testing. It should be noted that CE-CERT has an extensive database of tunnel blanks, such that the blanks are well characterized and can be compared to those of other experimental programs. To condition the tunnel for DPF-level measurements, a natural gas burner was operated to elevate CVS tunnel temperatures above 200°C and temperatures in the exhaust transfer line above 700°C to remove wall deposited PM. Recent testing in the MEL has shown that this reduces background PM contamination and provides for more robust measurements at DPF PM emission levels.

In addition to tunnel blanks, trip blanks, static blanks and dynamic blanks were performed. Each type of blank corresponds to a possible contamination scenario. The trip blanks represent carrying filters to the test site, but not taking them out of their holders. The static blanks represent loading and unloading filters without going to the test site. The dynamic blanks represent loading filters into filter holders and connecting them in the secondary dilution tunnel, but not pulling a sample flow. The dynamic blanks are placed in the secondary dilution tunnel for the same period as a complete test cycle. The trip, static and dynamic filter weights are typically within the repeatability of reference filter weights. During this PMP study, one full set of quality control filters were sampled and their weights were all within reference filter repeatability limits of 2-3 µg. The overall uncertainty for these filter weights is 2.5 µg at one standard deviation or 7.5 µg at three standard deviations.

PM mass samples were collected using 47 mm diameter, 2.0 µm pore Gelman Teflon membrane filters. Pre- and post-filter mass measurements were made using a Cahn ultramicrobalance (resolution is 1 µg) in a temperature (25°C) and humidity (40% RH) controlled environmental weighing chamber.

Although the filter masses for the test cycles can be relatively low, it was decided that filters would be collected over only single cycles, since the cycle times are similar in duration to those of the FTP engine dynamometer test. For comparison, the engine dynamometer FTP is 20 minutes in duration, the ETC Urban and cruise cycles are each 10 minutes long, the UDDS is approximately 18 minutes long, and the creep is 14 minutes long. As such, they provide a measure of the repeatability/accuracy that can be obtained over a standard certification cycle.

PMP Measurement System

The PMP measurement system and its associated suite of instruments are generically described in section 2.4. Two PMP double dilutions systems were utilized for this program. The first system is essentially the same system that has been in extensive use at CARB's heavy-duty chassis dynamometer facility in Los Angeles, as discussed above and in Herner et al. [2007]. It utilizes a Matter Engineering MD-19 rotating disk diluter for the first stage PMP dilution (PND1) at 150°C, an evaporative tube heated to 300°C, and a Dekati ejector diluter for the second stage of dilution (PND2). The particles are then counted using a CPC. A TSI 3790 with a 23 nm size cut was used with this system, since it is currently approved for the PMP system.

CE-CERT also designed a second PMP-based double dilution system. This system is experimental and mimics the sample treatment of the PMP protocol. It is designed as an alternative and to provide comparison with the approved PMP rotating head MD-19 design. This PMP design is denoted the “MEL” system throughout the rest of the report. The MEL system utilizes a modified design of the ISO 8178 partial flow single venturi fractional flow sampler, as shown in Figure 3-3. The venturi provides the main control of the sample flow and overall dilution ratio. The venturi creates a negative pressure causing sample to flow from the CVS to the venturi. A metered flow was added to the transfer tube, between the CVS and the venturi, to provide a hot (150°C), first stage dilution (PND1) at a dilution ratio of 10 to 1. The primary dilution utilized a simple Swaglock tee where the sample was introduced into the straight line dilution air flow at 90 degrees. The evaporation tube (ET), heated to 300°C, was added between the first stage and the venturi. The ET also maintained a residence time of 200 ms, as specified by the PMP protocol. The metered flow through the venturi creates the second stage of dilution (PDN2). The venturi flow is temperature controlled to 25°C. The sample flow can be changed by varying the sample tube inner diameter (ID). The sample tube ID determines how much sample is drawn for a given venturi pressure drop. For the PMP program, the sample tube was selected to achieve an overall dilution of ~ 100 to 1. The design intention of the MEL PMP system was to compare a low cost diluter (MEL) with a more sophisticated diluter such as the MD-19 system. Since only a single TSI 3790 is available for this program, the CE-CERT system utilized a TSI 3760A (11 nm) and TSI 3025A (3 nm) for particle counts, as discussed below. The placement of the CPCs was after the second stage of dilution, denoted “to particulate sampling system” in Figure 3-3. The MEL system was also not evaluated against the PMP calibration criteria [Andersson et al., 2007].

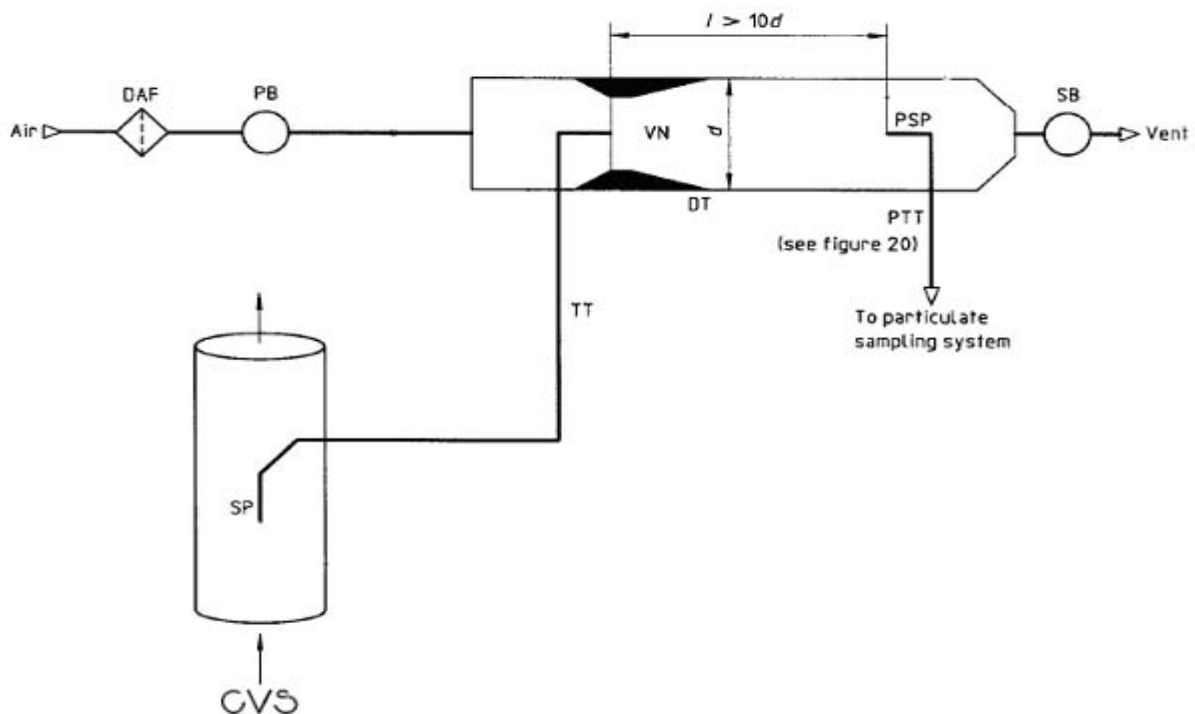


Figure 3-3. Partial flow dilution system with single venturi, concentration measurement and fractional sampling method [modified from ISO 8178-1:1996]

The two PMP designs are compared in Table 3-2. This table lists the PMP specifications that could influence the effectiveness of the repeatability of particle number measurements with removal of volatiles. The MEL design had three times less first stage dilution (PND1) and the same PND1 heated dilution temperature set point, but a much longer residence time to achieve this temperature set point. The ET and final stage of dilution were configured similarly between both designs. A photograph of the general connections for the two PMP systems is provided in Figure 3-4.

Table 3-2 PMP designs comparisons between the MEL and MD-19 systems.

PMP Design	PND1				VPR	PND2	
	DR	Temp (C)	Heat Length (in)	Flow (slpm)	Temp (C)	DR	Temp (C)
MEL	10	150	36	10	300	10	20
MD-19	30	150	6	20	300	10	20

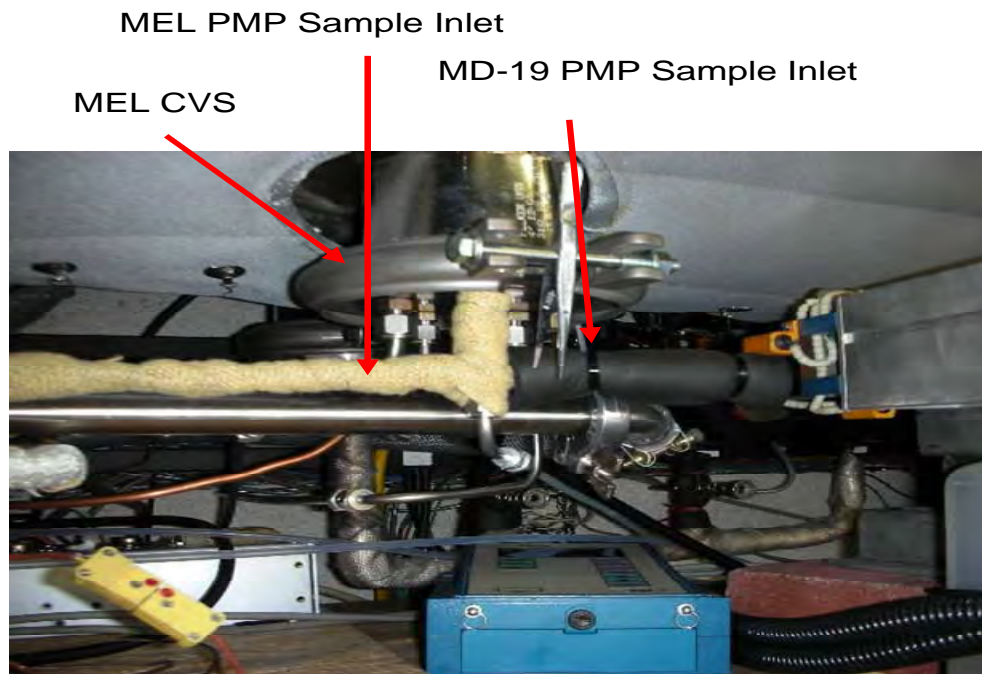


Figure 3-4. Sampling Set-up for PMP Systems.

There was a difference in sample residence time between the two PMP dilution systems used in this study, which is important to consider when comparing the two PMP diluters. The MEL dilution system had a lower residence time and was designed with bypass flow of 15 lpm to try and minimize residence time. The MD-19 setup did not have a bypass and used larger transfer lines, and thus typically had longer residence times. In this case, residence time is a combination of time to get the sample to an instrument (transport time) and the time it takes the instrument to respond to a step increase (response time). The residence time for the MEL PMP dilution system CPC 3760A is around six seconds and the residence times for the MD-19 dilution system CPC 3760A and CPC 3790 are ten and six seconds, respectively. The four second difference between the residence times for the two 3760's is accounted for in the transport delays between the MEL and MD-19 PMP configurations. The 3790 showed a four second faster residence time compared to the MD-19 3760.

Condensation Particle Counters and Configurations

As discussed in section 2.4, one goal of this program was to evaluate the limitations of the imposed 23 nm size cut for the PMP program through the use of CPCs with different lower size cuts. For these measurements, a TSI 3790 was used below the MD-19 PMP system. To provide a smaller size cut for comparison with the TSI 3790, two TSI 3025A CPCs (3 nm) were also used. One of the 3025A CPCs was placed downstream of the MD-19 PMP sampling system to provide a direct comparison with the TSI 3790. The second 3025A CPC was placed downstream of the CE-CERT PMP sampling system to provide a direct comparison with measurements made with the MD-19 system. The 3025A CPCs were operated at a flow rate of 1.5 lpm. This has an impact on their counting efficiency. When the 3025As are operated at a flow rate of 0.3 lpm, there is an internal split of 10:1 for the flow reaching the detector. When the 3025As are operated at a flow

rate of 1.5 lpm, there is an internal split of 50:1 for the flow reaching the detector, so not as many particles make it to the detection region.

Two additional TSI 3760A CPCs were placed downstream of the MD-19 PMP system and the MEL PMP system, respectively, to provide additional intercomparisons. It should be noted that one of these 3760A CPCs was internally redesigned to utilize a 1 lpm instead of a 1.5 lpm flow rate. This flow rate difference was compensated for in all calculations, by multiplying the measured values for the CPC with the lower rates by 1.5 to correct for the flow difference.

A TSI 3022 CPC (7 nm) was used to sample directly from the primary tunnel and provided some indication of the impacts of the removal of solid particles by the PMP systems. The 3760As also do not have a correction for coincidence. Coincidence occurs when two particles pass the detector at the same. Coincidence becomes significant above a raw measurement level of 10,000 #/cc.

Other Real-Time Instruments

A Dekati mass monitor (DMM), a TSI DustTrak™ and the UC Riverside fast-scan scanning mobility particle sampler (SMPS) (f-SMPS) [Shah and Cocker, 2005] were additional instruments that were used in conjunction with this program. The f-SMPS is an in-house CE-CERT instrument that provides a complete scan over the size range ~5-200 nm, on a time scale sufficient to capture transient operation. For this program, the f-SMPS was set up to scan the ~5-200 nm once every 5 seconds. The f-SMPS was utilized for measurements both from the primary tunnel and below the MD-19 PMP system. For some measurements off the primary tunnel, the f-SMPS did experience some difficulty in adjusting to the pressure changes in the primary dilution tunnel, although this did not appear to have a measurable impact on the size distributions.

The DMM and the DustTrak™ were both connected directly to the primary dilution tunnel. The Dekati DMM measures PM mass concentrations through a combination of an electrical mobility diameter via particle charging and an aerodynamic diameter via inertial impaction over six stages of electrometers [Lehmann et al., 2004]. This allows the estimation of size as well as particle mass with the assumption of a log normal distribution.

The Engine Exhaust Particle Size (EEPS) [Johnson et al., 2004] that was used in the corresponding CARB chassis dynamometer testing program was also used in this program. The EEPS was utilized for direct measurement from the primary dilution tunnel for nearly all of the tests. A few preliminary tests were initially conducted with the EEPS placed downstream of the MD-19 PMP system, but these measurements showed that the count rate was insufficient for sampling with a multichannel instrument.

Engine Parameters

During these emissions tests, the J1939 signal was also collected from the engine ECM. This signal provides real-time (~10 Hz) estimated and measured signals for engine parameters such as torque, power, speed, boost, temperatures, etc. Brake specific power is not a direct output from J1939 protocols, but can be calculated from other J1939 parameters, as discussed in Miller et al. [2007].

Quality Assurance/Quality Control Measures for Real-time PM instruments

The CE-CERT MEL has existing QA/QC procedures for the measurement of all regulated gaseous emissions and PM mass, as summarized in Appendix E.

During testing all CPCs, the EEPS, and other CE-CERT instruments were verified for proper operation each morning as the laboratory was warming up. Verification involved checking the CPC's zero, span, and sample flow. The zero was performed by placing a hepa capsule on the CPC inlets and waiting for the CPC to stabilize. All CPCs showed a good zero value during the week of testing. The CPC flows were verified using a dry cell displacement flowmeter and were found to be repeatable and meeting manufacturer specifications. The final check was to use a common "pseudo" span with all the CPCs simultaneously sampling room air. The pseudo span measurements are discussed in greater detail in Appendix F. CPC tunnel blanks were also collected shortly before and after the on-road testing. The on-road CPC blanks were 0.31 and 0.37 #/cc for the 3790 and 3760A CPCs, respectively, and 0.65 #/cc for the 3025A CPC. CPC tunnel blanks were not subtracted from the sampled values when calculating emissions, as prescribed by the PMP (Andersson et al. 2007).

A separate experiment was conducted to evaluate the calibration of the various particle number count and sizing instruments utilized in the on-road measurements. The experiment was conducted in CE-CERT's atmospheric chamber, which can be used to readily create and characterize particles with well defined characteristics. The particles were created by injecting a hydrocarbon particle precursor into the chamber and initiating nucleation with the chamber light source. This procedure created nice, nearly spherical particles with a nominal size between 70 and 170 nm, which is above all of the cut-off diameters for the utilized CPCs. Although there are some differences between the different CPCs, overall, the data show good comparability between CPCs used in the on-road testing. The results of these chamber calibration verification experiments are discussed in greater detail in Appendix F.

As discussed above, the PMP systems were also not evaluated against the PMP calibration criteria [Andersson et al., 2007].

In addition to the discussed QA/QC procedures, multiple investigators witnessed various and different aspects of the testing, providing key critical on-site oversight and expert critique to the various aspects of over-the-road program.

4.0 Emissions Results for Chassis Dynamometer Laboratory Testing

4.1 Gas-Phase Emissions

The gas-phase emissions are provided for NO_x, NMHC, and CO in Figure 4-1 to Figure 4-3, respectively, for each of the test conditions. The bars for each test condition represent an average over all tests at that condition, with the error bars representing one standard deviation. The emissions are presented in grams per mile (g/mi) for the speed-time trace cycles, such as the UDDS and the cruise, and in grams per hour (g/hr) for the idle condition. It should be noted that the gas-phase and PM mass emissions values presented here for the chassis dynamometer testing were QA/QC checked, but did not undergo the full QA/QC process controls typically utilized by this facility due to issues with data availability as the laboratory was being upgraded. Nevertheless, the quality of the data was deemed to be sufficient for the purposes of this study, and any changes expected from the full QA/QC evaluation would be expected to be very minor and not at a level that would impact any conclusions.

For NO_x emissions, the truck emission rates were on the order of 10 g/mi for the UDDS and 7 g/mi for the cruise. These emissions values are comparable to those found in other testing of medium-duty diesel trucks [Clark et al., 2007]. The percentage of NO₂ as a function of total NO_x varied depending on the test cycle, with highest percentage of NO₂ seen for the cruise cycle and the lowest seen for the idle. The higher NO₂ ratios for the cruise could be attributed to higher temperatures in the aftertreatment system.

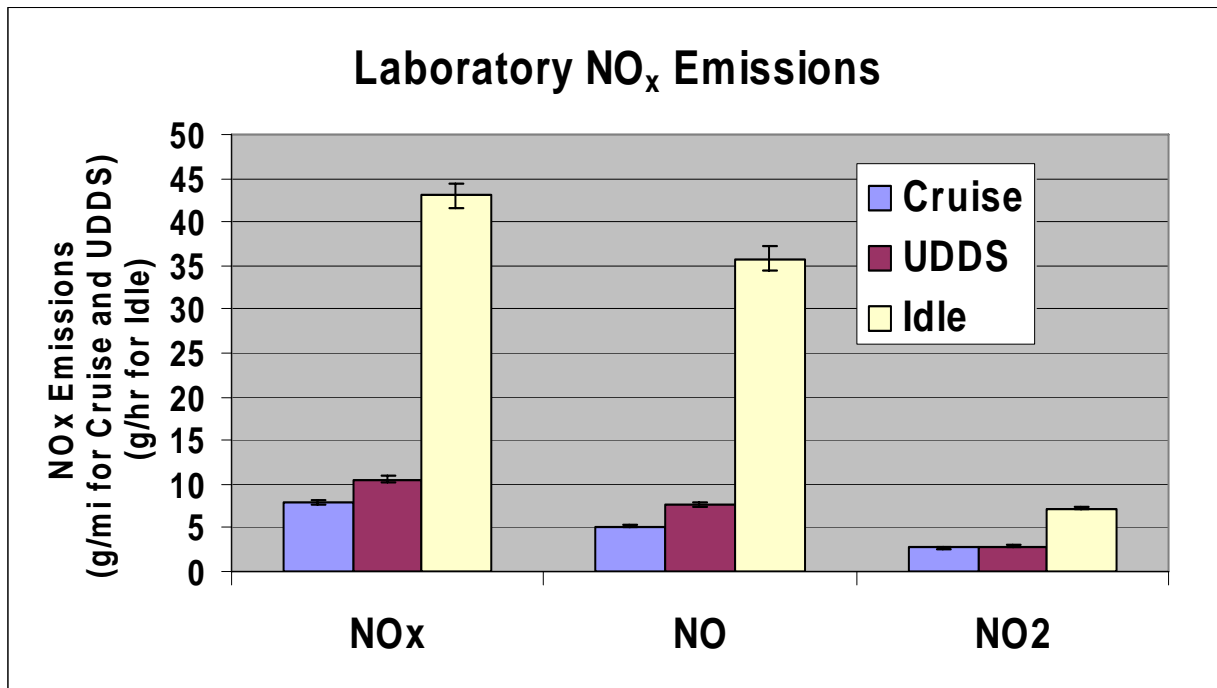


Figure 4-1. NO_x Emissions Results.

THC emissions varied for the different test cycles. THC emissions for the cruise cycle were essentially below the detection limits on average. THC emissions for the UDDS and the idle were measurable but still relatively low. The THC emissions for the cruise vs. the UDDS cycle could be attributed to the higher aftertreatment temperatures achieved during the cruise cycle.

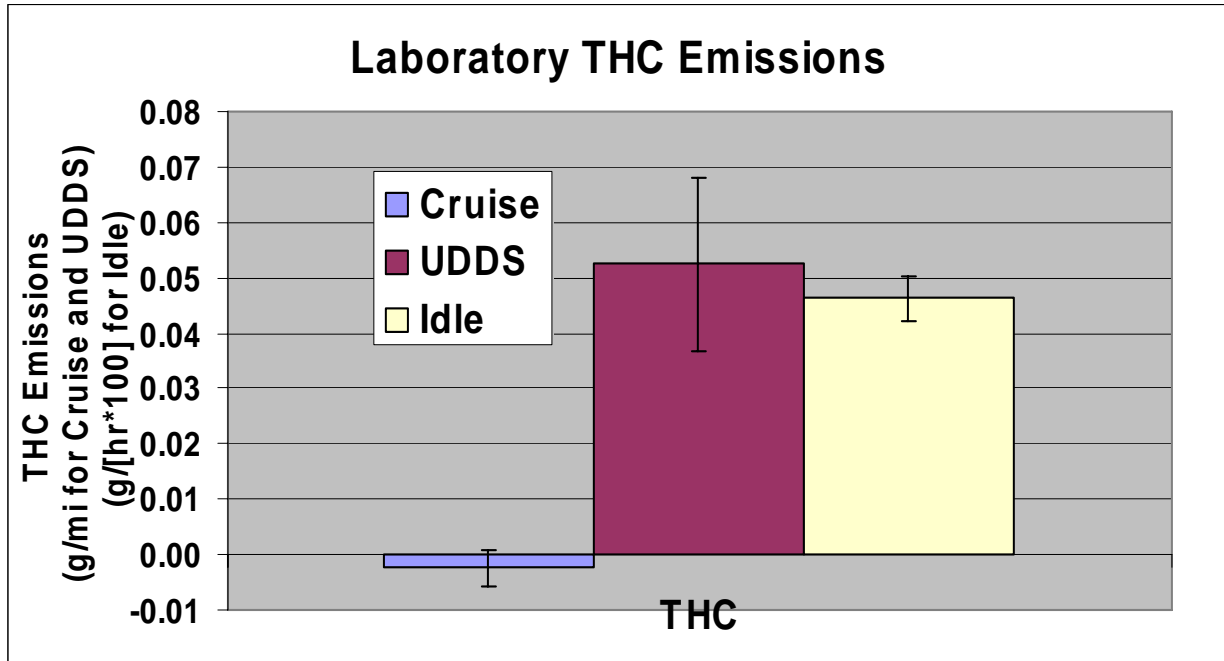


Figure 4-2. THC Emissions Results

CO emissions also varied for the different test cycles. CO emissions for the cruise cycle were very low and near the detection limits (note the scale is multiplied by 100). CO emissions for the UDDS and the idle were well within the measurable range, but were still low compared to NO_x emission levels. The CO emissions for the cruise vs. the UDDS cycle could be attributed to the higher aftertreatment temperatures achieved during the cruise cycle.

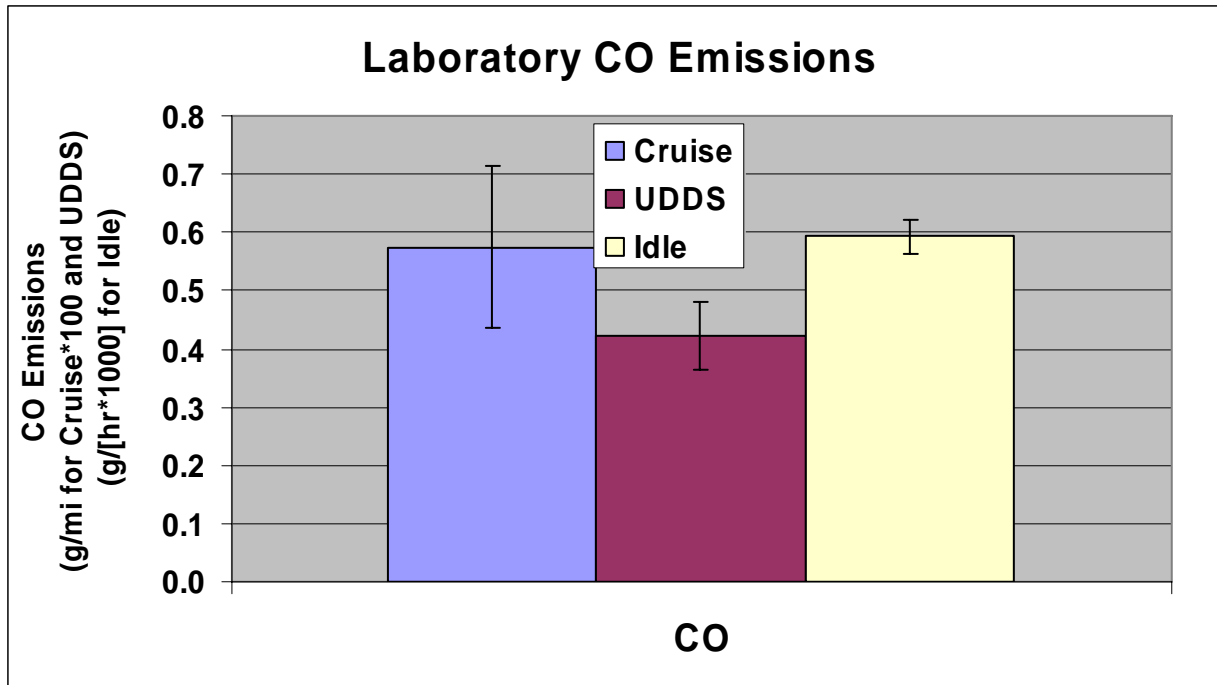


Figure 4-3. CO Emissions Results

4.2 PM Mass Results

The PM mass results are shown in Figure 4-4 for average emissions for each cycle, with the error bars as one standard deviation. These values are fairly low and consistent with what would be expected for a vehicle with an engine equipped with a DPF. The measurements were all well above the tunnel blank levels for the driving cycles, which were 1.6 mg/mi for the UDDS and 0.6 mg/mi for the 50 mph cruise. The idle emissions were essentially at the same level as the tunnel blanks, which were 29 mg/hour. The PM filter masses for the laboratory study are provided in Figure 4-5. Over the time periods for the test cycles for the cruise and the UDDS, the filter masses were well above the blank and detection levels. The filter masses for the idle were comparable to those of the tunnel blanks for the same time period of 35-45 minutes, ~11 µg. It should be noted that the tests were conducted over testing periods of approximately 35 to 45 minutes, which is approximately twice as long as the typical certification test over the Federal Test Procedure (FTP). Hence, certification test filter mass levels would likely be less than those measured in the laboratory portion of this work. On the other hand, current wall-flow DPFs typically reduce PM to well below the 2007 PM standard, so PM mass levels for devices performing near the certification levels should be more readily measureable.

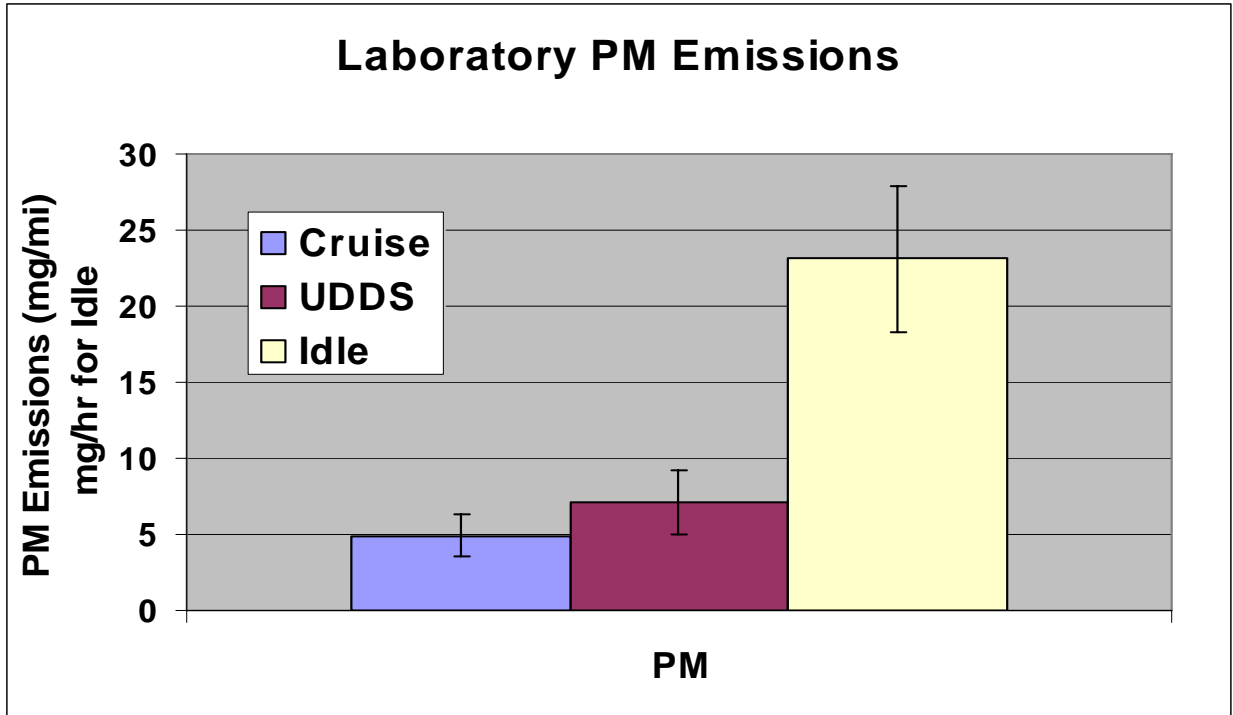


Figure 4-4. PM Emissions Results

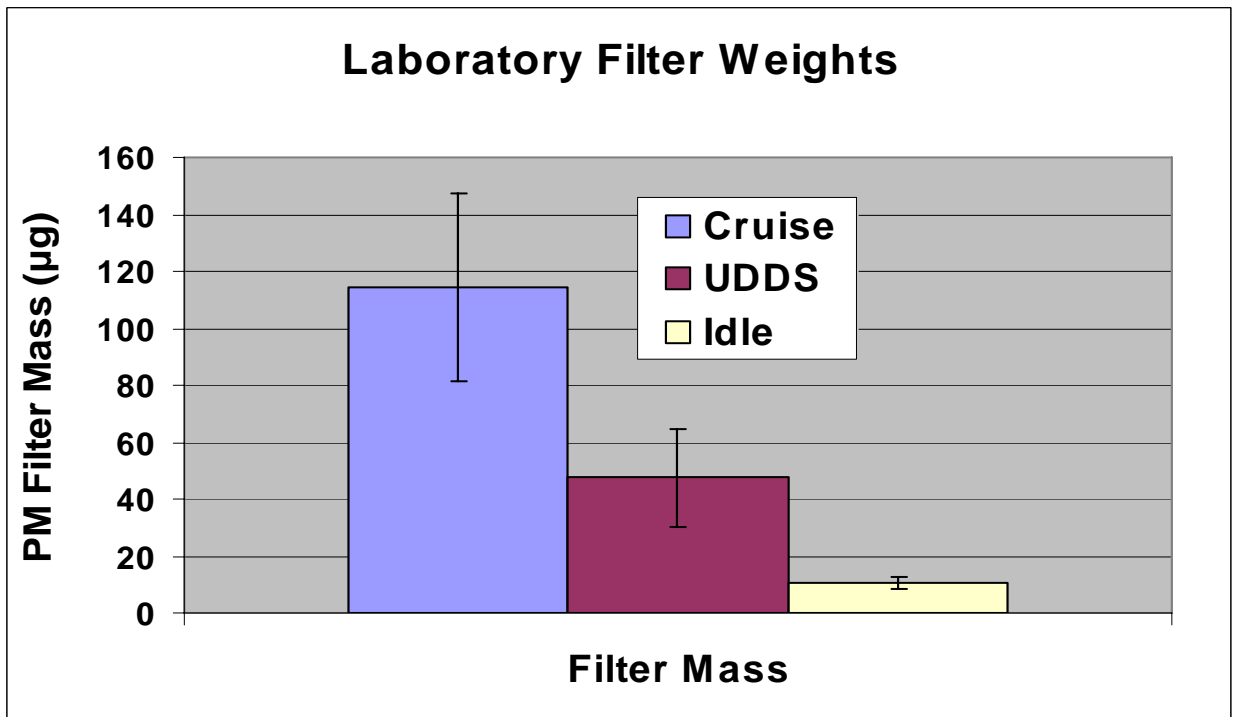


Figure 4-5. PM Filter Masses

4.3 PMP and other Particle Number Results

The CPC data for the UDDS and the 50 mph cruise are shown in Figure 4-6 and Figure 4-7. Figure 4-6 shows the data averaged over all the test points. The particle number counts for the 3790 were below the European standard for light-duty vehicles (8×10^{11} particles/mi) for both the UDDS and cruise cycles, noting that the scale for the 3790 is multiplied by 10. As shown in Figure 4-6, the results show a large variability when averaged over all tests. The nature of this variability is further investigated in Figure 4-8 and Figure 4-9. These figures show the individual test results for the UDDS and cruise cycles, respectively. The UDDS cycle data shows that there is one test in particular has a considerably higher particle count rate than the others, with another test that is also higher than most of the other measurements. Similarly, the cruise cycle data also shows a few data points with significantly higher emissions rates than the other data points. These data will be discussed further in real-time data results in section 4.5.

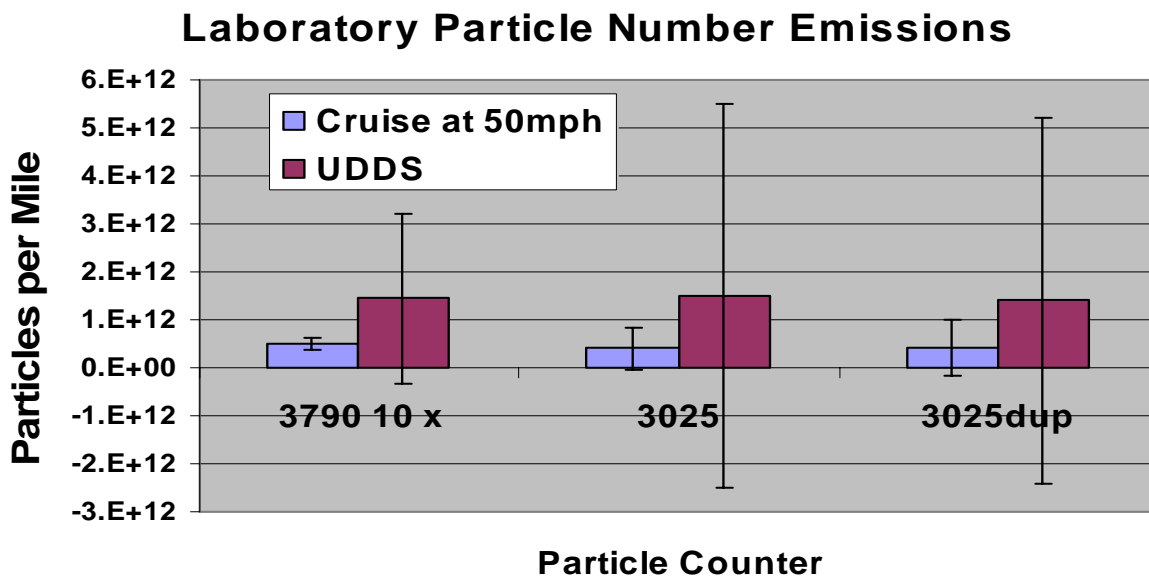


Figure 4-6. Particle Number Counts for different CPCs for the UDDS and the Cruise, including all Test Runs.

Some scenarios were examined to look at the potential use of outlier criteria to improve the repeatability of the particle number measurements. Figure 4-7 shows the UDDS and cruise particle number counts with the data points determined to be outliers via two different scenarios removed. Two separate scenarios for outliers were investigated. For the first scenario, outliers were removed using some of the same protocols used in the PMP for PM mass, as discussed in Andersson et al. [2007]. Using these protocols, a point is considered an outlier if it is outside the range of two standard deviations of the average of the ‘rest’ of the tests, or the other tests conducted. It is important to note that these procedures were applied to PM mass in the European studies, not particle number, so the application of this outlier criteria to particle number is outside the limits of the PMP protocols. While this protocol captured the highest outlier in each

case, the second highest outlier point was not always identified using this technique. As such, an additional outlier comparison is included where both of the two highest outliers were removed.

With the “PMP outlier criteria” applied, the PMP compliant 3790 CPC (23 nm) shows relatively low variability, but the small cut point CPC 3025s (3 nm) still show considerable variability. The variability for the 3025s does improve when the highest two outlier points are both removed. After the removal of outliers, there are some trends of higher particle number counts for the 3025As compared with the 3790 and for the UDDS compared with the cruise. While significant outliers were not observed in CARB’s previous study [Herner et al., 2007] or in the on-road tests described below, the laboratory tests seem to indicate that the use of outlier criteria might be useful in the application of particle number measurements.

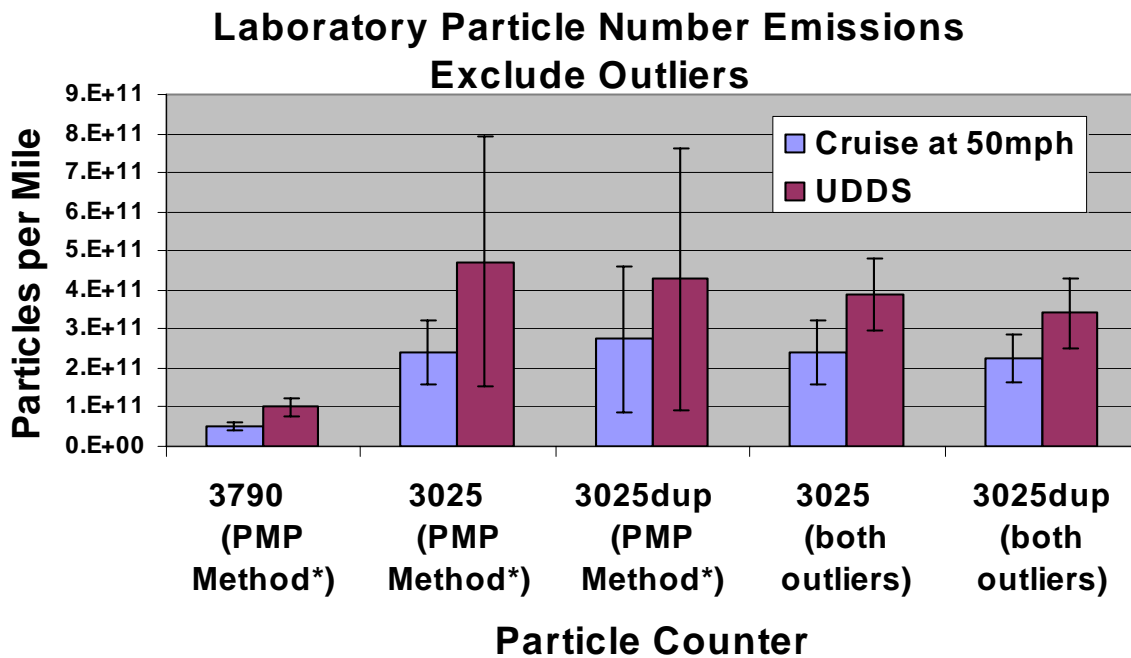


Figure 4-7. Particle Number Counts for different CPCs for the UDDS and the CPC, excluding the Test with the Highest Particle Concentration for each Cycle. * Note this outlier criteria is typically used in the PMP protocol for PM mass, not particle number.

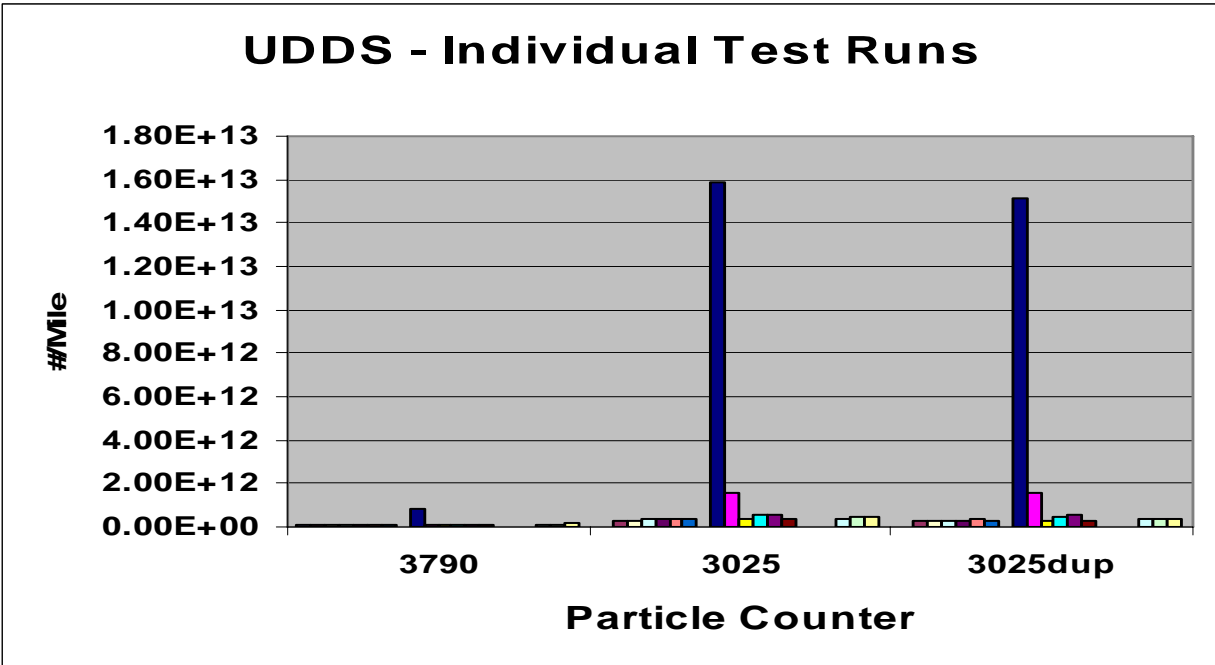


Figure 4-8. Particle Number Counts for Individual Test Runs for the UDDS.

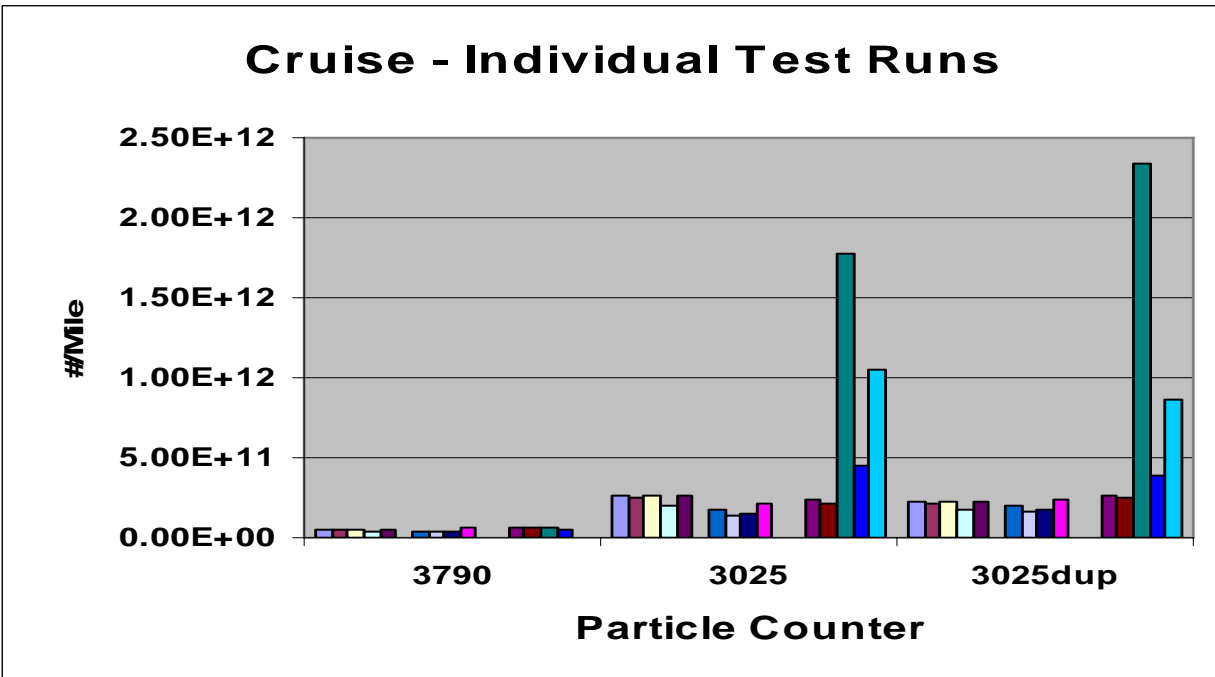


Figure 4-9. Particle Number Counts for Individual Test Runs for the Cruise.

There was a reasonable correlation between the two 3025A CPCs. A correlation plot between the two instruments is presented in Figure 4-10. The CPCs show the best correlation over the UDDS, with an R^2 of 0.99. The correlation for the UDDS is also reasonably good at 0.95, but with a slope and intercept indicating a slight positive bias between the systems.

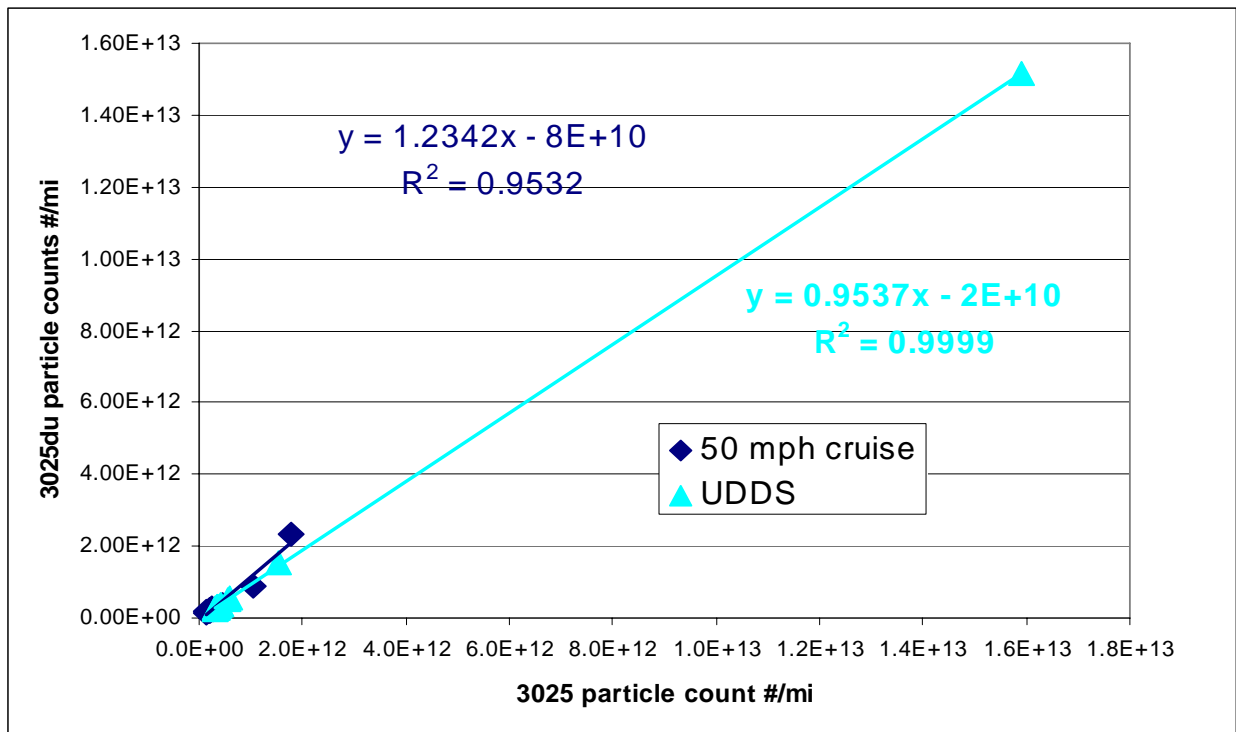


Figure 4-10. Correlation between two 3025A systems.

One of the proposed advantages of the particle number measurements is that they are more repeatable at low measurement levels. A comparison of the coefficients of variation (COVs) for the particle number measurement and the PM mass measurements is provided in Figure 4-11. Interestingly, these results show that the COV comparison between the PM mass and corresponding particle number measurements depends on how outliers are addressed. With no outliers removed, the COV for the PM mass is comparable to or slightly worse than that for the PMP-compliant 3790 CPC for the cruise cycle, but the COV for the PM mass is better than that for the 3790 CPC for the UDDS. When the PMP outliers are removed, the COV for the 3790 for the UDDS cycle improves to a slightly better but comparable value to the PM mass. The COVs for the 3025s are both higher than those for either the 3790 or the PM mass measurements with or without the PMP outlier tests. Only with the highest two outliers removed for the 3025s do their COV values improve to levels comparable to those for the PM mass and the 3790. It is important to note that the European PMP design is based on the 3790 size cut point, so the larger variability seen for the 3025As is not representative of the European protocols. It should also be noted that no tests were performed to examine the impacts of any artifacts in the PM mass measurements.

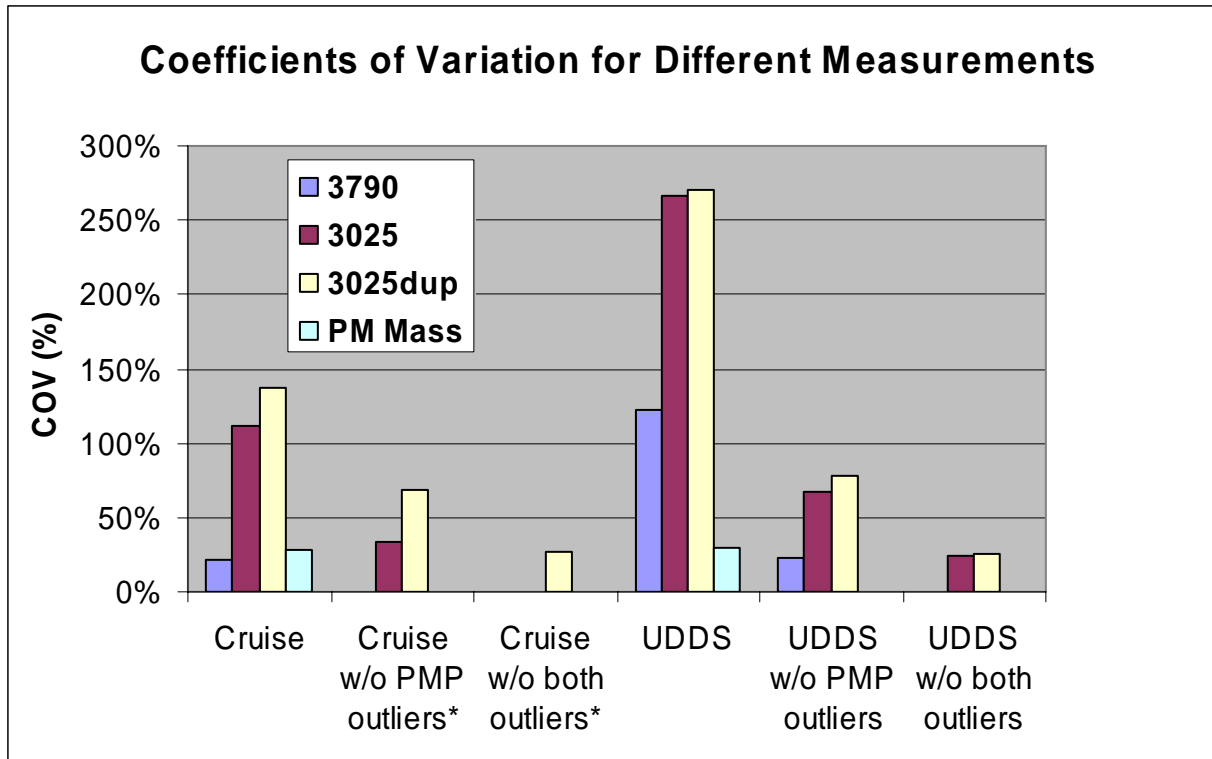


Figure 4-11. Coefficients of Variation for Various Instruments. * Note this outlier criteria is typically used in the PMP protocol for PM mass, not particle number.

4.4 Particle Size Distributions

Average size distributions for the UDDS and cruise cycles are presented in Figure 4-12 and Figure 4-13. These size distributions were collected by the DMS off the primary tunnel, and hence are not necessarily representative of the size distributions that would be measured below the PMP system. For both cycles, the size distributions show a significant contribution of smaller particles in the nucleation mode. These data show that a significant number of nucleation mode particles were emitted for each cycle. The nucleation mode was typically observed once a critical temperature was reached on the post emission control device. This temperature was 310°C for this DPF device configuration. It appears that the nucleation mode particles may be attributed to the conversion of SO₂ to SO₃, which is likely aided by a Pt catalytic coating on the DPF. This is consistent with previous studies that have shown an important contribution of sulfate to nucleation particles following an aftertreatment system [Kittelson et al., 2006; Grose et al., 2006]. This is also consistent with ion chromatography measurements of particle samples collected during cycles where nucleation was observed, which showed sulfate comprised a significant fraction of the PM mass. The size distributions (in dN/DlogDp) for individual tests for the UDDS and Cruise cycle are provided in Appendix G. The size distributions in terms of dV/DlogDp are also provided in Appendix G for the UDDS and Cruise cycles.

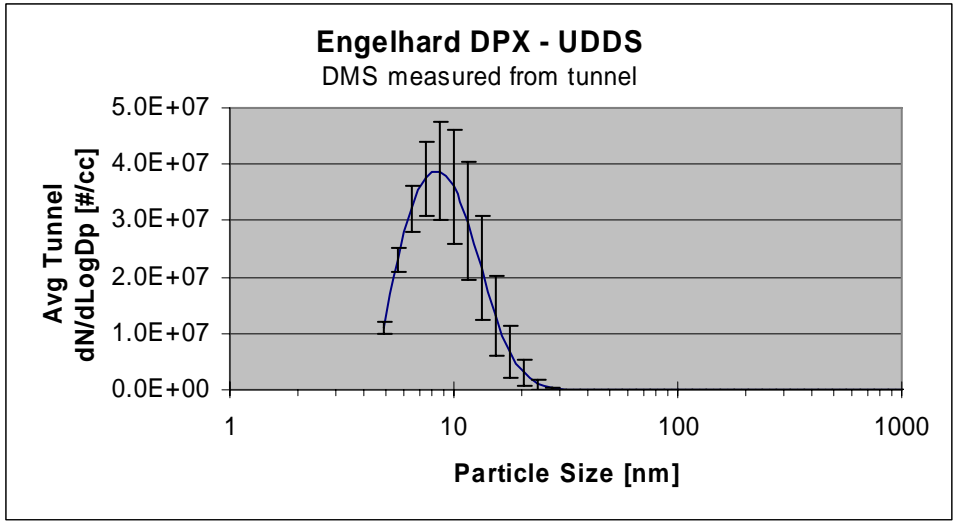


Figure 4-12. Average Size Distribution for UDDS tests (dN/dLogDp).

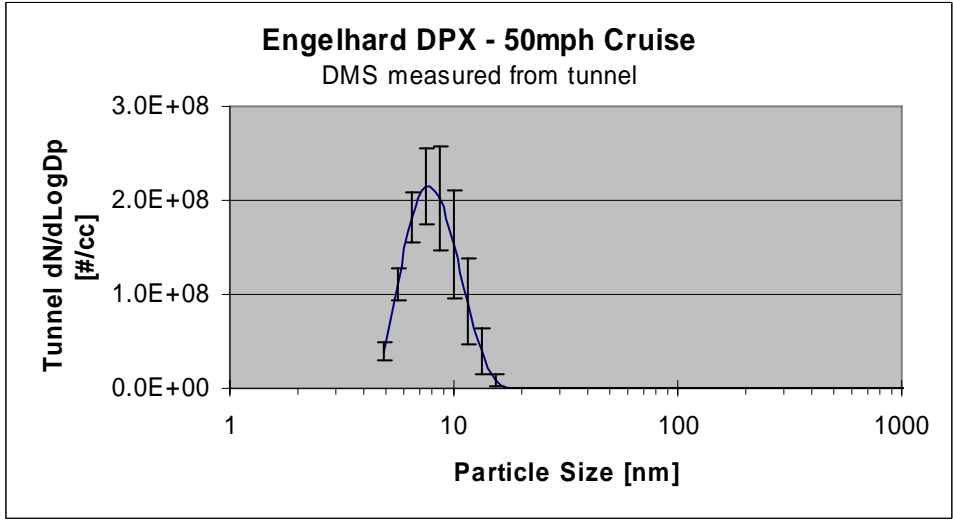


Figure 4-13. Average Size Distributions for Cruise Tests (dN/dLogDp).

4.5 Real Time CPC, EAD, EEPS, and PAS Results

In this section, real-time particle number results for the various test cycles are discussed. The results include the various particle number measurements made. Real-time data for the PAS is provided in Appendix G.

UDDS Results

Figure 4-14 shows the real-time results for the various CPCs and the EAD for a cycle with two back-to-back UDDS cycles. These measurements are representative of the general behavior seen during the course of the UDDS measurements. The EAD measurements were obtained from the main tunnel, while all the CPCs measured below the PMP system. The EAD clearly shows

elevated particle counts during the high speed driving portions of the cycle. Under these conditions, exhaust temperature levels are sufficiently high to produce nucleation particles, as discussed earlier. Figure 4-15 shows the real-time size distributions from the EEPS, which was directly connected to the primary tunnel, with the two corresponding peaks in the size range for nucleation particles. Note that while there are considerable nucleation particles in the primary tunnel during the peaks in the UDDS cycle, these particles were not seen by the 3790 CPC that is below the PMP system. The 3025As below the PMP did show some response to the nucleation particles, although it is dampened due to the VPR.

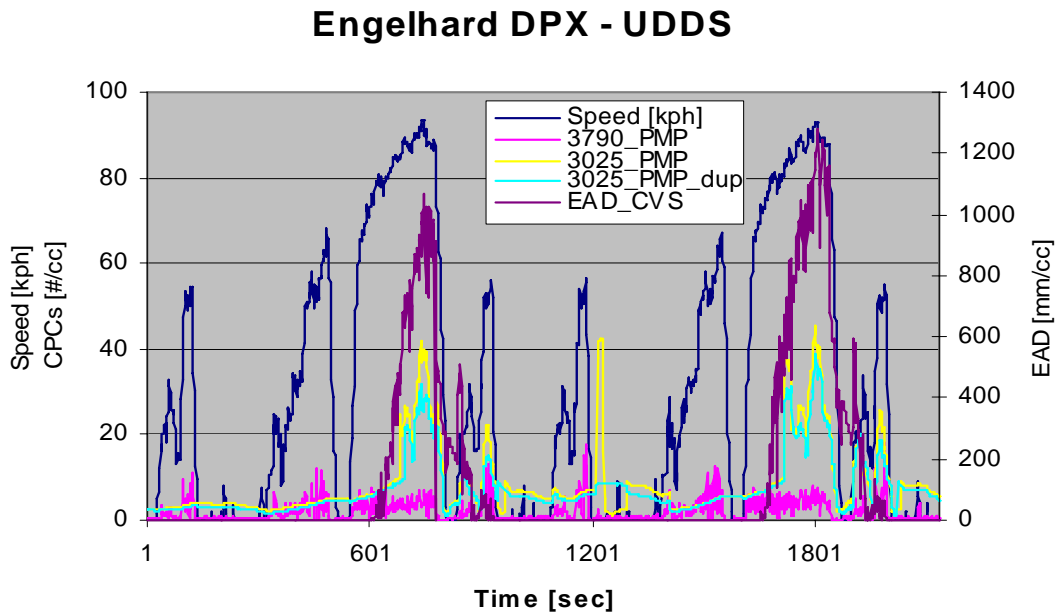


Figure 4-14. Real-Time Particle Number Counts for Various Instruments for the UDDS 2x

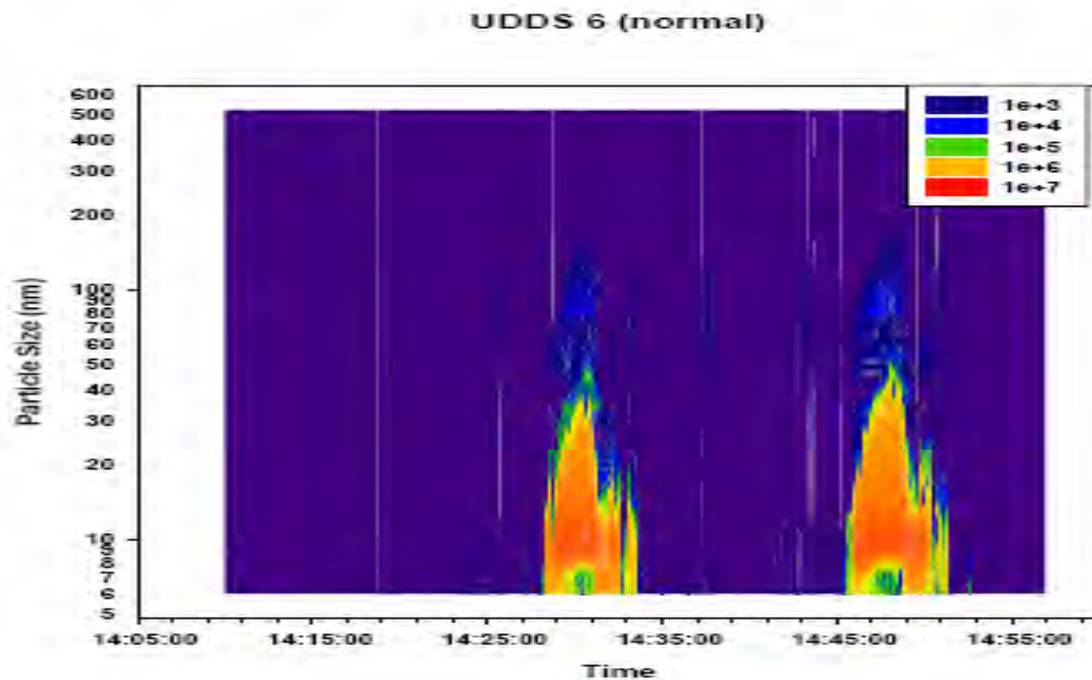


Figure 4-15. EEPS data for UDDS 2x Cycle

The CPC particle counters are all located below the PMP system, and hence are counting only particles that are considered to be solid within the PMP operational definition. The data show a dampened but still visible response from the two 3025As (measures particles > 3 nm) below the PMP during the nucleation events, but not from the 3790 (measures particles > 23 nm). This could be due to several factors. There could be some inefficiency in the PMP in eliminating more volatile or sulfate-derived nucleation particles in the smaller size ranges. Some breakthrough could be due to incomplete evaporation, the shrinking of larger more volatile particles, or evaporation and renucleation after the evaporation tube. Particles composed of sulfuric acid and hydrocarbons could also pyrolyze into solid-like particles as they pass through the PMP. Interestingly, the 3025As also show some particle counts for the final hill of the UDDS cycle around 900 and 1900 seconds in the plot that are not seen by the EAD, which has a size cut of 10 nm.

The 3790 has shorter internal averaging and the resolution of its response is considerably greater than the 3025As. This can be seen in some sections of the plot, where a small peak is observed in the 3790, while the event is broadened or washed out in the 3025As.

The real-time data also provide further detail on the nature of the outlier tests. For the UDDS, one test exhibited a significantly higher particle number count than the others, as shown in Figure 4-8. The real-time CPC results for this test are provided below in Figure 4-16, along with exhaust temperature. The results show the 3025A CPCs exhibited several spikes up to the 40,000 to 100,000 particles/cc level at conditions where the PMP was providing a 300 to 1 dilution from the primary tunnel. This was well above the PMP recommended sampling range. The 3790 CPC

also registered high particle count rates for one of these events. As the events on the 3025A CPC were observed for both CPCs, they appear to represent real events as opposed to issues with an instrument or sampling system. Further investigation is needed to better understand the nature of these events. It should be noted that unusually large spikes in total particle counts have been observed by some other researchers downstream of an aftertreatment system (Kittelson, 2008).

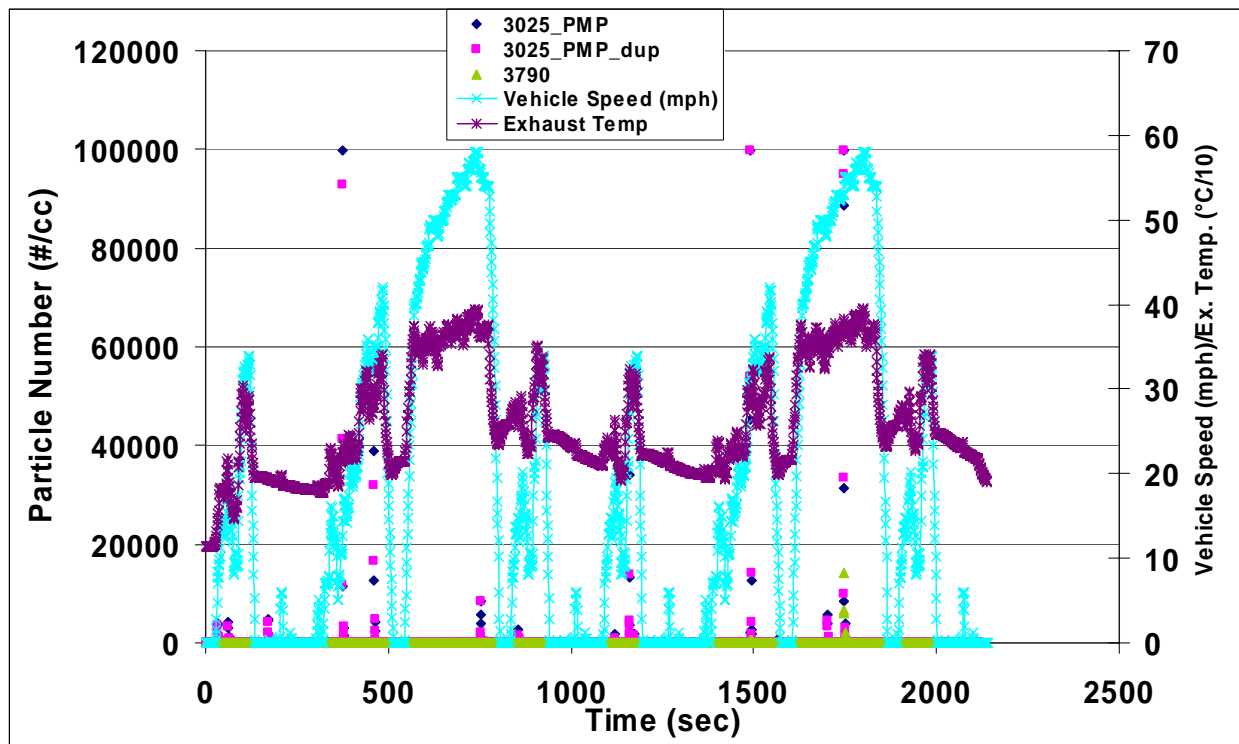


Figure 4-16. Real-Time CPC data for outlier UDDS conducted on 6/1/07 Run 1

Cruise

The real-time particle counts for the cruise cycle show considerably less transient behavior, as would be expected. Figure 4-17 and Figure 4-18, respectively, show a series of CPC 3025A and CPC 3790 data collected below the PMP. The corresponding EAD signal, collected directly from the primary tunnel, is also shown in Figure 4-17. The EAD signal shows a relatively steady-state signal, with a series of oscillations. The oscillations in the graph correlate with the engine fan turning on and off, thereby increasing and decreasing the engine load. The EAD signal shows the nucleation particles form and remain relatively steady once a high enough exhaust temperature is reached and maintained. The data for the CPC 3025s and the 3790 show a generally flat line for particle counts, with a few random, nominal spikes in the count data. This indicates that the nucleation particles are largely eliminated as they travel through the PMP system.

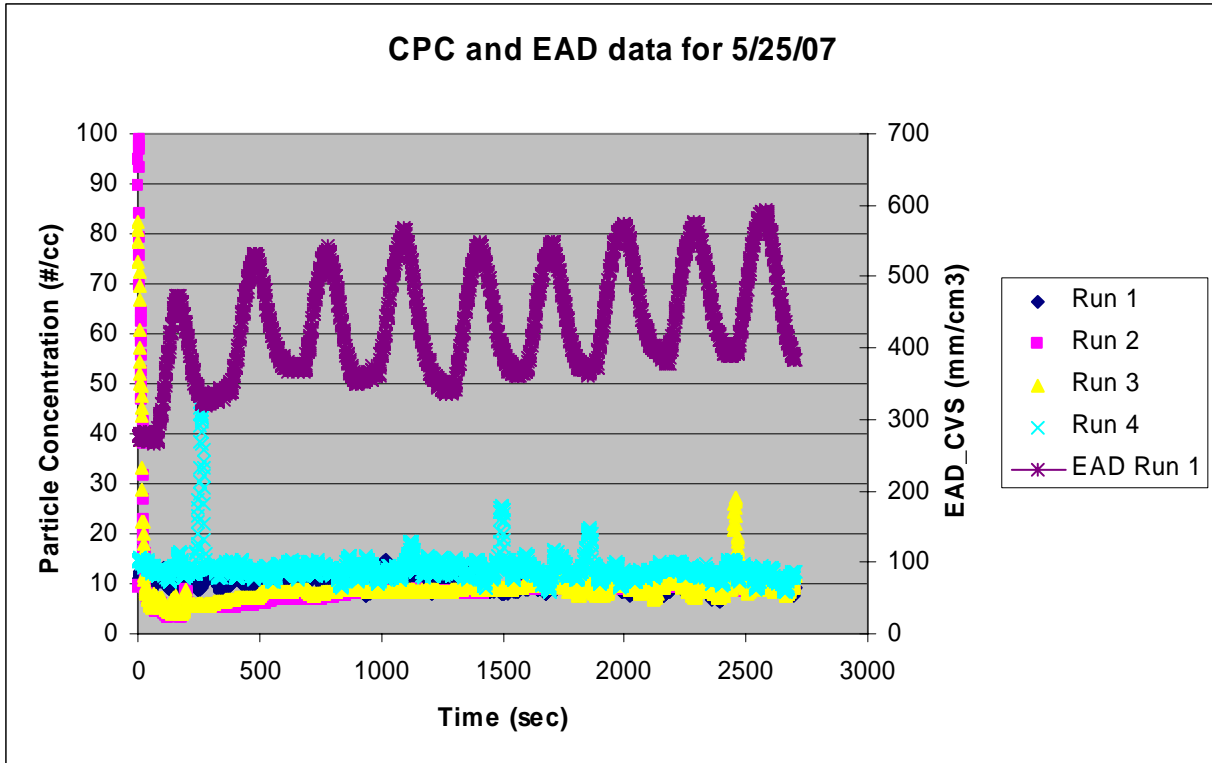


Figure 4-17. CPC 3025A data runs from 5/25/07 over the 50 mph cruise.

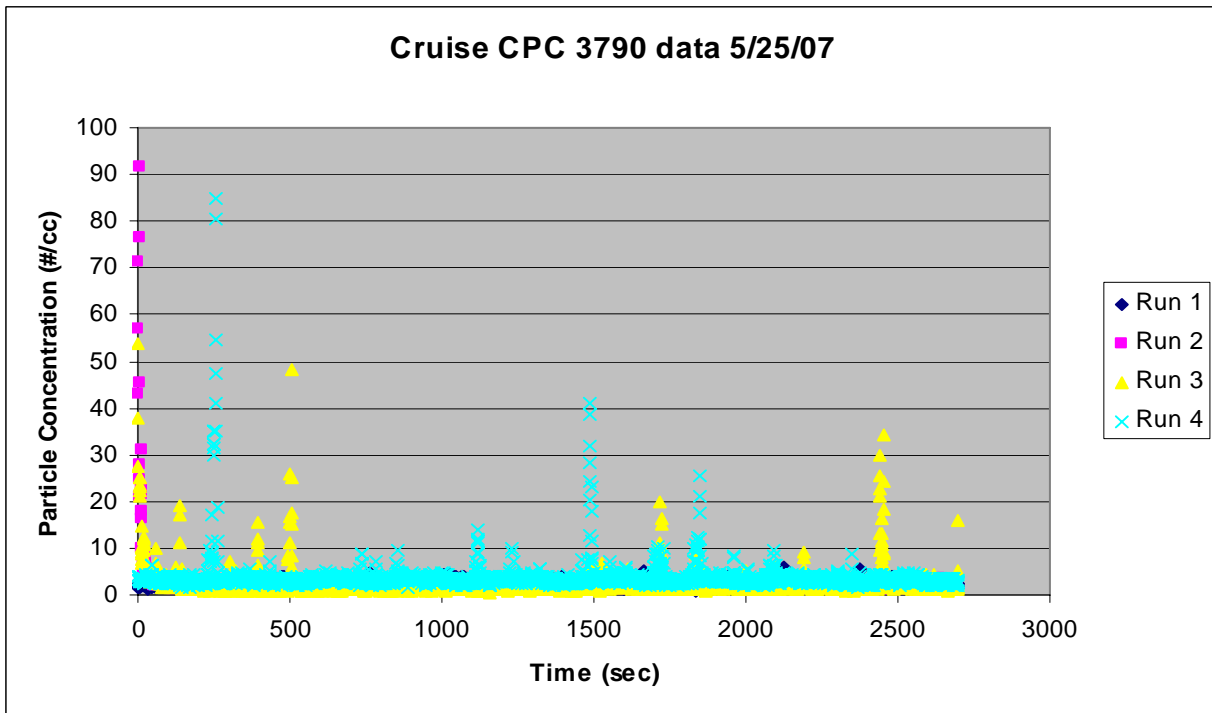


Figure 4-18. CPC 3790 data runs from 5/25/07 over the 50 cruise.

The formation of the nucleation particles can be more readily seen in Figure 4-19, which shows EEPS data during the warm-up and an actual 50 mph cruise. The data show there is little particle formation as the engine warms up until it reaches a certain exhaust temperature level. At that point, nucleation begins and continues as long as the elevated temperatures are maintained. Note the EEPS data also show the oscillation due to the engine fan.

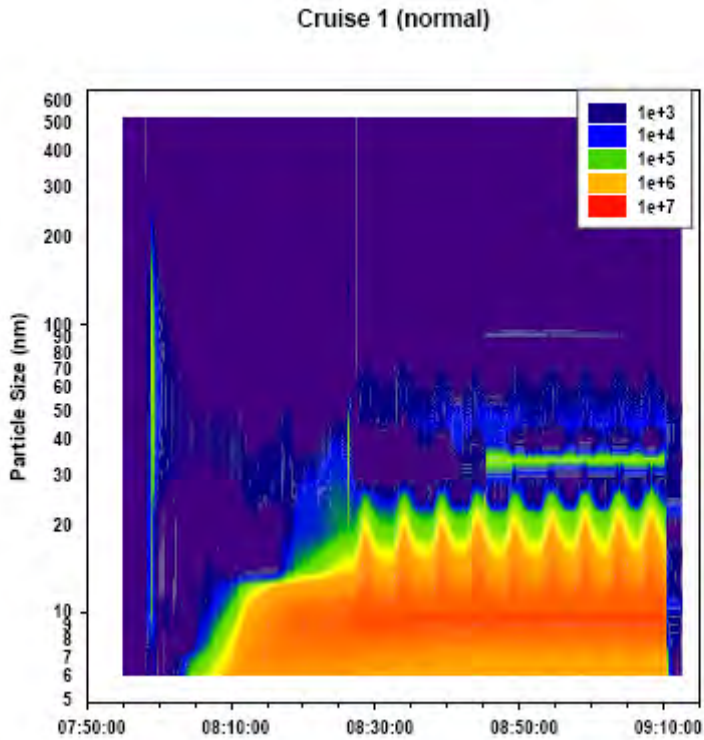


Figure 4-19. EEPS data for a 50 mph Cruise with the Corresponding Warm-up

Two cruise cycles showed particle counts that were well above the typical test values. The CPC 3025A data for each of these tests is presented in Figure 4-20. For the highest particle count cruise test (Run 3 5/30/07), the CPC both show a pattern of consistently elevated particle counts that show a steady decline over the course of the test cycle. These data also show an oscillation that is consistent with the engine fan turning on and off. This oscillation is also seen in the EAD data. The cruise with the second highest particle counts (Run 5 5/30/07), showed a single spike to a count level of nearly 40,000 particles/cc with some other smaller spikes also seen in the cycle. In both cases, the behavior is observed for both CPCs, indicating the data represent a real event. Further investigation is needed to better understand the nature of these events.

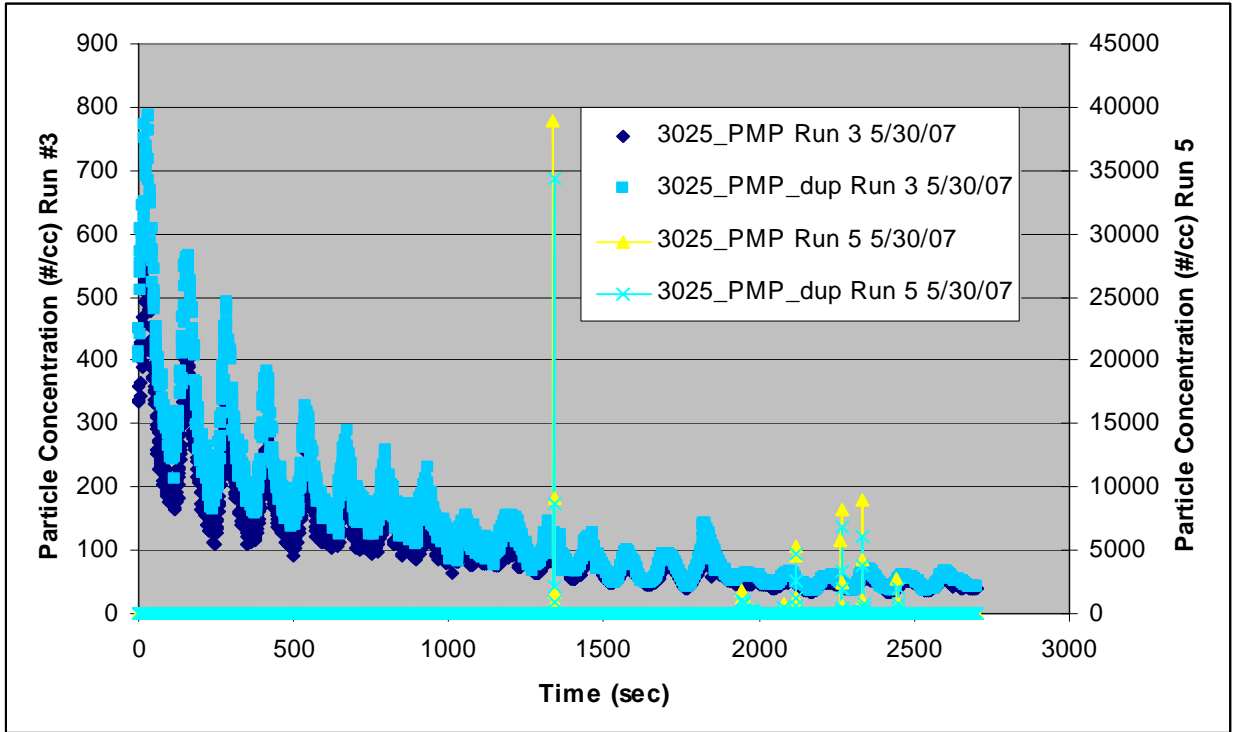


Figure 4-20. CPC 3025A data for two outlier test runs over the 50 mph cruise.

Idle

For the idle testing, the PMP dilution system was not available, so all the real-time instruments sampled directly from the tunnel. Real-time data from the CPC 3022 and the EAD are shown in Figure 4-21 for an entire day of idle operation. These data show that the particle concentration levels are essentially flat with the CPC 3022 showing some small spikes throughout the course of the sampling period. The peak in particle concentration for the EAD at the very start of sampling can be attributed to the engine being turned on and initial start up emissions.

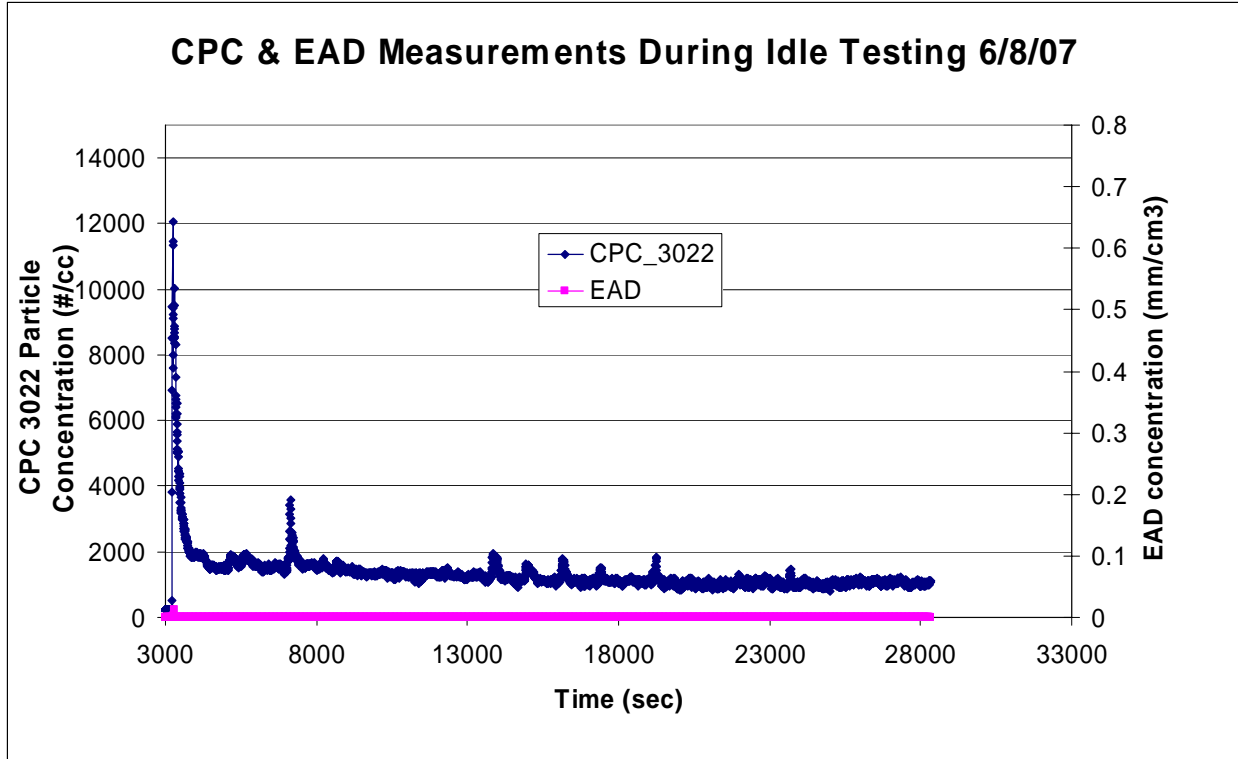


Figure 4-21. CPC and EAD measurements during Idle Testing

Temperature Experiment with the PMP System

For one cruise test run at 50 mph, the parameters for the PMP system were varied to provide a greater understanding of the impacts of the system on particle counts. Specifically, the ET on the PMP system was turned off after the particle number concentration had reached a semi-steady state condition. Figure 4-22 shows real-time data for a number of different particle counting instruments during this run. The EAD data show the onset and continuation of nucleation once the critical exhaust temperature is achieved, as shown in Figure 4-19, and the oscillations due to the engine fan turning on and off. The EAD measurements were made in the primary tunnel. Measuring below the PMP, the EEPS and the two 3025A's measured a significant increase in particle counts once the ET sample temperature decreased to 160°C. The two CPCs quickly reach their maximum concentration of 10^5 , while the EEPS is measuring $4-8 \times 10^5$. This discrepancy is attributed to the previous observed trend of lower particle emissions measured with the EEPS during cruise cycles rather than the presence of a lot of particles in the 3 – 5.6 nm range [Herner et al., 2007]. The 3790, however, which measures only particles greater than 23 nm, is barely affected by turning off the ET. This is consistent with some of the findings of the European PMP program, which concluded that hot dilution alone, i.e., without the ET, is sufficient to eliminate most volatiles in the >23 nm range from light-duty diesel vehicles [Andersson, 2008].

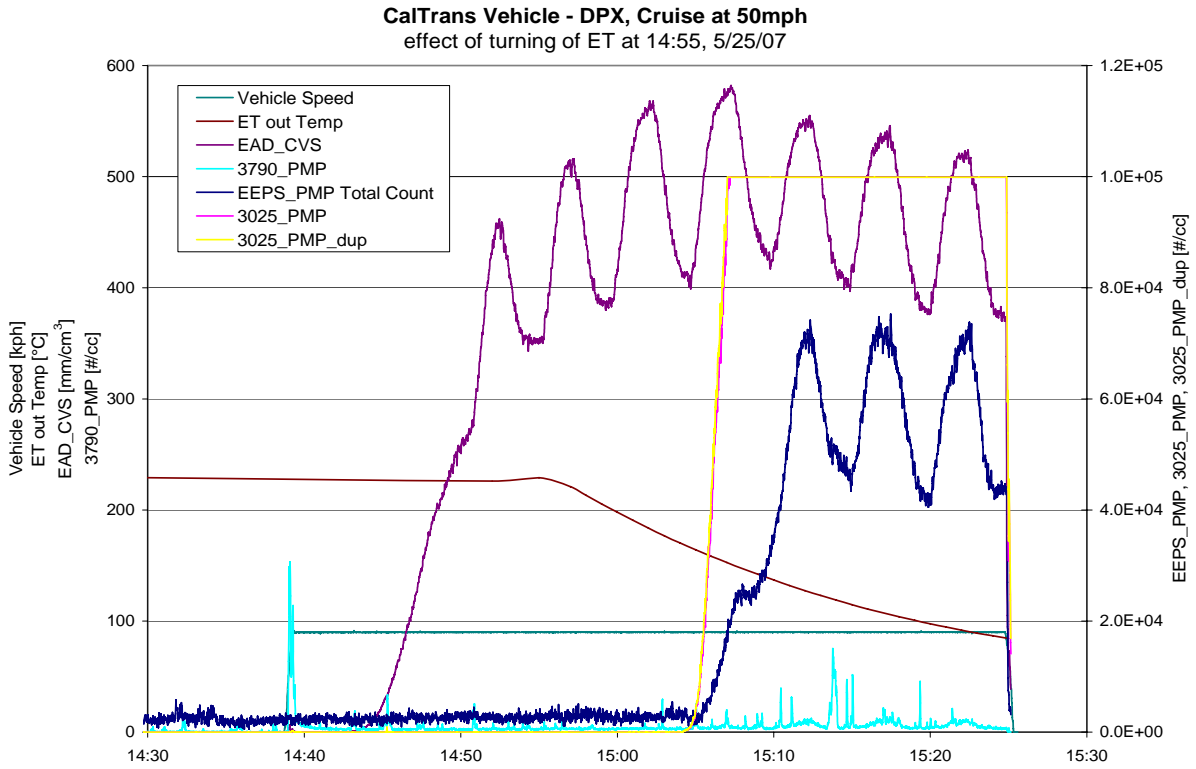


Figure 4-22. Real-Time Particle Counts for Various Instruments for a 50 mph Cruise.

5.0 On-Road Emissions Results

5.1 Gas-Phase Emissions

The gas-phase emissions are provided for NO_x, NMHC, and CO in Figure 5-1 through Figure 5-3 below for each of the test cycles in a grams per mile (g/mi). The gas-phase emissions are provided in a Table form in Appendix H. Appendix H also provides graphs of the results for gas-phase emissions on a g/bhp-hr basis. Note that for each test cycle, the results are also separated based on the direction or route that was taken to complete the cycle, as discussed above in the experiment section. It was decided to break the cycles down based on direction because analysis showed that cycles run in opposite/different directions were not as repeatable as we have observed previously for standard cycles. In order to study the true measurement error/repeatability without the complications of road conditions, it was decided that the cycles should be separated based on the specific route/direction. A more complete discussion of the experimental variability due to directionality and why this separation was chosen is provided in Appendix I.

For NO_x, the integrated emissions varied from approximately 13 g/mi to near 52 g/mi (5 g/bhp-hr to 23 g/bhp-hr) depending on the test cycle (see Figure 5-1). These values are comparable to those found in a previous study of this truck without a DPF over other on-road cycles [Cocker et al., 2004a]. The NO_x emissions are highest on a g/mi and g/bhp-hr basis for the creep cycle since it is a very low speed, low power, transient cycle that covers only a short distance. The differences between the other cycles are smaller, with slightly lower NO_x emissions on a per mile basis found for the cruise cycle, which is less transient and run at higher speeds. The NO_x emissions for the creep cycle were more comparable to those of the other cycles when they were normalized by fuel consumption. The fuel-specific NO_x emissions results, as well as the NO_x emissions normal by work, are provided in Appendix H.

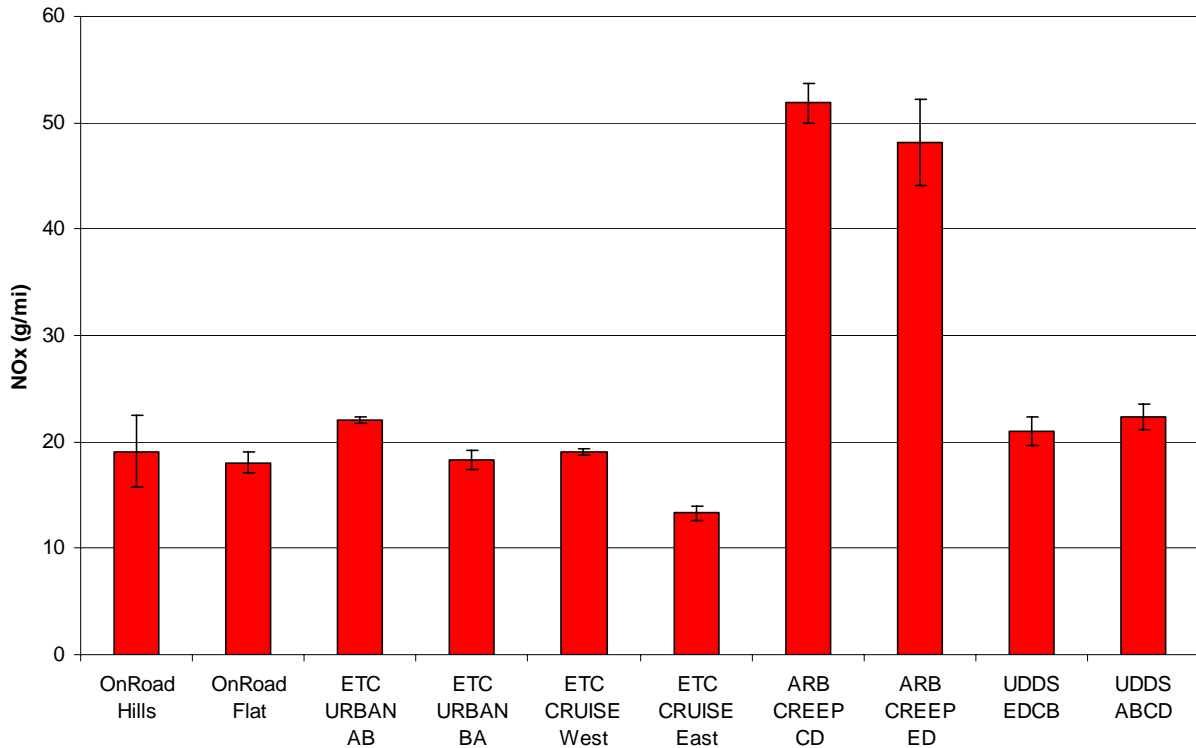


Figure 5-1. NO_x Emissions Results on a g/mi basis.

NMHC and CO were both close to the detection limits of the MEL laboratory configuration. It is important to understand the measurement levels in order to evaluate the overall emissions results for these pollutants. Comparisons of concentration measurements for NMHC, CH₄, and CO for different test cycles and for the ambient background are provided in Table 3-1.

Table 5-1. THC, CH₄, and CO Concentration Measurements.

Cycle	THC ppm			CH ₄ ppm			CO ppm		
	ave	stdev ¹	amb	ave	stdev ¹	amb	ave	stdev ¹	amb
OnRoad Varies	3.9	1.3	2.6	1.8	0.3	2.1	2.2	2.8	0.5
OnRoad ToThermal	4.1	1.6	2.6	2.1	0.3	2.1	2.4	3.3	0.5
ETC URBAN	2.7	0.2	2.6	2.1	0.2	2.1	0.7	0.8	0.5
ETC CRUISE	2.5	0.1	2.6	2.0	0.1	2.1	1.8	0.8	0.5
ARB CREEP	4.6	1.1	2.6	2.2	0.1	2.1	0.9	3.1	0.5
UDDS	3.1	1.8	2.6	2.1	0.2	2.1	1.2	4.0	0.5

¹ – this standard deviation is the average standard deviation with-in the test cycle. This standard deviation indicates the measured dynamic range.

Since NMHC levels were very close to ambient levels/detection levels, the NMHC and CO figures are scaled based on the MEL lower detection limits. The magnitude of the scale is approximately ten times the lower detection limit for NMHC and CO measurement at the 99% confidence level. The NMHC 99% confidence detection limits range from ~0.3 g/mi for the creep to ~0.01 g/mi for the cruise. The NMHC measurement uncertainty takes into account the subtraction of THC and CH₄ measurements with a correction for background dilution air. The CO 99% confidence detection limits range from 0.4 g/mi for the creep to 0.02 g/mi for the cruise. The measurement uncertainty takes into account the calibration range of the CO measurements

and the correction for background dilution air. These scales used in the figures provide a context for understanding the measurement levels in comparison to MEL detection capabilities.

NMHC emissions are presented on a g/mi basis in Figure 5-2. Ambient THC and CH₄ for most cycles are within 1 ppm C₁ of the sample measurement making background correction significant, as shown in Table 3-1. Thus, the NMHC measurement is at the detection limit of the MEL operation, with the exception of some of the traffic flow measurements and the creep cycle, where a slightly larger and more readily measurable THC concentration was found (~5 ppm C₁). The high concentration and large deviation on the creep NMHC is a result of THC measurements being higher and spiking on a subset of the creep cycles compared to others. This can be seen in the real-time data provided in Appendix H.

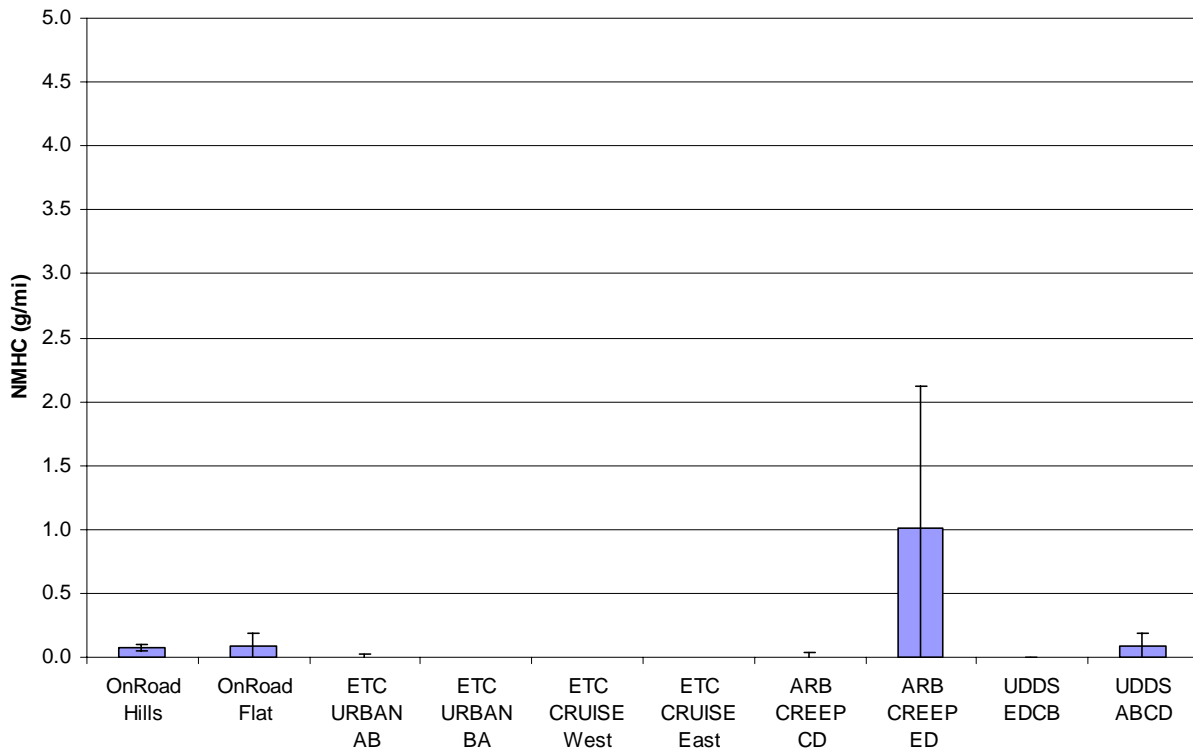


Figure 5-2. NMHC Emissions Results on a g/mi basis

CO emissions are shown on a g/mi basis in Figure 5-3. Typical ambient CO concentrations are less than 0.5 ppm, which is only 2 ppm less than most of the exhaust measurements, as shown in Table 3-1. Again, the reason for the higher deviation is due a higher CO measurement for some of the creep cycles compared to the others and not due to background correction, as shown in the real-time data. Although some cycle trends may exist for CO, the measurement variability and the low measurement levels make it difficult to draw conclusions in these trends for this data set. The real-time data results are provided in Appendix H.

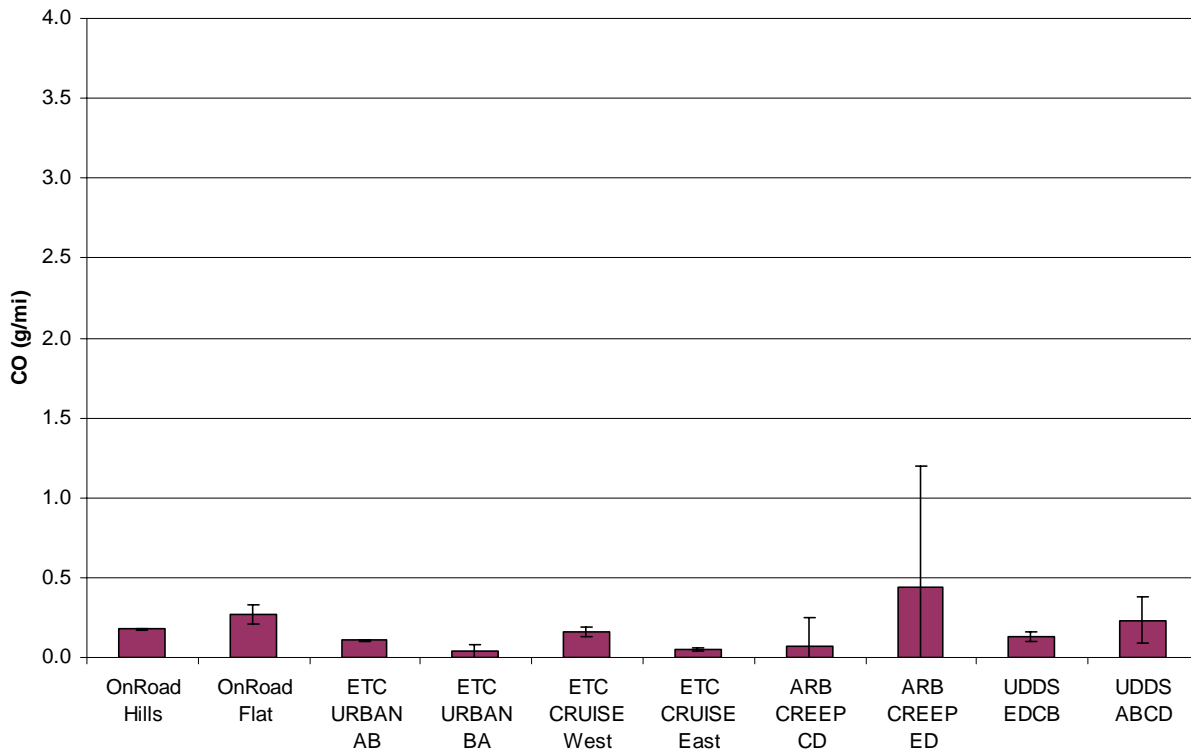


Figure 5-3. CO Emissions Results on a g/mi basis

5.2 PM Mass Results

Figure 5-4 through Figure 5-6 show the PM mass emissions and related measurements for the driving cycles and the flow-of-traffic tests for gravimetric measurements and the TSI DustTrak and Dekati DMM PM systems.

Gravimetric PM

The integrated gravimetric PM emissions for the on-road testing are presented in Figure 5-4. The gravimetric results are presented for all tests within a cycle without direction grouping, since the measurements are all near the detection limits. Average PM emissions for the standard test cycles varied from a negative value for the ETC Urban cycle to 9 mg/mi (4 mg/bhp-hr) for the creep cycle. PM emissions were slightly over 26 mg/mi (6 mg/bhp-hr) for the flow-of-traffic test. It is important to note that for nearly all of the cycles, the PM masses were near the measurable limit, as discussed below. This is especially true for the creep cycle, which is very short in duration. The difficulty in making mass measurements at these levels is reflected in the error bars for the creep and other cycles. Note that the on-road flow of traffic measurement has no error bar since only a single test was conducted at that condition.

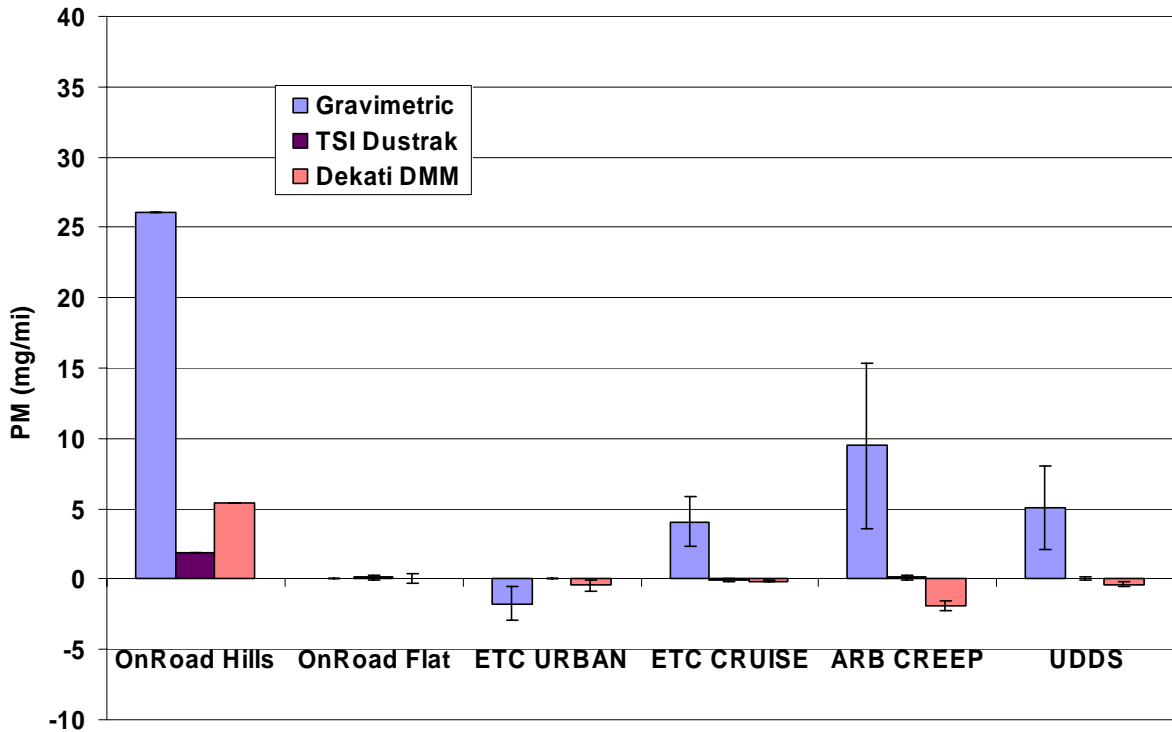


Figure 5-4. Particulate matter results on a g/mi basis

The PM emissions rates on a mg/mi and a g/bhp-hr basis are comparable to those seen in previous studies and to the 2007 certification levels. The 2007 PM emission certification level is 10 mg/bhp-hr based on a 20 minute FTP engine dynamometer emission test. Other studies have shown that post trap gravimetric emission levels are in the range of 10% of the standard or around 1-2 mg/bhp-hr [Khalek, 2005, 2006, 2007; Bosteels et al. 2007]. Even though the gravimetric PM measurements are not statistically significant, all measurements except for the creep cycle are around 1-2 mg/bhp-hr, in agreement with the previous studies [Khalek, 2005, 2006, 2007; Bosteels et al. 2007]. More recent work with integrated OEM production trap equipped engines have showed post trap PM emission levels of around 0.5mg/bhp-hr [unpublished]. The PM emission rates on a mg/mi basis are also similar to those seen in other studies [Herner et al. 2007; Kimura et al. 2004].

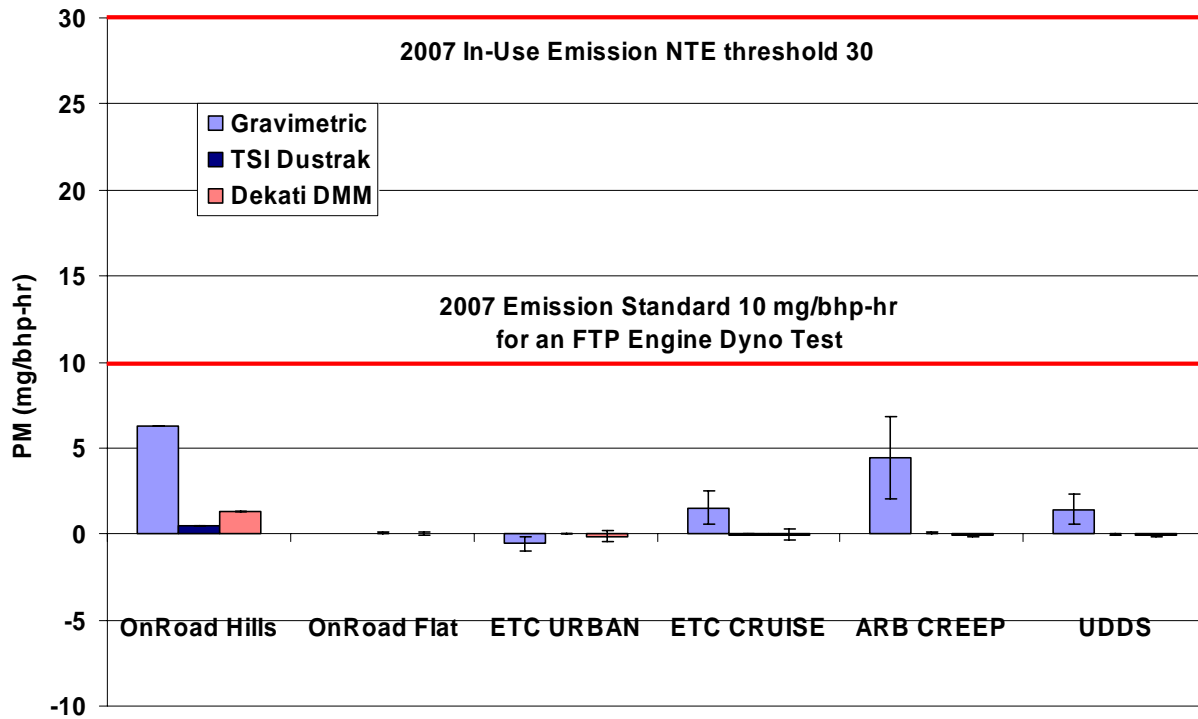


Figure 5-5. Particulate matter results on a mg/bhp-hr basis

The gravimetric PM mass measurements are close if not at the detection limits of the MEL PM measurement system. Figure 5-6 shows the filter weights sampled for all the tests. Typical average filter weights for each cycle ranged from slightly negative on the ETC Urban cycle to ~7 μg on the ETC cruise cycle. As a comparison, the filter weight on the 1 hr on-road cycle was 221 μg . The higher filter mass for the on-road test was due to a longer sample and there were nucleation events that caused that filter weight to be around 221 μg , as discussed below. Typical tunnel blanks are on the order of 5 μg over a 30 minute sample or equivalent to 2 μg and 4 μg , respectively, over cycle times for the ETC cycle (10 minutes) and the UDDS cycle (17 minutes). Other types of blanks were also collected including trip blanks, static blanks, and dynamic blanks. The mass for these other types of blanks were typically within the repeatability limits for the reference filter, or approximately 2-3 μg . The overall uncertainty of the filter weights is approximately 2.5 μg at one standard deviation or 7.5 μg at three standard deviations. All of the measurements for this program are either at or below this level, with the exception of the one on-road test.

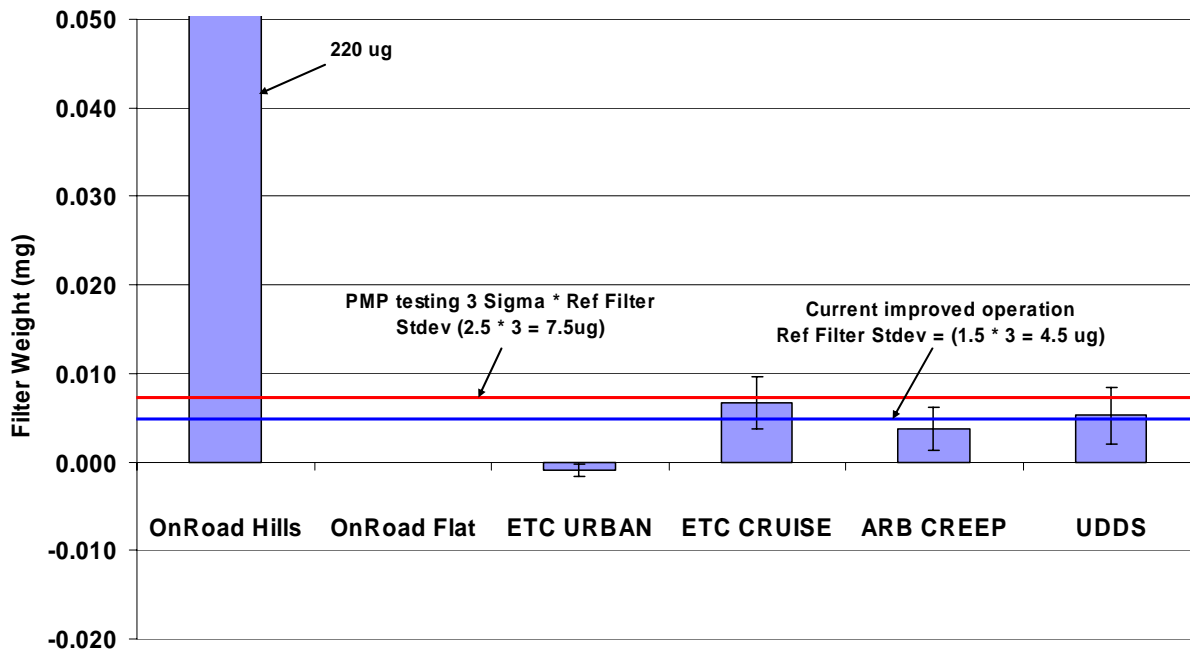


Figure 5-6. Particulate matter results on a filter weight basis (mg/filter).

CE-CERT is currently making improvements to our PM sampling and analysis system, such as increasing sample filter flows, lowering dilution (minimum CFR40.1060 level of DR=6), and improving reference filter repeatability to around 1 μg . We estimate that CE-CERT's future three standard deviation detection limit will be around 3-4 μg at best. This is a significant improvement, but still a long way away from accurate post-DPF measurement evaluation for the driving cycles performed.

Real-Time PM Mass Emissions – DustTrak

The real time PM emission measurements for both the DMM and DustTrak were closer to 0 mg/bhp-hr emissions levels than the filter weights, and sometimes were negative. This could be due in part to artifacts that might be observed on the filters but not with the real-time mass instruments. It is hard to draw a comparison from the real-time DustTrak to gravimetric filter methods since the gravimetric filter method was not statistically significant for many of the filter measurements. The best comparison can be seen by looking at the on-road test where the DustTrak measured only 1.8 mg/mi (0.44 mg/bhp-hr) and the gravimetric filter method gave ~26 mg/mi (6 mg/bhp-hr) with a filter weight of greater than 200 μg . The DustTrak showed a factor of 14 times less mass on a mg/mi and mg/bhp-hr basis for this test.

The best explanation as to why the DustTrak is an order of magnitude lower than the gravimetric PM mass compared to engine out levels is due to a failure of the DustTrak to scatter light efficiently at the smaller peak size distribution produced by post trap emissions. The DustTrak principal of operation is to measure light scattered by particles. The manufacture claims that light is scattered from 100 nm and above, although they do not document the DustTrak minimum light

scattering capabilities. Engine out PM peak mass is typically around 100 nm [Shah and Cocker, 2005] thus making the DustTrak a potentially reasonable approach to measure engine out PM emissions. Numerous tests performed on this same truck without a DPF show that the DustTrak typically agrees with gravimetric PM to within 10-20%, if a correction factor to normalize to the filters is used [Johnson et al., unpublished]. For this study, much of the PM mass on the on-road testing is due to nucleation, as discussed below, hence the DustTrak measurement principal could be a limitation in this size range. Overall, it appears the DustTrak light scattering measurement principal is not well suited for trap equipped engines.

Real-Time PM Mass Emissions – Dekati Mass Monitor

The real-time DMM values are also closer to 0 mg/bhp-hr than gravimetric methods, with many values below zero. This could be due, in part, to artifacts measured by the filters. During the on-road flow-of-traffic driving, the DMM did see a fair amount of mass in the primary tunnel that tracked engine load and operation events. The DMM sampled only 5 mg/mi (1.5 mg/bhp-hr), however, where the gravimetric method measured over 26 mg/mi (6 mg/bhp-hr). The DMM PM mass sampled is about 5 times less compared to the filter based method on a mg/mi basis and on a work specific basis. In order to understand the DMM mass capabilities, the concentration measurements need to be examined. For these measurements, the DMM analog out concentrations were used. The DMM analog out concentrations were generally around $\pm 5 \mu\text{g}/\text{m}^3$ for the prescribed driving cycles and around $20 \mu\text{g}/\text{m}^3$ for the on-road tests. For concentrations lower than $50 \mu\text{g}/\text{m}^3$, the digital signal recorded by the DMM should be used in order to prevent analog conversion biases causing measurement loss, as discussed in Appendix D. There are also smaller adjustments that could be made related to flow compensation, although these corrections are small compared to the scales for this data (10-20%).

5.3 Particle Size Distributions

Size is an important physical characteristic of particles and is an important factor in understanding the results of this study. Average size distributions for the different test cycles were developed for each of the test cycles based on f-SMPS measurements from the primary tunnel. For each individual test, the real-time f-SMPS data were averaged over the entire cycle for each size range. The individual test results for a given cycle were then averaged to determine the average size distribution for the cycle, with the error for each size range given as the standard deviation of the individual test results for that specific size range.

The average size distributions for the ETC cruise, ETC Urban, and the CARB creep cycles are shown in Figure 5-7, Figure 5-8, and Figure 5-9, respectively. The cruise cycle shows a size distribution with a mean diameter of approximately 23 nm, while the size distributions for the urban and creep cycles show a mean diameter closer to 100 nm. This indicates that for the cruise cycle, there is a significant contribution from nucleation particles in the lower size ranges, whereas the urban and creep cycles produce primarily accumulation mode particles. The particle counts drop sharply near 200 nm because this is near the end of the instrument size range, rather than an actual sharp decline. The particle count rates for the cruise cycle are also much higher than those of either the urban or creep cycles. The second peak for either cruise size distribution is very similar to the creep and urban size distribution magnitude and mean diameter. Additional

real-time, f-SMPS data results are provided below, which show the occurrence of nucleation particles in real-time during the cruise as well as the UDDS cycle, which is not included in this section.

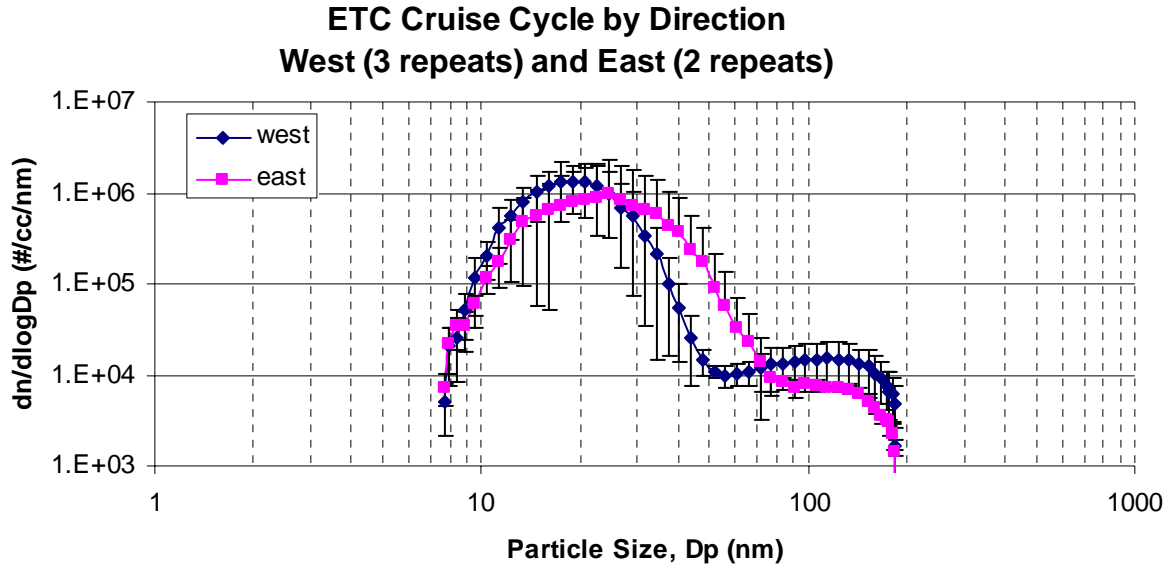


Figure 5-7. Average Size Distribution for ETC Cruise Cycle using the f-SMPS.

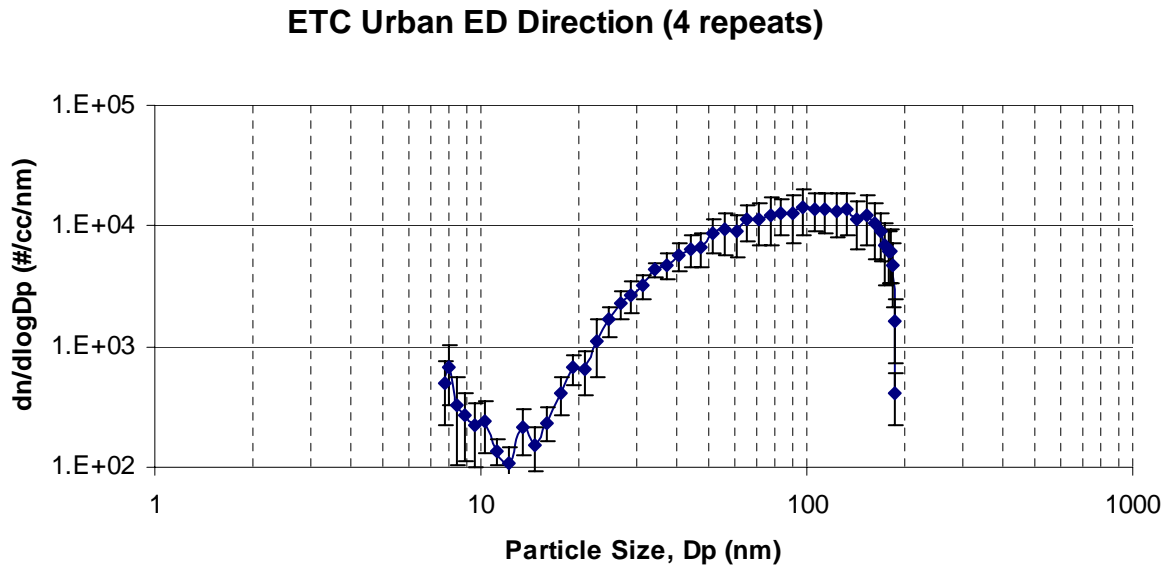


Figure 5-8. Average Size Distribution for ETC Urban Cycle using the f-SMPS.

CARB Creep BA Direction (4 repeats)

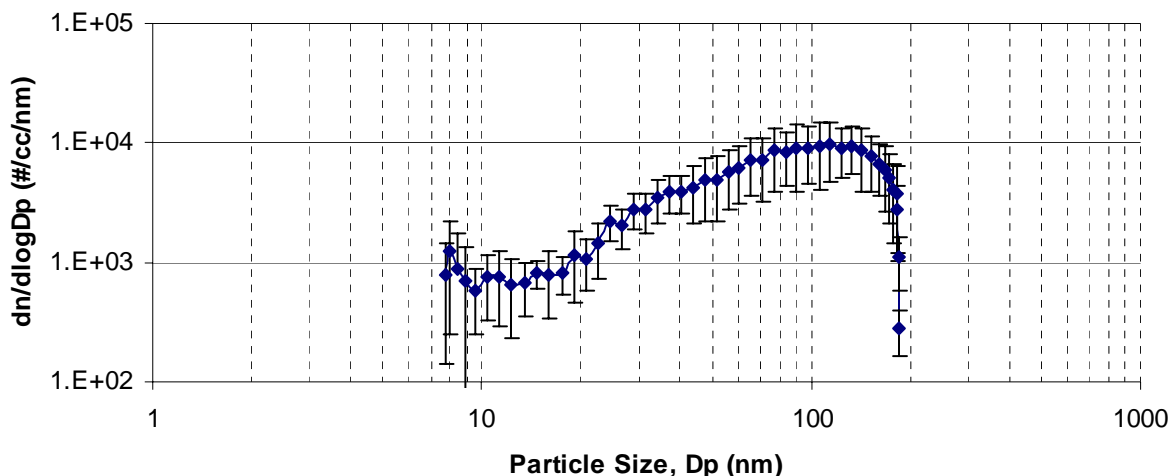


Figure 5-9. Average Size Distribution for CARB Creep Cycle using the f-SMPS.

5.4 PMP and other Particle Number Results

The particle number concentrations for the different cycles are shown in Figure 5-10 grouped by direction and Figure 5-11 with no direction grouping. Both Figures are in log scale. Particle number concentration results are also provided in Appendix J. The CPCs with the higher size cuts, the 3760A and the 3790, are shown separately in Figure 5-12 for cycles grouped by direction and Figure 5-13 without directional grouping. The CPCs with the lower size cuts, the 3022 and the 3025As, are shown separately in Figure 5-14 for cycles grouped by direction and Figure 5-15 without directional grouping. The results for particle number are presented both with and without directional grouping since the PMP specifications call for a minimum number of tests of 5. Although the directional grouped tests provide more consistent test-to-test variability, the number of tests in each group is typical below 5, as seen in Table 5-2. As such, both cases are presented. Additionally, OnRoad or flow-of-traffic tests were conducted over two different conditions. The OnRoad Hills data were taken from test runs where the truck was driven on a steep climb on the road out of Indio toward Blythe, CA and on the trips to and from Indio to Riverside, CA that featured a combination of hills and downhill driving. The OnRoad Flat driving conditions were obtained during trips between Indio and Thermal, CA. Figure 5-12 through Figure 5-15 are all shown in arithmetic scales to allow closer comparisons between the CPCs with similar cut points without the complications of scaling between the instruments. The results represent the average of all test runs for the specified test cycle with the error bars representing one standard deviation.

Cycle	OnRoad Hills	OnRoad Flat	ETC Urban AB	ETC Urban BA	ETC Cruise west	ETC Cruise east	ARB Creep CD	ARB Creep ED	UDDS ABCD	UDDS EDCB
count	3	4	2	5	4	3	2	5	4	4

Table 5-2. Number of Tests for Each Cycle Grouped by Direction

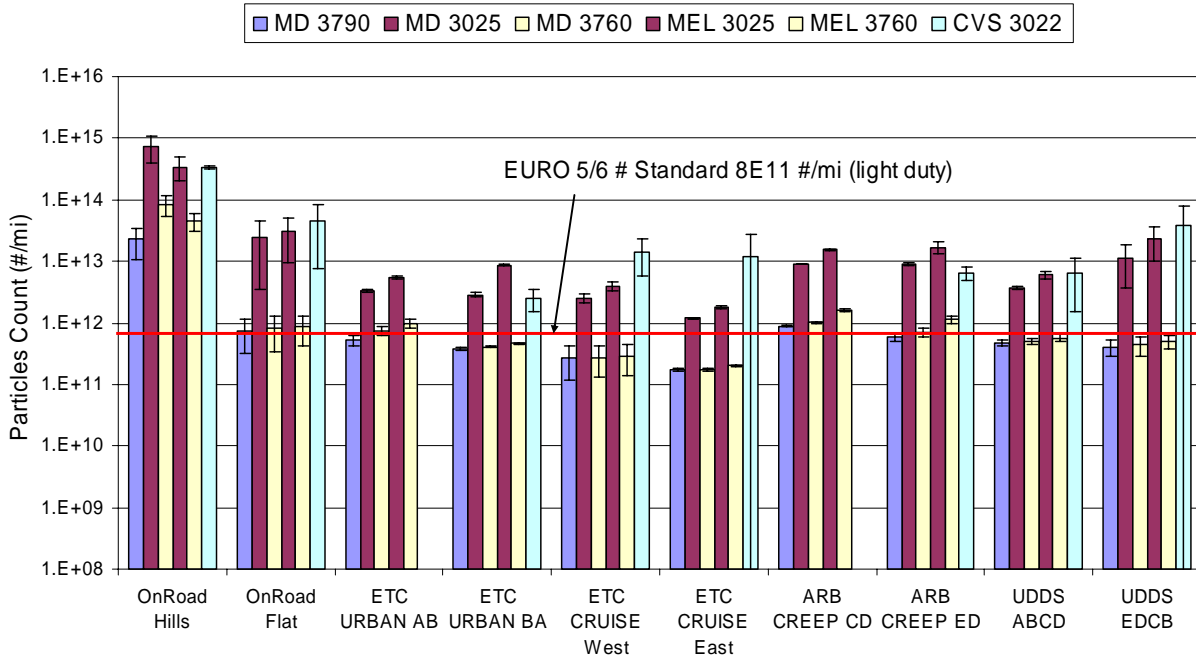


Figure 5-10. Particle number rate (#/mi) for all CPC's on driving cycles grouped by direction and flow-of-traffic tests (Note log scale y-axis)

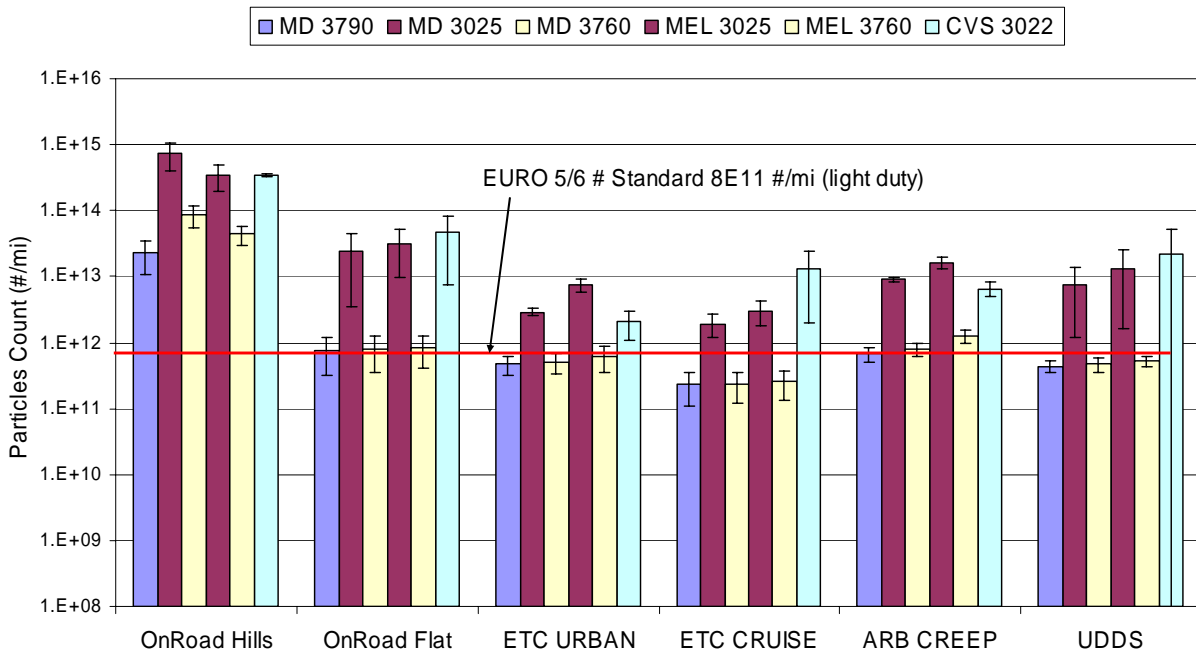


Figure 5-11. Particle number rate (#/mi) on driving cycles not grouped by direction and flow-of-traffic tests (Note log scale y-axis)

The results in Figure 5-10 and Figure 5-11 show that the particle number measurements depend on the test cycle, test route and the size cut for the CPC. The particle number measurements for the 3760A and the 3790 are considerably lower than those for the 3022 or the 3025A. This is

consistent with the fact that lower cut CPCs should see higher counts compared to higher cut CPCs. The 3790 (>23 nm) and the 3760A (>11 nm) CPCs have higher cut points compared to the 3022 (>7 nm) or 3025A (>3 nm) CPCs. This is consistent with the laboratory results, showing that a significant fraction of the particles are not being counted using the current PMP size cut of 23 nm. The 3022 is also connected directly to the primary tunnel, and hence sees more volatile particles that will not be seen by CPCs below the PMP systems.

The CPCs with the higher cut points are presented in Figure 5-12 and Figure 5-13. The ARB Creep cycle showed the highest particle number per mile compared to all the other standard cycles. The ETC Urban particle number measurements were comparable or slightly higher than those for the UDDS. The east-bound cruise particle number measurements were below those of the west-bound cruise and the other standard cycles. The west-bound cruise has a more prominent nucleation mode and overall higher particle counts than found for the east-bound cruise, as discussed further in the real-time data section and Appendix K. The two cycles where nucleation was most prominent, the west-bound cruise and the UDDS, did not show significantly higher particle counts compared to the other standard cycles overall, however. This indicates that the PMP system was effective in eliminating the nucleation particles seen in the primary tunnel under these conditions.

For the higher cut point CPCs, the emissions over the standard cycles are generally below the European standard for particle number of 8×10^{11} #/mi for light-duty vehicles. They are, however, higher than the typical levels measured for DPF-equipped light-duty vehicles in the PMP light-duty inter-laboratory correlation exercise (LD-ILCE), which were generally below the 2×10^{11} #/km (3.22×10^{11} #/mi) level [Andersson et al., 2007]. For the particle number counts in g/bhp-hr, the values ranged from approximately 7.6×10^{10} #/bhp-hr for the east-bound cruise to 3×10^{11} #/bhp-hr for the Creep. These are comparable to slightly below values recently measured in Europe by Bosteels et al. [2007] as part of a study by the Association for Emissions Control by Catalyst (AECC), which are around 3×10^{11} #/bhp-hr for the ETC cycle run.

On the other hand, the OnRoad Hills particle number measurements were about one to two orders of magnitude higher than any of the other standard driving cycles. The OnRoad Hills tests were associated with higher engine loads and exhaust temperatures consistently of 300°C or more. Under these conditions PM emissions and concentrations for all types of particles increased significantly, including solid, non-solid, and nucleation particles. Significant nucleation particle formation was observed by all the real-time particle counters (EEPS, f-SMPS and CPC's). In fact, on the OnRoad Hills tests, the 3022 and the low cut point CPCs all saturated at the maximum count rate, thus the values reported represent absolute lower bounds. The high cut point 3760s also reached concentrations above 10^4 #/cc, which is above the maximum stated range for the instruments and in a region where coincidence effects become significant.

For one of the OnRoad Hills tests, where there was significant nucleation, the PM gravimetric filter was analyzed by ion chromatography. It was found that of the 220 µg total mass, 50 µg was sulfate. Since sulfate absorbs water in a ratio of 2 to 1, another 50 µg of mass is also associated with sulfate. Approximately half of the mass was due to sulfate, and the remainder was likely due to organic carbon or elemental carbon. In the companion chassis dynamometer portion of this project, nucleation was also observed during conditions of elevated exhaust temperatures,

and sulfate also comprised a significant fraction of the PM mass. Previous studies have also shown a prevalence of sulfate in nucleation particles formed following aftertreatment systems, and that the level of nucleation increased with increasing exhaust temperature [Kittelson et al., 2006; Grose et al., 2006]. More detailed analyses of the chemistry of the particles below the PMP could provide additional insight into the phenomena that are occurring under these high load conditions.

The high nucleation particle counts for the OnRoad Hills driving for the PMP could be some breakthrough or inefficiency in eliminating more volatile or sulfate-derived particles at very high concentrations. The breakthrough could be due to incomplete evaporation or evaporation and renucleation after the evaporation tube. Particles composed of sulfuric acid and hydrocarbons could also pyrolyze into solid-like particles as they pass through the PMP.

The 3790 CPC showed the lowest average particle per mile rate compared to the other high cut point CPCs (3760As) for all of the driving cycles and flow of traffic driving. This is again consistent with the fact that the 3790 has a higher cut point than the 3760A. A paired, two tail t-test showed that the differences between the 3790 and 3760As were statistically significant at the 99% confidence level for all cycles but the east-bound ETC Cruise cycle.

The route direction of driving cycles also had a significant effect on the particle number rate per mile, similar to the effect on the regulated emissions. Particle number emissions for the west-bound cruise cycles were higher than those for the east-bound cruise cycles. The west-bound cruise cycles were conducted uphill, had higher exhaust temperatures, and showed greater nucleation than the east-bound cruise cycles. A more detailed discussion of the differences in the cruise cycle directions is presented below in the real-time data section and Appendix K.

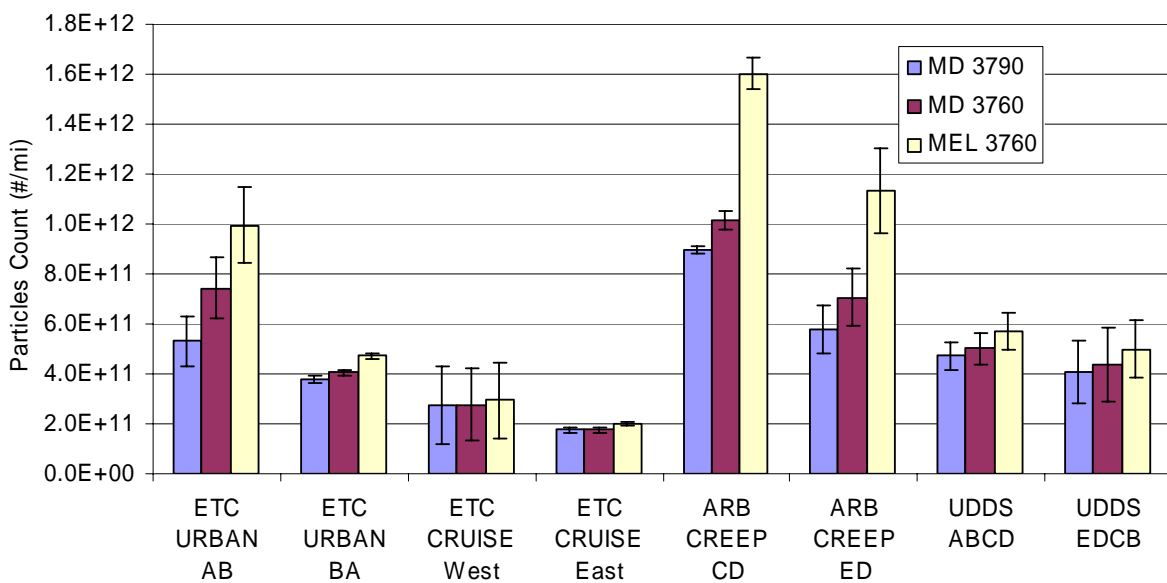


Figure 5-12. Particle number rate (#/mi) for similar cut point CPC's (3760A and 3790) for driving cycles grouped by direction

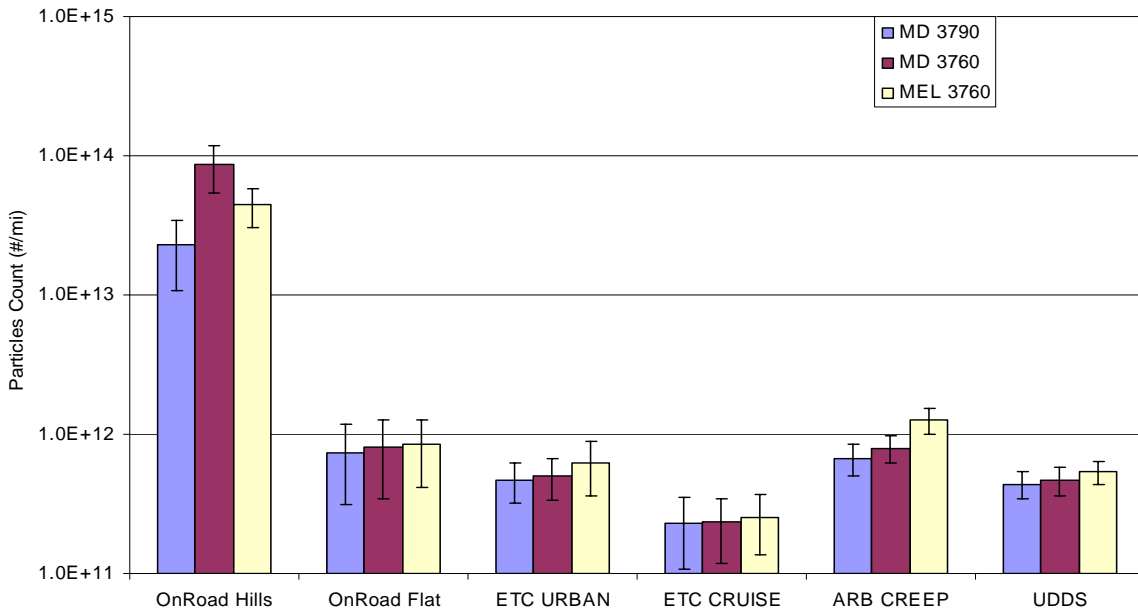


Figure 5-13. Particle number rate (#/mi) for similar cut point CPC's (3760A and 3790) for driving cycles grouped by direction and flow-of-traffic tests (log scale).

The test cycle trends for particle number for the smaller size cut instruments, shown in Figure 5-14 and Figure 5-15, are less consistent. The 3022 CPC showed a statistically significant higher particle number count than the 3025A for some of the cruise cycles where nucleation was found. The higher 3022 response over the 3025A can be attributed to the fact that the 3022 is connected to the primary tunnel and the 3025A is connected to the PMP dilution system. The PMP dilution system is designed to eliminate volatile nucleation particles, thus the most of the small nucleation particles seen by the 3022 would not be seen by the 3025As. Nucleation events were also identified in the UDDS cycle tests, although this cycle does not show consistent trends between different CPCs. The comparisons between CPCs for the UDDS are also complicated by fairly high variability for the 3022 measurements. The OnRoad Hills tests showed significant nucleation and saturated the low cut point CPCs, so the reported values represent only lower bounds on the particle number counts and comparisons between CPCs under these conditions can not be quantified.

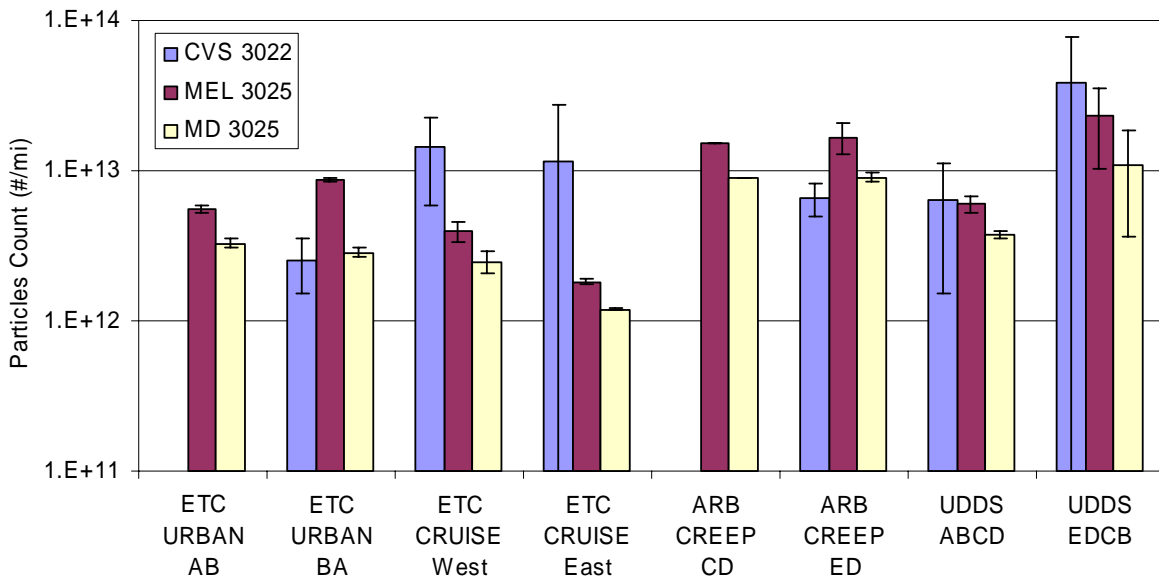


Figure 5-14. Particle number rate (#/mi) for similar cut point CPC's (3025A and 3022) for driving cycles grouped by direction (log scale).

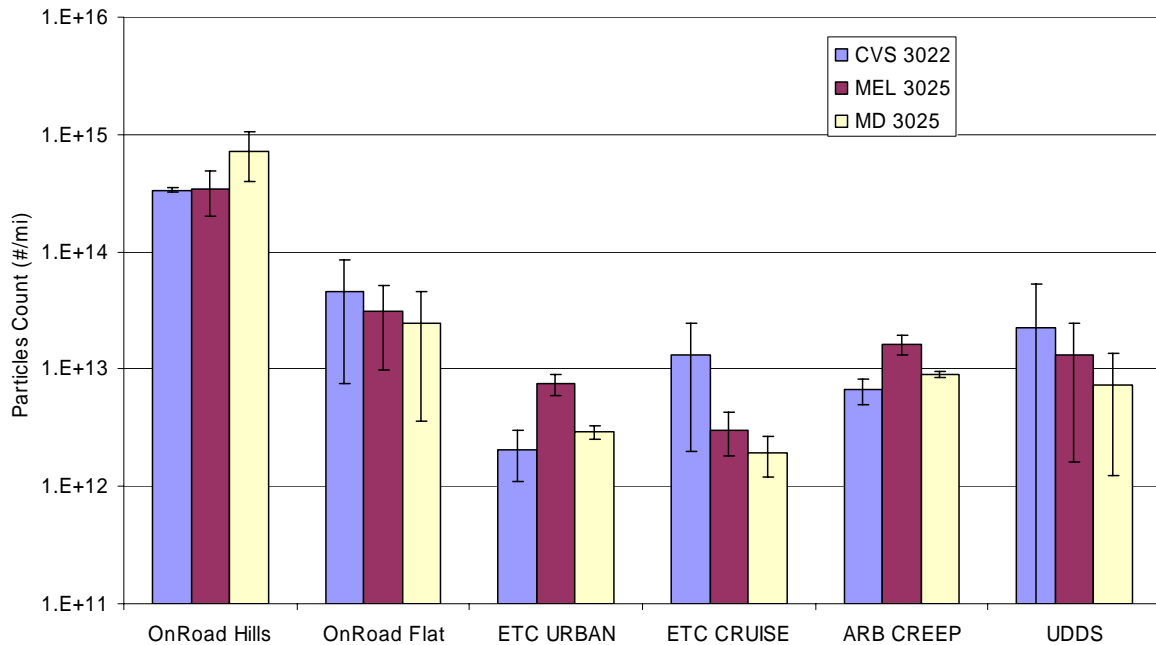


Figure 5-15. Particle number rate (#/mi) for similar cut point CPC's (3025A and 3022) for driving cycles not grouped by direction and for flow-of-traffic tests (log scale).

The 3022 particle number measurements for the creep and ETC urban cycles were comparable to or lower than the 3025As. Since significant nucleation was not observed for these cycles, the

particles may be less organic and less susceptible to being eliminated in the PMP system. It is also possible that some particles may be evaporated in the PMP and subsequently renucleate below the PMP. Given the variability observed in the testing, however, definitive particle number trends between the UDDS, creep, and urban cycles could not be identified for the CPCs with the smaller size cut.

One other trend seen for the standardized cycles is that the integrated particle number levels for the CPCs below the MEL PMP are generally higher than those for the comparable CPCs below the MD-19 PMP system for the standard cycles. This indicates that differences in the systems design can contribute to differences in the particle number measurements. Since the error bars in the graphs represent testing variability in addition to the variability associated with the instruments themselves, a paired t-test is needed to truly understand the significance of instrument differences within a given test cycle. A paired, two tail t-test showed the differences in the averages between the two 3760As on the different PMP systems were statistically significant at a 99% confidence level for the UDDS, Creep, and Cruise cycles and at greater than a 95% confidence level for the Urban cycle. Paired, two tail t-test results for the 3025As for the two different PMP systems showed that their differences were statistically significant at greater than a 99% confidence level for all cycles except the ETC Urban AB and UDDS EDCB and ARB Creep ED. For the ETC Urban AB, UDDS EDCB and ARB Creep ED, the differences for the 3025As were still statistically significant at confidence levels ranging from 90 to 95%, depending on the cycle.

Interestingly, measurements for the flow of traffic tests show the opposite trend, with the MD 3760A reading higher than that of the MEL 3760A, as seen in Figure 5-13. The low cut point CPCs were typically saturated on-road, so the CPCs between the two systems cannot be compared (see Figure 5-15). The main difference between the flow-of-traffic data the cycle tests is the particle number concentrations are much higher for the flow-of-traffic data. This suggests a possible measurement issue in either the sampling system (PMP diluter and transfer tubing) or in the CPC measurement instrument. The CPC measurement principle is fairly simplistic and robust suggesting most of the deviation comes from the sampling system. The PMP dilution ratios are relatively constant and could not account for the differences seen between the on-road tests and the driving cycle tests. It is possible that the higher concentrations for the flow-of-traffic tests are causing different formation/elimination mechanisms between the two diluter systems, but additional testing would be needed in this area.

CPC day-to-day variability is considered in Figure 5-16 and Figure 5-17. The figures show the day-to-day averaged measurements for all the UDDS cycles performed at the standard PMP settings. The UDDS cycle was chosen because it was repeated over more days than the other cycles. The high cut point CPCs are shown in Figure 5-16 with a linear y-axis and the low cut point CPCs are in Figure 5-17 with a log y-axis due to the large CVS 3022 signal relative to the other 3025A CPCs.

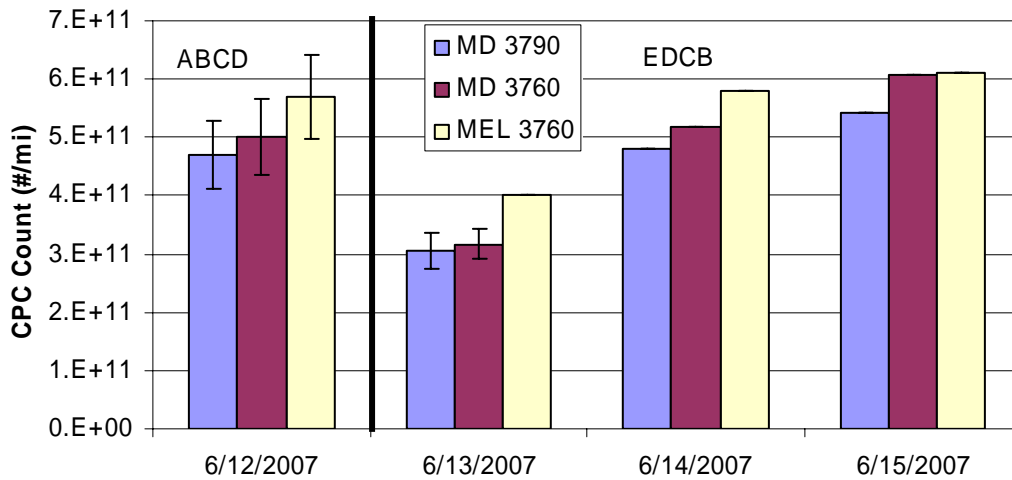


Figure 5-16. Particle number rate (#/mi) for the UDDS cycle over four separate days and two different driving directions to show day to day trends for similar cut point CPC's (3760A and 3790)

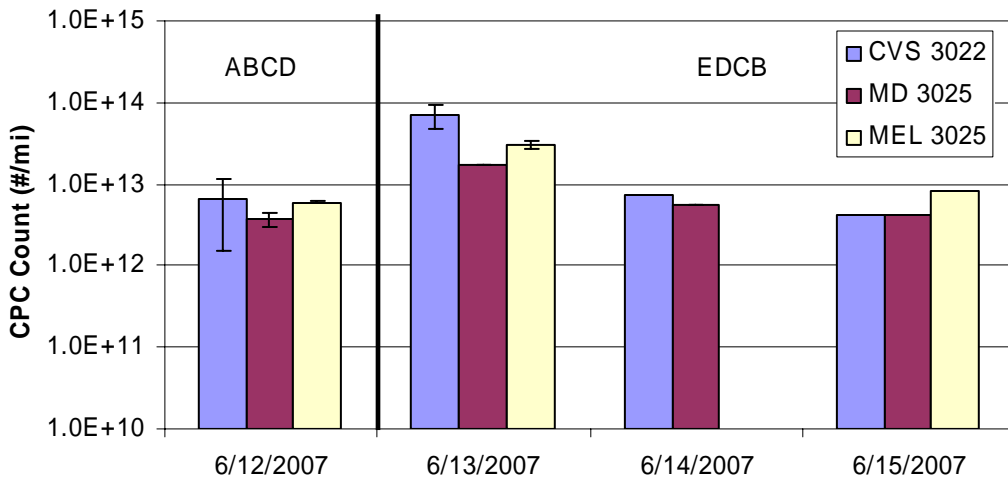


Figure 5-17. Particle number rate (#/mi) for the UDDS cycle over four separate days and two different driving directions to show day to day trends for similar cut point CPC's (3025A and 3022) Note y-axis log scale.

The CPC readings for a given test cycle varied from day-to-day. It appears the trend is less significant for the high cut point CPCs compared to the low cut point CPCs. The high cut point CPCs varied by a factor of at most two between days where the lower cut CPCs varied by a factor of ~5-10 for the 3025A and ~15 for the 3022.

The lower day-to-day variability for the high cut CPCs compared to the low cut CPC's could be partly due to the level of the signal and the nature of the particles measured. The high cut point CPCs are measuring on the order of 10 – 40 #/cc with a maximum of 100 #/cc. The low cut point CPCs are averaging 100-200 #/cc, but during heavy loads the values are much larger at around

1,000 to 10,000 #/cc, with much more dynamic range. The lower cut CPCs are spanning a larger portion of their measurement range and, at the highest concentration levels, could even be experiencing some measurement issues such as coincidence that is not identical between CPC's.

One potential advantage of particle number measurements is better repeatability at low mass levels. Figure 5-18 and Figure 5-19 show the COVs for particle number, PM mass, and NO_x for each cycle. The first figure shows the COV results for the cycles grouped by direction and the second figure shows the same results, but with all the cycles averaged together. In these figures, the OnRoad tests were eliminated since they were conducted over different routes and the Urban AB and Creep CD were eliminated since only two tests were conducted under these conditions.

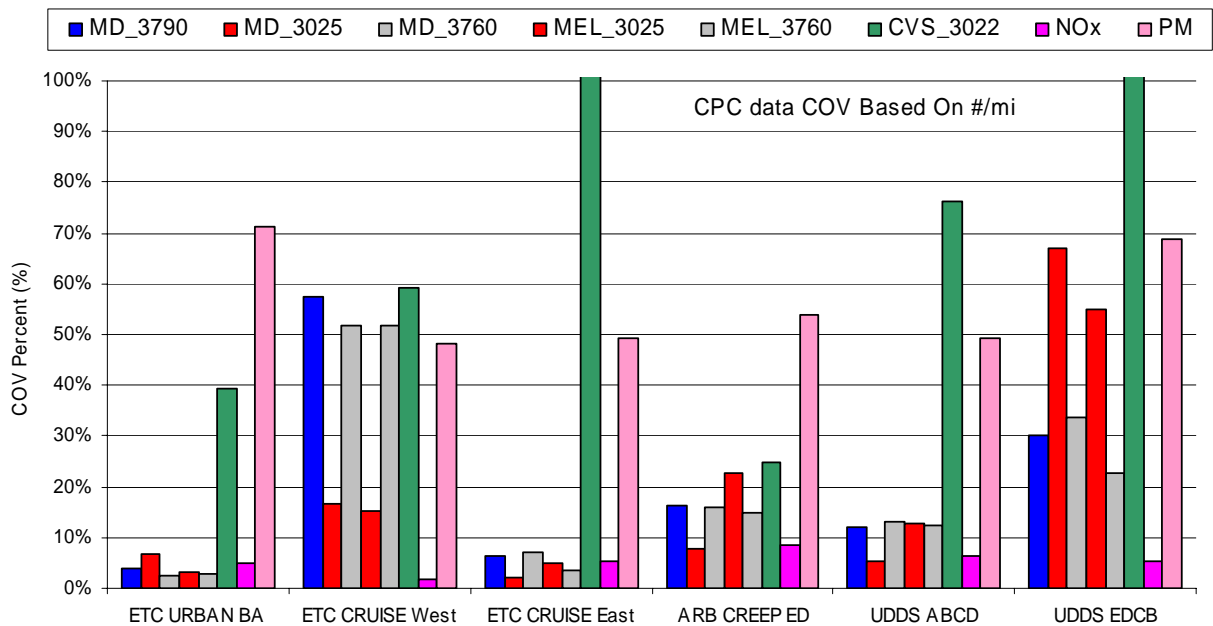


Figure 5-18. Coefficient of Variation for all CPC's and selected regulated measurements for on-road driving cycles grouped by direction

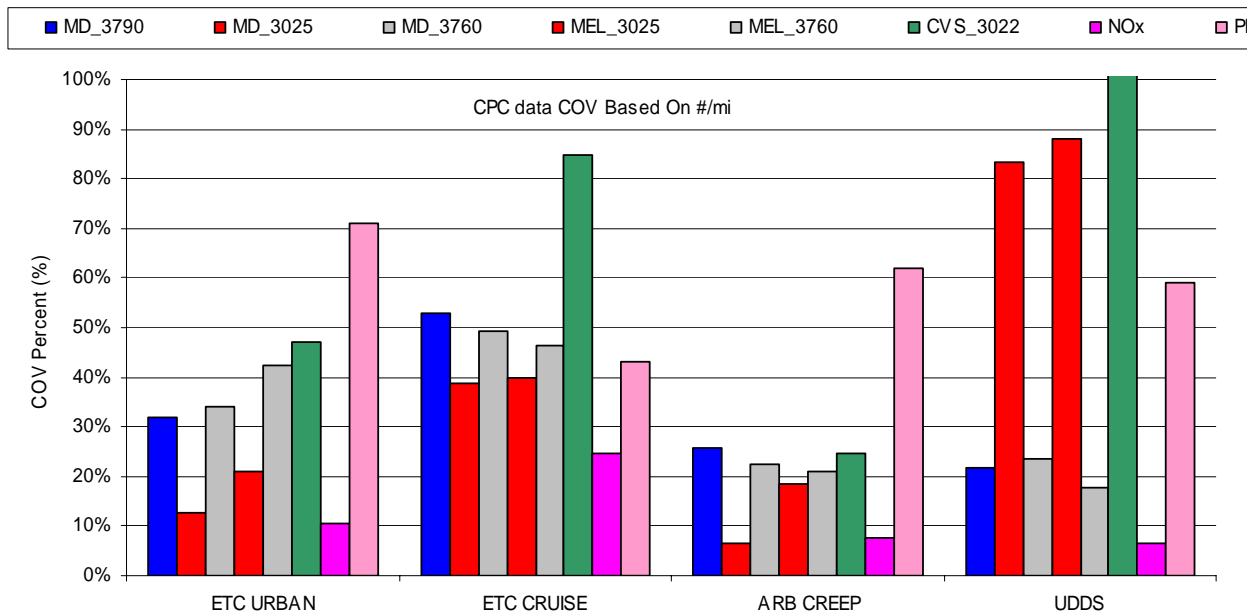


Figure 5-19. Coefficient of Variation for all CPC's and selected regulated measurements for on-road driving cycles not grouped by direction

In comparison with the PM filter mass COVs, the particle number measurements generally had lower COVs. For the ETC urban, creep and east-bound cruise cycles, the COVs for all CPCs were lower than the PM mass COV. The higher cut point CPCs also had lower COVs compared to PM mass for the UDDS cycle and the lower cut point CPCs had lower COVs compared to PM mass for the west-bound cruise. For the east-bound cruise and UDDS cycles, the 3022 COVs were higher than those for PM mass. The higher variability for the 3022 can be attributed to the impacts of more volatile nucleation particles that are either completely eliminated or are present in much smaller numbers below the PMP system. Although nucleation events did contribute to higher variability and outliers in the measurements directly from the dilution tunnel, these outliers did not impact the repeatability of the 3790 measurements below the PMP, unlike in some of the laboratory measurements. One other factor of importance in comparing the COVs between gravimetric measurements and particle number is that the particle number measurements are well above the minimum detection limits (MDLs) whereas the gravimetric measurements were at or below the MDLs or were comparable to background levels.

For the intercomparisons between the CPCs, the differences in COVs depended on the size cut, sampling location, and the cycle. The COVs for the 3022s are higher than those of the CPCs below the PMP system for all cycles but the west-bound cruise and creep. There were no strong trend differences between the high cut point CPCs and low cut point CPCs below the PMP, with the exception of the west-bound cruise and the UDDS EDCB, which showed opposite trends. In cases where higher variability was found for the higher cut point CPCs (3760A and 3790), this can be attributed to the very low count rates for these cycles and the fact that there were no nucleation events to affect the lower cut CPCs response. The high cut point CPCs can still count at these lowest number levels, but did show greater variability.

5.5 Real Time PM Number Results

In this section, real-time particle number results for the various test cycles are discussed. Additional analysis of the real-time data is also provided in Appendix K. The results include the various particle number measurements made, as well as some other variables such as exhaust temperature and calculated J1939 brake horsepower. The exhaust temperatures were measured at the stack (post CRT) and not before the catalyst. Some of the figures show multiple cycles or cycles that are sampled at different physical times. For ease of analysis, the actual cycles are joined together as snippets representing just the cycle data and eliminating any gaps in time between segments of the cycle. Figures where the data is not continuous is identified by “Not Continuous Test” and often show discontinuous jumps in the data.

In order to compare the CPC real-time data measured at different sampling locations in the sampling setup (i.e., CVS and the two PMP systems), the CPC's had to be normalized and time aligned to some reference. All the figures show real-time CPC data normalized to the MD19 dilution system (MD19 dilution ratio [DR] ~ 300 vs. MEL DR ~ 100). The reason for normalizing to a common dilution is to understand of differences between systems with dilution ratio removed. The MD-19 dilution level was chosen as the basis since the MD-19 is being used in response to the European regulations. Time alignment was performed using the J1939 brake horsepower calculated from ECM signals. All the CPC data shown in the following real-time figures is time aligned to engine power and normalized to the MD-19 PMP dilution of 300.

There are four prescribed driving cycles considered in the following real-time analysis. The ETC cruise, UDDS, ARB creep and ETC urban driving traces. In addition to the prescribed driving cycles some flow-of-traffic on-road driving tests are also analyzed. The flow-of-traffic data was added because the real-time PM results were significantly different from the prescribed driving cycle results. The reason for considering the real-time CPC data is to evaluate particle formation modes. Another consideration is to see the effectiveness of the PMP dilution for removing particles detected in the primary dilution tunnel (3022, EEPS and f-SMPS) versus those measured down stream of the PMP system (3760A's, 3790 and 3025A's) on a second by second basis.

ETC cruise

Figure 5-20 shows the real-time CPC data for a west bound and east bound ETC cruise cycle (test ID 200706121134_MEL.xls). Figure 5-20 shows a typical cruise cycle for the lower cut point CPCs (3025A and 3022). The lower cut point CPC show a very large initial spike during the beginning of the west bound ETC cruise. The 3022 measures an order of magnitude higher number concentration during the initial particle peak at the beginning of the cycle compared to both PMP diluted 3025A's. The 3025As on both PMP dilution systems also spikes about an order in magnitude over the typical cruise value of (100 #/cc). The higher count rate for the primary tunnel 3022 compared to the PMP diluted 3025A's suggests the particles are volatile in nature and are not counted by the 3025As below the PMP systems or are significantly reduced. The effects of these nucleation events are seen in some of the integrated plots comparing west-bound and east-bound cruise cycles. However, even with the nucleation event, the particle counts below the PMP are still comparable to or lower than other cycles without nucleation, such as the

ETC Urban. The differences between the 3025A measurements below the MEL and MD-19 PMP systems are discussed in greater detail in Appendix K.

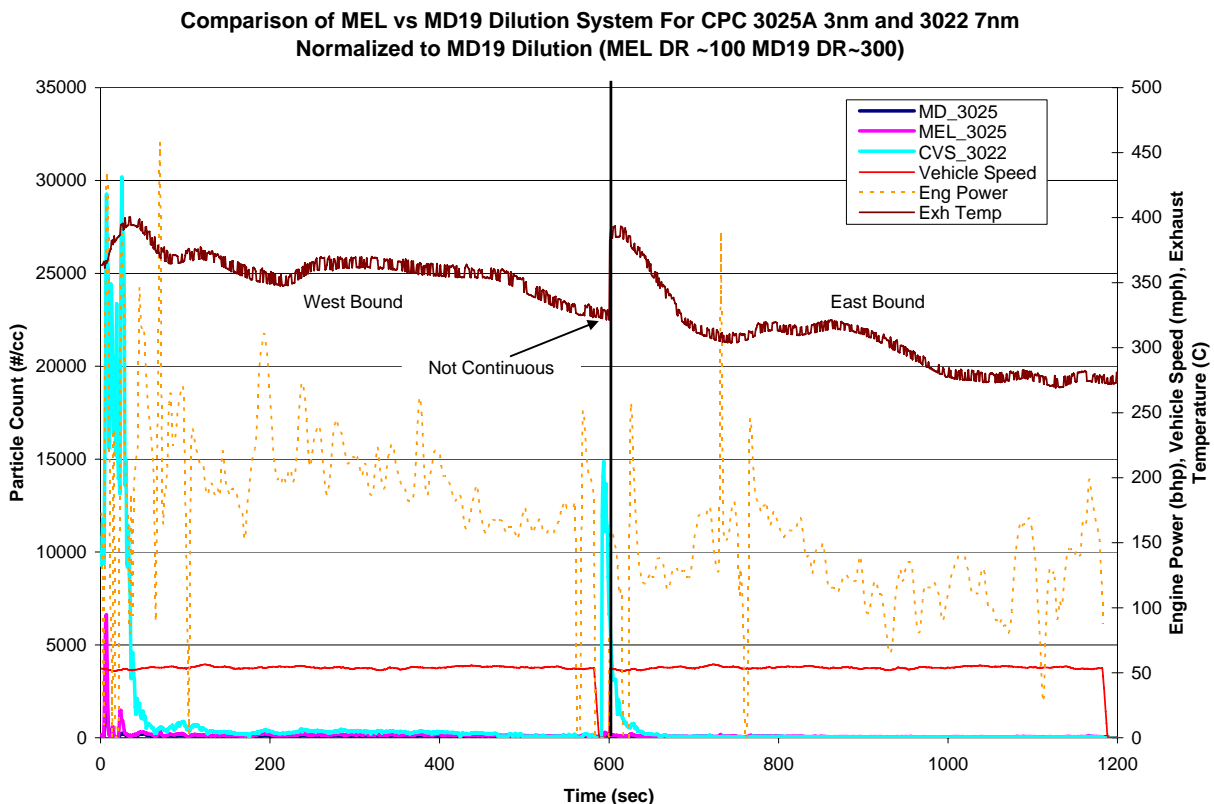


Figure 5-20. Real-time particle rate (#/cc) for the 3025A and 3022 CPCs on the ETC cruise cycle

Figure 5-21 shows a three second averaged f-SMPS distribution scan of the same ETC cruise cycle. The f-SMPS measurements were made from the primary dilution tunnel. The f-SMPS scan shows a high concentration nucleation mode spike occurs with an average diameter centered around 15 nm. The small diameter concentration spike supports the idea that the particles are from a nanoparticle nucleation burst. In comparing cycles where the nanoparticles form or don't form, the nanoparticles tend to form under conditions/cycles where elevated temperatures occur. For the cruise cycle, the nanoparticles form only when the exhaust temperature is at elevated levels. The conversion of SO_2 to SO_3 at elevated temperatures likely plays an important role in this nanoparticle formation.

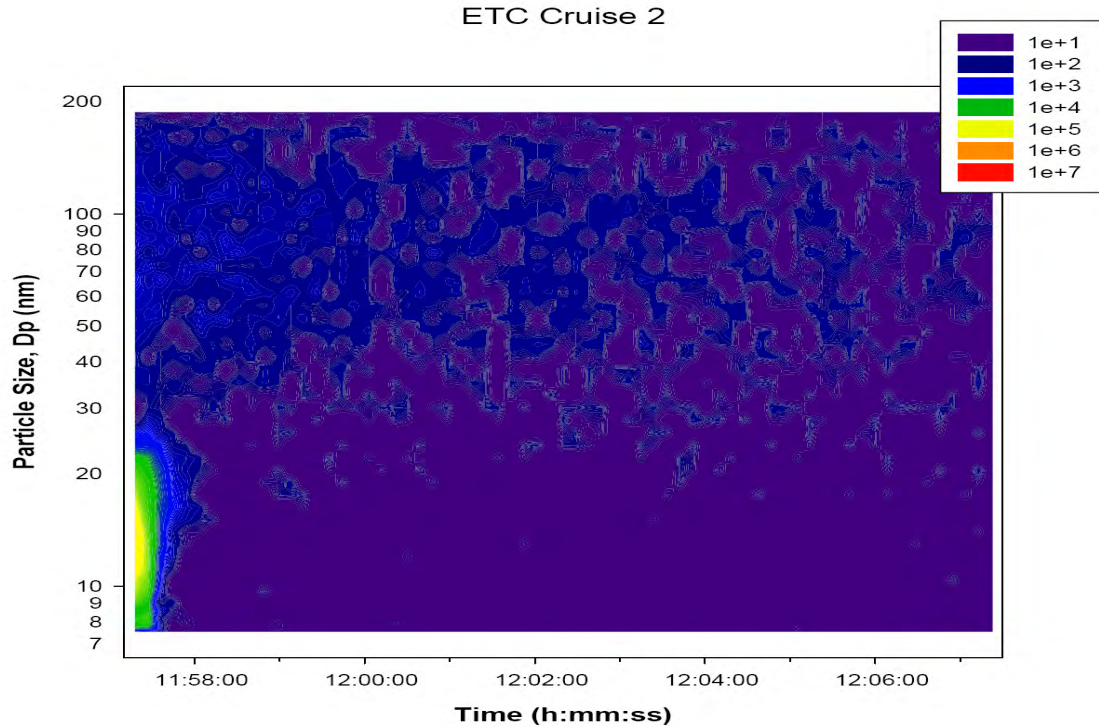


Figure 5-21 f-SMPS size distribution for the westbound ETC cruise cycle $dN/d\log(D_p)$

The high cut point CPCs (3790 and 3670As) did not show the nucleation event in real-time. The high cut point CPCs showed relatively good correlation and a prolonged peak in the particle counts from approximately the middle of the west-bound cruise to the end of the west-bound cruise. The nature of this prolonged peak is not understood at this time. The real-time data for the high cut point CPCs is provided in Appendix K.

UDDS

Real-time particle number measurements for the UDDS cycle are presented below in Figure 5-22 through Figure 5-25 (test ID 200706131258_MEL.xls). Note that the speed traces feature the four main peaks present in the UDDS speed trace, but in a different order from that found in the traditional trace. This is due to logistical considerations in accommodating the trace within the confines of the available real-world roadways. For ease of analysis, the actual cycles are joined together as snippets representing just the cycle data with gaps in time between cycle phases. The data is not continuous for Figure 5-22 and Figure 5-24, as shown directly on the figures by the phrase “Not Continuous Test” and the discontinuous jumps in the data.

Figure 5-22 shows the real-time data for the low cut point CPCs (3025A and 3022) over the UDDS cycle. Figure 5-22 also shows three sections of the cycles denoted as detail A, B, and C that are discussed in greater detail in Appendix K. The final hill of the UDDS shows a large spike for the low cut point CPC in the primary tunnel and down stream of the PMP diluter, while very low CPC concentrations are measured during the rest of the UDDS. Although it appears that the low cut point CPCs are noisy in looking at the overall UDDS figure, when one looks at the detail figures (discussed in Appendix K) it is apparent that the CPCs are responding to engine load.

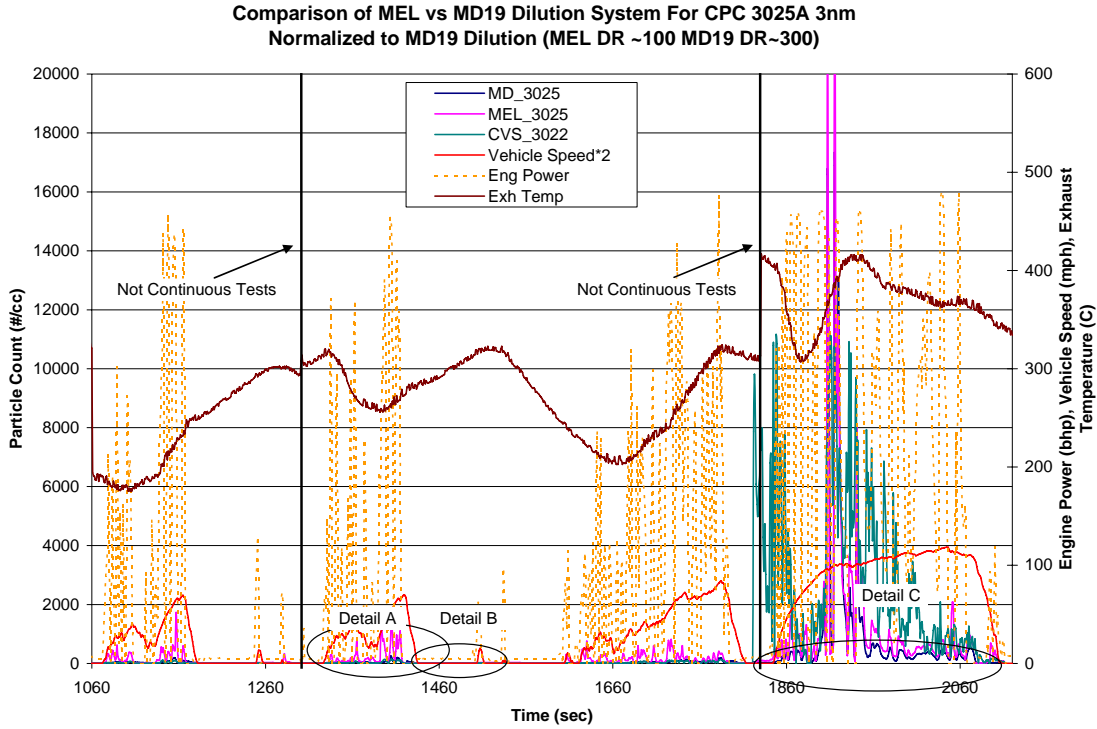


Figure 5-22. Real-time particle rate (#/cc) for the 3025A and 3022 CPCs on the UDDS cycle

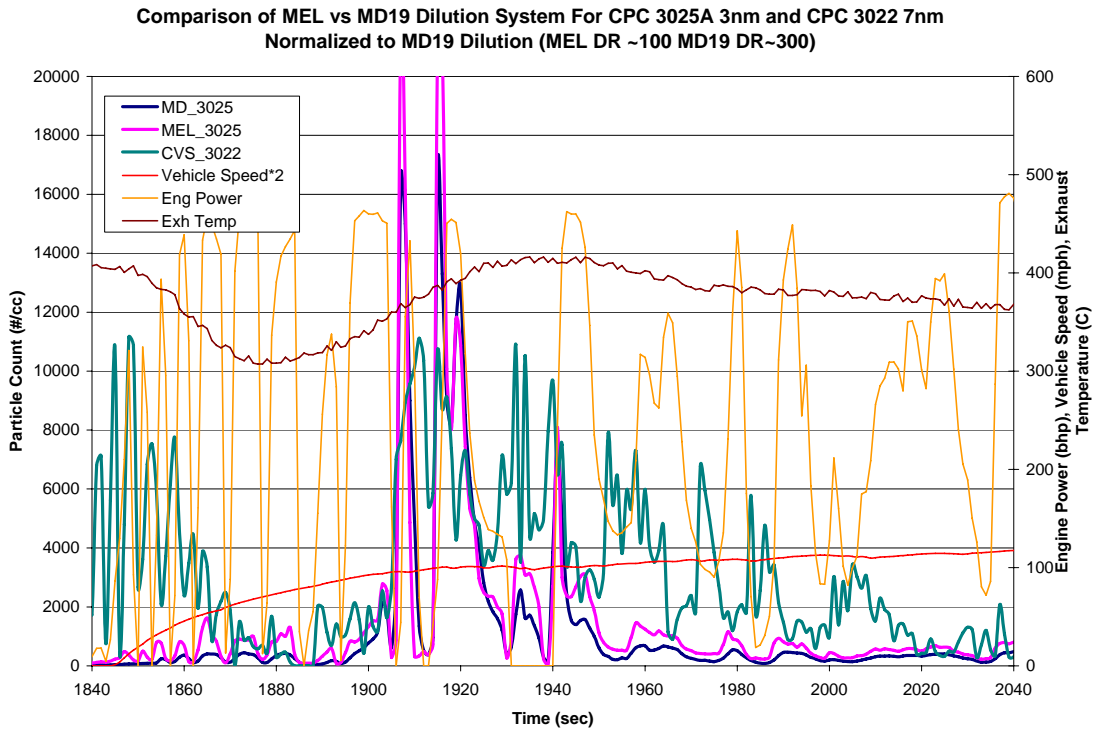


Figure 5-23 Detail C. Real-time particle rate (#/cc) for the 3025A and 3022 CPCs on the UDDS cycle

The high cut point CPCs are considered in Figure 5-24. Figure 5-24 shows the CPC 3790 and 3760A instruments utilized for particle number measurements as well as the exhaust temperature and engine power for the entire UDDS cycle. Again the 3760s and the 3790 measure similar particle number counts and overall, the high cut point CPC data show the more transient nature of the UDDS cycle as compared to the cruise cycle. The three detailed sections denoted in Figure 5-24 also show that the CPC data is again responding to the work done by the engine to reach targeted driving speeds, as discussed in greater detail in Appendix K.

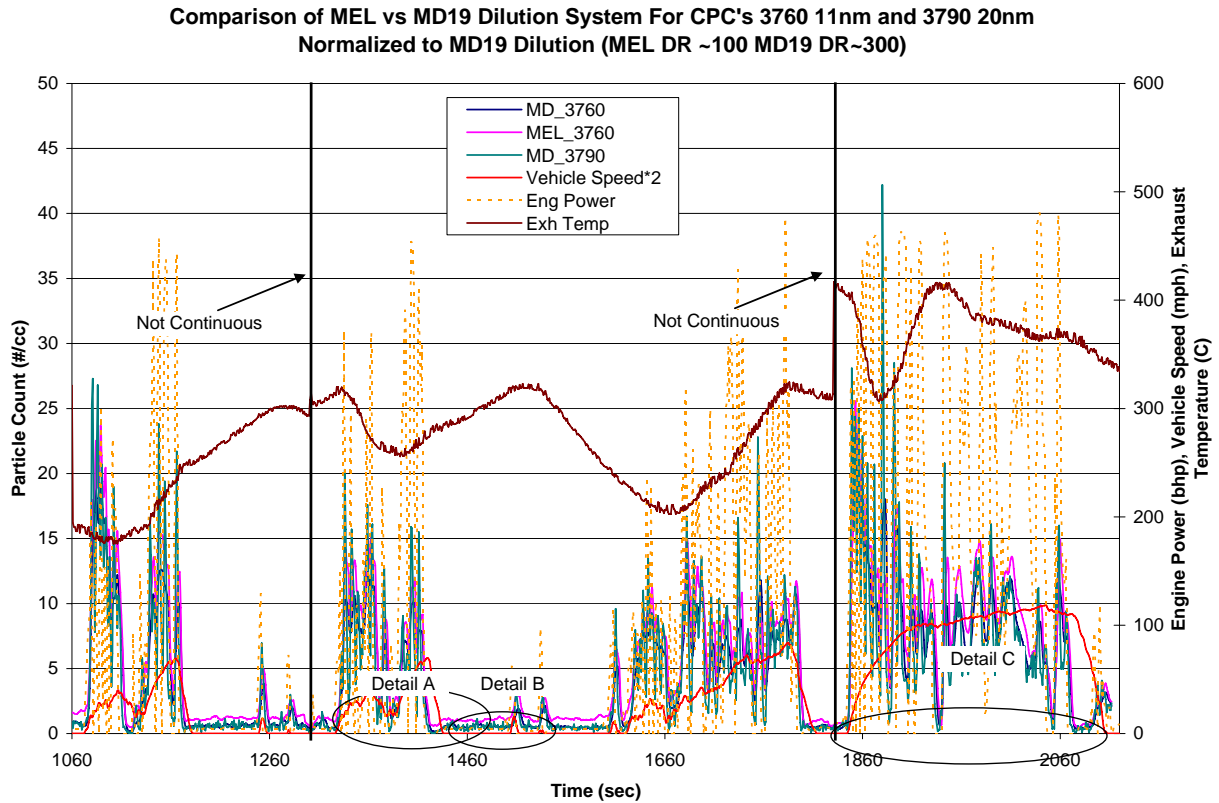


Figure 5-24. Real-time particle rate (#/cc) for CPCs 3790 and 3760 on the UDDS cycle

The f-SMPS data in Figure 5-25 provides an additional view of the particle size distributions in the primary tunnel during the entire UDDS cycle. The f-SMPS measurements over the UDDS were low, indicating few volatiles particles, except for the large hill in detail C where the f-SMPS showed a nucleation spike in the CVS tunnel. The location of the spike agrees with the CPC measurements. The peak f-SMPS particle diameter appears to be around 25 nm. The peak f-SMPS peak diameter is above the 3790 CPC cut size of 23 nm.

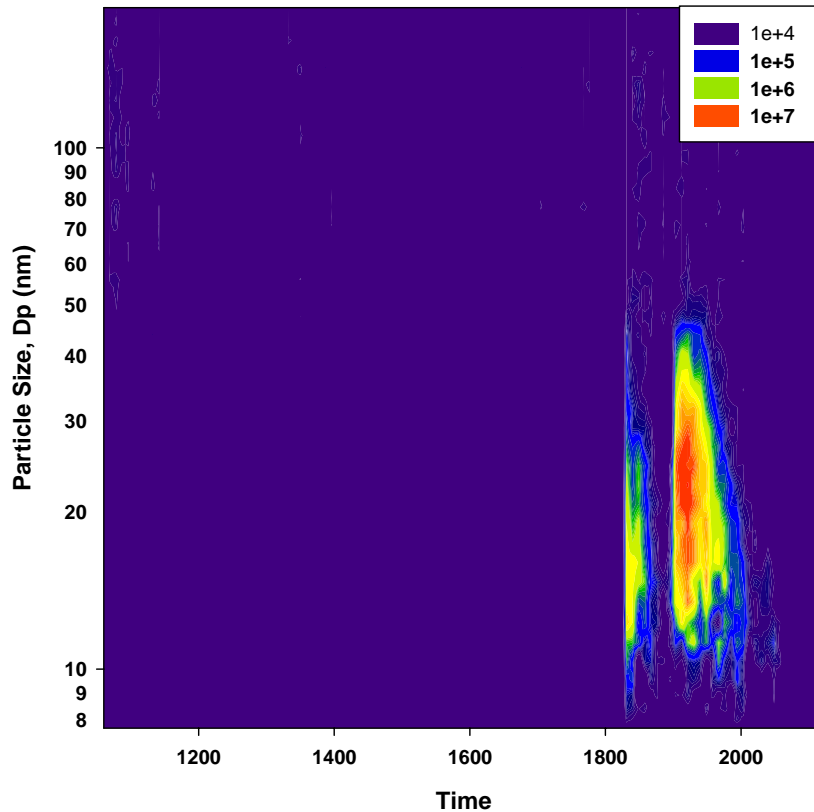


Figure 5-25. f-SMPS size distribution over a typical 20 minute UDDS cycle $dN/d\log(D_p)$

ETC Urban and CARB Creep Cycles

The ETC urban and ARB creep cycles are combined and shown for the low and high cut point CPCs in Figure 5-26 and Figure 5-27. The three detailed section in each of these figures are discussed in greater detail in Appendix K. Figure 5-26 shows the low cut point CPC3025A's for the creep and urban cycles. The low cut point CPC data is very transient and shows a similar trend as the UDDS CPC data, but the exhaust temperatures were lower. The exhaust temperature for the creep cycles is fairly constant and low, around 125°C. For the ETC urban cycles, the temperature is higher at 250°C, but not high enough to initiate nucleation. The large step in temperature is not real and shows the discontinuity in physical time between the creep cycles and the ETC urban cycle. The f-SMPS data shows particle formation is very low suggesting no nucleation events during either the creep or urban cycles. The F-SMPS data is provided in Appendix K.

Comparison of MEL vs MD19 Dilution System For CPC 3025A 3nm
 Normalized to MD19 Dilution (MEL DR ~100 MD19 DR~300)

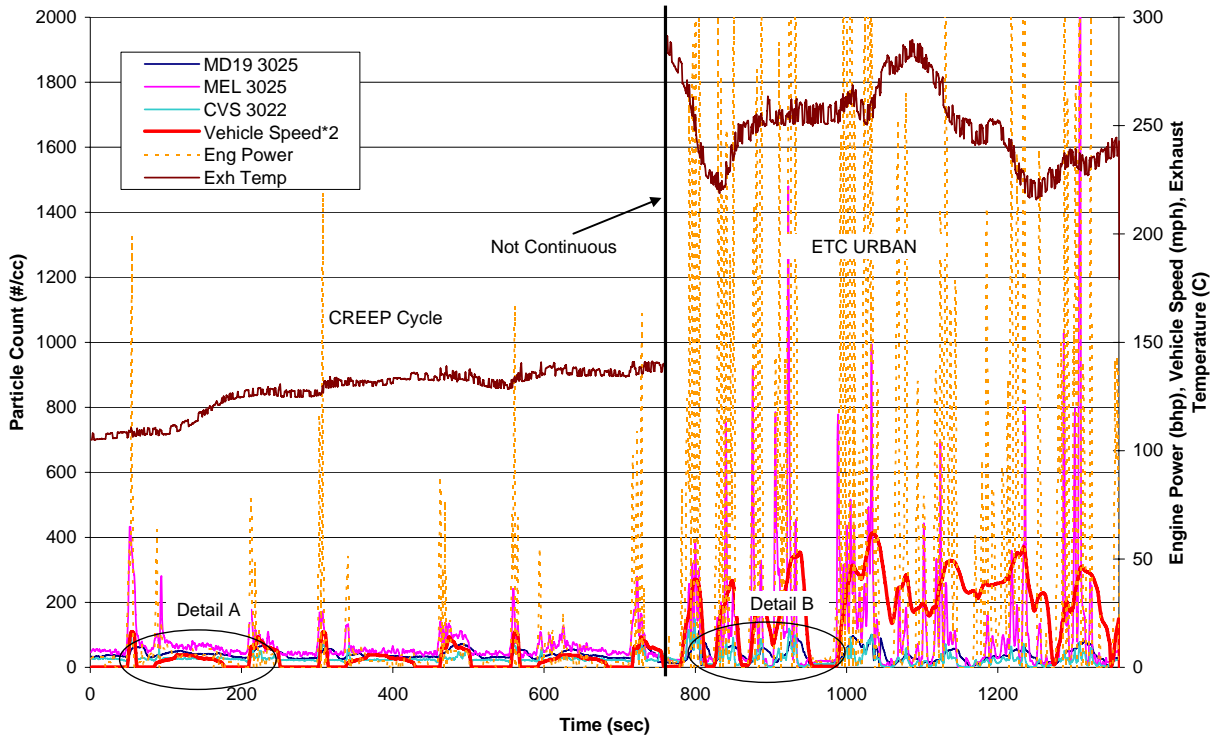


Figure 5-26. Real-time particle rate (#/cc) for CPCs 3025A on the creep and urban cycles

Figure 5-27 shows the same complete creep and urban driving schedules as before, but this time for the higher cut point CPCs (3790 & 3760). The data show that particle number for these cycles is transient and shows spikes with accelerations similar to the UDDS behavior.

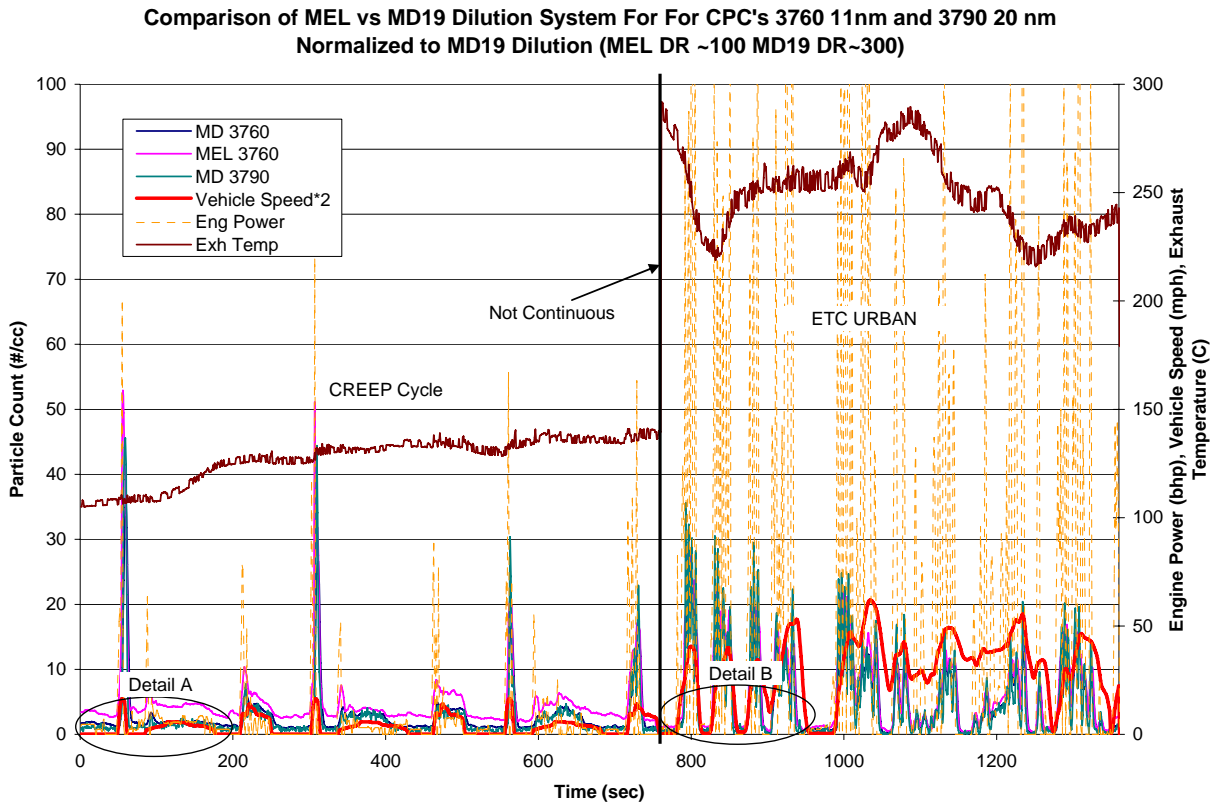


Figure 5-27. Real-time particle rate (#/cc) for CPCs 3790 and 3760 on the creep and urban cycles

Flow-of-traffic

Emissions were measured during three separate flow-of-traffic segments of operation. The three driving segments represented flat driving between Indio and Thermal, CA, steep hill climbing on the road out of Indio toward Blythe, CA, and a combination of hills and down hill driving on the return trip from Indio to Riverside, CA. The behavior of the emissions data for the flat road driving was similar to that of the standard cycles, so it is not discussed further here.

The test runs for the trips between Riverside and Indio, CA and to Blythe, CA both contained higher load operation. The test run to Blythe, CA was specifically run to try to force a regeneration event to remove any built-up PM in the DPF. For both of these higher load test runs, the high cut point CPCs showed concentration levels more than two orders of magnitude higher than the maximum of 100 #/cc found for the prescribed cycles. The real-time data for high cut point CPCs for the measurements taken on the return trip from Indio to Riverside, CA are provided in Figure 5-28. The corresponding real-time data is provided in Figure 5-29. The MD 3790 malfunctioned just after starting the cycle, thus all 3790 data is invalid. The low cut point CPCs quickly reached saturation during both of these test runs. The high cut point 3760s also reached concentrations above 10^4 #/cc, which is above the maximum stated range for the instruments and in a region where coincidence effects become significant. The measurements for all instruments were highest during the first half of the trip, since this was when the truck was climbing in elevation. The second half of the trip was largely downhill, and particle

concentrations declined to much lower levels with no saturation. It was also observed that, in contrast to the standard cycle data, the signal for the MD-19 high cut point CPCs was higher than that for the MEL CPCs. The details of the flow of traffic real-time measurements for the test runs to Blythe, CA and the low cut point CPCs are described in greater detail in Appendix K.

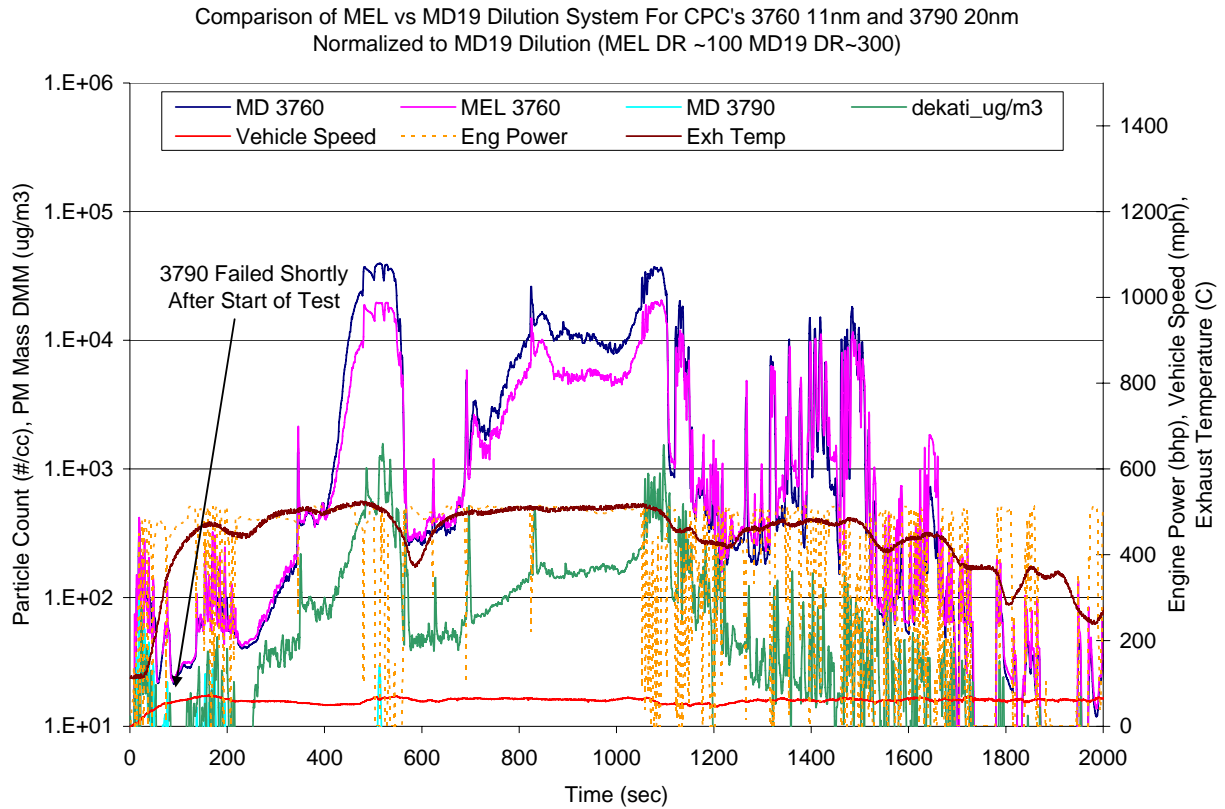


Figure 5-28. Real-time particle rate (#/cc) for similar cuts point CPCs (3790 and 3760) with Dekati DMM mass concentration ($\mu\text{g}/\text{m}^3$) for the flow-of-traffic Indio to Riverside run

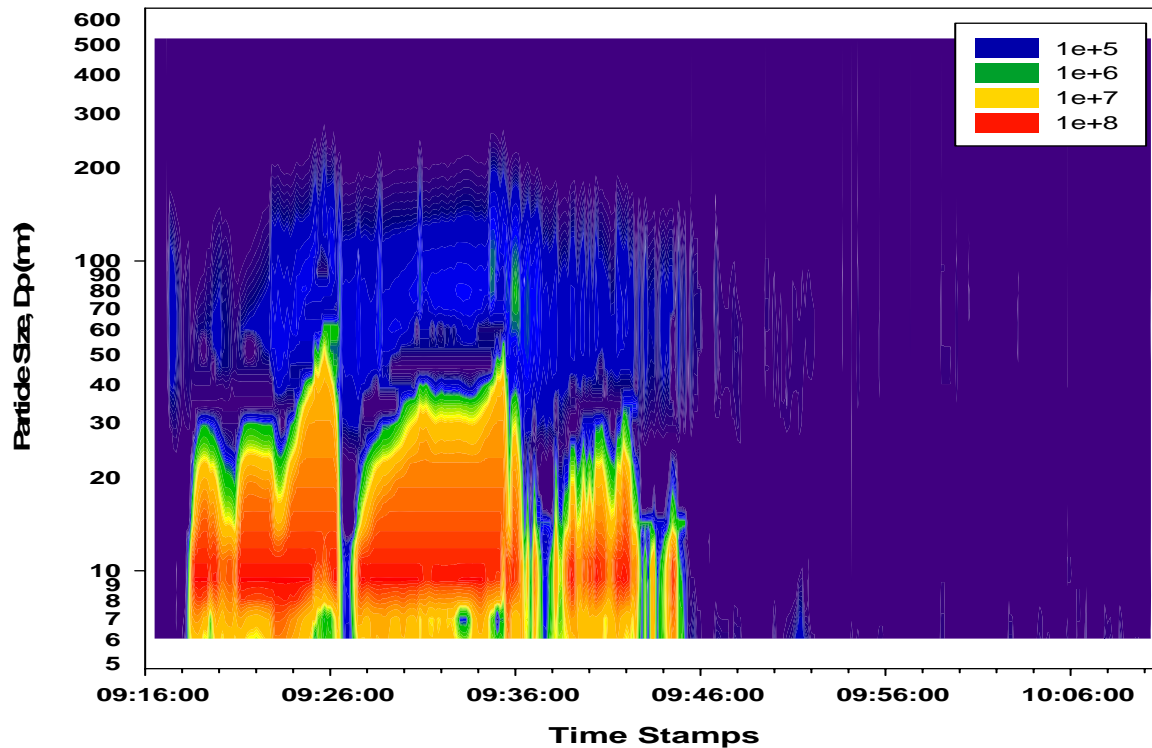


Figure 5-29. EEPS size distribution for Riverside to Indio flow-of-traffic Run $dN/d\log(D_p)$

MD19 High Dilution and MEL High Temperature Evaluation Runs on UDDS Cycle

Toward the end of the testing session, some additional tests were conducted in an effort to better characterize the PMP system. These tests were conducted on two separate UDDS cycles. For one test, the dilution ratio for the MD-19 was increased from ~300 to ~1400. A corresponding increase in the dilution ratio for the MEL PMP system could not be achieved due to its inherent design, so the MEL system was run using its standard operating conditions. For the second test, the temperature of the ET for the MEL system increased from 300°C to 500°C. The ET temperature for the MD-19 could not be increased so the MD-19 PMP system was run at its standard operating conditions. For both tests, it was found the results different configurations for the PMP systems did not show significant differences from those for the standard PMP operating conditions. This indicates that the PMP specifications were sufficient to eliminate the more volatile particles under typical UDDS operating conditions. The real-time data associated with these tests is discussed in greater detail in Appendix K. It would be interesting to conduct a similar experiment during an on-road driving conditions where significantly higher counts were observed below the PMP. Under these more extreme conditions, it is possible that high dilution or higher ET temperatures could have a greater impact on the distribution of particles seen below the PMP.

5.6 Intercomparisons Between CPCs and the PMP Dilution Systems

Two correlation analyses were considered, an integrated correlation analysis and a real-time second by second correlation analysis. The integrated correlation analysis provides a more robust evaluation between two systems without issues of time alignment and dynamic response. This is useful for determining true biases between systems. The real-time second-by-second correlations provide a different perspective. With the real-time correlation, one can investigate qualitative information on dynamic response (high or low spread), and possible issues at different magnitudes where correlations do not follow a linear relationship. The integrated correlation results are provided below in this section. The real-time correlation results are discussed in greater detail in Appendix K.

The MEL and MD-19 PMP systems are compared by examining the integrated results for all the flow-of-traffic cycles and contrived driving cycles. Figure 5-30 shows the high cut point CPCs correlation data for all the test cycles (left figure) and the data with the flow-of-traffic tests removed (right figure). Since the standard driving cycle data has much lower count levels than the flow-of-traffic measurements, these data are presented separately in the right hand figures to adequately show their details. Figure 5-31 shows the correlation data for the low cut point CPCs, but only using the standard cycles since the low cut point CPCs were saturated. The correlation for the complete data set for the high cut point CPCs shows that the MEL system measured lower by a factor of two for the high cut CPCs compared to the MD-19 system. This comparison agrees with the flow-of-traffic data presented earlier that the MEL was lower than the MD-19. If one filters out all the flow-of-traffic data and focuses on the data sampled during the standardized driving cycles, the MEL system measured higher values by a factor of two for the low cut CPCs, with no bias for the high cut point CPCs. This agrees with much of the real-time data and integrated cycle averaged data presented earlier where the MEL CPCs measured lower for the flow-of-traffic tests, but higher for the contrived driving cycles.

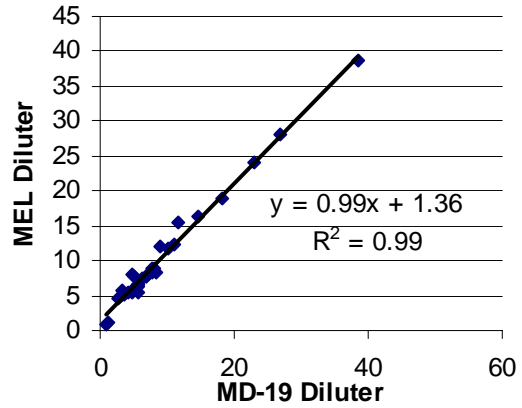
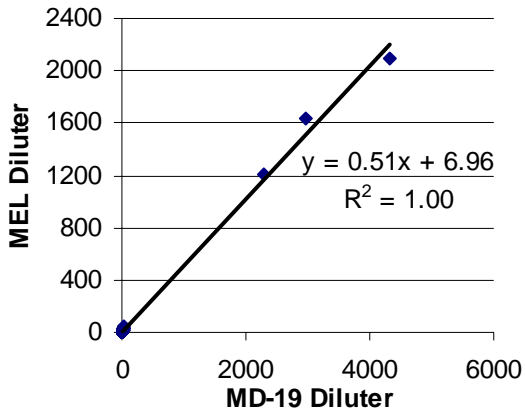


Figure 5-30. CPC 3760A correlation full data set and reduced data set with flow-of-traffic data removed

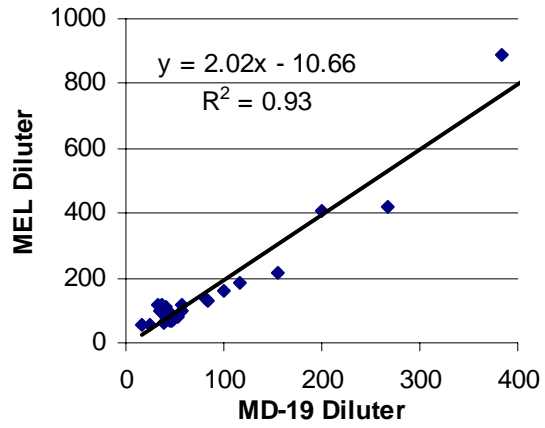
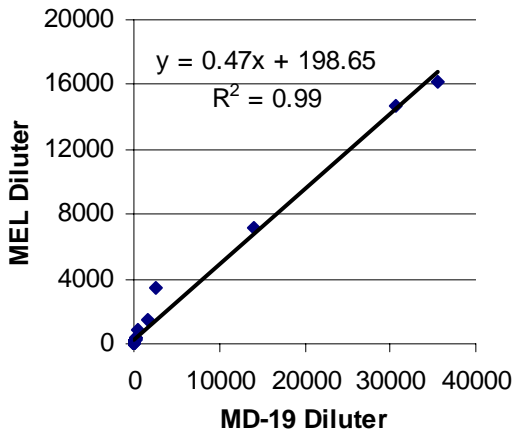


Figure 5-31. CPC 3025A correlation full data set and reduced data set

6.0 Summary

This study was designed to evaluate the performance of the European PMP protocol for the measurement of “solid” particle number under both laboratory and on-road conditions. The PMP system is designed to measure “solid” particles that are operationally defined as ones having a diameter between 23 nm and 2.5 μm and of sufficiently low volatility to survive a residence time of 0.2 seconds at 300°C. Laboratory was conducted at the California Air Resources Board’s (CARBs) heavy-duty vehicle emissions laboratory in Los Angeles. On-road testing was conducted over the road with CE-CERT’s Mobile Emissions Laboratory (MEL). Testing was conducted on two different diesel trucks equipped with diesel particle filters (DPFs). Between the laboratory and on-road testing a range of instruments were tested, including a full rotating disk diluter PMP system with a 23 nm cut point 3790 condensation particle counter (CPC), a second alternative PMP system for the on-road testing, additional CPCs with lower cut points (3-7 nm) and higher cut points (11 nm), an EEPS, an f-SMPS a DMS, an EAD, and a PAS. The laboratory tests were performed over multiple iterations of a UDDS cycle, a 50 mph cruise, and an idle. The on-road tests were conducted over a series of standard cycles such as the UDDS, the urban and motorway segments of the European ETC cycle, and the CARB creep cycle, as well as under typical on-road highway conditions.

A summary of the results is as follows:

Chassis Dynamometer Laboratory Testing

- PM mass emissions levels were on the order of 5-10 mg/mi, consistent with the levels of reduction expected for a DPF. PM mass levels were approximately 40 to 120 μg per filter, which is sufficiently above the tunnel blank and detection levels to allow accurate measurements. It should be noted that the tests were conducted over testing periods of approximately 35 to 45 minutes, which is approximately twice as long as the typical certification test over the Federal Test Procedure (FTP). Hence, certification test filter mass levels would likely be less than those measured in the laboratory portion of this work. On the other hand, current wall-flow DPFs typically reduce PM to well below the 2007 PM standard, so PM mass levels for devices performing near the certification levels should be more readily measureable.
- The particle number counts for the 3790 were below the European standard for light-duty vehicles for both the UDDS and cruise cycles. The coefficient of variability (COV) of the 3790 measurements was comparable to that of PM mass for the cruise, but greater than that of PM mass for the UDDS at ~120%.
- The COVs of the lower cut point 3025As were all greater than that of the PM mass and ranged from 110 to 270%. The high variability was primarily due to outlier tests for both the cruise and the UDDS cycles with significantly higher counts than the others in the sets. Although the variability was most significant for the 3025A CPCs with the lower size cut point (3 nm), the PMP-compliant 3790 (23 nm) also exhibited significant outliers for the UDDS.

- The removal of outliers improved the repeatability of measurements for the PMP-compliant 3790 and well as the 3025As. It also suggests the possible importance for developing statistical methods for outliers, which are not currently incorporated into the PMP protocol, to get consistently repeatable particle number measurements.
- It is significant to note that the outlier events are believed to represent real differences in particle number emissions that can be seen with the PMP system, but may be masked in the mass measurement. During some of the outlier tests, the 3025A CPCs exhibited several spikes up to the 40,000 to 100,000 particles/cc level at conditions where the PMP was providing a 300 to 1 dilution from the primary tunnel. It should be noted that unusually large spikes in total particle counts have been observed by some other researchers downstream of an aftertreatment system (Kittelson, 2008). For one test, there was also a consistently high particle count level that trended downward throughout the test.
- Real-time data for measurements taken in the primary tunnel showed that significant nucleation occurred once a critical temperature was reached on the post emission control device exhaust. This temperature was 310°C for this DPF device configuration. It appears that the nucleation mode particles may be attributed to the conversion of SO₂ to SO₃, which is likely aided by the catalytic washcoat on the DPF. This is consistent with previous studies that have shown sulfate makes an important contribution to nucleation particles downstream of an aftertreatment system [Kittelson et al., 2006; Grose et al., 2006].
 - The real-time size distributions for the UDDS cycle showed elevated particle counts during the high speed driving portions of the cycle. Under these conditions, exhaust temperature levels are sufficiently high to produce nucleation particles. The corresponding UDDS size distributions for showed a significant contribution of smaller particles in the nucleation mode.
 - The real-time 50 mph cruise data showed the onset and subsequent continuous formation of a nucleation mode once the critical temperature was reached. The size distributions for the 50 mph cruise showed a significant contribution of smaller particles in the nucleation mode.
- The temperature of the evaporative tube for the PMP system was found to have little impact on the 3790 particle concentration during a nucleation event, indicating that the more volatile particles are in the size range below 23 nm.
- For NO_x emissions, the truck emission rates were on the order of 10 g/mi for the UDDS and 7 g/mi for the cruise. The percentage of NO₂ as a function of total NO_x varied depending on the test cycle, with highest percentage of NO₂ seen for the cruise cycle and the lowest seen for the idle.
- THC and CO emissions were very low, and were either near or below the instrument detection limits.

On-Road Testing

- PM filter mass measurements were near detection limits for most standard driving cycles, with emissions levels of 10 mg/mi or 4 mg/bhp-hr or less. PM mass increased markedly for the higher load on-road cycles conducted on a steep grade and during uphill segments

of road. The filter masses for the standard cycles were generally below the three standard deviation detection limit of 7.5 µg per filter.

- Particle number counts varied depending on the cycle, operating mode, sampling location, and measurement instrument.
- The CPC particle number count levels follow a trend that is consistent with the size cuts of the respective instruments, with the particle counts for the 3760s (~11 nm) and the 3790 (23 nm) being considerably less than those of the 3022 (7 nm) and the 3025As (3 nm). The 3022 CPC, which was connected to the primary tunnel as opposed to below the PMP system, also showed higher counts than the other CPCs below the PMP system when volatile nucleation particles formed.
- For the 3790 and 3760A CPCs below the PMP systems, particle number counts were relatively high for the higher load on-road tests. Under these conditions PM emissions and concentrations for all types of particles increased significantly, including solid, non-solid, and nucleation particles. For the high load on-road tests, the high cut point 3760s reached concentrations above 10^4 #/cc, which is above the maximum stated range for the instruments and in a region where coincidence effects become significant. Of the standard cycles, particle number was highest on a per mile basis for the creep cycle. The particle counts for the ETC Urban and UDDS were lower, with the ETC cruise cycles being lowest. The particle counts for the 3790 for the standard cycles were generally below the European particle number standard for light-duty vehicles, with the exception of some creep cycles.
- For the 3022 and 3025A systems, there were less consistent trends between the cycles. The 3022 measured higher particle numbers than the 3025As during some cruise cycles where a strong nucleation mode peak was observed. The particle number readings for the 3022 and the 3025As all saturated at the maximum count rate for the higher load on-road tests. Although these measurements represented only absolute lower limits, the particle number levels were considerably higher for the on-road tests than the standard cycles.
- The particle number measurements below the PMP showed a lower coefficient of variation than the PM filter mass measurements for nearly all cycle/CPC combinations. The COV for the low cut point 3022 that sampled directly from the primary dilution tunnel was higher than those for the CPCs below the PMP system for nearly all cycles. This can be attributed to variability in nucleation and or other volatile particles eliminated by the PMP, especially for the UDDS and cruise. Although nucleation events did contribute to higher variability and outliers in the measurements directly from the dilution tunnel, these outliers did not impact the repeatability of the 3790 measurements below the PMP, unlike in some of the laboratory measurements. There were no strong trend differences between COVs the high and low cut point CPCs below the PMP.
- The rotating disk PMP system (denoted MD-19) and the ISO 8178 partial flow PMP system (denoted MEL) showed good agreement for the 3760A and 3790 CPCs with the higher size cuts. This was found for both the integrated and the real-time results. The good intercomparisons for the 3760s are found on most cycles with the exception of the creep cycle. The intercomparisons between the MD-19 and the MEL PMP systems for the 3025As showed greater differences between the systems, including more transient data for the MEL system. The MEL and MD-19 systems also showed biases relative to one another, with the MEL higher than the MD-19 for the standard cycles and the MD-19 system being higher than the MEL for the higher load on-road driving conditions.

- For some cycles, nucleation particles were formed. These nucleation particles were generally formed during portions of the cycle when elevated exhaust temperatures were found. The nucleation particles showed a strong response with the 3022 CPC in the primary tunnel. The instruments below the PMP showed a much weaker response during nucleation events for the standard cycle, but relatively high levels for the more aggressive on-road tests.
 - The on-road test runs representing steep hill climbing or a combination of hills and down hill driving showed significant nucleation throughout the test runs and that the levels were quite high for the high and low cut point CPCs below the PMP. These driving conditions were characterized with higher engine loads and exhaust temperatures consistently above 300°C or more. The high cut CPCs were measuring concentrations over 10^4 and the low cut CPCs were saturated at 10^5 and 10^7 for the 3025A and 3022, respectively.
 - A PM filter sampled from one of these high load tests showed a significant contribution from sulfate and associated water mass (~45%). This suggests that SO₂ to SO₃ conversion in the catalyst plays an important role in these nucleation events. Previous studies have also shown a prevalence of sulfate in nucleation particles formed following aftertreatment systems, and that the level of nucleation increased with increasing exhaust temperature [Kittelson et al., 2006; Grose et al., 2006].
 - For the more aggressive cycles, the high particle counts measured below the PMP could indicate that the PMP sampling train has some inefficiencies in removing nucleation mode particles at such high levels or that there is a slight breakthrough of volatiles through the PMP due to incomplete evaporation, evaporation and renucleation after the evaporation tube, or pyrolysis.
 - A nucleation event is observed near the beginning of the ETC cruise. This event contributes to some of the variability in the particle number measurements for that cycle.
 - Nucleation was also observed during the highest speed/load portion of the UDDS.
- NO_x emissions ranged from 13 to ~22 g/mi for the ETC Urban, ETC cruise, and UDDS cycles, with NO_x emissions for the ETC cruise generally being the lowest. NO_x emissions for the creep cycle were considerably higher than those for the other cycles, and were on the order of 50 g/mi. The higher NO_x emissions for the creep cycle are due to its transient nature and short distance.
- THC and CO emissions were very low and near the instrument detection limits.

7.0 Discussion and Implications

An important objective of this study was to evaluate the PMP protocol under a robust set of experimental conditions from laboratory to on-road, in-use testing. This included a comparison of different PMP-compliant systems, comparisons of particle counters with different size ranges, comparisons of particle number with PM mass, comparisons under different driving cycles or conditions, and comparisons of the variability of different methodologies. A number of important observations were made in this program that can be used to critically evaluate the PMP protocol and to suggest further areas of study. Some important issues of note include:

Particle number offers the potential to more readily characterize emissions at the low levels currently exhibited by current wall-flow DPFs, which are often only a small percentage of the certification value. In this study, particle number emissions compared favorably with PM mass emissions for the on-road testing. PM mass measurements for nearly all the on-road test conditions were near or below detection limits and tunnel blank levels, indicating it is difficult to obtain a true, quantifiable value. Particle counts, on the other hand, were readily measured at the levels seen in the on-road testing and represented real quantifiable values. For the laboratory testing, the advantages of the particle number measurements were less clear as the mass levels were higher due to longer test times, the filter masses were in a readily quantifiable range, and outliers were found in the particle number measurements. Recent studies have also suggested that PM mass loadings for certification of engines emitting at levels close to the current US 2007 standards, as opposed to the actual tailpipe PM emissions levels for DPF-equipped engines, are adequate to get a precise mass measurement [Khalek, 2005].

The variability between the different PMP particle number counts and the PM mass depended on the cycle, sampling location and time, the specific test instrument, and other experimental conditions. For the on-road tests, the variability or COVs for the particle number counts below the PMP were all lower than those for the PM mass measurements for nearly all testing scenarios. For the laboratory tests, however, outliers were found on both the 50 mph cruise and the UDDS. It does appear that the outlier events represent real differences in particle number emissions that can be seen with the PMP system but may be masked in the mass measurement. Unusually large spikes in total particle counts have been observed by some other researchers downstream of an aftertreatment system (Kittelton, 2008). Such outliers below the PMP, especially for the 3790, were not observed in the on-road testing or in CARB's previous PMP work. It is possible that the outliers represent small, localized regeneration events in the DPF, emphasizing the need to better understand the fill level of the DPF. This is probably a more critical point for active DPF, as opposed to passive DPF, such as those used here.

The overall combined laboratory and on-road results seem to indicate that particle number can provide a more repeatable measurement for current wall-flow DPFs with particle emission levels well below the 2007 US PM mass standard, but not necessarily at PM levels near the standards. Additionally, the PMP methodology provides a new metric with which to better understand PM emissions. The development of statistical techniques for the removal of outlier tests for particle number should be considered. These statistical outlier criteria are not currently incorporated into the PMP protocols. The need for statistical techniques to remove outliers could also increase the number of tests required to achieve a valid measurement or necessitate that a certain number of

tests be run for a valid measurement. In comparing the COVs for gravimetric measurements and particle number, it is again worth noting that the particle number measurements are well above the detection limits, whereas the gravimetric measurements were not in many cases for the on-road test. Thus, while the PM mass measurements have a lot of scatter at these levels, the particle number measurements have outliers that can be removed using statistics.

The particle number measurements for the low cut point CPCs (3025s – 3 nm) were approximately an order of magnitude higher than those for the PMP-compliant (3790 – 23 nm) and the other high cut point CPCs (3760As -11 nm) below the PMP system for both the on-road and laboratory measurements. This means that a significant fraction of particles are not being counted using the current 23 nm cut size either due to size and/or volatility. This has the advantage of removing nucleation particles that can contribute to variability, but also removes the ability to characterize these same small particles. The negative impacts of greater system variability were seen for the lower cut point CPCs in the laboratory testing, but not the on-road testing. Greater differences between different PMP-compliant dilution systems were also found for the lower cut point CPCs than the higher cut point CPCs for the on-road testing.

Under more aggressive driving conditions with higher exhaust temperatures, significant nucleation was observed, with very high count levels below the PMP system. These particles had a large sulfate contribution that may not have been eliminated by the current PMP dilution system. The finding that sulfate makes an important contribution to nucleation particles following an aftertreatment system is consistent with previous studies [Kittelson et al., 2006; Grose et al., 2006]. This finding suggests that certification level tests may not be sufficient to understand or characterize particle count levels that may occur on the road. The robustness of the PMP sampling system under these conditions also needs to be better understood. Other methods can be considered for developing systems for PMP-compliant applications. Previous studies, for example, have used a ‘catalytic stripper’ that combines a sulfur-trap that eliminates sulfur compounds and an oxidation catalyst that eliminates hydrocarbons to provide a potentially more robust technology for removing nucleation particles and providing for more consistent measurements [Abdul-Khalek and Kittelson, 1995; Kittelson et al., 2005].

These results also suggest that additional information on the chemistry of the particles would be of value to determine specifically what types of particles are being measured below the PMP system. This could include analysing the chemical character of elemental and organic carbon, sulfuric products, hydrocarbons (HCs), PAHs, water and trace elements/metals, and metal oxide particles from engine wear or lube oil packages.

For the on-road tests, where two PMP compliant dilution systems were compared, some significant differences were identified. It appears there is a significant difference in the two PMP systems depending on measurement level. At high concentrations, the MD-19 high cut point CPCs measured higher values, while at low to moderate concentrations, the MD-19 CPC counts were lower for the low cut point CPCs when compared to the MEL system. Further research is needed to better understand these system differences. Also, some systematic evaluations of different designs and different parameters with the PMP system operation should be evaluated. This could include different temperatures, dilution ratios, or residence time for the sampling system or CPCs with different cut points.

The effectiveness of the PMP system should be evaluated in California over a wider range of vehicles and aftertreatment technology applications, similar to what has been accomplished in Europe. The focus of this project and previous CARB efforts for heavy-duty diesel has been on passive DPF systems. A recent investigation by CARB researchers on the PMP “Golden Vehicle” also included an active regeneration system. Further studies are needed on DPF technologies that meet the US 2007 PM standards that typically have both a passive element as well as an active element. Information upstream of the DPF may also be of interest in understanding the impact of different DPFs. These studies should include the examination of different DPF fill level states and regeneration. The effectiveness of the PMP system in measuring particle number from a vehicle system equipped with a DPF + NO_x aftertreatment system, such as an SCR system, may also be of interest in looking to future applications.

8.0 References

Abdul-Khalek, I.S. and D.B. Kittelson. 1995. "Real Time Measurement of Volatile and Solid Exhaust Particles Using a Mini-Catalyst," SAE Paper No. 950236, SAE International Congress & Exposition, Detroit, MI, February 27-March 2, 1995.

AECC – Association for Emissions Control by Catalysts, 2005 “AECC Light-Duty Test Programme – PMP Measurements. Working paper No. GRPE-PMP-15-1. 15th PMP working meeting, Geneva, May 31st.

Andersson, J., Giechaskiel, B., Munoz-Bueno, R., and Dilara, P. 2007. Particle Measurement Programme (PMP) Light-duty Inter-laboratory Correlation Exercise (ILCE_LD) Final Report No. GRPE-PMP-18-2. 18th PMP working meeting, January.

Andersson, J. and Clarke, D., 2005 “Inter-Laboratory Correlation Exercise: Updated Framework and Laboratory guide for HD Engine Testing. Document for the UK Department for Transportation. Working paper No. GRPE-PMP-15-4. 15th PMP working meeting, Geneva, May 31st.

Andersson, J. 2008. personal communication.

Ayala, A. and Herner, J.D. 2005. Transient Ultrafine Particle Emission Measurements with a New Fast Particle Aerosol Sizer for a Trap Equipped Diesel Truck. SAE technical paper 2005-01-3800. Presented at the October SAE fuels Conference, Texas, October.

Ayala, A. Kado, N.Y., Okamoto, R.A., Holmen, B.A., Kuzmicky, P.A., Kobayashi, R., and Stiglitz, K.E. 2002. Diesel and CNG Heavy-duty Transient Bus Emissions over Multiple Driving Schedules: Regulated Pollutants and Project Overview.” *Journal of Lubricants and Fuels*, SAE Transactions, Vol. 111, pp. 735-747. (also SAE technical paper No. 2002-01-1722)

Bosteels, D., May, J., Nicol, A.J., Such, C.H., Andersson, J.D., Sellers, R.D., 2007. Investigation of the Feasibility of Achieving Euro VI Heavy-Duty Diesel Emissions Limits by Advanced Emissions Controls. Presentation on the Association of Emissions Control by Catalyst website. www.aecc.be. September.

Brook, R.D., Brook, J.R. Urch, B., Vincent, R., Rajagopalan, S., Silverman, F. 2002. Inhalation of fine particulate air pollution and ozone causes acute arterial vasoconstriction in healthy adults. *Circulation*. 105: 1534-1536.

Cambustion, www.cambustion.co.uk – see website for information on DMS500.

Chow, J.C., Watson, J.G., Pritchett, L.C., Pierson, W.R., Frazier, C.A., and Purcell, R.G. (1993) Thermal/Optical Reflectance Carbon Analysis System: Description, Evaluation, and Application in U.S. Air Quality Studies. *Atmospheric Environment*, vol. 27A, p. 1185.

- Clark, N.N., Gautam, M., Wayne, W.S., Lyons, D.W., Thompson, G., and Zielinska, B., 2007. Heavy-duty Vehicle Chassis Dynamometer Testing for Emissions Inventory, Air quality Modeling, Source Apportionment, and Air Toxics Emissions Inventory, E-55/59 All Phases. Final Report to the Coordinating Research Council. August. Available at www.crcao.com.
- Cocker, D.R., Shah, S.D., Johnson, K.C., Miller, J.W., and Norbeck, J.M. (2004a) Development and Application of a Mobile Laboratory for Measuring Emissions from Diesel Engines. 1. Regulated Gaseous Emissions. *Environ. Sci. Technol.* 38, 2182.
- Cocker, D.R., Shah, S.D., Johnson, K.C., Zhu, X., Miller, J.W., and Norbeck, J.M. (2004b) Development and Application of a Mobile Laboratory for Measuring Emissions from Diesel Engines. 2. Sampling and Toxics and Particulate Matter. *Environ. Sci. Technol.* 38, 6809.
- Dilara, P. and Andersson, J. 2005. Report on First Results from LD Interlab. Working Paper No. GRPE-PMP-15-2 for the 15th PMP Working Meeting, Geneva, May.
- Grose, M.; H. Sakurai; J. Savstrom; M. R. Stolzenburg; W. F. Watts, Jr.; C. G. Morgan; I. P. Murray; M. V. Twigg; D. B. Kittelson; and P. H. McMurry, 2006. "Chemical and Physical Properties of Ultrafine Diesel Exhaust Particles Sampled Downstream of a Catalytic Trap," *Environ. Sci. Technol.*; 2006; 40(17) pp 5502 – 5507.
- Herner, J.D., Robertson, W.H., and Ayala, A. 2007. Investigation of Ultrafine Particle Number Measurements from a Clean Diesel Truck using the European PMP Protocol. SAE technical paper 2007-01-1114.
- Ibald-Mulli, A., Wichmann, H.E., Kreyling, W., Peters, A. 2002. Epidemiological evidence on health effects of ultrafine particles. *J. Aerosol Med. – Dep. Clear. Effect Lung.* 15(2): 189-201.
- Johnson, T., Caldow, R., Pocher, A., Mirme, A. and Kittelson, D. 2004. A New Electrical Mobility Particle Sizer Spectrometer for Engine Exhaust Particle Measurements. SAE technical Paper No. 2004-01-1341.
- Kasper, M. The Number Concentration of Non-Volatile Particles - Design Study for An Instrument According to the PMP Recommendations. *SAE Technical Paper.* 2004-01-0960
- Khalek, I.A. 2005. 2007 Diesel Particle Measurement Research. SwRI Final Report No. 03.10415 to the Coordinating Research Council under project E-66-Phase 1, May.
- Khalek, I.A. 2006. 2007 Diesel Particle Measurement Research. SwRI Final Report No. 03.10415 to the Coordinating Research Council under project E-66-Phase 2, March.
- Khalek, I.A. 2007. 2007 Diesel Particle Measurement Research. SwRI Final Report No. 03.10415 to the Coordinating Research Council under project E-66-Phase 3, September.

Kimura, K., Alleman, T.L., Chatterjee, S., and Hallstrom, K. (2004) Long-Term Durability of Passive Diesel Particulate Filters on Heavy-Duty Vehicles. SAE Technical Paper No. 2004-01-0079.

Kittelson, D., T. Hands, C. Nickolaus, N. Collings, V. Niemelä, and M. Twigg, 2004. “Mass Correlation of Engine Emissions with Spectral Instruments,” JSAE paper number 20045462.

Kittelson, D. B., W. F. Watts, J. C. Savstrom, J. P. Johnson, 2005. “Influence of Catalytic Stripper on Response of PAS and DC,” *Journal of Aerosol Science* 36 1089–1107.

Kittelson, D. B., W. F. Watts, J. P. Johnson, C. Rowntree, M. Payne, S. Goodier, C. Warrens, H. Preston, U. Zink, M. Ortiz, C. Goersmann, M. V. Twigg, A. P. Walker, and R. Caldow. 2006. On-Road Evaluation of Two Diesel Exhaust Aftertreatment Devices, *Journal of Aerosol Science*, v 37, n 9, September, 2006, p 1140-1151.

Kittelson, D. B. (2008) personal communication regarding on-going studies at the University of Minnesota.

Lehmann, U., Niemela, V., and Mohr, M. 2004. New Methods for Time-Resolved Diesel Engine Exhaust Particle Mass Measurement. *Environ. Sci. Technol.*, vol 38, pp. 5704 – 5711.

Matter, U., Siegmann, H.C., and Burtscher, H. 1999. Dynamic Field Measurements of Submicron Particles from Diesel Engines. *Environ. Sci. Technol.*, vol. 33, pp. 1946-1952.

Miller, J.W., Johnson, K., Durbin, T.D., and Cocker, D.R. (2007) Measurement Allowance Project – On-Road Validation. Final Report to the Measurement Allowance Steering Committee. August.

Mohr, Martin. Evaluation of a Particle Number Measurement Procedure. 2005. UNECE Working paper No. GRPE-PMP-15-3

Oberdorster, G. 2001. Pulmonary effects of inhaled ultrafine particles. *International Archives of Occupational and Environmental Health*. 74(1): 1-8.

Peters, A., Wichmann, H.E., Tuch, T., Heinrich, J., Heyder, J. 1997. Respiratory effects are associated with the number of ultrafine particles. *American Journal of Respiratory and Critical Care Medicine*. 155(4): 1376-1383.

Pope, C.A., Burnett, R.T., Thun, M.J., Calle, E.E., Krewski, D., Ito, K, Thurston, G.D. 2002. Lung cancer, cardio-pulmonary mortality, and long term exposure to fine particulate air pollution. *Journal of the American Medical Association*. 287(9): 1132-1141.

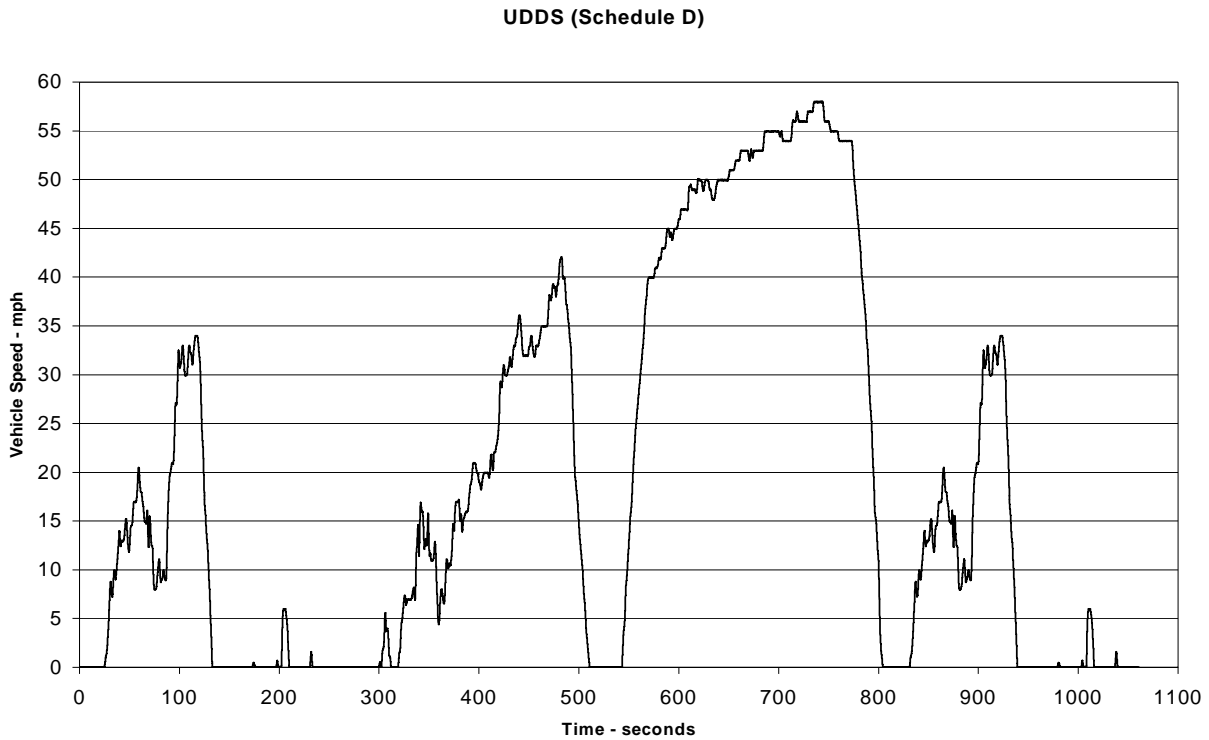
Reavell, K., T. Hands, and N. Collings, 2002. “A Fast Response Particulate Spectrometer for Combustion Aerosols,” SAE paper 2002-01-2714.

Shah, S. and Cocker, D.R. 2005. A Fast Scanning Mobility Particle Spectrometer for Monitoring Transient Particle Size Distributions. *Aersol Sci. Technol.*, vol. 39, 519-526.

Appendix A – Test Cycles

UDDS

Federal heavy-duty vehicle Urban Dynamometer Driving Schedule (UDDS) is a cycle commonly used to collect emissions data on engines already in heavy, heavy-duty diesel (HHD) trucks. The test cycle is a transient test cycle with a short cruise section, and hence exercises both the test vehicle and the PMP system over a fairly wide range of operation. This cycle covers a distance of 5.55 miles with an average speed of 18.8 mph and maximum speed of 58 mph.



The European ETC cycle

The ETC test cycle (also known as FIGE transient cycle) has been introduced, together with the [ESC](#) (European Stationary Cycle), for emission certification of heavy-duty diesel engines in Europe starting in the year 2000 (*Directive [1999/96/EC](#) of December 13, 1999*). The ESC and ETC cycles replace the earlier [R-49](#) test.

The ETC cycle has been developed by the [FIGE](#) Institute, Aachen, Germany, based on real road cycle measurements of heavy duty vehicles (*FIGE Report 104 05 316, January 1994*). The final ETC cycle is a shortened and slightly modified version of the original FIGE proposal.

Different driving conditions are represented by three parts of the ETC cycle, including urban, rural and motorway driving. The duration of the entire cycle is 1800s. The duration of each part is 600s.

- Part one represents city driving with a maximum speed of 50 km/h, frequent starts, stops, and idling.
- Part two is rural driving starting with a steep acceleration segment. The average speed is about 72 km/h
- Part three is motorway driving with average speed of about 88 km/h.

FIGE Institute developed the cycle in two variants: as a chassis and an engine dynamometer test. Vehicle speed vs. time over the duration of the cycle is shown in Figure A-2.

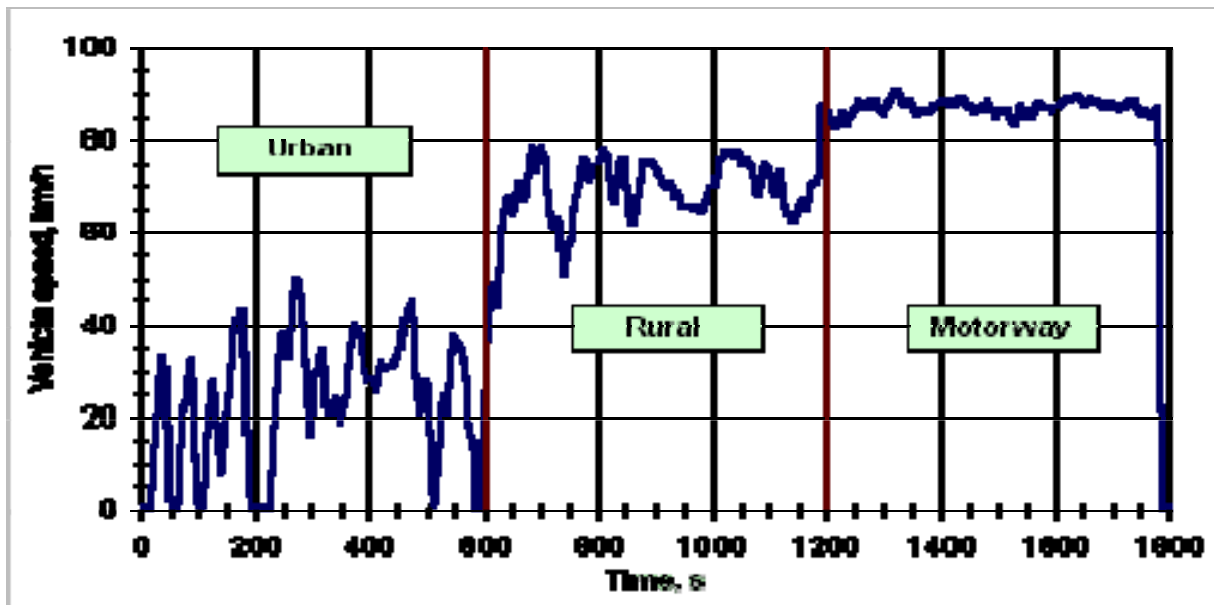
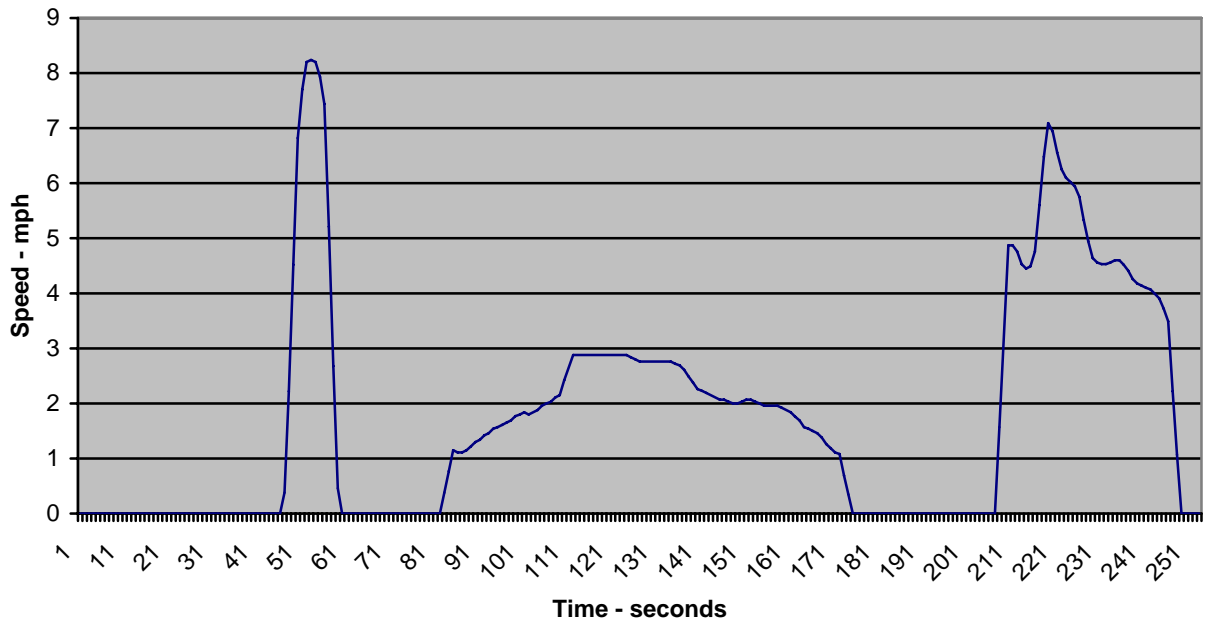


Figure A-2. ETC Transient Cycle - Vehicle Speed

CARB Creep Cycle

The CARB Creep Cycle is the second segment of the CARB 4-mode test cycle. The creep cycle represents driving in heavily congest freeway traffic. This cycle covers a distance of 0.12 miles over a period of 253 seconds with an average speed of 1.8 mph.

HHDDT Creep mode cycle



Appendix B – Time Response Experiments with PMP System

An experiment was conducted to evaluate the time response of PMP system in sampling from the primary dilution tunnel. The interest was in seeing how the MD-19 system 'averages' the real time particle count signal (i.e. measurements taken below our PMP look like moving averages of measurements taken in the tunnel). For this experiment, two 3025A CPCs were utilized, with one sampling from the primary dilution tunnel, and the other sampling below the PMP system. For this experiment, a vehicle with a new DPF was utilized, so no nucleation was observed (see Herner et al., 2007). This allowed a direct comparison of the concentrations in the CVS to those below the PMP, without the complication of losing nucleation particles through the PMP system.

CONCLUSION – In general, it was found that the PMP sampling train time averaged or broadened the signal in the real-time, but this does not affect the time integrated particle counts.

Test Set-up

The parameters for the test set-up were as follows:

PMP Settings: PND1 = 23 @150°C, ET = 300°C, PND2 = 10 for a total dilution of 230 compared to the CVS.

3025_PMP - CPC 3025A (size cut 3nm) measuring particle count below PMP

3025_CVS - CPC 3025A (size cut 3nm) measuring particle count in the CVS

Test Vehicle - Isuzu MHDD with CRT aftertreatment

Test Cycle – The Central Business District (CBD), which consists of 14 repeated accelerations to 20mph, as illustrated below.

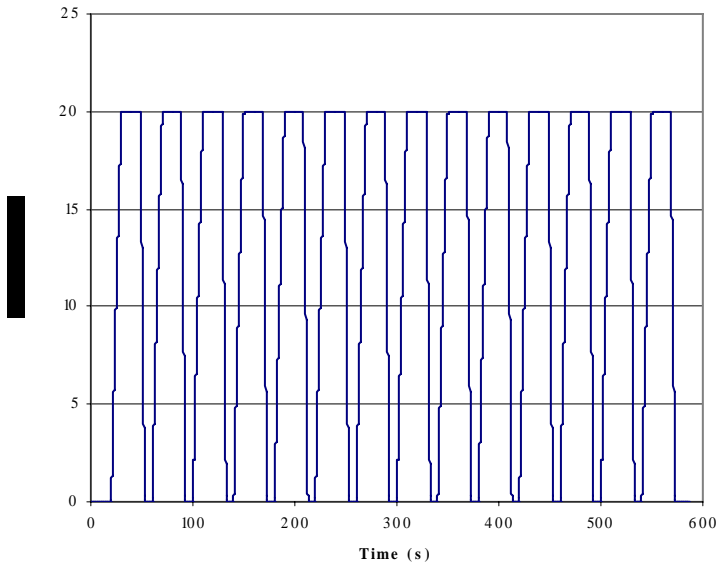


Figure B-1. CBD Cycle Speed-Time Trace

Figure B-2 shows particle count data for the entire test sequence, consisting of a 30min warm up at 50 mph followed by 3 back to back runs of the CBD cycle.

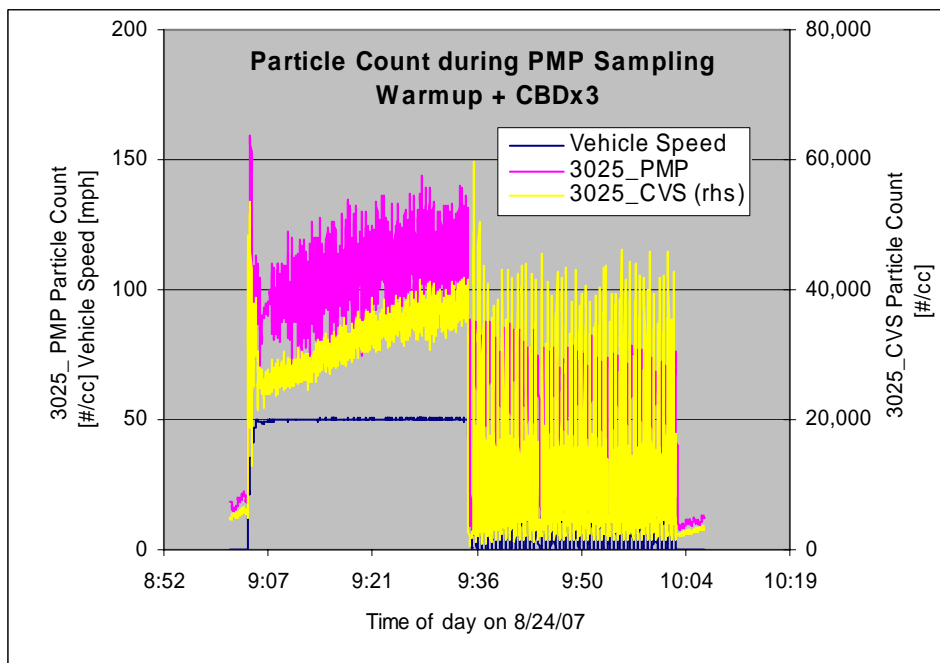


Figure B-2. Particle Counts for the Full Test Sequence with a 50 mph warm-up and 3 back-to-back CBDs

Figure B-3 provides a closer look at the particle counts during one of the typical CBD sequences. This graph shows a 5 minute segment of the CBD. The 3025_CVS particle count nicely correlates with the operation behavior for the truck engine. On each acceleration to 20 mph, two

gear shifts are visible followed by the steady state particle emissions during the short 20mph cruise. This level of resolution is not seen in the 3025_PMP data due to the averaging effect of the MD-19 PMP setup.

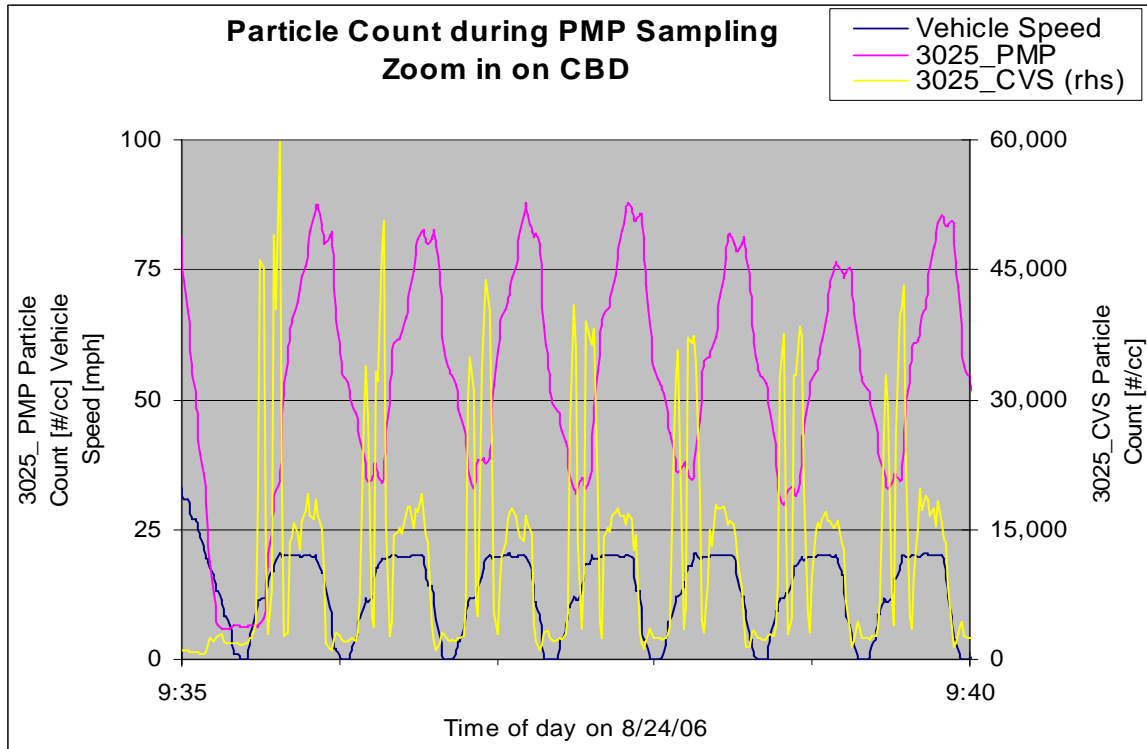


Figure B-3. Particle Counts for a 5 Minute Segment of the CBD

In Figure B-4, you see the PMP dilution setpoint (230) in pink, and the ratio of the concentration from the 3025_PMP and 3025_CVS in blue. Since this vehicle does not have a nucleation mode with a large fraction of volatile particles, this ratio is expected to remain constant. During the first segment of driving with a cruise at 50 mph from ~9:00 to 9:30, the ratio of the particle concentrations between the two instruments remains the same as that of the dilution ratio, consistent with expectations. During the second segment of driving, from ~9:35 to 10 AM, a more transient CBD was run. During this segment, the concentration ratio between the CPC in the CVS and that below the PMP changes, consistent with the observations in Figure B-3 that the CPC below the PMP sees a delayed response, and hence the concentration peaks and valleys for the instruments at the two locations are seen at different times.

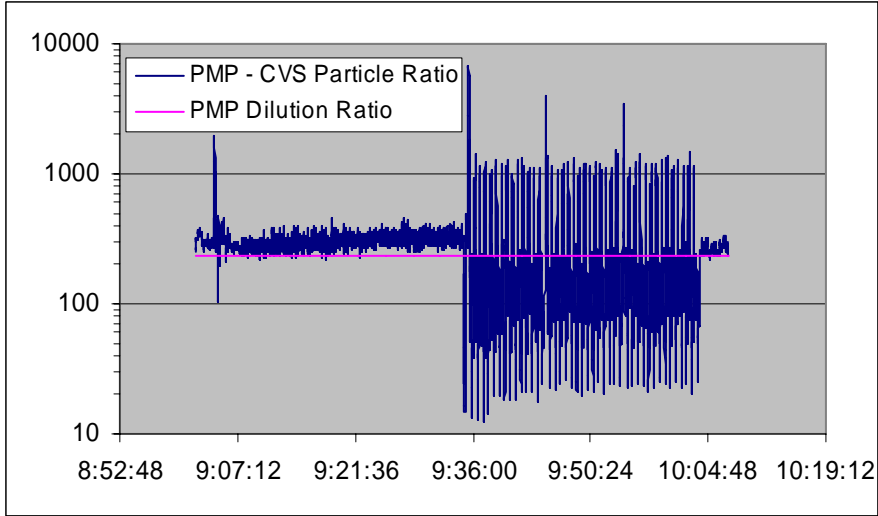
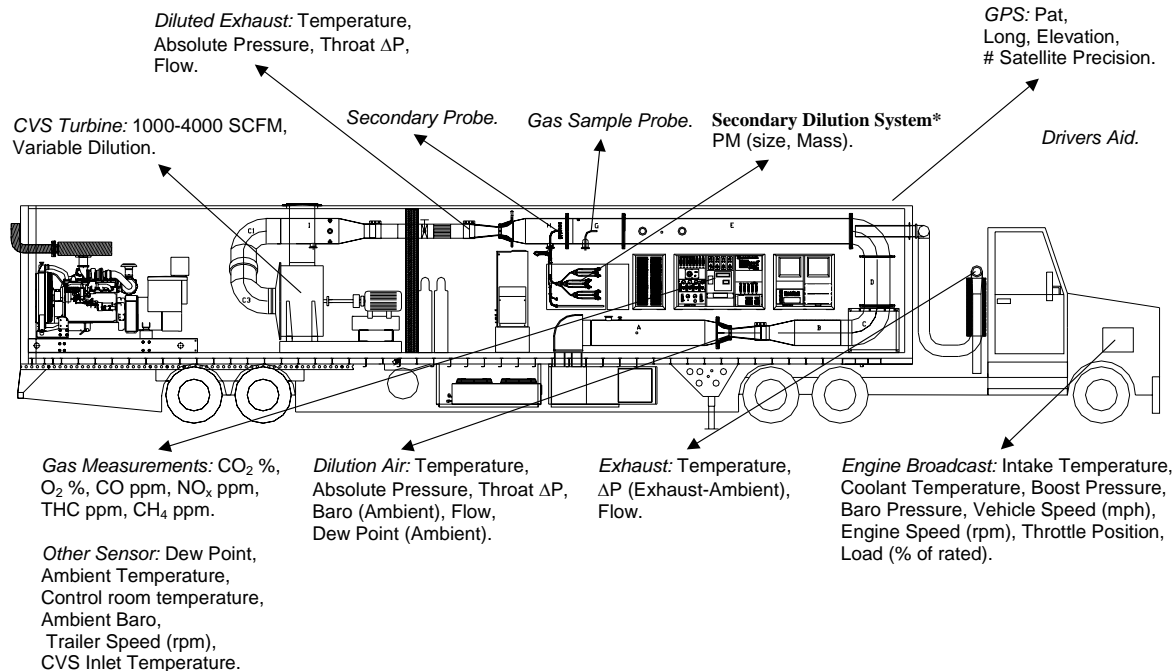


Figure B-4. Dilution Ratio Comparisons

Appendix C – Background Information on UCR’s Mobile Emission Lab

Extensive detail is provided in (Cocker, et al., 2004a,b) so this section is provided for those that may not have access to that reference. Basically the mobile emissions lab (MEL) consists of a number of operating systems that are typically found in a stationary lab. However the MEL lab is on wheels instead of concrete. A schematic of MEL and its major subsystems is shown in the figure below. Some description follows.



Major Systems within the Mobile Emission Lab

The primary dilution system is configured as a full-flow constant volume sampling (CVS) system with a smooth approach orifice (SAO) venturi and dynamic flow controller. The SAO venturi has the advantage of no moving parts and repeatable accuracy at high throughput with low-pressure drop. As opposed to traditional dilution tunnels with a positive displacement pump or a critical flow orifice, the SAO system with dynamic flow control eliminates the need for a heat exchanger. Tunnel flow rate is adjustable from 1000 to 4000 scfm with accuracy of 0.5% of full scale. It is capable of total exhaust capture for engines up to 600 hp. Colorado Engineering Experiment Station Inc. initially calibrated the flow rate through both SAOs for the primary tunnel.

The mobile laboratory contains a suite of gas-phase analyzers on shock-mounted benches. The gas-phase analytical instruments measure NO_x, methane (CH₄), total hydrocarbons (THC), CO, and CO₂ at a frequency of 10 Hz and were selected based on optimum response time and on road stability. The 200-L Tedlar bags are used to collect tunnel and dilution air samples over a complete test cycle. A total of eight bags are suspended in the MEL allowing four test cycles to

be performed between analyses. Filling of the bags is automated with Lab View 7.0 software (National Instruments, Austin, TX). A summary of the analytical instrumentation used, their ranges, and principles of operation is provided in the table below. Each modal analyzer is time-corrected for tunnel, sample line, and analyzer delay time.

Gas Component	Range	Monitoring Method
NO _x	10/30/100/300/1000 (ppm)	Chemiluminescence
CO	50/200/1000/3000 (ppm)	NDIR
CO ₂	0.5/2/8/16 (%)	NDIR
THC	10/30/100/300/1000 & 5000 (ppmC)	Heated FID
CH ₄	10/30/100/300/1000 & 5000 (ppmC)	Heated FID

Summary of gas-phase instrumentation in MEL



Photograph of MEL during Testing

Appendix D – A General Description of the Locations for the Off-Road Testing



Figure D-1. Generic Map of Greater Los Angeles Area including the Riverside, Palm Springs, and Indio Areas.

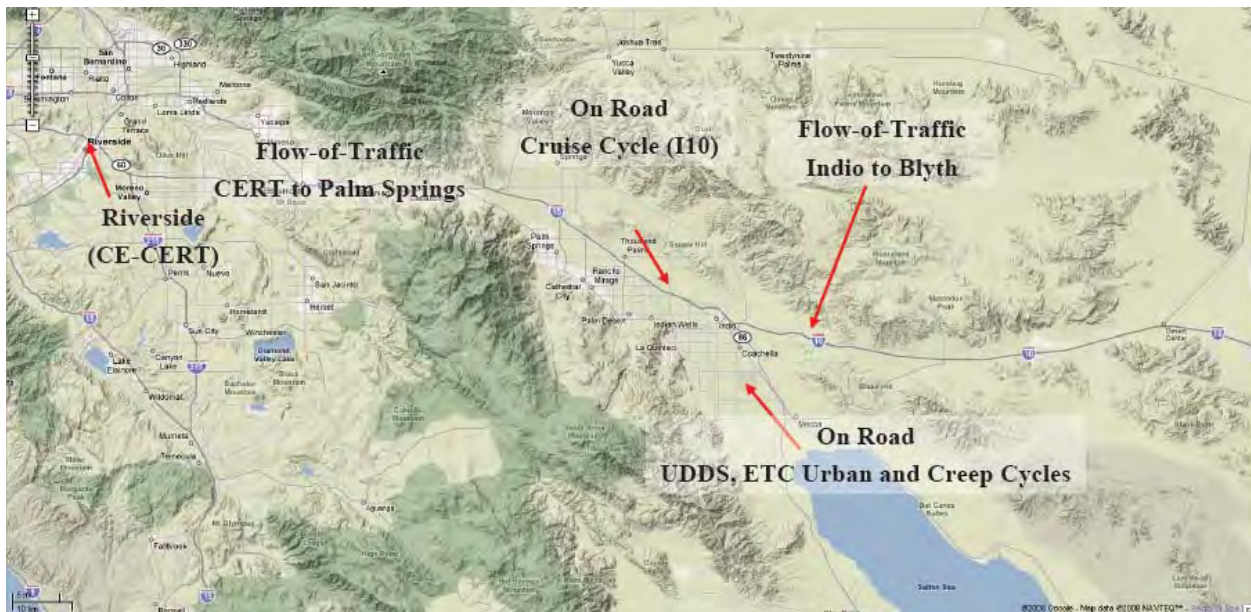


Figure D-2. Map of Greater Riverside, Palm Springs, and Indio Areas Showing Locations for Various On-Road Cycle and Flow-of-Traffic Test Runs were conducted.

Appendix E – Quality Assurance/Quality Control

Internal calibration and verification procedures are performed regularly in accordance with the CFR. A partial summary of routine calibrations performed by the MEL as part of the data quality assurance/quality control program is listed in Table E-1. The MEL uses precision gas blending to obtain required calibration gas concentrations. Calibration gas cylinders, certified to 1 %, are obtained from Scott-Marrin Inc. (Riverside, CA). By using precision blending, the number of calibration gas cylinders in the lab was reduced to 5 and cylinders need to be replaced less frequently. The gas divider contains a series of mass flow controllers that are calibrated regularly with a Bios Flow Calibrator (Butler, New Jersey) and produces the required calibration gas concentrations within the required ± 1.5 percent accuracy.

In addition to weekly propane recovery checks which yield >98% recovery, CO₂ recovery checks are also performed. A calibrated mass of CO₂ is injected into the primary dilution tunnel and is measured downstream by the CO₂ analyzer. These tests also yield >98% recovery. The results of each recovery check are all stored in an internal QA/QC graph that allows for the immediate identification of problems and/or sampling bias.

Table E-1. Summary of Routine Calibrations

EQUIPMENT	FREQUENCY	VERIFICATION PERFORMED	CALIBRATION PERFORMED
CVS	Daily	Differential Pressure	Electronic Cal
	Daily	Absolute Pressure	Electronic Cal
	Weekly	Propane Injection	
	Monthly	CO ₂ Injection	
	Per Set-up Second by second	CVS Leak Check Back pressure tolerance ±5 inH ₂ O	
Cal system MFCs	Annual	Primary Standard	MFCs: Drycal Bios Meter
	Monthly	Audit bottle check	
Analyzers	Pre/Post Test		Zero Span
	Daily	Zero span drifts	
	Monthly	Linearity Check	
Secondary System Integrity and MFCs	Semi-Annual	Propane Injection: 6 point primary vs. secondary check	MFCs: Drycal Bios Meter & TSI Mass Meter
	Semi-Annual		
Data Validation	Variable	Integrated Modal Mass vs. Bag Mass	
	Per test	Visual review	
PM Sample Media	Weekly	Trip Tunnel Banks	
	Monthly	Static and Dynamic Blanks	
Temperature	Daily	Psychrometer	Performed if verification fails
Barometric Pressure	Daily	Aneroid barometer ATIS	Performed if verification fails
Dewpoint Sensors	Daily	Psychrometer Chilled mirror	Performed if verification fails

Appendix F – CPC Chamber Calibration Experiment and Pseudo Span Results from the On-Road Testing

Pseudo Span Checks

During the on-road testing, a pseudo span check was performed on the CPCs each morning. A pseudo span value was performed by letting each CPC sample from the control room simultaneously. The inlet tube was removed from each CPC so it was sampling directly from the control room. The pseudo span value was allowed to stabilize and recorded. Figure F-1 shows the pseudo span values for each day of testing. The pseudo spans show some variation over the course of the 5 tests days, but this is likely due to changes in the surrounding ambient environment. The 3025s also showed some divergence from the other CPCs on a few days (6/13 and 6/14), but no unusual trends were found in the actual emissions test data for those days.

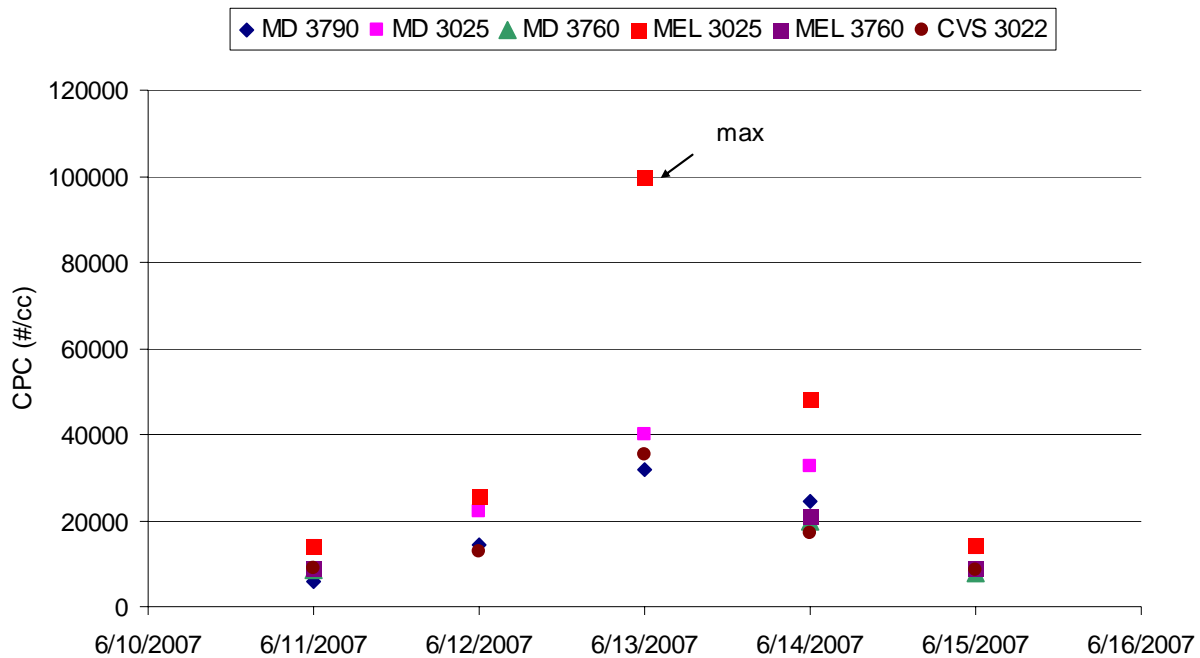


Figure F-1. CPC start up control room concentration values (pseudo daily span check). (CPC MEL 3760A corrected for flow 1.0 vs. 1.5 lpm)

Atmospheric Chamber Calibration Check

A separate experiment was conducted to evaluate the calibration on the various particle number count and sizing instruments utilized in the on-road measurements. The experiment was conducted in CE-CERT's atmospheric chamber, which can be used to readily create and characterize particles with well defined characteristics. The particles were created by injecting a hydrocarbon particle precursor into the chamber and initiating nucleation with the chamber light source. This procedure created nice, nearly spherical particles with a nominal size between 70 and 170 nm, which is above all of the cut-off diameters for the utilized CPCs. A nominal size distribution for one of the sample runs is provided in Figure F-2. One disadvantage of the experimental set-up was that the experiments were conducted at low pressures, such that a long time was required for sampling.

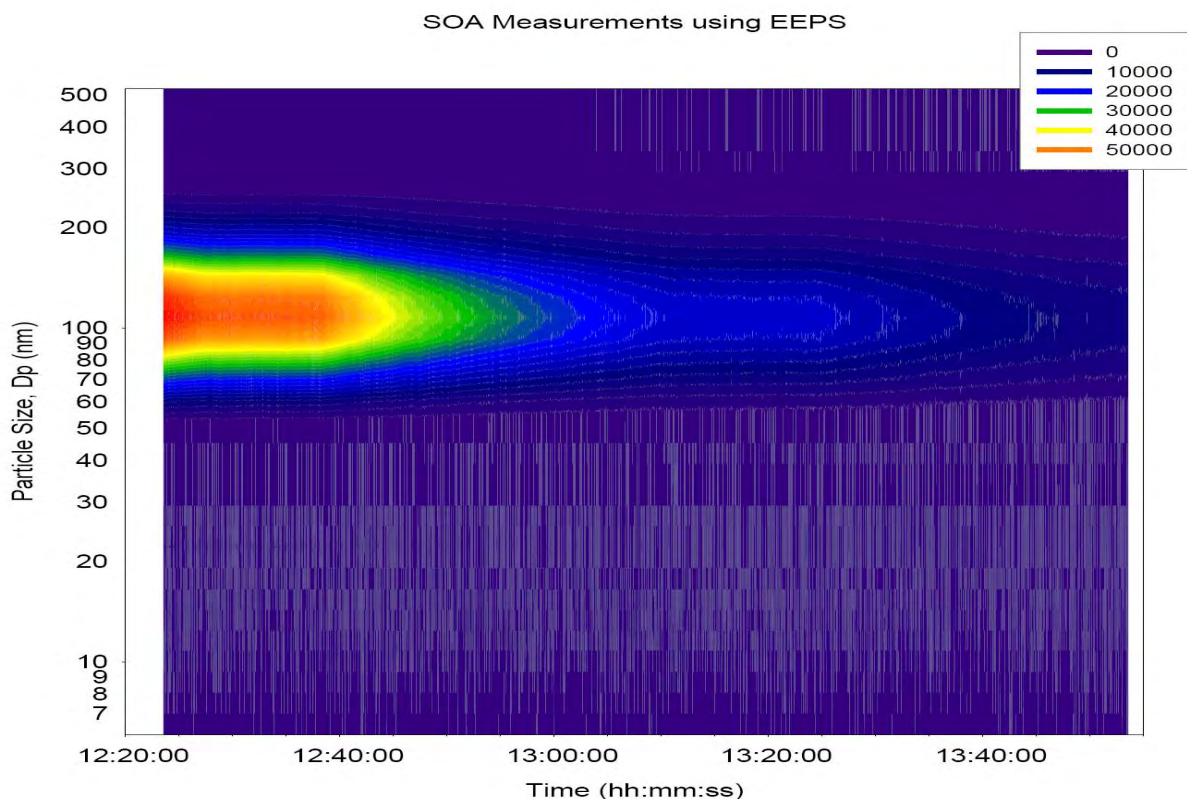


Figure F-2. fSMPS Size distribution of the particle calibration source on all the CPC's, EEPS, and fSMPS $dN/d\log(D_p)$

Particle number comparisons were made over a range in particle number concentrations from 1.2×10^3 particles/cc to 6×10^4 particles/cc. The resulting calibration correlation for each of the CPCs is presented in Figure F-3 and F-4, where the MD-19 3025A CPC is used the reference CPC. It should be noted that the 3760A and 3790 instruments are limited to a maximum concentration of 10^4 /cc, and hence were not included in the higher concentration measurements. Although there are some differences between the different CPCs, overall, the data show good comparability between CPCs used in the experiments.

A regression was performed and a standard error of estimate was made for each instrument over the concentration range. The standard error of estimate (SEE) provides a statistical measure of the error about a least squares regression line. The correlation coefficients for the 3790 was 0.9998 and had a standard error of estimate of 54 #/cc over the reduced range of calibration data. The 3025A's showed a higher correlation of 0.99998 with a standard error of estimate of 236 #/cc for all the data and 69 #/cc for data below 10^4 #/cc. The lowest correlation and highest standard error estimate was from the two 3760A CPCs. The MD19 3760A correlations was around 0.98 with a standard error of estimate of 355 #/cc for data below 10^4 #/cc. The MEL 3760A had a higher correlation of 0.9998 and a lower standard error of estimate of 51 #/cc than the MD19 3760A.

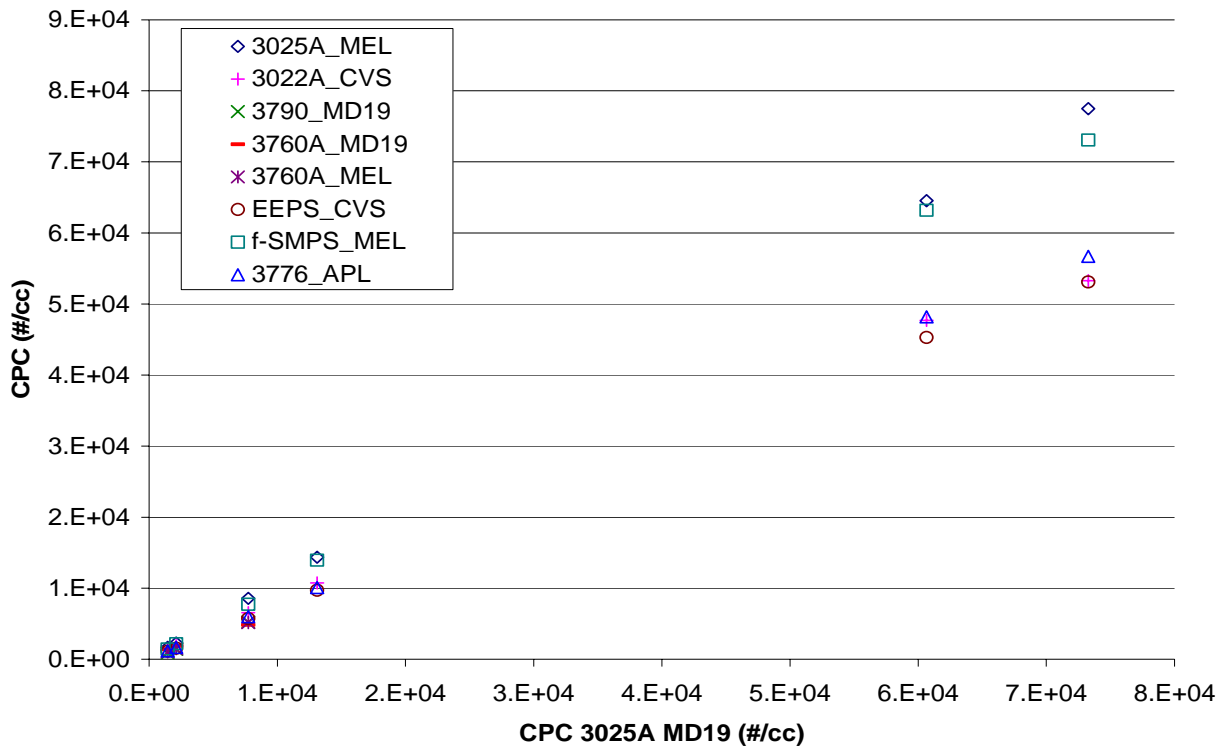


Figure F-3. Particle number response from all CPC, EEPS and f-SMPS instruments above 10⁴

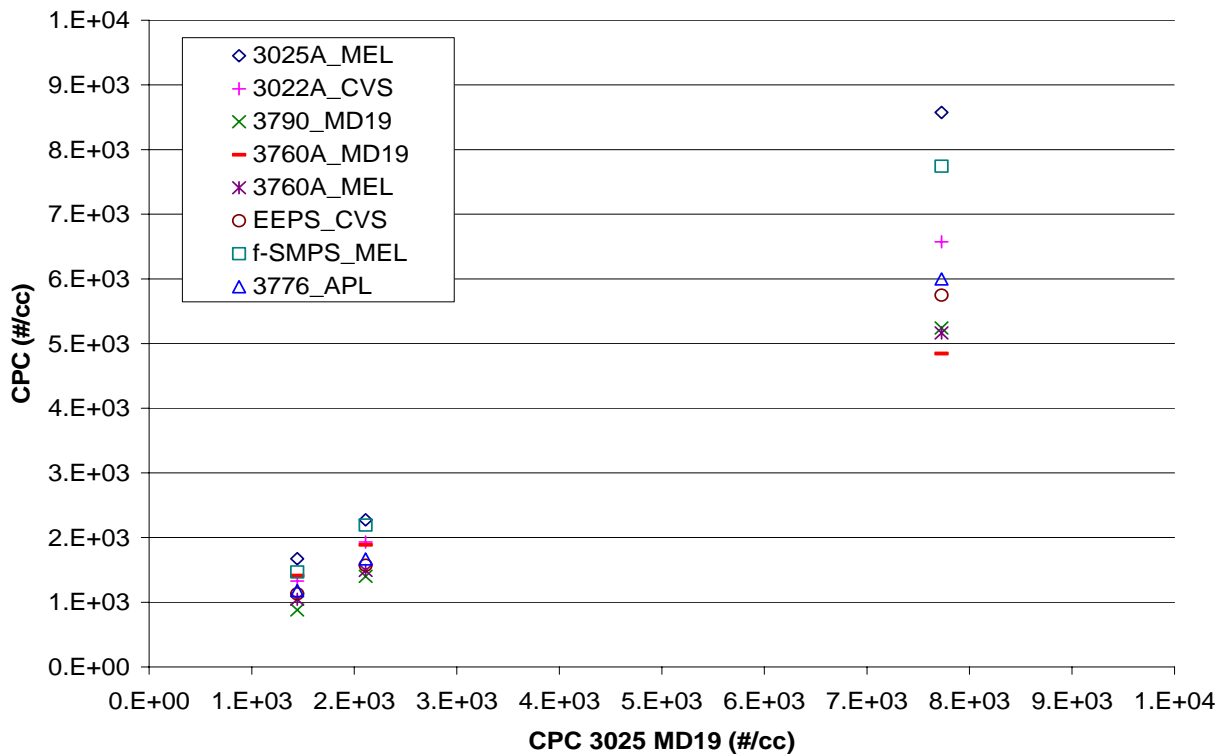


Figure F-4. Particle number response from all CPC, EEPS and f-SMPS instruments below 10⁴

If you take the standard error estimate and divide by each calibration point you get a feel for the associated error at that measurement. The percent error of each point ranged from less than 1% to as much as 25%. The 3776 instrument, which remained in the chamber, had the lowest SEE/span ratio at less than 1%. The SEE/span ratios for the other instruments were on average as follows: 5% for the 3790, 5% for the 3022A, 4% for the 3025A, 20% for the MD19 3760A, and 4% for the MEL 3760A. Note these averages were based on only data below 10^4 #/cc. For the CPCs capable of measuring above 10^4 #/cc, their average SEE/span ratios tended to be lower at concentration levels above 10^4 #/cc.

The particle concentrations utilized in this calibration exercise were above the levels found in the on-road test experiments. For the 3790, the maximum concentration for the on-road driving cycle tests was 100 particles/cc. For the 3025A, the concentration levels were typically between 500~1000 particles/cc for the on-road driving cycle tests, with peaks in particle concentration of 6000 particles/cc when there was nucleation. The 3022 saw a wider range of particle number concentrations since it was less diluted in the primary tunnel and also observed the semi-volatile nucleation mode. It is suggested that further experiments at a much lower concentration may be of value. During the flow of traffic on-road tests, on the other hand, concentrations levels for all CPCs were orders of magnitude higher than this calibration data.

Appendix G – Additional Test Data for the Chassis Dynamometer Testing Portion of the Study

Size Distribution Data

The size distribution results for individual tests for the UDDS and Cruise cycle, respectively, are shown in Figure G-1 and Figure G-2. The size distributions in terms of $dV/D\log D_p$ are provided in figure G-3 for the UDDS and Figure G-4 for the Cruise. These plots show a bi- or tri-modal distribution of particles is possible, with the possibility of some particle mass in the coarse mode.

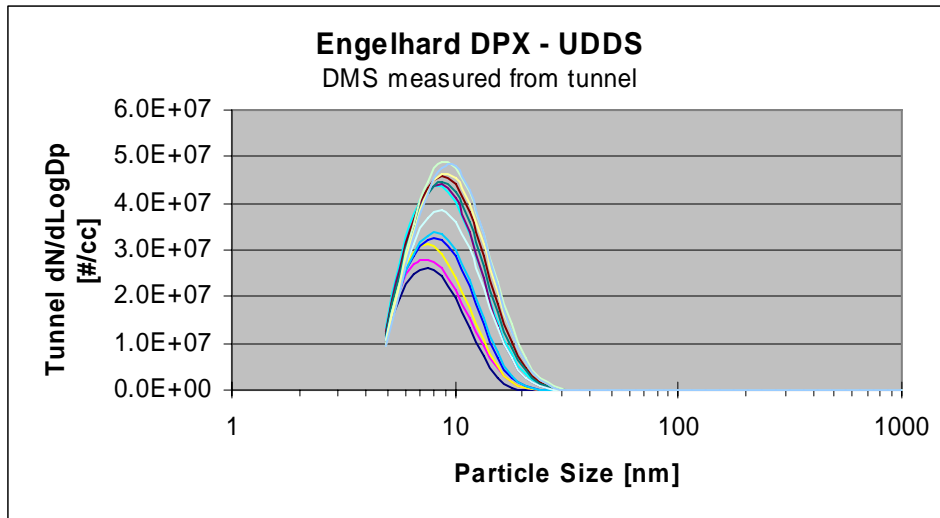


Figure G-1. Size Distributions for Individual Tests for UDDS tests ($dN/d\log D_p$).

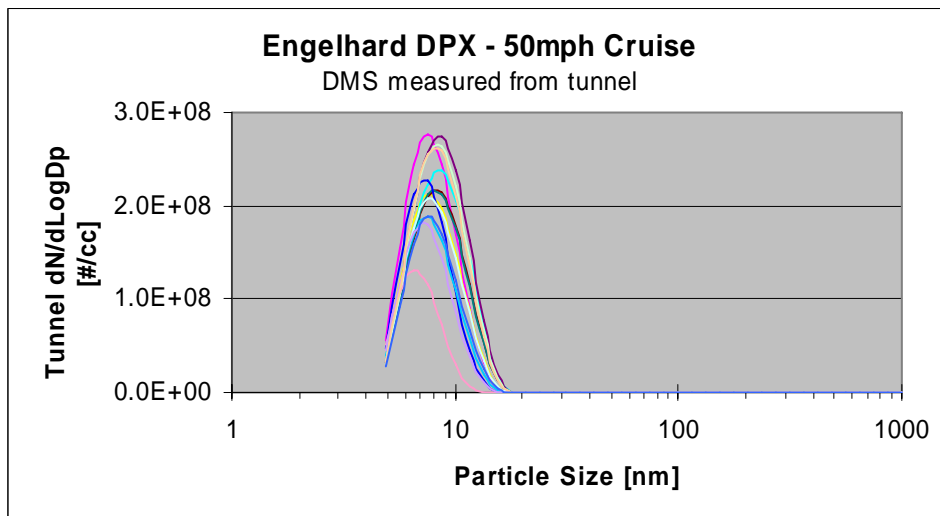


Figure G-2. Size Distributions for Individual Tests for Cruise tests ($dN/d\log D_p$).

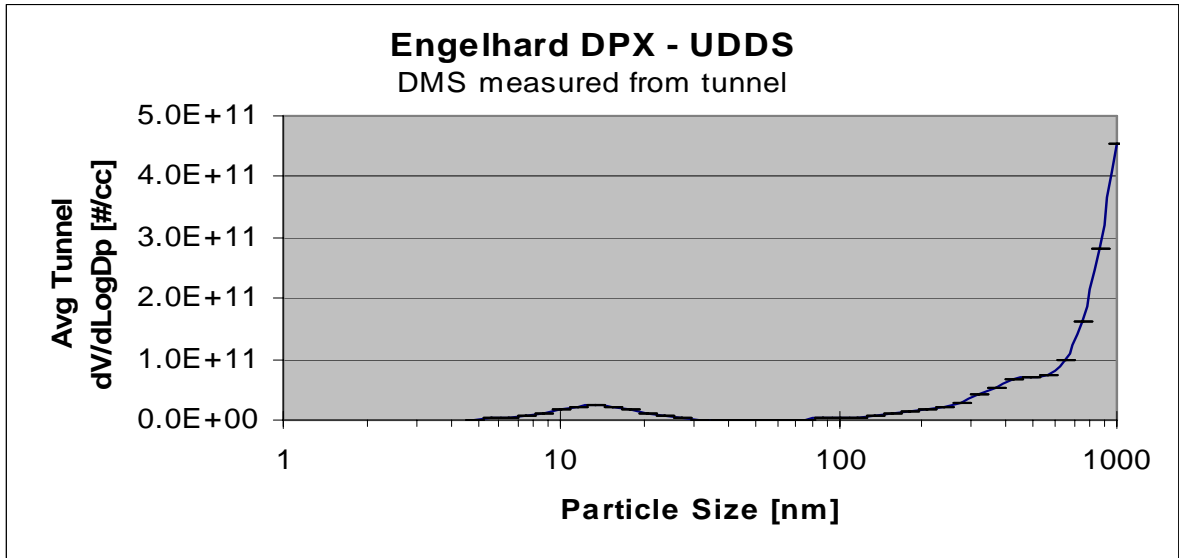


Figure G-3. Average Size Distribution for UDDS tests ($dV/d\text{LogDp}$).

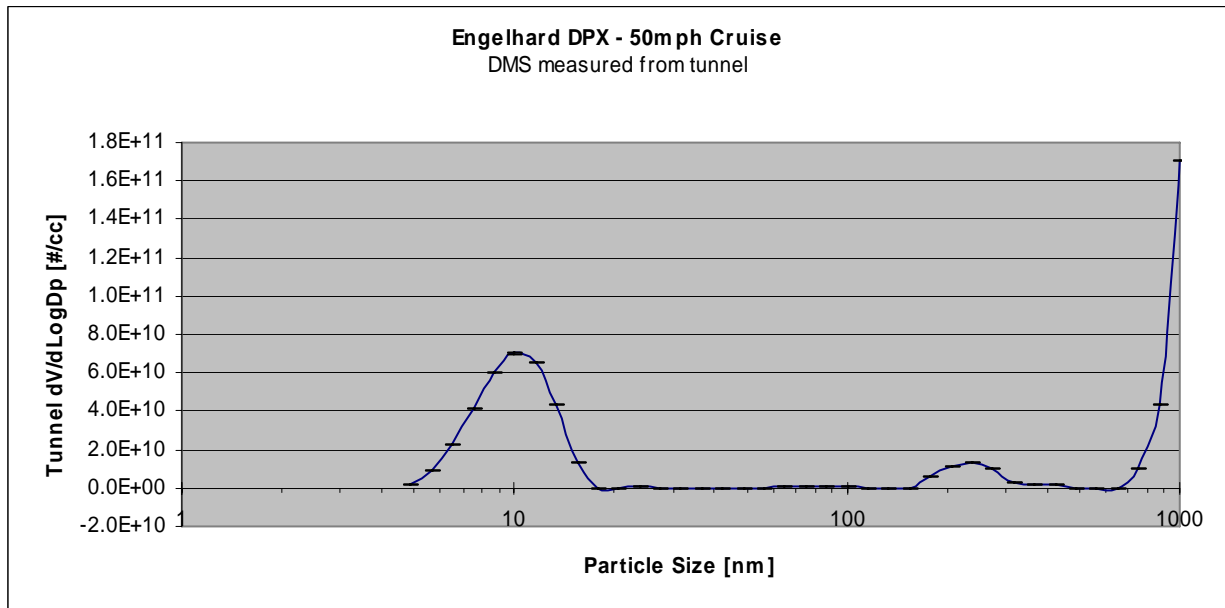


Figure G-4. Average Size Distribution for Cruise tests ($dV/d\text{LogDp}$).

PAS Real-Time Data

The real-time data for the Photoelectric Aerosol Detector (PAS) is presented in Figure G-5 for a 2x UDDS cycle. The PAS is designed to measure particle bound PAH's and soot, with a greater response to PAH's. In ambient applications, its output is considered synonymous with particle bound PAHs. For the UDDS cycle, the PAS signal varies from approximately 3 to 35 femtoamps

(fA) throughout the cycle. Interestingly, the PAS shows peaks for some of the intermediate hills, but not for the highest speed peak.

Although the PAS signal is optimized for measurement of PAHs, the only thing the PAS signal correlates to is the emissions of 190 nm particles, as measured with the EEPS directly from the tunnel, suggesting a correlation with soot. Interestingly, the correlation does not hold when higher emissions of 190 nm particles are observed at the high temperature parts of the cycle when nucleation is occurring.

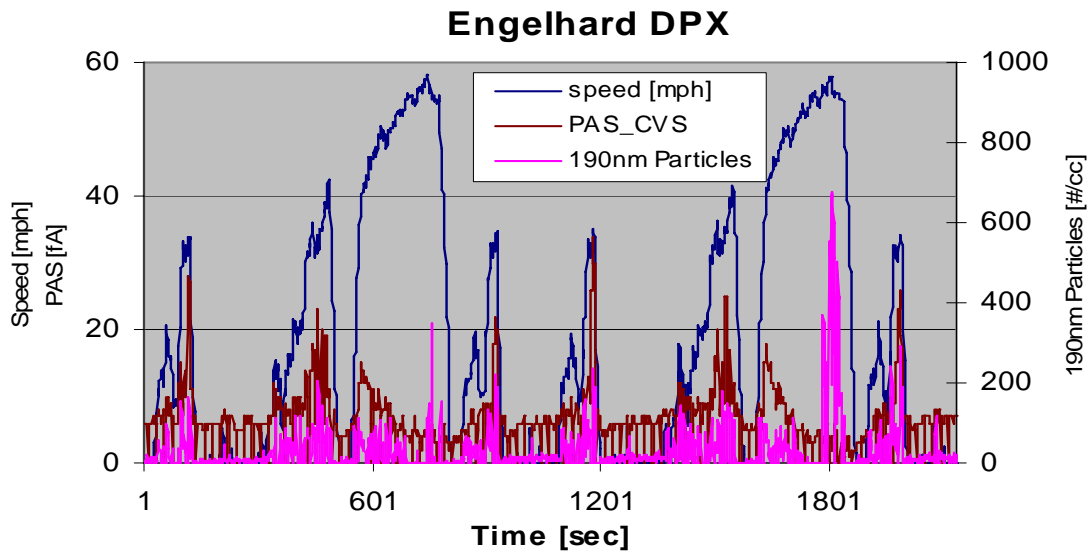


Figure G-5. Real-Time Particle Count Data for the PAS and 190 nm EEPS signal over a UDDS 2x.

Real-time PAS data for a series of 50 mph cruise cycles conducted over a full day is presented in Figure G-6. The PAS signal for the 50 mph cruise is considerably lower than that for the UDDS, with data typically in the 2 fA or less range, over a longer sampling period. It should be noted some of the portions of the cruise daily test trace are zero points, which represent breaks between test cycles.

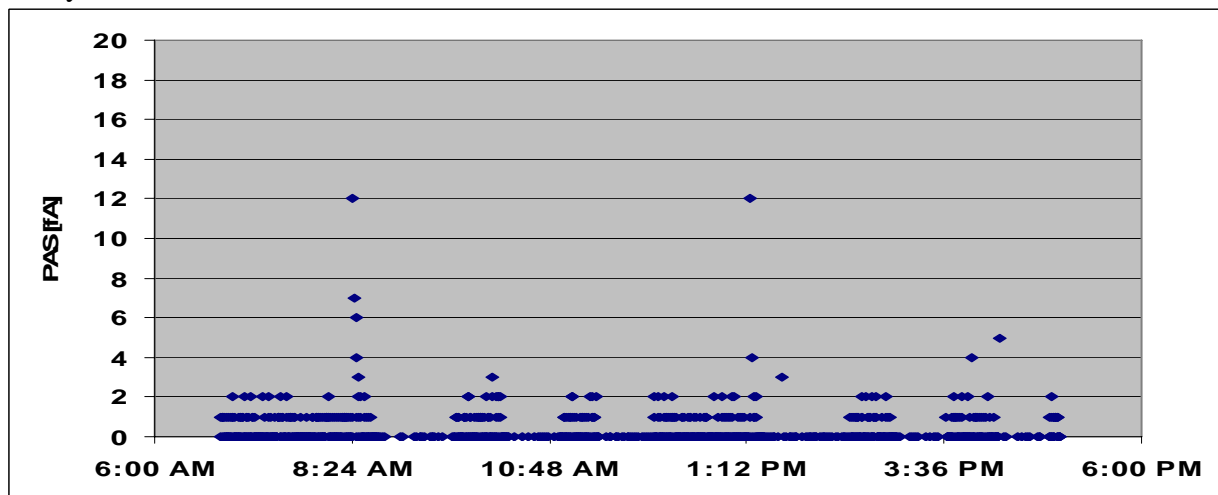


Figure G-6. Real-Time Particle Count Data for the PAS over full day of 50 mph cruises.

Appendix H – Supplemental Gas-Phase Test Results for the On-Road Testing

A summary of the gas-phase emissions results for the on-road testing is provided in Table H-1.

Table H-1. Gas-Phase and Gravimetric PM Phase Emissions Results with Standard Deviations

Cycle	count	NMHC g/mi		CO g/mi		NO _x g/mi		PM mg/mi	
		ave	stdev	ave	stdev	ave	stdev	ave	stdev
OnRoad Hills	3	0.07	0.02	0.18	0.01	19.1	3.4	26.1	n/a
OnRoad Flat	4	0.08	0.11	0.27	0.06	18.1	1.0	0.0	0.0
ETC URBAN AB	2	0.00	0.02	0.11	0.00	22.1	0.3	0.0	0.0
ETC URBAN BA	5	-0.03	0.01	0.04	0.04	18.2	0.9	-1.7	1.2
ETC CRUISE West	4	-0.01	0.00	0.16	0.03	19.0	0.3	2.2	2.2
ETC CRUISE East	3	-0.02	0.01	0.05	0.01	13.3	0.7	2.2	2.0
ARB CREEP CD	2	0.00	0.05	0.07	0.17	51.8	1.8	9.0	12.8
ARB CREEP ED	5	1.01	1.11	0.44	0.76	48.1	4.0	5.9	4.7
UDDS ABCD	4	-0.02	0.01	0.13	0.03	21.0	1.4	5.9	2.9
UDDS EDCB	4	0.08	0.11	0.23	0.14	22.4	1.2	3.8	2.6

NO_x emissions are normalized by work and fuel consumption, respectively, in Figures H-1 and H-2. The NO_x emissions for the creep cycle remain much higher than those of the other cycles when normalized by work. The creep cycle does show better comparability when normalized by fuel use, however, see Figure H-2.

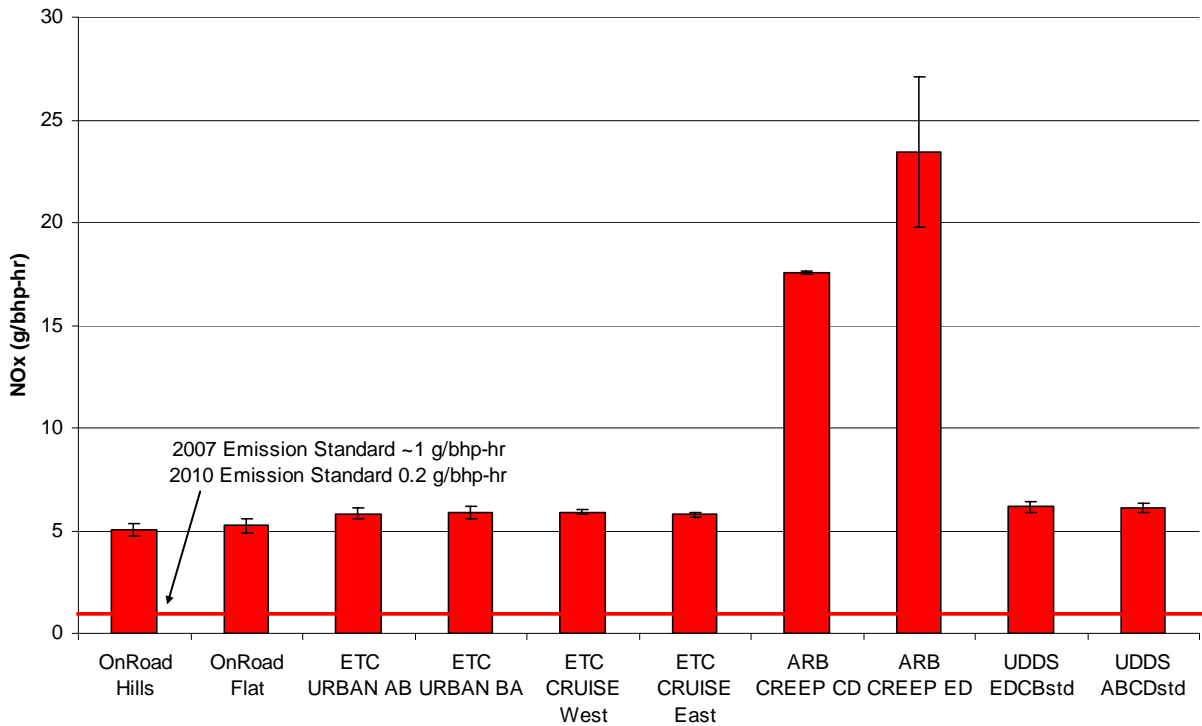


Figure H-1. NO_x Emissions Results on a g/bhp-hr basis.

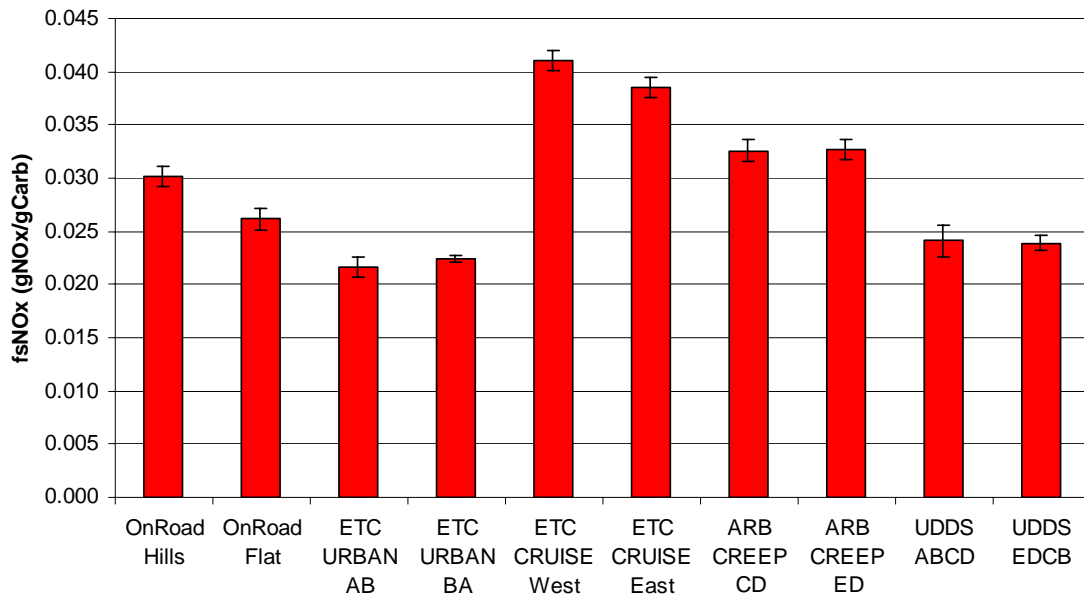


Figure H-2. Fuel specific NO_x results using carbon balance.

NMHC emissions are presented on a g/bhp-hr basis in Figure H-3. The NMHC figure is scaled based on the MEL lower detection limits since NMHC levels were very close to ambient levels. The magnitude of the scale is approximately ten times the lower detection limit for NMHC measurement at the 99% confidence level. The measurement uncertainty takes into account the subtraction of THC and CH₄ measurements with a correction for background dilution air.

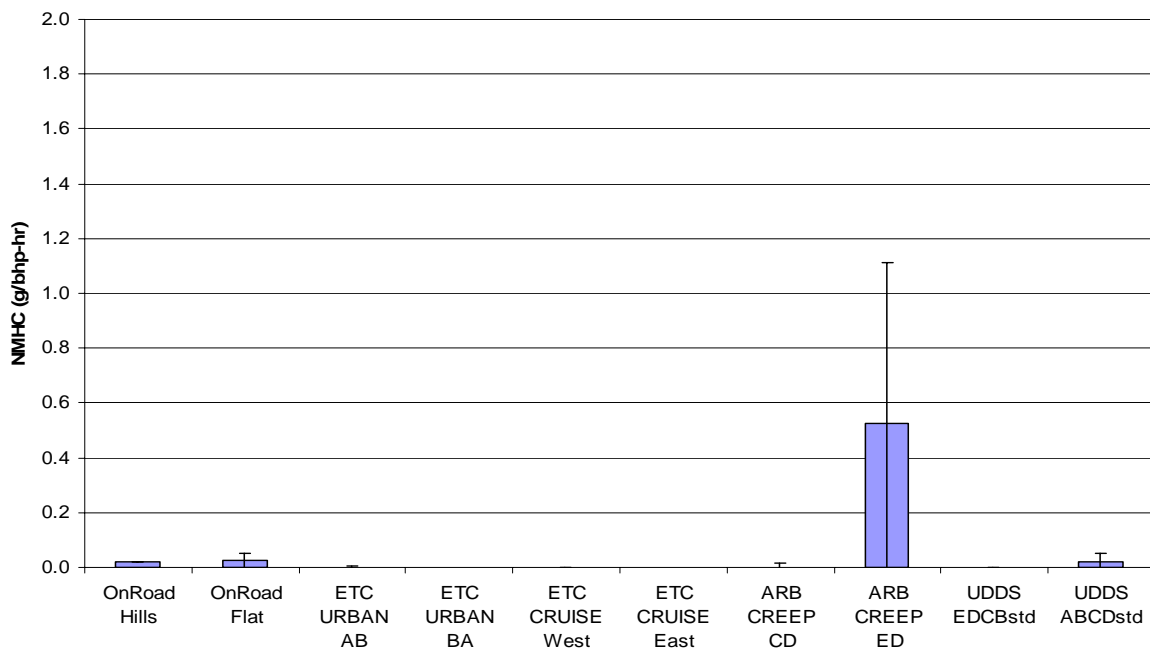


Figure H-3. NMHC Emissions Results on a g/bhp-hr basis

The high concentration and large deviation on the creep NMHC is a result of THC measurements being higher on some of the creep cycles compared to others. This can be explained in part by examining the real-time data, as shown Figure H-4. This Figure shows some spikes in the THC concentration during the first creep of a two creep sequence. This could be due to the fact that the engine is idling for a period before the start of the first creep, as preparation for the test run were being made. Thus, the engine may not have been sufficiently warmed up. CO, NO_x, CO₂ and engine load also showed differences in the initial stages of the two creep cycles, so the NMHC spike was not a result of THC measurement error, but most likely a real measured event.

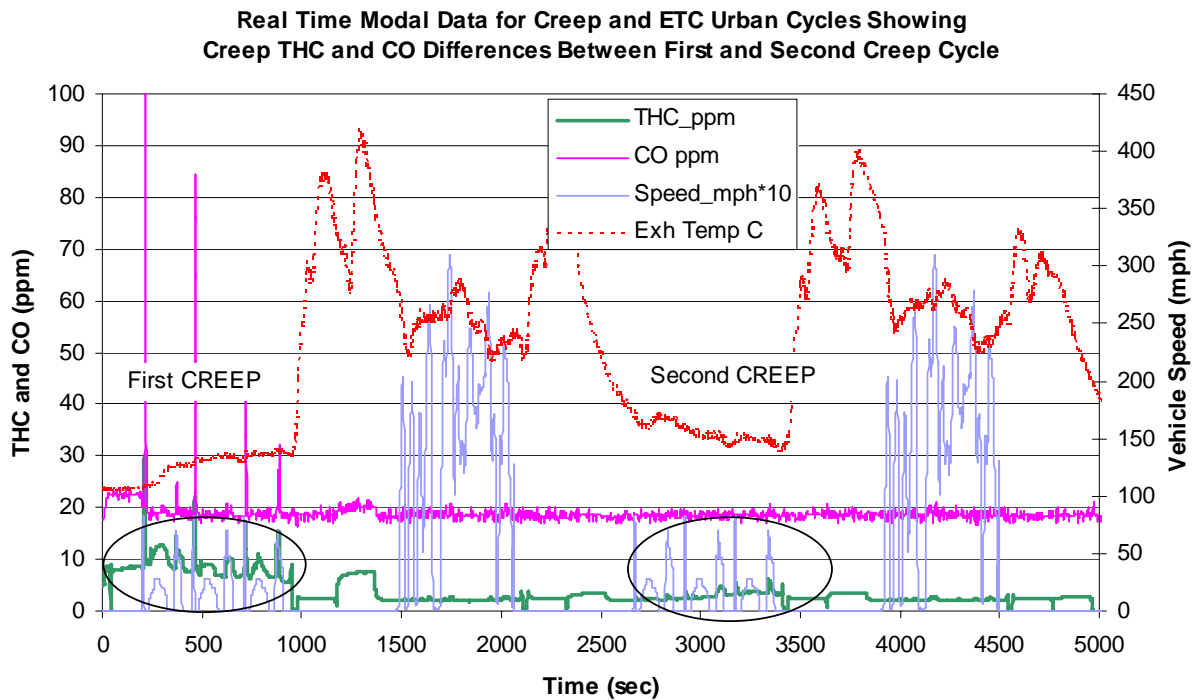


Figure H-4. Plot of Real-Time THC and CO Emissions for the Creep and ETC Urban cycles.

CO emissions are shown on a g/bhp-hr basis in Figure H-5. This figure is also scaled based on the MEL lower detection limits, since CO levels were very close to ambient levels. The magnitude of the scale is approximately ten times the lower detection limit for CO measurement at 99% confidence limit.

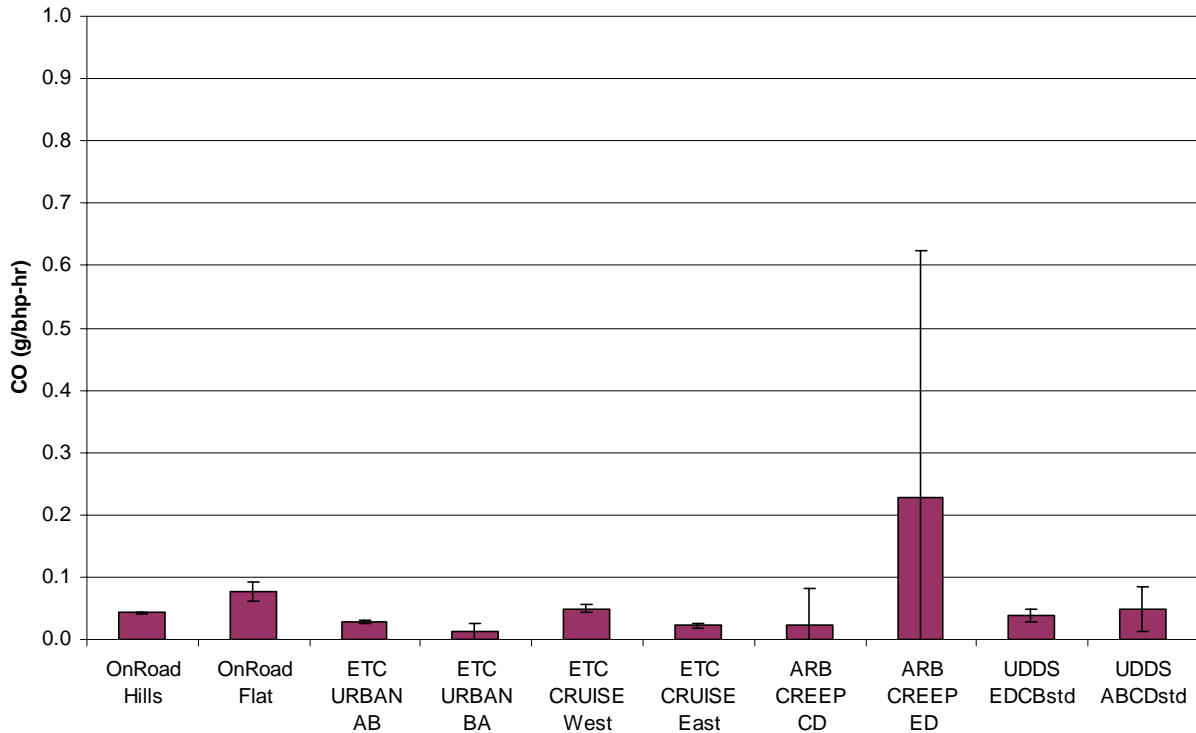


Figure H-5. CO Emissions Results on a g/bhp-hr basis

CO₂ emissions are presented in figure H-6 and H-7, respectively, on a g/mi and g/bhp-hr basis. Typical flow-of-traffic CO₂ emissions are 2 kg/mi at steady flow conditions, with CO₂ emissions ranging as high as 5 kg/mi in congested conditions simulated with the creep cycle, where the average speed is less than 5 mi/hr. The brake specific CO₂ emissions are flatter across the cycles, with the exception of the creep cycle. On a brake specific basis, CO₂ emissions are lowest for the steady state cruise and highest for the creep cycle. This truck consumed approximately 3 or 4 times as much fuel for a creep cycle on a per mi or per engine power basis compared to the cruise cycle.

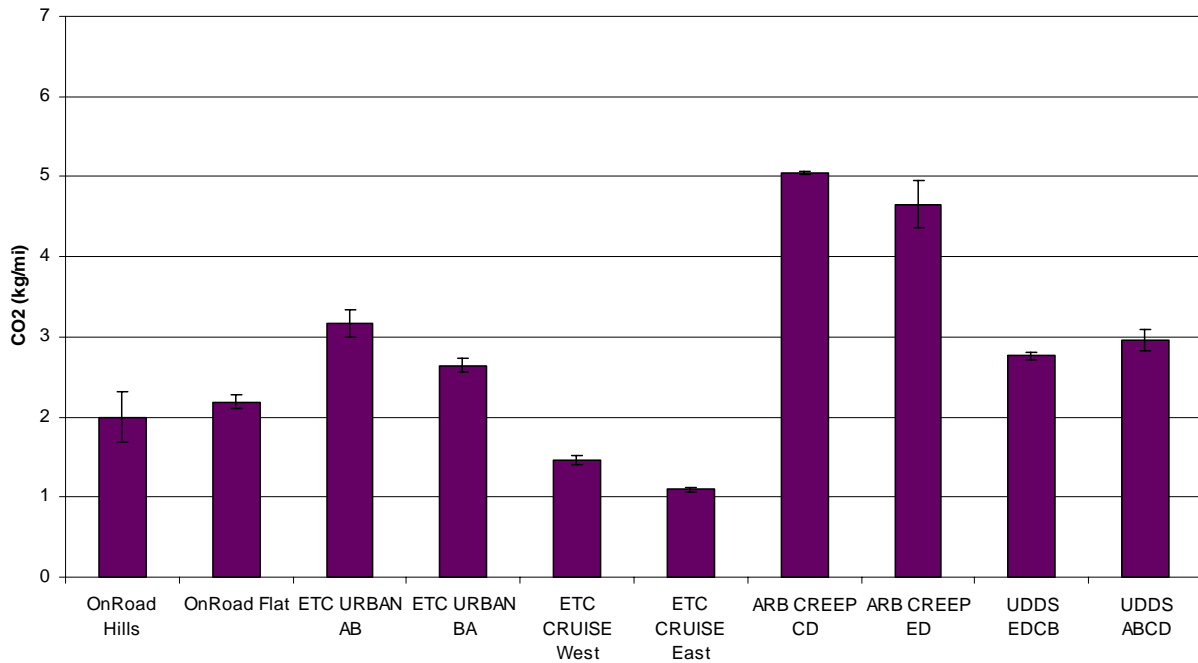


Figure H-6. CO₂ Emissions Results on a kg/mi basis

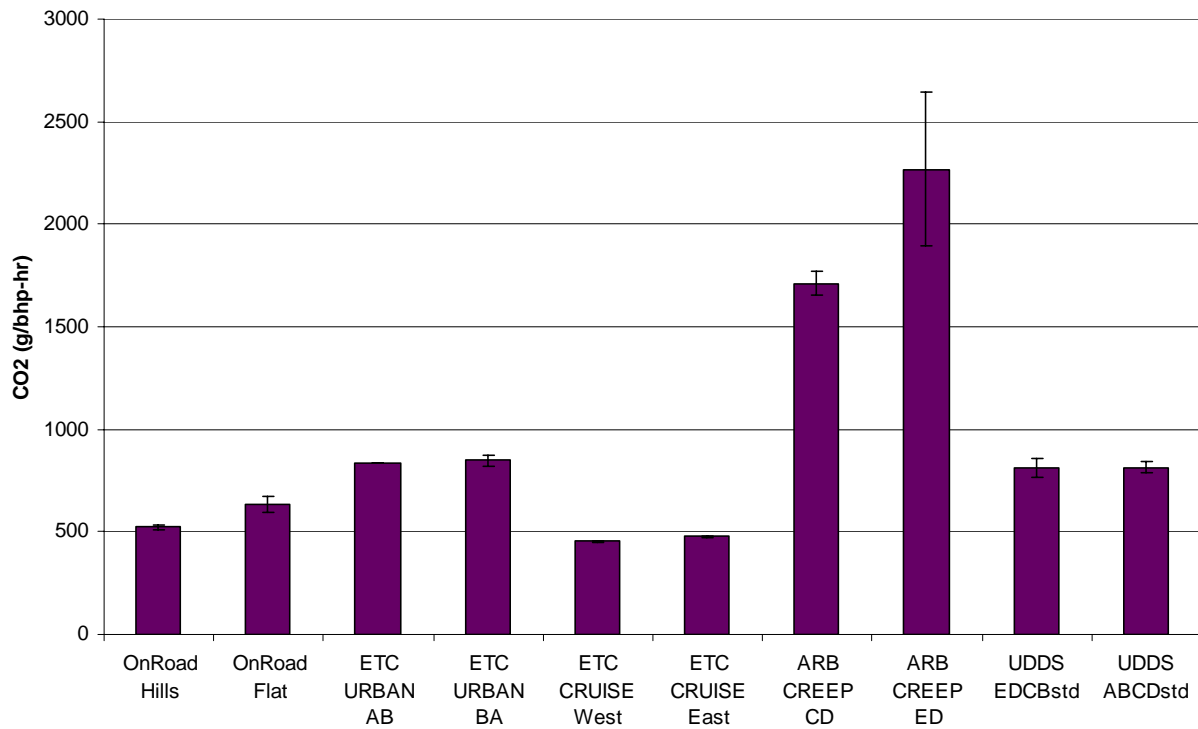


Figure H-7. CO₂ Emission results on a g/bhp-hr basis

CO₂ is useful for providing an analysis of the fuel consumed based on ECM estimates and fuel consumed based on a balance of carbon from CO₂, THC, and CO emissions. Figure H-8 shows

the MEL carbon balance fuel consumption compared with the ECM fuel consumption. The MEL and ECM carbon mass balance agree within 3%, where the MEL is slightly lower than the ECM fuel rates. This level of agreement is similar to that found in previous MEL studies [Cocker et al., 2004a]. This good correlation is an indicator that the on-road emissions masses are reliable and consistent within expectations.

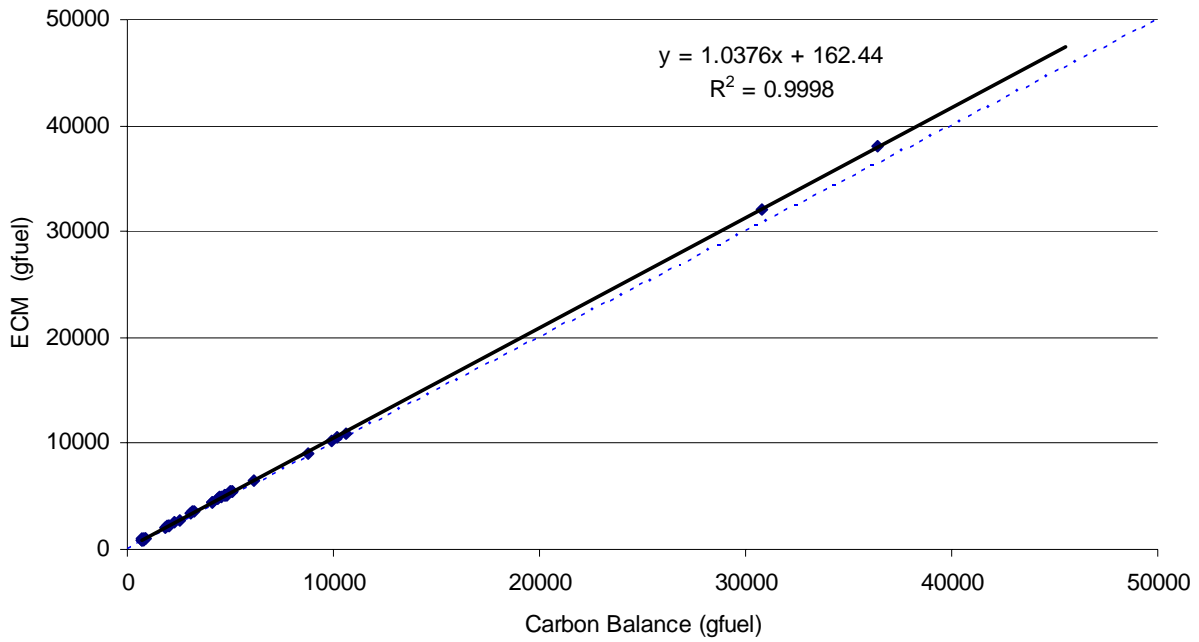


Figure H-8. Flow-of-traffic and Standardized cycles fuel consumption carbon balance correlation between emissions measured and ECM fuel rate

Appendix I – On-Road Test Route Repeatability for Gas-Phase Measurements

An important aspect of this program is evaluating the repeatability of the PMP sampling methodology and other associated emissions. In order to evaluate the systematic variability in the measurement methods, it is also important to understand and control sources of variability in the testing process as well. In the on-road testing for the present program, a series of standard drive cycles were utilized including the UDDS, ETC, and CARB creep cycles. In evaluating cycle repeatability, it was found that some of the variations in the test data could be explained by differences in the course route for a particular cycle. As such, the data presentation in the main text is based on separation of different directions within each test cycle. The details of test variability based on test route directionality are explained in greater detail in this Appendix.

Data validation is based on repeatability, reproducibility, and traceability. Repeatability is the repeat of measurement within a test; reproducibility is the ability to recreate data at a separate time or experimental location; and traceability is the ability to measure a standard or some reference to a standard. Repeatability is a good measure of how variable results are for a group of tests performed over a short sequence test period. Although the focus of the study is on particles, gaseous emissions repeatability is a more reliable metric for overall variability for test conditions.

While it is well understood that particle number measurements will likely have greater variability than standard gaseous measurements at engine out levels, it is important to examine the variability of gaseous measurements to ensure the test cycles are repeatable in and of themselves. The focus for test repeatability in this study is based on NO_x and CO₂ and not THC, CH₄, NMHC and CO. As discussed in section 5, the concentration measurements of THC, CH₄, and CO for the CRT equipped diesel engine are too low and too close to ambient values to be effectively used for repeatability determination. Table I-1 shows the corresponding concentration levels for NO_x and CO₂. It is of note that the levels of NO_x and CO₂ are well above ambient levels and detection limits, and as such, detectability issues do not limit the repeatability of the measurements.

Cycle	NO _x ppm			CO ₂ ppm		
	ave	stdev ¹	amb	ave	stdev ¹	amb
OnRoad Varies	115.0	100.0	0.03	1.30	1.02	0.033
OnRoad ToThermal	78.9	77.3	0.03	1.03	0.93	0.033
ETC URBAN	42.6	47.6	0.03	0.68	0.68	0.033
ETC CRUISE	117.8	29.5	0.03	0.98	0.24	0.033
ARB CREEP	36.9	25.4	0.03	0.41	0.33	0.033
UDDS	48.5	45.5	0.03	0.71	0.65	0.033

¹ – this standard deviation is the average standard deviation with-in the test cycle. This standard deviation indicates the measured dynamic range.

Table I-1. NO_x and CO₂ Concentration Averages for the Test Runs with all Runs Utilized

The magnitude and variation of NO_x and CO₂ emissions are shown in Table I-2 below. The NO_x and CO₂ repeatability, as measured by coefficient of variation (COV), is greater than 5% for all the driving schedules, except the flow-of-traffic testing between Indio and Thermal, although most of the standard cycles, except for the cruise, have a variability of 10% or less. Although these variability estimates may initially appear to be reasonable, they are considerably higher

than the values CE-CERT has seen in the past for repeatability (COVs) of similar measurements. In earlier studies with the CE-CERT MEL, typically COVs of less than 5% for NO_x and CO₂ on standard cycles have been obtained.

Cycle	count	NO _x g/mi			CO ₂ g/mi		
		ave	stdev	COV	ave	stdev	COV
OnRoad Varies	3	19.1	3.4	18%	1999	308	15%
OnRoad ToThermal	4	18.1	1.0	5%	2186	84	4%
ETC URBAN	7	19.4	2.0	10%	2791	273	10%
ETC CRUISE	8	18.9	6.0	32%	1452	381	26%
ARB CREEP	7	49.2	3.8	8%	4764	308	6%
UDDS	10	21.8	1.4	6%	2878	143	5%

Table I-2. Mass Emission Rate NO_x and CO₂ Averages for the Test Runs with all Runs Utilized

Potential sources of error can be more readily understood by examining engine operation data more closely, as shown in Table I-3 for torque, fuel flow, and boost pressure. These data show that for all cycles, at least one of the engine operational parameters has a COV in excess of 10%. This indicates that there appears to be some instability in the engine operation over the various cycles. If the engine torque, fuel rate and boost pressure are not repeatable, it is understandable that there will be some impact on the emissions results as well. A comparison chart of NO_x and CO₂ with the engine operational variables provided below in Figure I-1.

Cycle	count	eTourque %			eFuel cc/sec			eBoost kPa		
		ave	stdev	COV	ave	stdev	COV	ave	stdev	COV
OnRoad Varies	3	43.8	1.5	4%	13.78	0.14	1%	90.3	1.0	1%
OnRoad ToThermal	4	26.5	2.8	11%	8.84	0.92	10%	54.8	6.3	11%
ETC URBAN	7	10.6	1.1	10%	4.48	0.47	10%	23.4	2.7	12%
ETC CRUISE	8	36.4	10.5	29%	8.91	2.06	23%	39.7	13.5	34%
ARB CREEP	7	2.0	0.5	23%	1.48	0.12	8%	3.2	0.8	26%
UDDS	10	15.0	1.2	8%	7.05	1.49	21%	31.4	1.0	3%

Table I-3. Averages for Engine Parameters for the Test Runs with all Runs Utilized

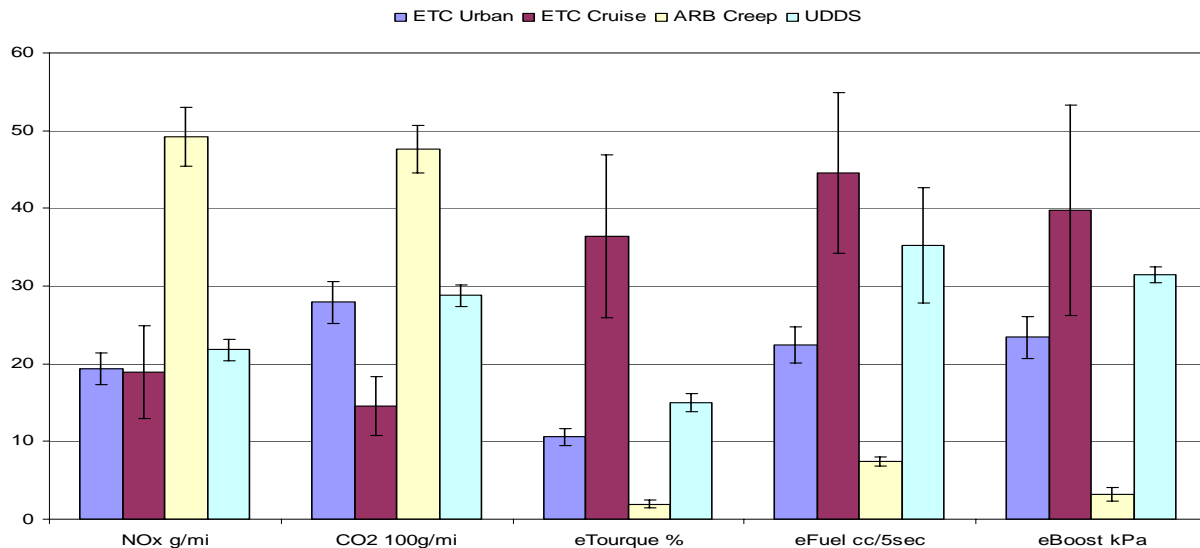


Figure I-1. Averages for NO_x and CO₂ and Engine Parameters for the Test Runs with all Runs

To further investigate the slightly higher than expected COVs, the drive cycles were reanalyzed with the data separated based on direction each of the drive cycles were run in. The ETC cruise cycles were performed on the I10 freeway, with five east bound and three west bound repeats, but in the same physical location on the I10. In this section of the I10, there is a slight uphill grade for the west bound direction and down hill grade for the east bound direction. The trade winds are also from the west to the east, but on the days we tested the winds were light.

The ETC urban, ARB creep and UDDS cycles were performed on farm road near Thermal airport. The basic layout and all start and stop points based on physical stop signs that we encountered is shown in section 3-3. For each of these cycles, the cycles were initially performed in a clockwise direction (i.e., in an ABCDE direction). The testing was than modified to run counter clockwise (i.e., in an EDCBA direction) for purposes of safety. The 2.8 mile distance has a slight uphill grade from A to B.

The emissions results grouped by common test mode (i.e. same section of road going the same direction) are presented in Tables I-4 and I-5 and in Figure I-2. Tables I-2 and I-3 above show the repeatability data for NO_x, CO₂ and the engine parameters with the data grouped by similar direction. These data are also shown graphically in Figure I-1. These data show a considerable improvement in test repeatability, although the creep and UDDS still have some outliers that are keeping their COVs high.

Cycle	count	NMHC g/mi		CO g/mi		NOx g/mi		PM mg/mi	
		ave	stdev	ave	stdev	ave	stdev	ave	stdev
OnRoad Varies	3	0.07	0.02	0.18	0.01	19.1	3.4	26.1	n/a
OnRoad ToThermal	4	0.08	0.11	0.27	0.06	18.1	1.0	n/a	n/a
ETC URBAN_AB	2	0.00	0.02	0.11	0.00	22.1	0.3	38.6	8.7
ETC URBAN_BA	5	-0.03	0.01	0.04	0.04	18.2	0.9	-1.7	1.2
ETC CRUISE_Est	3	-0.01	0.00	0.16	0.03	19.0	0.3	12.1	7.6
ETC CRUISE_Wst	3	-0.02	0.01	0.05	0.01	13.3	0.7	4.7	2.3
ARB CREEP_CD	2	0.00	0.05	0.07	0.17	51.8	1.8	33.0	21.2
ARB CREEP_ED	5	1.01	1.11	0.44	0.76	48.1	4.0	5.9	4.7
UDDS_EDCB	4	-0.02	0.01	0.13	0.03	21.0	1.4	5.9	2.9
UDDS_ABCD	6	0.08	0.11	0.23	0.14	22.4	1.2	3.8	2.6

Table I-4. Emission Rate Averages for the Test Runs Separated by Route

Cycle	count	eTourque %			eFuel cc/sec			eBoost kPa		
		ave	stdev	COV	ave	stdev	COV	ave	stdev	COV
OnRoad Varies	3	43.8	1.5	4%	13.78	0.14	1%	90.3	1.0	1%
OnRoad ToThermal	4	26.5	2.8	11%	8.84	0.92	10%	54.8	6.3	11%
ETC URBAN_AB	2	12.1	0.3	2%	5.12	0.37	7%	26.9	2.7	10%
ETC URBAN_BA	5	10.0	0.3	3%	4.23	0.11	3%	22.0	0.8	4%
ETC CRUISE_Est	3	37.0	1.3	4%	9.03	0.32	4%	40.4	2.7	7%
ETC CRUISE_Wst	3	26.4	1.0	4%	6.94	0.18	3%	27.1	0.8	3%
ARB CREEP_CD	2	2.5	0.1	4%	1.64	0.00	0%	4.4	0.0	1%
ARB CREEP_ED	5	1.7	0.3	19%	1.42	0.05	4%	2.7	0.2	7%
UDDS_EDCB	4	14.6	1.2	8%	5.65	0.13	2%	31.5	1.3	4%
UDDS_ABCD	6	15.3	1.2	8%	7.99	1.17	15%	31.4	0.8	3%

Table I-5. Engine Parameter Averages for the Test Runs Separated by Route

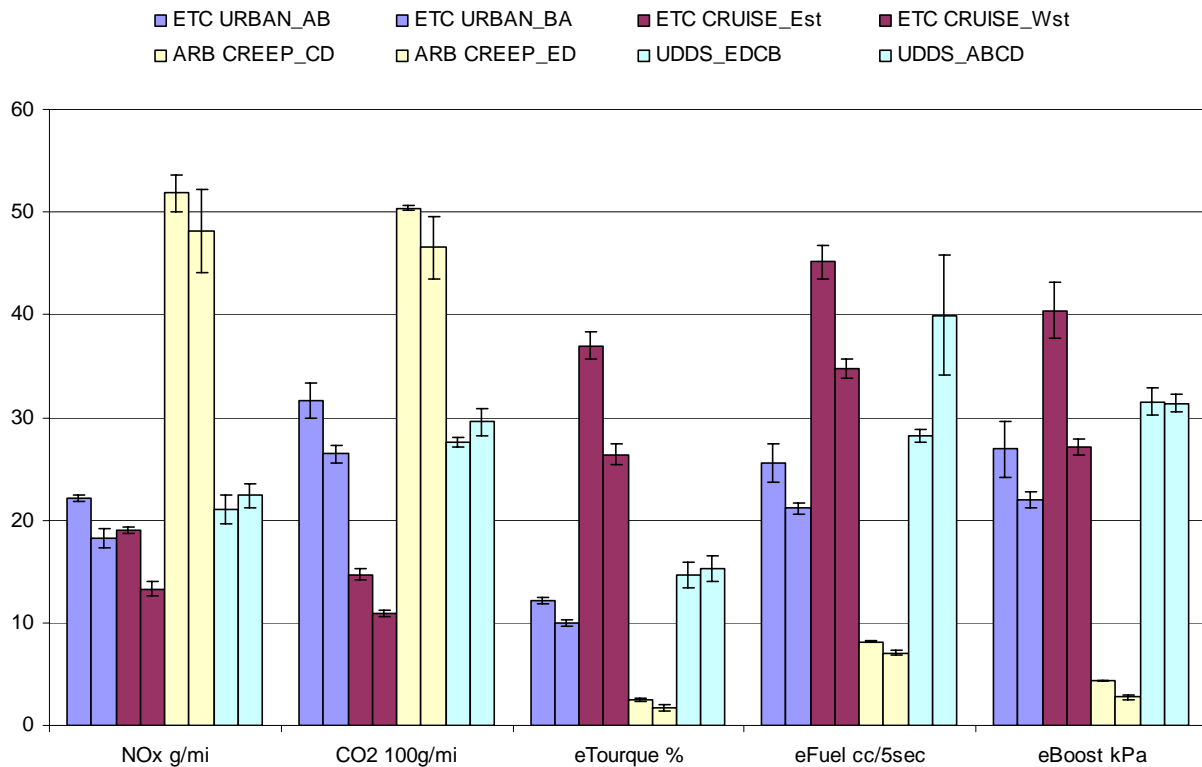


Figure I-2. Averages for NO_x and CO₂ and Engine Parameters for the Test Runs Separated by Route

The creep had one outlier that appears to be a real data point. If the point is removed, all the engine and emissions data would fall within 5%. There is no physical reason to remove the point so it was kept in the reduced data evaluation. The difficulty with the creep cycles is that the distance and emission levels are lower so the variability increases.

The UDDS data does not show any outliers that would warrant removing data points to improve COVs. There seems to be some random conditions between each test that caused all the variability. The trend is clear when looking at emissions and load data on a common plot. Notice in Figure I-3 below how NO_x follows engine load and CO₂ follows fuel consumption from test to test. For the first two points the direction was ABCDE and the remaining points are EDCBA. The emissions tracked what was happening at the engine, but nothing explains the engine variability which caused the emissions COV to be greater than 5%. Compared to past work at Thermal, the MEL system showed a typical NO_x COV for five repeats over three days was less than 2%. One other interesting fact is that there is not much difference between directions for the UDDS cycles. One reason is the UDDS cycle is long and requires going from A to E so the net elevation change is zero compared to all the other cycles where the net elevation change was either positive or negative depending on the direction.

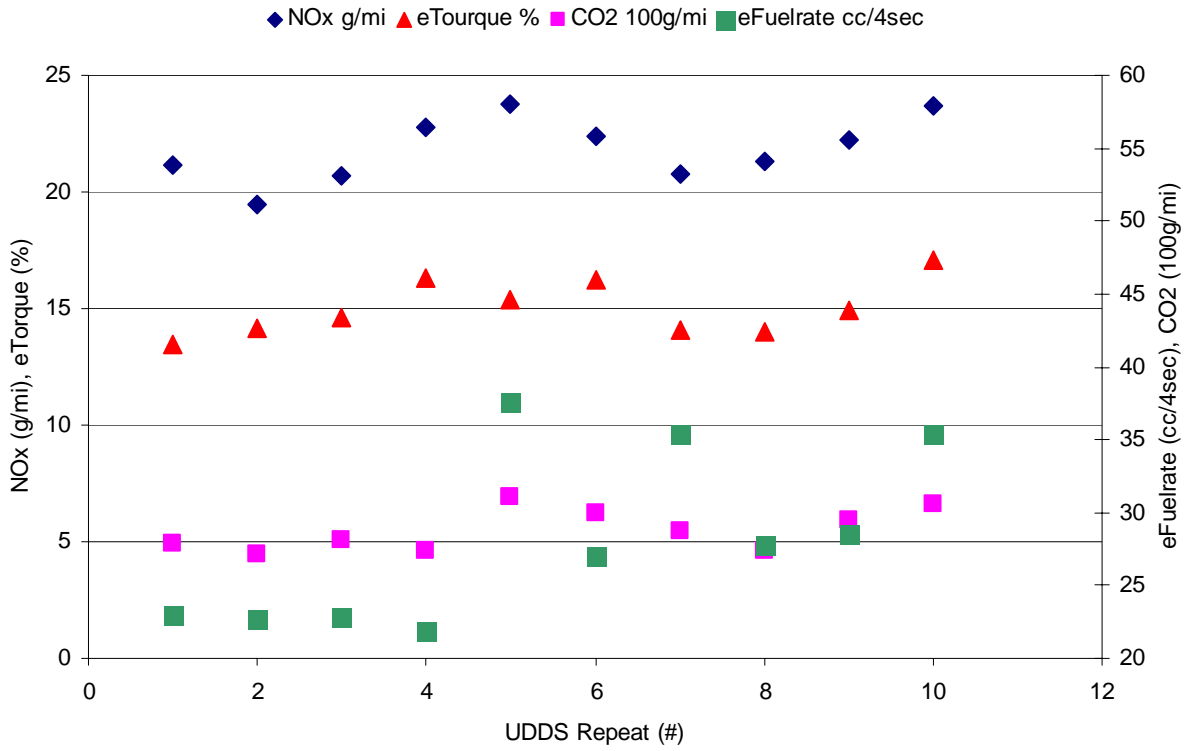


Figure I-3. Averages for NO_x and CO₂ and Engine Parameters as a Function of UDDS Test Iteration

Appendix J – Supplemental Integrated PM Mass and Number Information for the On-Road Testing

Particle number concentration values are provided in the Tables below for the different CPCs and for the different drive cycles. Interestingly, the ARB Creep Cycle showed the lowest concentration levels compared to the other cycles, whereas the creep had the highest particle number values on a g/mi basis for the standard cycles. The reason for the high particle number per mile for the Creep cycles, with correspondingly low concentrations, is because of the much shorter distance traveled compared to the other cycles.

Table J-1. MD-19 CPC statistics for cycles separated by direction and flow-of-traffic tests

Cycle	count	MD-19 3790 #/cc			MD-19 3025 #/cc			MD-19 3760 #/cc		
		ave	stdev	COV	ave	stdev	COV	ave	stdev	COV
OnRoad Hills	3	2.3E+13	1.2E+13	53%	7.2E+14	3.3E+14	46%	8.6E+13	3.2E+13	37%
OnRoad Flat	4	7.4E+11	4.3E+11	58%	2.4E+13	2.1E+13	85%	8.0E+11	4.6E+11	57%
ETC URBAN AB	2	5.3E+11	1.0E+11	19%	3.3E+12	2.4E+11	7%	7.4E+11	1.2E+11	16%
ETC URBAN BA	5	3.8E+11	1.6E+10	4%	2.9E+12	1.9E+11	7%	4.1E+11	1.1E+10	3%
ETC CRUISE West	4	2.7E+11	1.6E+11	57%	2.5E+12	4.1E+11	17%	2.8E+11	1.4E+11	52%
ETC CRUISE East	3	1.7E+11	1.1E+10	6%	1.2E+12	2.5E+10	2%	1.8E+11	1.2E+10	7%
ARB CREEP CD	2	8.9E+11	1.5E+10	2%	8.9E+12	1.9E+10	0%	1.0E+12	3.8E+10	4%
ARB CREEP ED	5	5.8E+11	9.4E+10	16%	9.0E+12	7.1E+11	8%	7.1E+11	1.1E+11	16%
UDDS ABCD	4	4.7E+11	5.7E+10	12%	3.8E+12	2.1E+11	5%	5.0E+11	6.5E+10	13%
UDDS EDCB	4	4.1E+11	1.2E+11	30%	1.1E+13	7.3E+12	67%	4.4E+11	1.5E+11	34%

Table J-2. MEL CPC statistics for cycles separated by direction and flow-of-traffic tests

Cycle	count	MEL 3025 #/cc			MEL 3760 #/cc		
		ave	stdev	COV	ave	stdev	COV
OnRoad Hills	3	3.4E+14	1.4E+14	42%	4.4E+13	1.4E+13	32%
OnRoad Flat	4	3.1E+13	2.1E+13	68%	8.5E+11	4.4E+11	51%
ETC URBAN AB	2	5.6E+12	3.5E+11	6%	9.9E+11	1.5E+11	15%
ETC URBAN BA	5	8.7E+12	2.7E+11	3%	4.7E+11	1.4E+10	3%
ETC CRUISE West	4	3.9E+12	6.1E+11	15%	2.9E+11	1.5E+11	52%
ETC CRUISE East	3	1.8E+12	9.2E+10	5%	2.0E+11	6.9E+09	3%
ARB CREEP CD	2	1.5E+13	7.5E+10	0%	1.6E+12	6.6E+10	4%
ARB CREEP ED	5	1.7E+13	3.8E+12	23%	1.1E+12	1.7E+11	15%
UDDS ABCD	4	6.0E+12	7.8E+11	13%	5.7E+11	7.1E+10	12%
UDDS EDCB	4	2.3E+13	1.3E+13	55%	5.0E+11	1.1E+11	23%

Table J-3. MEL PMP diluter system specifications for cycles separated by direction and flow-of-traffic tests

Cycle	count	Dilution Ratio				
		ave	stdev	COV	stdev ¹	COV
OnRoad Hills	3	120.9	1.5	1.3%	5.5	4.6%
OnRoad Flat	4	108.3	1.2	1.1%	2.6	2.4%
ETC URBAN AB	2	106.5	3.0	2.8%	1.1	1.1%
ETC URBAN BA	5	108.2	0.5	0.5%	0.3	0.3%
ETC CRUISE West	3	111.1	4.4	4.0%	1.6	1.4%
ETC CRUISE East	3	113.7	2.1	1.9%	0.5	0.5%
ARB CREEP CD	2	108.5	0.1	0.1%	0.5	0.4%
ARB CREEP ED	5	105.0	2.4	2.3%	0.9	0.8%
UDDS EDCBstd	4	108.2	1.0	1.0%	1.1	1.1%
UDDS ABCDstd	6	107.9	1.7	1.5%	1.5	1.4%

¹ – this standard deviation is the average standard deviation with-in the test cycle. This standard deviation indicates the measured dynamic range.

Appendix K – Supplemental Real-Time PM Number Measurements for the On-Road Testing

Cruise

Figure K-1 shows real-time data for the cruise cycle, but includes the data prior to starting the ETC cruise cycles. Before the ETC cruise cycle started, the vehicle was idling and then accelerating to freeway ETC cruise speeds. During the rapid acceleration, maximum power was achieved for several short bursts during gear shifting to reach cruise speeds. The exhaust stack temperature increased during the acceleration from 100°C to 350°C. At about 275°C, the large 3022 CPC nucleation burst started and peaked about 30 seconds later near the peak in exhaust temperature. Exhaust temperature typically lags sudden engine load by two seconds, but during this initial increase in engine load the exhaust temperature lagged behind by approximately 30 seconds. It is believed the CRT is absorbing the heat during this lag, which suggests the peak catalyst temperature coincides with the peak exhaust stack measurement temperature.

The Dekati DMM mass concentration was more than 100 ug/m³ during the acceleration and the main nucleation burst. It is also interesting how the PMP diluted CPCs were measuring particle concentrations that followed the gear shifting with stack temperatures around 200°C suggesting that solid particles were being formed during hard accelerations. One possibility for the measured PM spikes on all the CPCs and DMM is that they could be due to the very high engine out PM emissions found during the combined acceleration and gear shifting. More work in understanding this phenomena is needed.

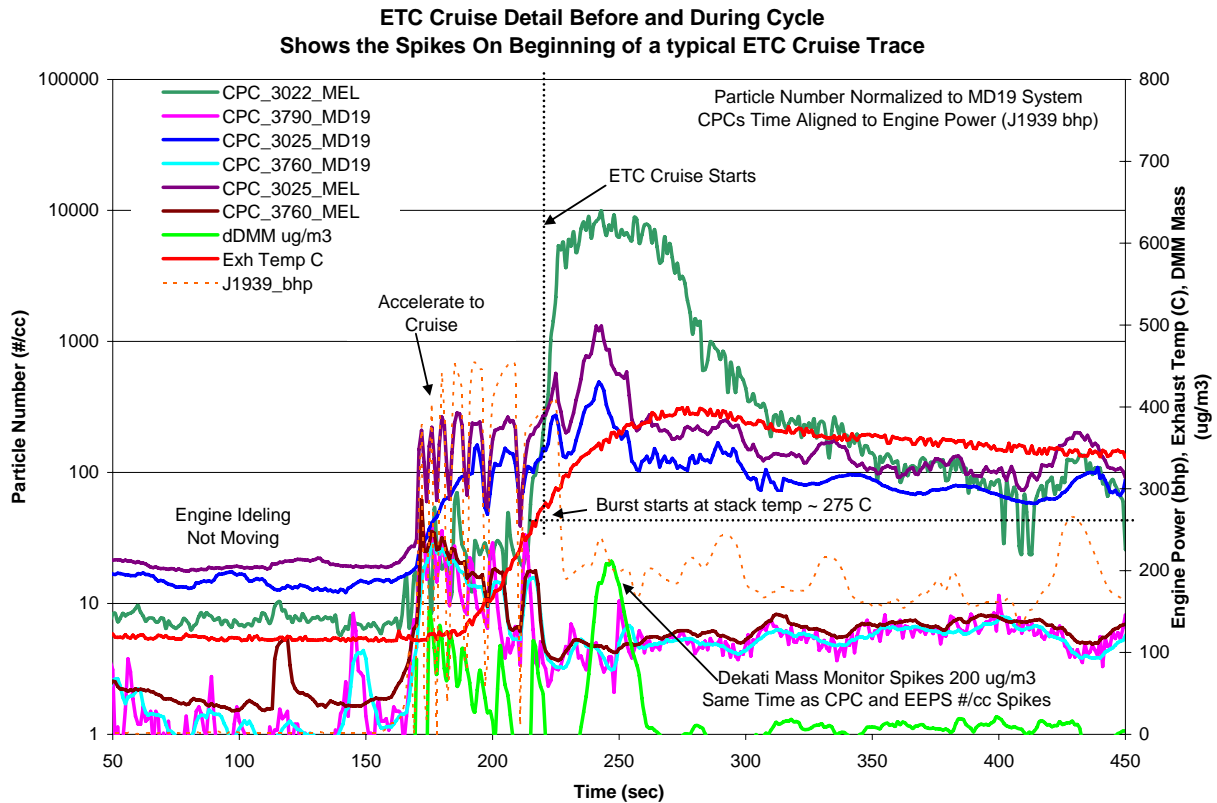


Figure K-1. Real-time particle rate (#/cc) all CPCs and Dekati DMM ($\mu\text{g}/\text{m}^3$) before and during the ETC cruise cycle (Note log y-scale axis)

A comparison of particle counts was made with the large initial nucleation spike on the cruise cycle removed, as shown in Figure K-2. The left two bars for each CPC are the west bound test direction and the right two are the east bound direction. The left blue bars are the 600 second cycle averages and the right red bars are the reduced 500 second averages. The reduced 500 second cycle emissions rate was calculated by simply removing the first 100 seconds of the cycle data. The particle number emissions rate ($\#/mi$) for the 500 second period dropped for some CPC's and remained comparable for other CPC's. The error bars were not significantly reduced or increased indicating the cycle repeatability is not dependent on the initial spike. The fact that the average measurement and the coefficient of variation did not vary significantly, suggest that engine conditioning prior to starting a repeatable particle number test does not bias the absolute emissions rate. Although not significant on an average basis, it is obvious from the real-time data that if the significant spike could be eliminated, repeatability statistics from averaging within the cycle itself could be improved by performing preconditioning. It is suggested all particle number repeated tests should consider engine and trap pre-conditioning before emissions testing.

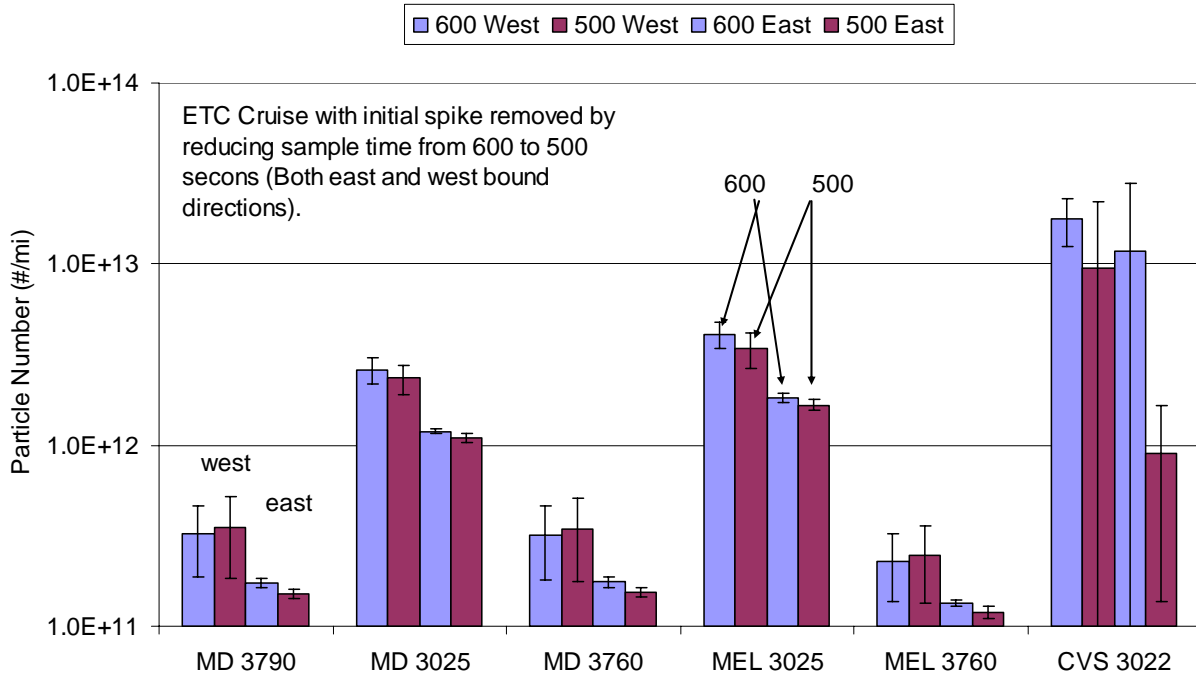


Figure K-2. ETC cruise cycle evaluation with and with-out spike during beginning of cycle for all CPC's log y-scale

Figure K-3 shows the cruise data for the lower cut point CPCs, but with a reduced y-axis scale so that the data from other parts of the cycle can be seen. The data show that the 3022 is reading consistently higher than the 3025As throughout the first cruise, although this is not the case for the second cruise. The data also show that the 3025As for the MEL and MD-19 dilution systems are of the same order of magnitude and show similar transient response to the slight engine load deviations. The particle counts for the MEL 3025A are biased higher than those for the MD-19 3025A, however. The MEL 3025A also follows engine load more closely than the MD-19 3025A system, as can be seen by the highlighted details of Figure K-3. There are two detail sections in Figure K-3 that show a transient deviation between the two PMP diluters. Figure K-4 shows a close up of the second detail section. As the engine load goes to zero, the MEL 3025A follows the cycle work, but the MD-19 3025A does not. The CPC correlation presented later also highlights similar differences in response between the MEL and MD19 PMP CPC measurement systems. This dynamic response appears to be more significant for the low cut point CPCs as compared to the high cut point CPCs.

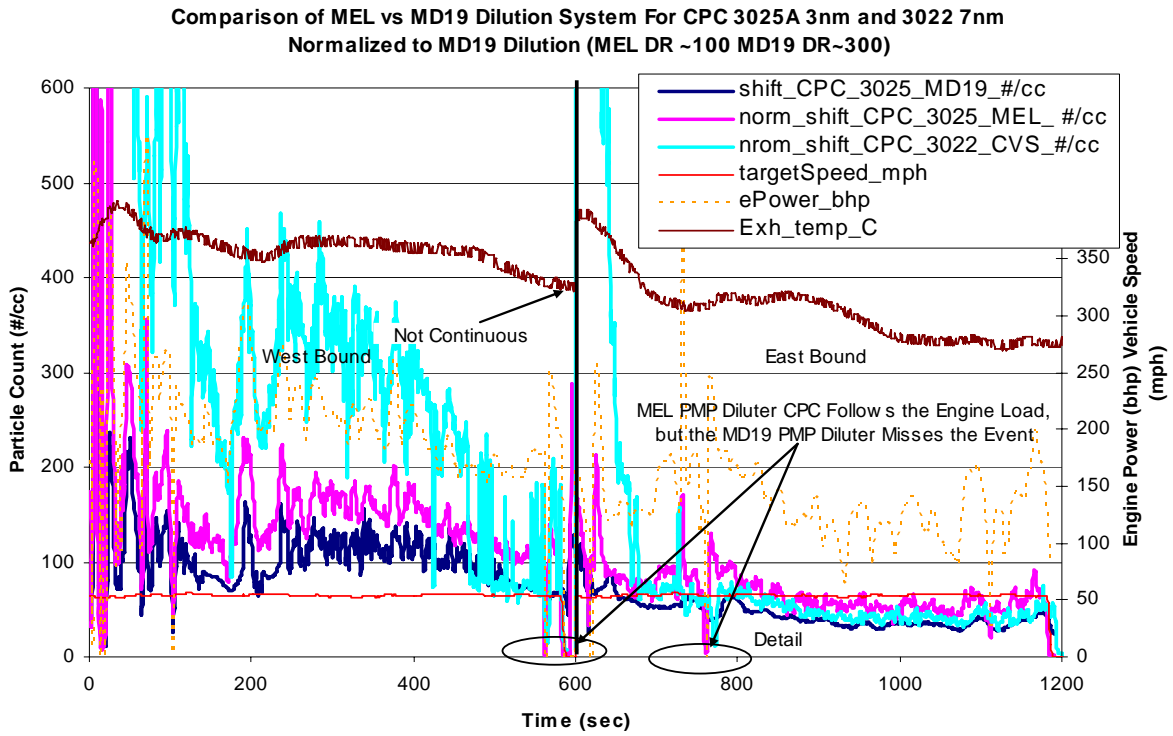


Figure K-3. Low cut CPC particle rate (#/cc) on the ETC cruise cycle reduced y-scale axis

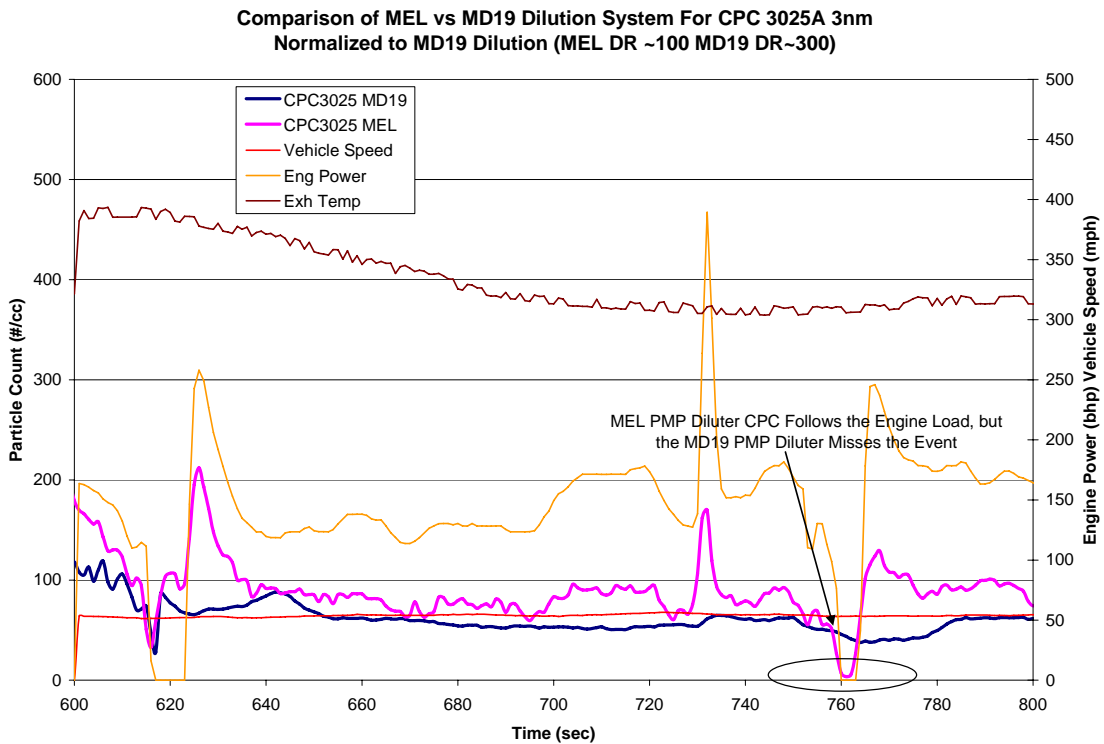


Figure K-4. Detail A low cut CPC particle rate (#/cc) on the ETC cruise

The high cut point CPCs (3760A and 3790) are considered next for the selected cruise cycle. The 3760s and the 3790 measured similar particle number counts, indicating the difference between the 11 nm and 23 nm size cut size cuts for these instruments did not have a significant impact on the particle number levels. During the west bound cruise, the higher cut point CPC's show a large peak in the middle of the cycle when exhaust temperature and engine load were relatively constant and decreasing, as shown in Figure K-5. Both 3025A's also may have slightly responded to this unknown event, but with much lower response and relative magnitude. The higher cut point CPC's did not follow engine load and are less transient compared to the 3025A and 3022 CPC measurements for the cruise cycle. The large peak measured on this cruise cycle could be specific for the selected cruise test. Additional analysis is needed to determine how significant the high cut point CPC event might be in actual on-road driving cruise conditions.

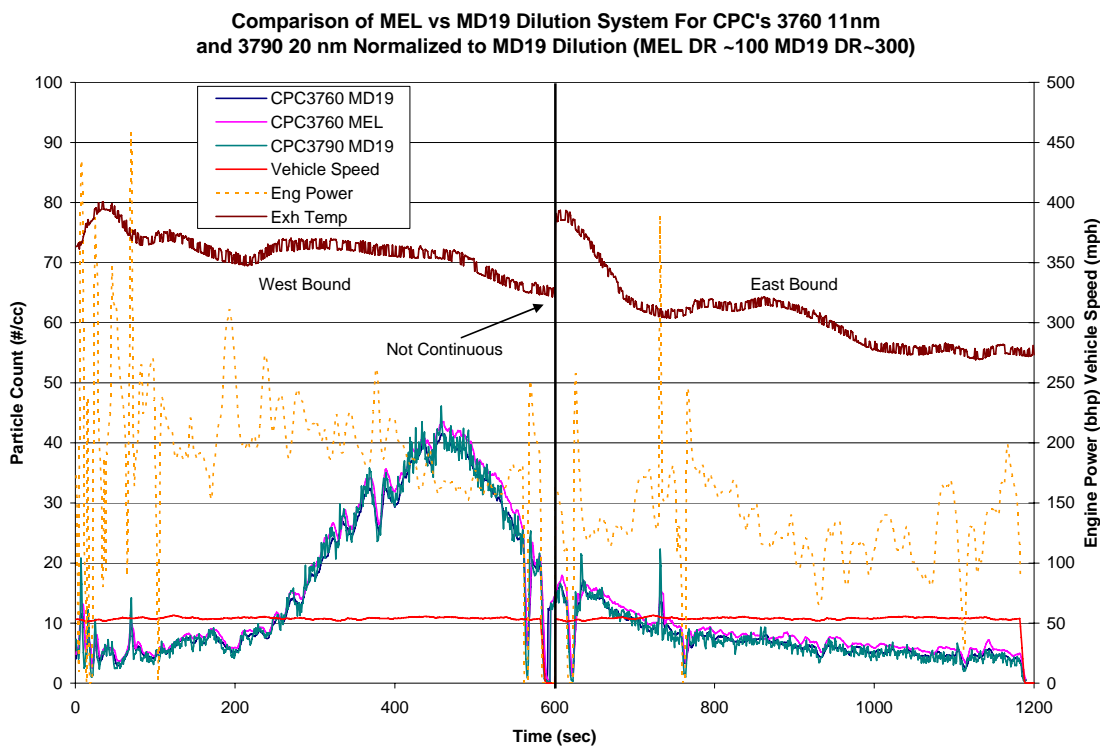


Figure K-5. Real-time particle rate (#/cc) for similar cuts point CPCs (3790 and 3760) on the ETC cruise cycle

UDDS

Figure K-6 shows the overall real-time data for a UDDS cycle. Figure K-7 through Figure K-9 show segments A, B, and C, as denoted in Figure K-6, in more detail. The 3022 low measurements for detail A and B suggest there are no nucleation events in the primary tunnel, but during detail C there is a large nucleation event.

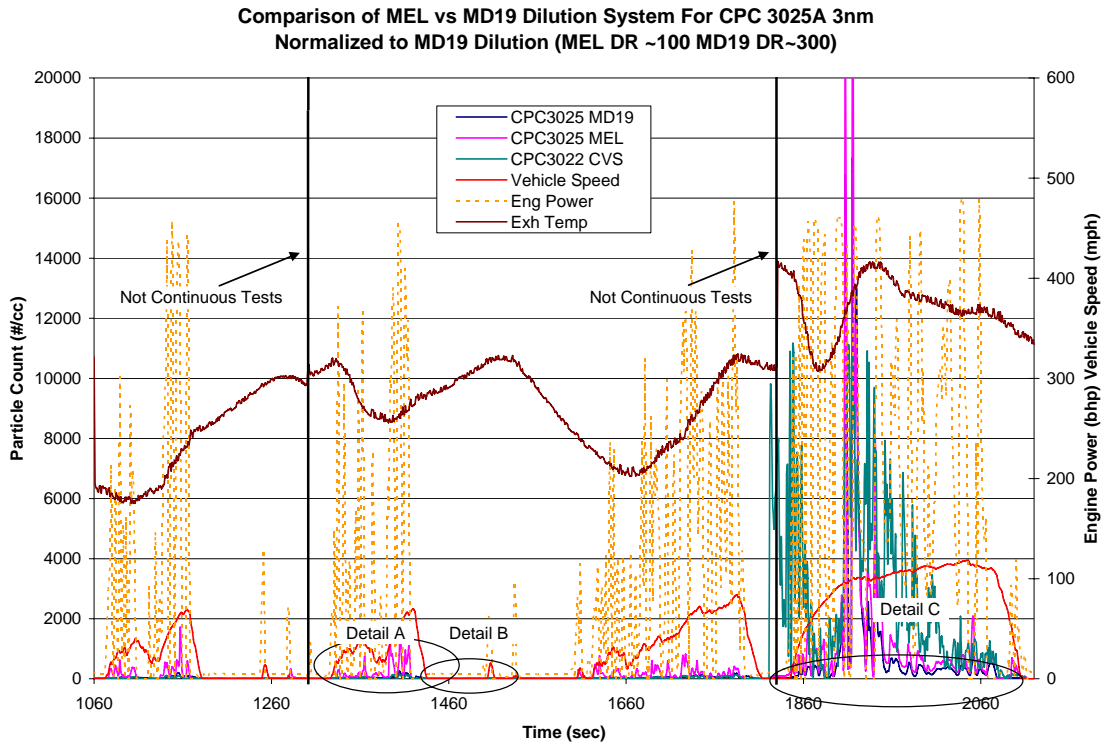


Figure K-6. Real-time particle rate (#/cc) for the 3025A and 3022 CPCs on the UDDS cycle

The behavior of the 3025A's when there is no nucleation in the primary tunnel is considered in detail A and B. For detail A, as shown in Figure K-7, the engine load is moderate and exhaust temperatures are increasing as vehicle speed is achieved. The MEL 3025A appears to have much more dynamic transient behavior than the MD-19 CPC and also records higher particle counts than the MD19 3025A. Near 1,400 seconds, the MEL 3025A spiked off scale, well above the 3022. The MD-19 3025A was also slightly higher than the 3022 during this event, but was not nearly as high as the MEL 3025A. Since both dilution systems are fairly robust, the dilution ratios should only vary by 10-20% between them. The nature of the differences between the 3025As below the different PMPs is not understood at this time.

Detail B in Figure K-8 shows the same trends as detail A, but with lighter overall engine load transients. The MEL 3025A still has a more transient behavior and shows a positive bias compared to the MD-19 3025A. The 3022 particle concentration is also lower than the 3025A's particle concentration down stream of the PMP diluters. Again, there is a relatively large MEL 3025A spike near 1610 seconds, where both the 3022 and MD-19 3025A barely registered the same load event. A similar engine load event occurred at 1510 seconds and this time the MEL 3025A CPC also did not respond with a large particle concentration spike.

The highest 3025A CPC particle concentrations were measured during the large hill shown in detail C, see Figure K-9. As before the MEL 3025A is biased higher and with more transient behavior compared to the MD-19 3025A. During parts of detail C, the 3022 measurements were higher than both 3025A's, suggesting there was a nucleation event in the primary tunnel. During most of the high 3022 measurements, the magnitude of the MEL and MD-19 3025A's measured

relatively low particle concentrations, due to the PMP eliminating non-solid particles. Around 1920 seconds, both 3025A's seemed to spike high, equaling the magnitude of the CVS 3022. The high 3025A measurement during the high 3022 measurement, suggests there is possible break through or small residual after the OC evaporation in the PMP diluter at the 3025A cut point size. The higher cut point CPCs (3760A and 3790) did not show this break down trend, as will be shown later. Thus, the possible PMP break down appears to be limited to the low cut point CPCs only. More analysis of primary tunnel size distribution and concentrations are necessary to analyze this theory further.

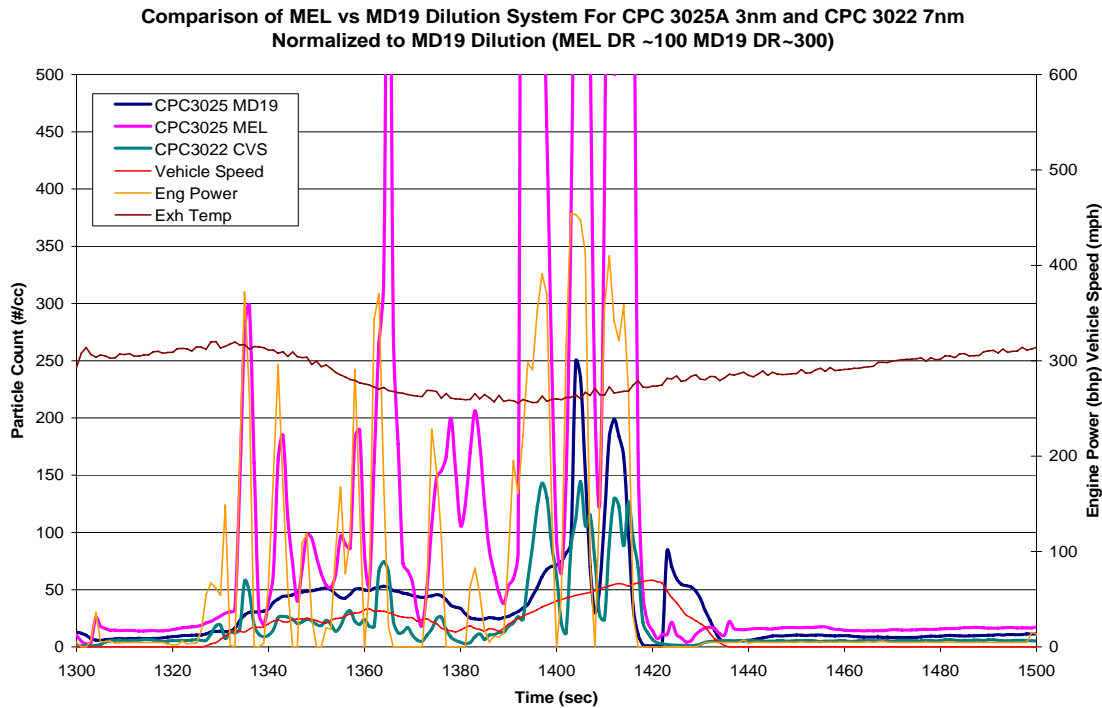


Figure K-7. Detail A. Real-time particle rate (#/cc) for the 3025A and 3022 CPCs on the UDDS cycle

Comparison of MEL vs MD19 Dilution System For CPC 3025A 3nm and CPC 3022 7nm
Normalized to MD19 Dilution (MEL DR ~100 MD19 DR~300)

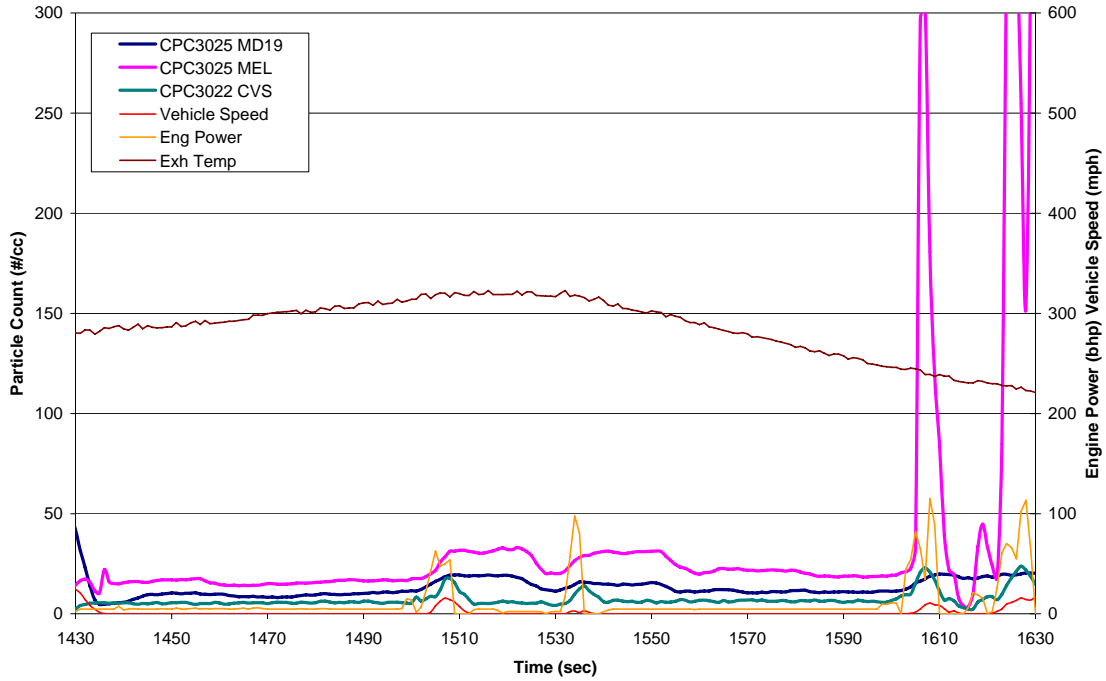


Figure K-8. Detail B. Real-time particle rate (#/cc) for the 3025A and 3022 CPCs on the UDDS cycle

Comparison of MEL vs MD19 Dilution System For CPC 3025A 3nm and CPC 3022 7nm
Normalized to MD19 Dilution (MEL DR ~100 MD19 DR~300)

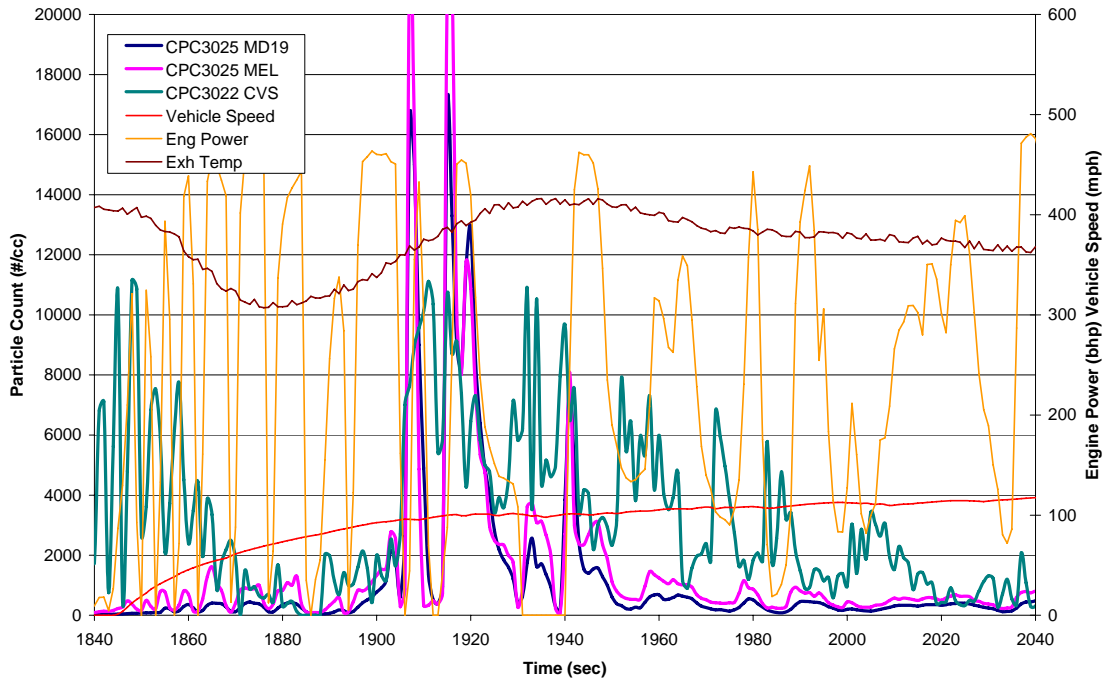


Figure K-9. Detail C. Real-time particle rate (#/cc) for the 3025A and 3022 CPCs on the UDDS cycle

Figure K-10 shows the overall real-time data for the UDDS cycle for the high cut point CPCs, with the same three areas detailed. Figures K-11 and K-12 show detailed areas A and C. Detail A and B showed similar detail for all the high cut point CPCs. Since detail B provides no new information, these results are not presented here.

Detail A in Figure K-11 represents moderate loads and showed slight transient CPC behavior. There is a significant response to engine load for all the high cut point CPCs. The MEL 3760A appears to be biased high during the peaks, but not for the steady state measurements. The 3790 appears to have the largest dynamic response with the MEL 3760A next and the MD-19 3760A last. The 3790 CPC measurements range from 2 #/cc during no-load condition to around 15 #/cc during moderate-transient-load conditions. The high CPC particle count with low primary tunnel 3022 measurements suggest the particles are largely solid.

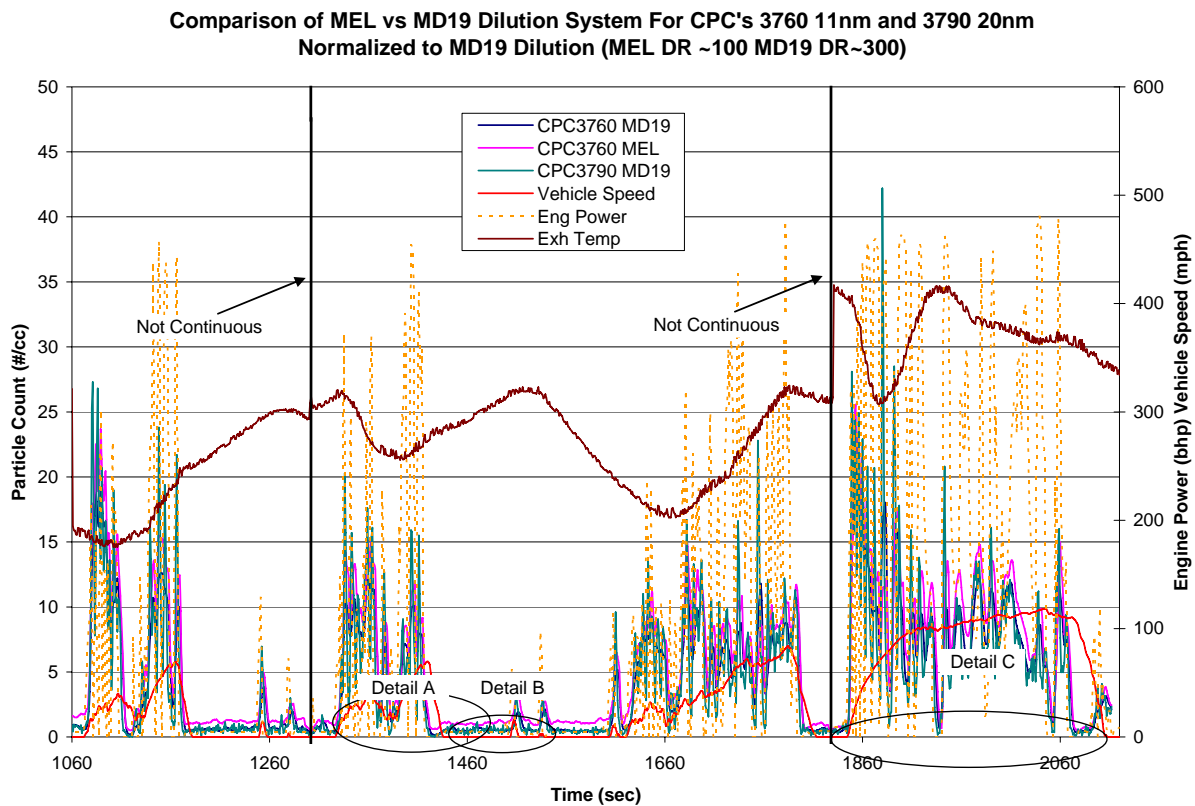


Figure K-10. Real-time particle rate (#/cc) for CPCs 3790 and 3760 on the UDDS cycle

Comparison of MEL vs MD19 Dilution System For CPC's 3760 11nm and 3790 20nm
Normalized to MD19 Dilution (MEL DR ~100 MD19 DR~300)

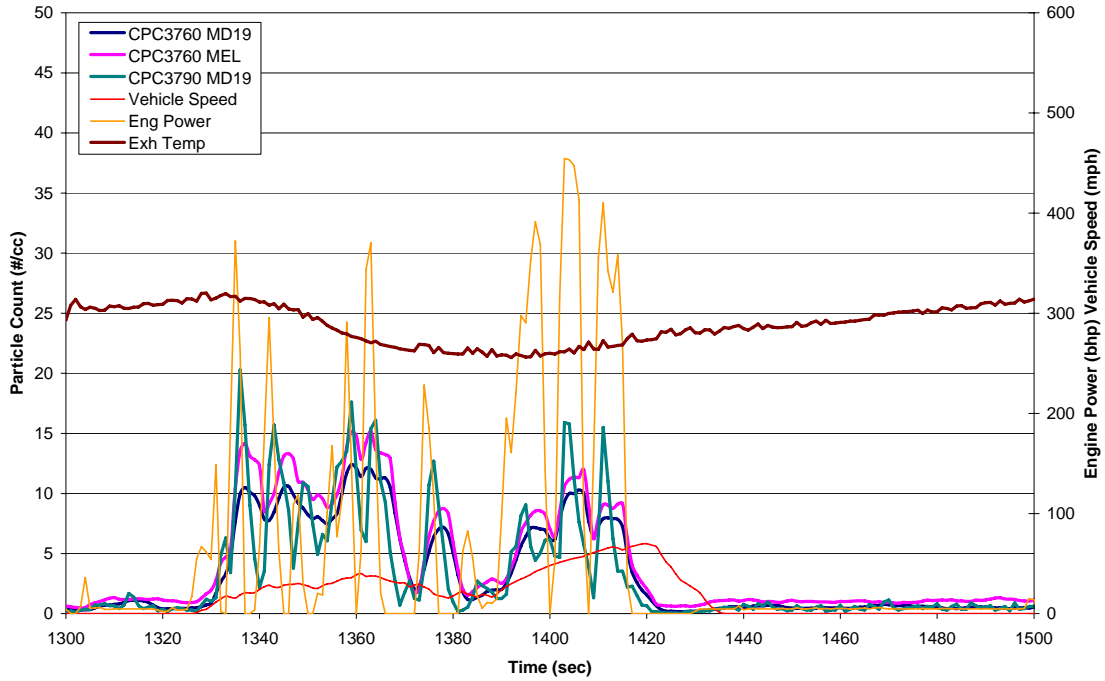


Figure K-11. Detail A. Real-time particle rate (#/cc) CPCs 3790 and 3760 on the UDDS cycle

Comparison of MEL vs MD19 Dilution System For CPC 3025A 3nm
Normalized to MD19 Dilution (MEL DR ~100 MD19 DR~300)

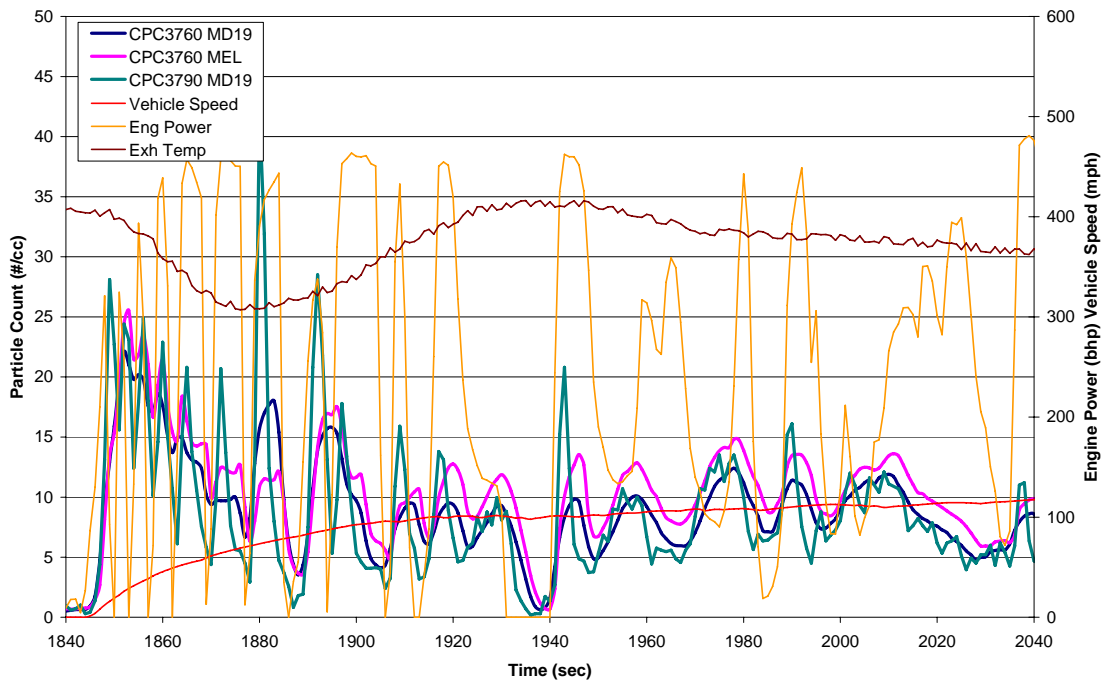


Figure K-12. Detail C. Real-time particle rate (#/cc) CPCs 3790 and 3760 on the UDDS cycle

ETC Urban and CARB Creep Cycles

Figure K-13 shows the overall cycle data for a combination Creep and Urban cycle, with the two detailed areas that are described below.

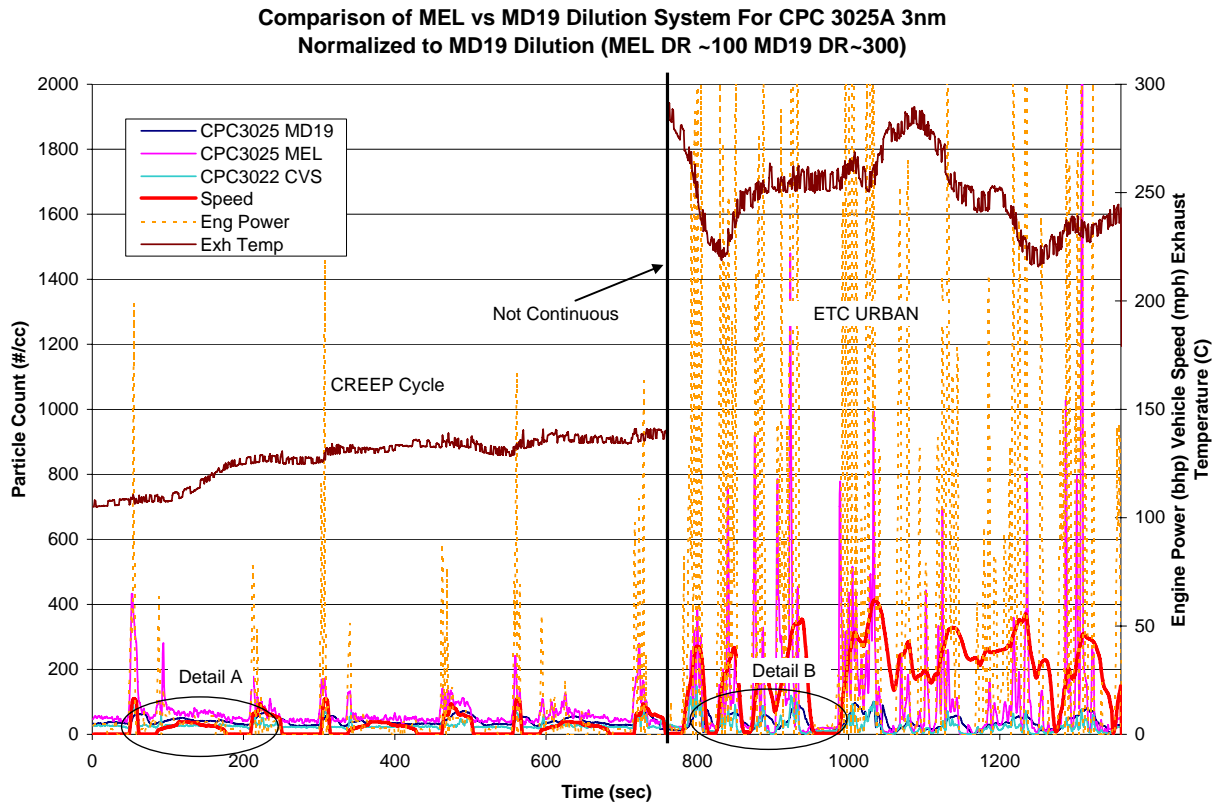


Figure K-13. Real-time particle rate (#/cc) for CPCs 3025A on the creep and urban cycles

Figure K-14 and K-15 are taken from a subset of the data in Figure 5-27, as shown by the detail circles. Figure K-14 shows the first detail section of the creep cycle with the same CPC y-axis as Figure 5-27, but only looking at the first 200 seconds of real time data. The three CPC's on both PMP dilution systems respond to the power spike with an increase in counts with very similar magnitudes, with the MEL 3760A being highest, followed by the MD-19 3790 with the MD-19 3760A being lowest. During the no load conditions, the MEL 3760A shows a slightly higher response than both MD-19 CPC's.

Figure K-15 shows a similar detail, but for the ETC urban driving schedule. Again all the CPC's measurements respond to work done by the engine, as expressed in brake horsepower. The 3790 shows a much greater dynamic range over both CPC 3760's. The MEL 3760A also appears to have more dynamic range compared to the MD-19 CPC 3760. Both 3760's have the same 11 nm cut point. The MD-19 3760A audited with ~40% more particles (below a concentration of 1000 #/cc) than the MEL 3760 during the morning of this test, but the MD-19 3760A shows a lower overall response and a lower peak response.

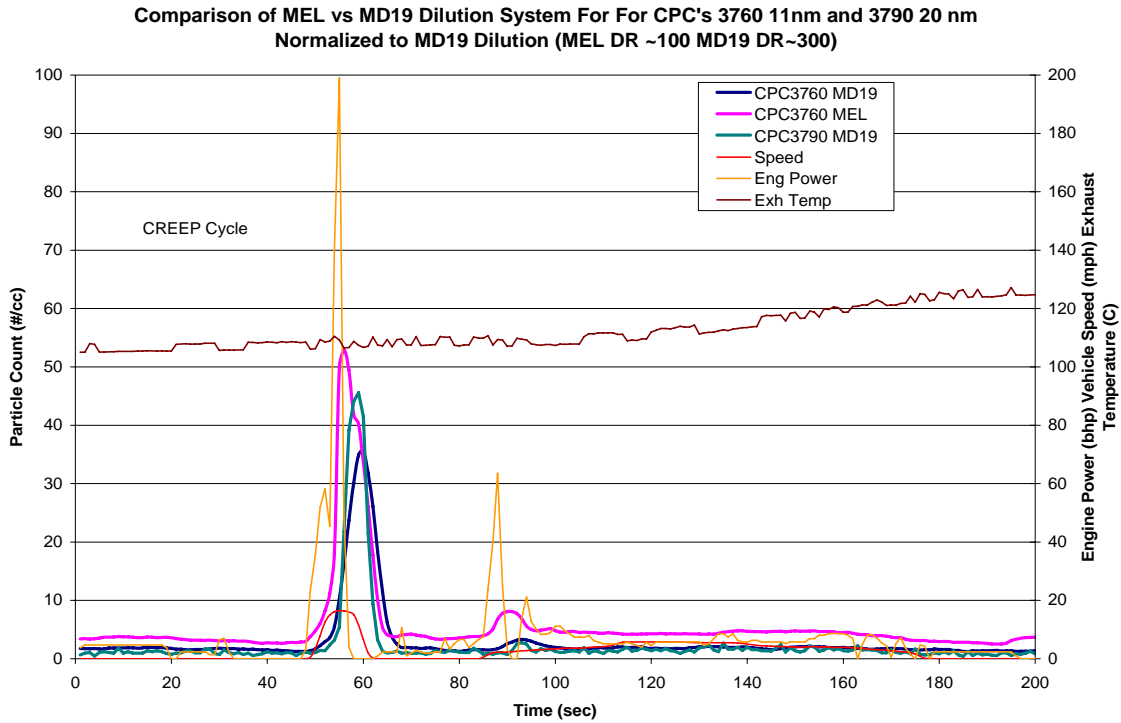


Figure K-14. Detail A. Real-time particle rate (#/cc) for CPCs 3790 and 3760, creep and urban cycles

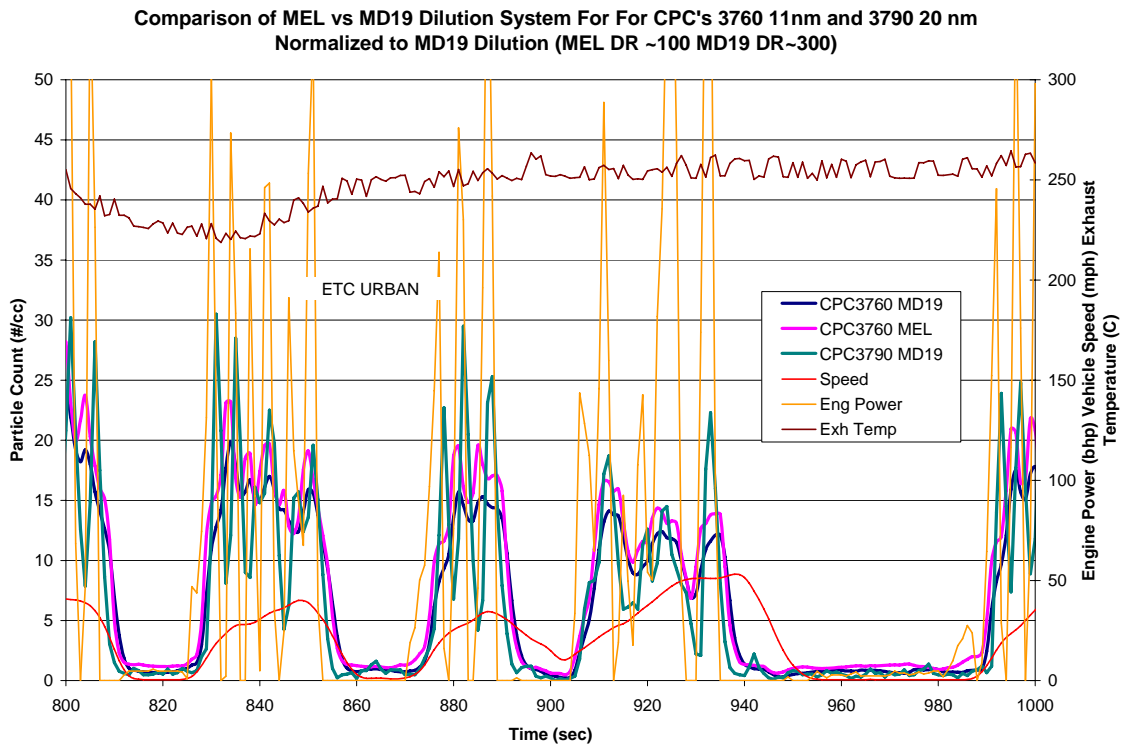


Figure K-15. Detail B. Real-time particle rate (#/cc) for CPCs 3790 and 3760 on the creep and urban cycles

The f-SMPS data is provided in Figure K-16 below. The data show a low count rate for the Creep and Urban cycle with no observable nucleation.

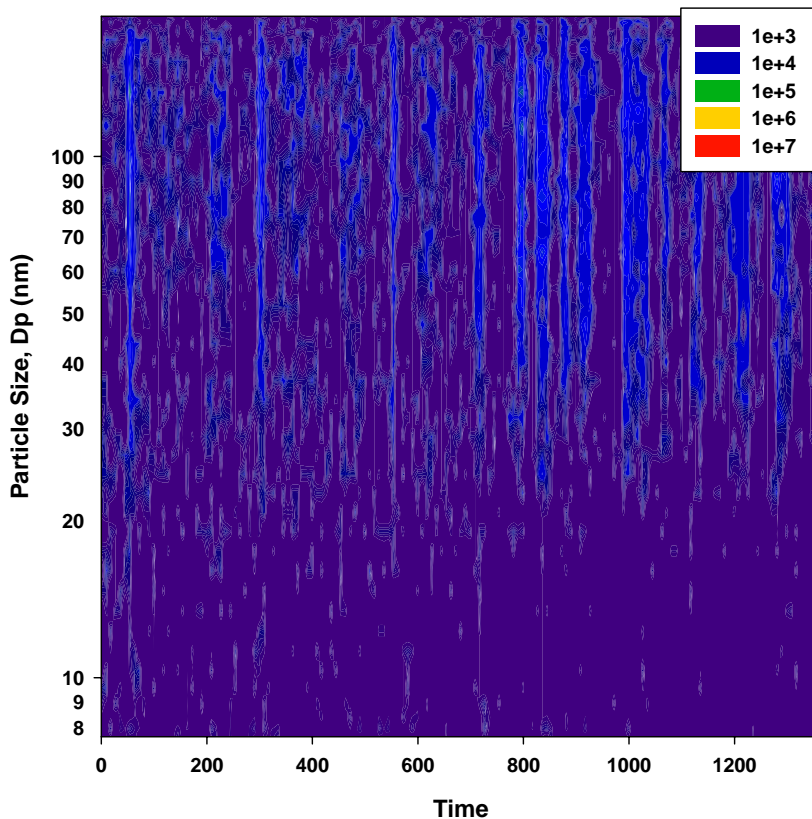


Figure K-16. f-SMPS size distribution over a typical ARB creep and ETC urban cycle $dN/d\log(Dp)$

Flow-of-traffic

The flow-of-traffic emissions were found to have significant differences compared to the prescribed driving cycles. There were three types of driving conditions that were identified with the flow-of-traffic data. They were flat driving, steep hill driving, and a combination of hills and down hill driving. The flat driving emissions behavior was similar to the prescribed driving cycles. Since it does not contribute any significant new information, the flat driving emissions are not considered in this analysis.

Two files are presented for the flow-of-traffic results. The flow-of-traffic data for the trip from Indio to Riverside following the I-10 and highway 215 freeways (test ID 200706150914_MEL.XLS) is presented above in the results section. The second trip is a round trip run towards Blythe where the engine ran near full load for around 20 minutes. The high sustained loads created a condition where the DPF was regenerating. Figure K-17 through Figure K-21 show the real time engine and CPC data for the Blythe run (test ID 200706141237_MEL.XLS). During the Riverside run, the MEL CPC 3760A stopped working after about 20 minutes and never recovered.

Flow-of-traffic - Blythe

It was believed that PM build up on the DPF had occurred and it was desired to force a regeneration event to allow evaluation of the emissions during and after a regeneration event. The I-10 freeway towards Blythe has a fairly long steep grade for about the first 20 miles, which was sufficient to create the desired regeneration event. The Blythe run loaded the engine to peak power for about 20 minutes, with sustained stack temperatures of around 500°C, and maintained fairly constant pre-CRT back pressure. The JM CRT is designed to regenerate at temperatures around 300°C, and the 500°C stack temperature was sufficient to establish regeneration. The fairly constant back pressure indicates that there was no PM adsorption on the CRT, since this would have increased back pressure.

The overall detail for the high cut CPC's is shown in Figure K-17 and the first 500 seconds are shown in Figure K-18 (note the log y-axis scale for the second figure). The first 1000 seconds is going up the hill towards Blythe and the last 1000 seconds is going down hill returning to Indio. The high cut CPCs measured more than two orders of magnitude higher signal compared to the maximum 100 #/cc on the prescribed driving cycles presented earlier. The MD19 3760A was around half that of the MEL 3760A near 150 seconds, but MD19 3760A was almost twice that of the MEL 3760A near 400 seconds, see Figure K-18. One factor in the shift in response as a function of magnitude could be related to coincidence. The two 3760A's are not coincidence corrected, thus measurements over 1E4 #/cc need to be evaluated on an absolute scale. Near 400 seconds, the MEL absolute 3760A count was 30,000 #/cc and the MD19 absolute count was 20,000 #/cc. Using the equation for coincidence correction the MEL 3760A should be multiplied by 1.35 and the MD 3760A should be multiplied by 1.22. The coincidence correction ratio between CPCs thus only contributes about 10% of the difference between the two 3760A CPC responses.

Another interesting point is the linear response to particle number by all high cut point CPCs as a function of time at sustained load and relatively constant stack temperature. The linearly increasing particle counts in the section from 50 to 200 seconds with the log y-axis scale suggests the data is increasing with an exponential trend. During this interval, the load was at peak power and fairly steady. The exhaust stack temperature was starting to level off. Its possible that the CRT catalyst temperature may have been still increasing. During this same time interval, the low cut CPCs both in the primary (3022) and the ones in the PMP diluters (3025A's) were all saturated, see Figure K-19, suggesting a large concentration of small particles. More analysis of EEPS and f-SMPS size distribution and concentration magnitude data could help understand the particle growth behavior and raw concentrations reached.

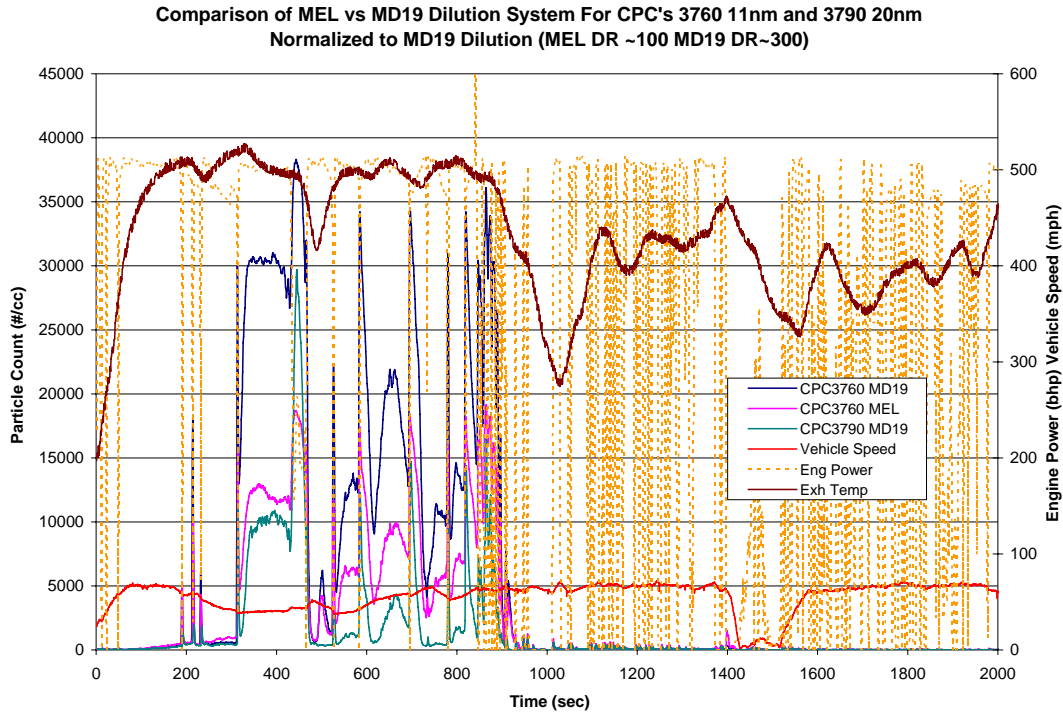


Figure K-17. Real-time particle rate (#/cc) for similar cuts point CPCs (3790 and 3760) for flow-of-traffic Blythe run

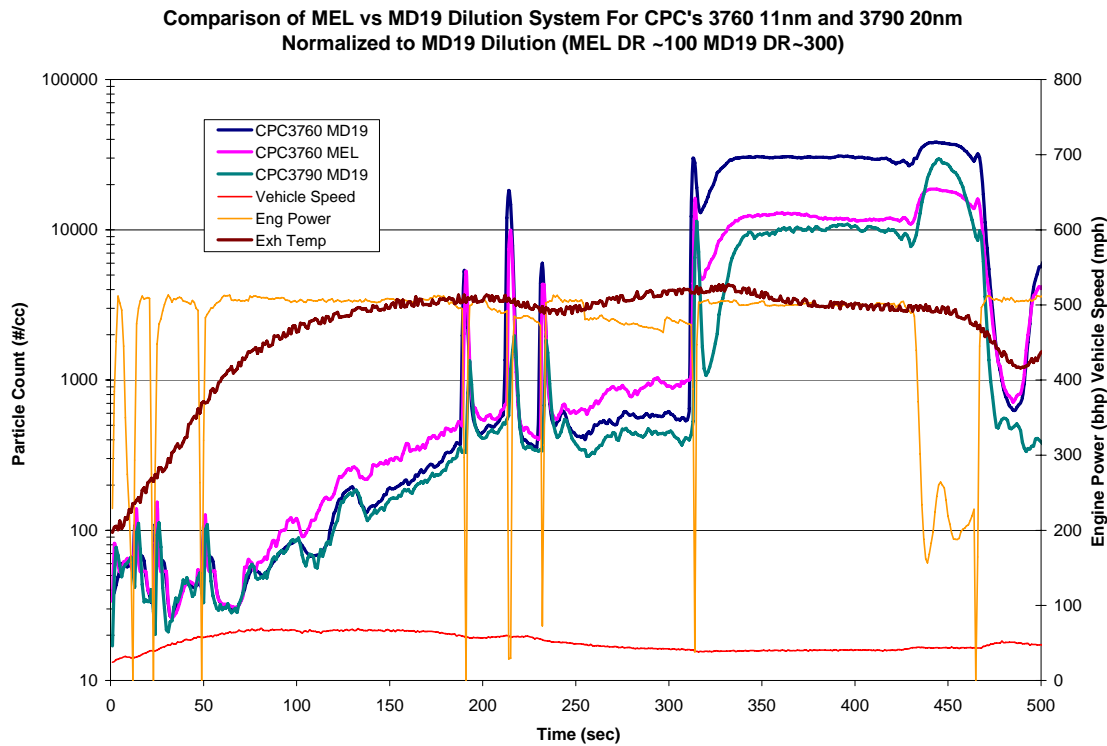


Figure K-18. 500 second detail for the real-time particle rate (#/cc) for similar cuts point CPCs (3790 and 3760) for flow-of-traffic Blythe run

The three spikes that occurred in the time interval between 150 to 250 seconds in Figure K-18 are a response to gear shifting to maintain speed going up the steep grade. One explanation for the #/cc spike occurring during shifting could be a result of over fueling which causes a very high concentration of particulate matter. It is interesting to point out how difficult this shift event would be to recreate on a chassis dyno and on an engine dyno due to dyno limitations for practically applying instant positive and negative torque. More investigation with the EEPS and f-SMPS data is necessary to analyze the size distribution and concentration magnitudes during these CPC spikes.

The low cut point CPCs are shown in Figure K-19 through Figure K-21. The low cut point CPC's were all saturated except for the first 80 seconds for the MEL and CVS CPCs and up to the first 150 seconds of the MD19 3025A CPC, see Figure K-19. The reason the MD-19 CPC saturated later compared to the MEL 3025A is due to the higher dilution ratio used with the MD PMP system. All the CPCs saturated at the manufactures specified limits, which were 1E5 for the 3025A's and 1E7 for the 3022. The saturation levels appear different in the graph, because they are normalized for the dilution ratios for the different systems to the MD-19 dilution ratio.

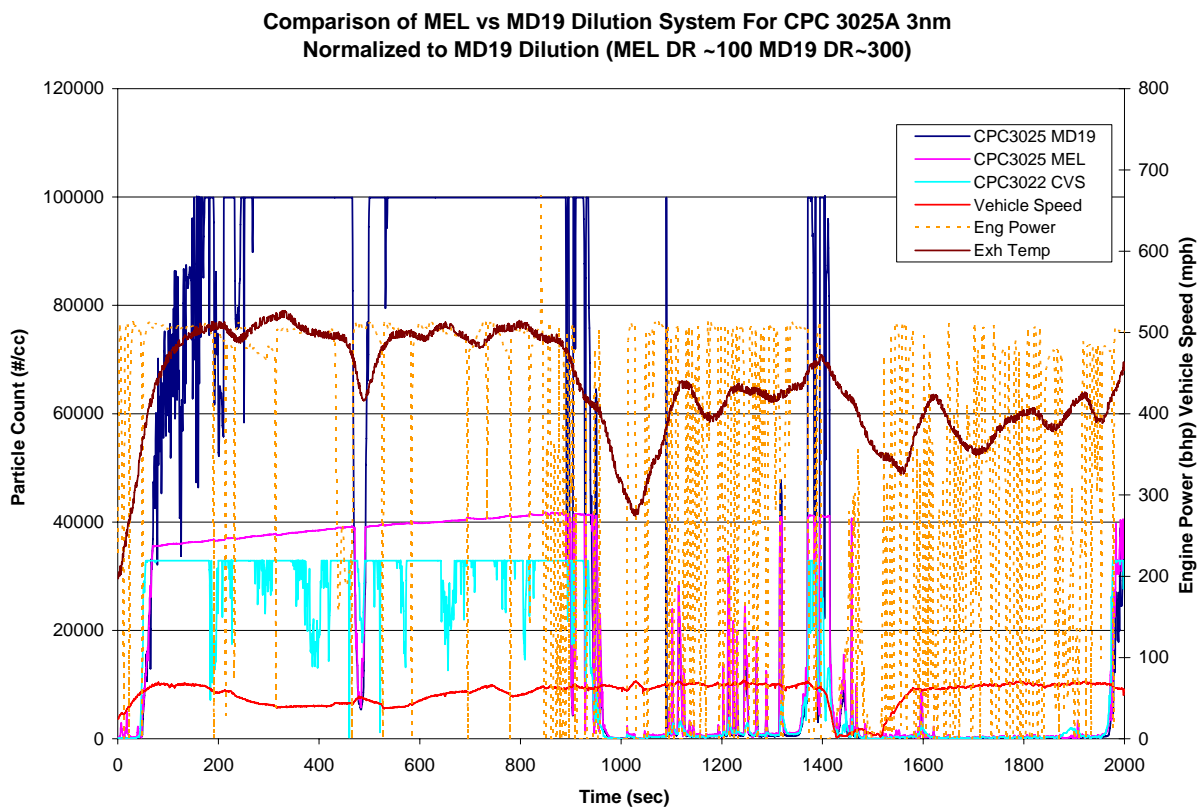


Figure K-19. Real-time particle rate (#/cc) for similar cut point CPCs (3025A and 3022) for flow-of-traffic Blythe run

Comparison of MEL vs MD19 Dilution System For CPC 3025A 3nm and CPC 3022 7nm
 Normalized to MD19 Dilution (MEL DR ~100 MD19 DR~300)

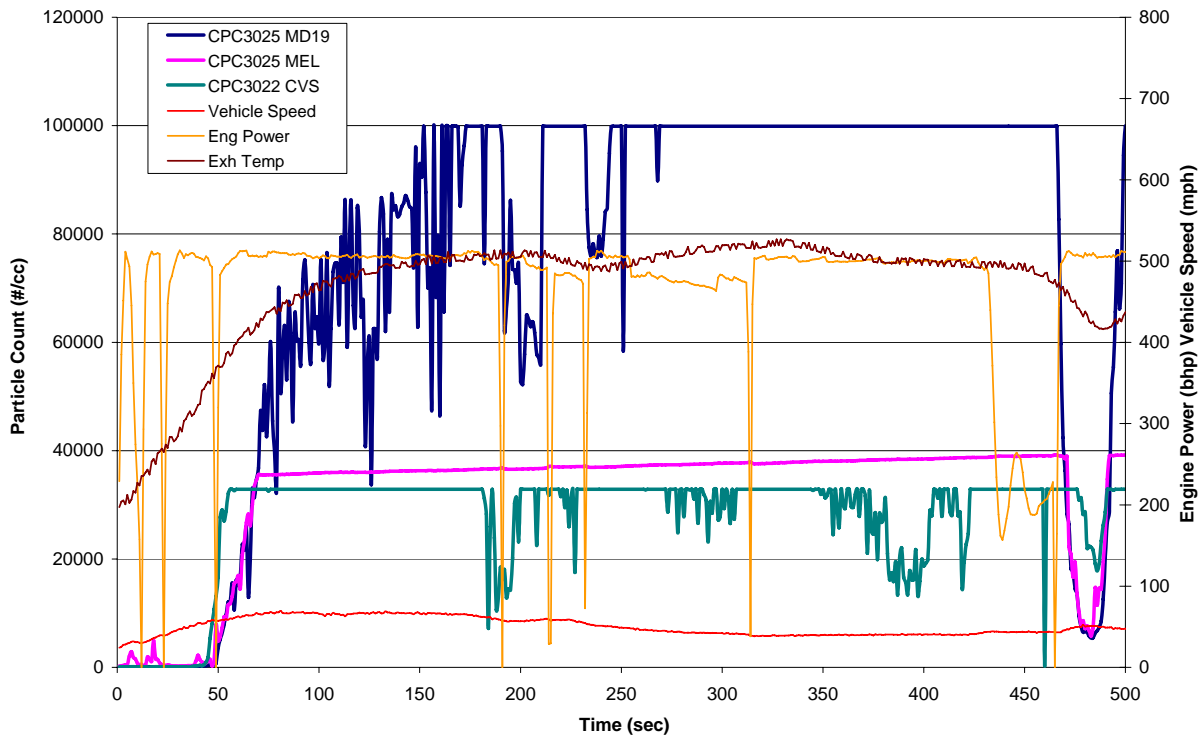


Figure K-20. 500 second detail for the real-time particle rate (#/cc) for similar cuts point CPCs (3025A and 3022) for flow-of-traffic Blythe run

Another interesting point is the MEL 3025A signal seems to be saturated, but still increasing. This can be explained by looking at the real time dilution ratio as shown in Figure K-21. As the flow-of-traffic Blythe run progresses, exhaust temperature is rising causing the CVS temperature to increase, which increases the PMP sample temperature. The sample temperature affects the sample flow by the ratio of absolute temperatures and thus the dilution ratio increases proportionally with increasing temperature, as shown by the Figure K-21. The flow-of-traffic high temperature also explains why the on-road-hill MEL DR was always slightly higher than the prescribed driving cycles DR by ~20%. The MD-19 diluter uses a rotating disk with small volumes machined into the face. Each rotation provides a certain sample flow to a larger flow that creates PND1. Since the MD-19 is a volume displacement device, its sample flow should also be proportional to temperature and thus its DR should vary with the temperature of the gas in the rotating disk. There are no corrections provided for temperature deviations from the MD-19 PMP configuration.

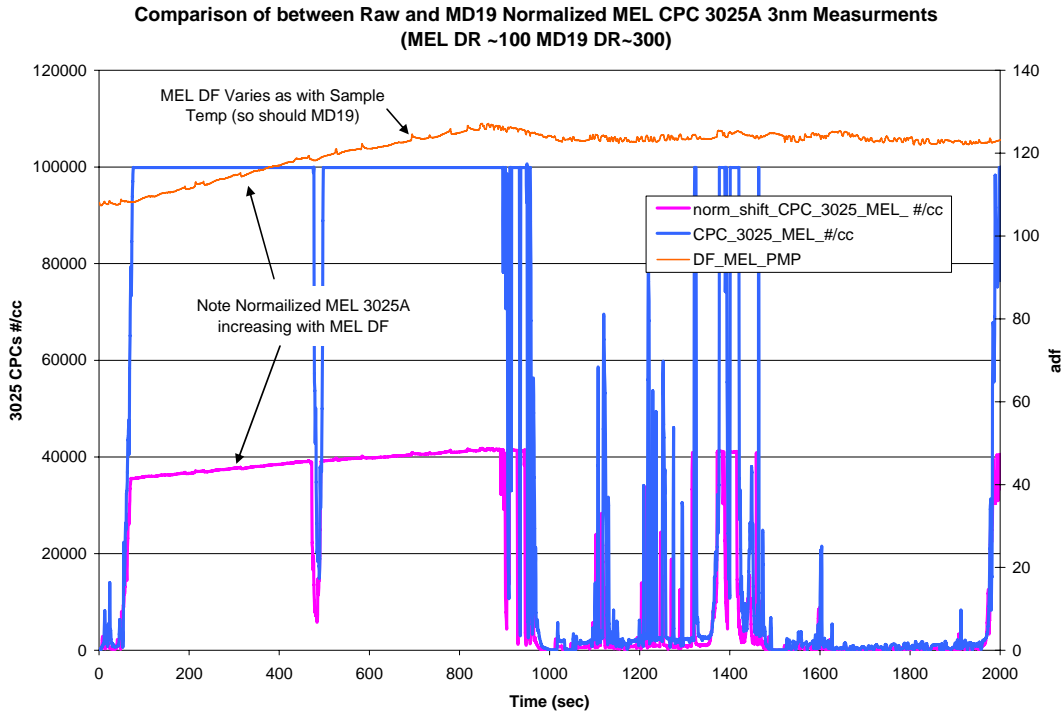


Figure K-21. Real-time particle rate (#/cc) for similar cuts point CPCs (3790 and 3760) with MEL dilution ratio for flow-of-traffic Blythe run

MD19 High Dilution and MEL High Temperature Evaluation Runs on UDSS cycle

During the fourth test day, it was decided to perform some additional experiments to investigate deviations from the standard PMP dilutions and VPR temperatures previously used in this study. The plan was to perform one UDSS with both the MEL and MD19 at a higher overall dilution and then a second UDSS at the original dilution but higher ET temperatures. The MD19 has a dial on the front of the diluter head that allows one to easily change from one dilution to another. The MD 19 was changed from a dial setting of 60 to 12.5 which changed the overall dilution ratio from ~300 to ~ 1400 (a factor of five). The MD-19 manufacture does not recommend going much lower than a dial setting of 12.5 so the overall DR of 1400 was the highest dilution possible with this MD-19 head. The head could be replaced and higher dilutions achieved if desired.

The MEL PMP dilution ratio was not as easy to increase. Given its inherent design of dilution through controlled flow and pressure drop, the only direct way to change dilution ratio was to replace the main inlet sample tube. Changing the inlet sample tube was not practical, so operators attempted to change some of the input parameters such as reducing the sample absolute pressure, reducing the available pressure drop, or increasing the flow to PND1. Only minor effects in the range of 10% were observed and thus the MEL PMP diluter was returned to its normal dilution settings for both UDSS cycles. It is interesting to note how difficult it was to change the dilution ratio, which is a positive point for repeatable operation, but not a benefit for dilution investigation.

The MD19 overall dilution ratio of 1400 increased only the first stage of dilution (PND1) from a DR of 30 to a DR of 150. The final stage of dilution (PND2) remained at 10 and the ET temperature stayed at 300°C. The sample flow decreased from 1.0 lpm to 0.2 lpm as a result of the new configuration and the PND1 dilution air flow remained the same at 30 lpm. The MEL PMP system was not modified for the first UDDS and thus provides a direct comparison with earlier UDDS tests.

The other part of the experiment was to increase the ET temperature to some significantly higher temperature for both PMP systems. The MEL system was capable of reaching 500°C at the ET section, but the MD-19 ET system was not adjustable. For the high temperature UDDS experiment, the MEL was set to a ET of 500°C and an overall DR of ~100 and the MD-19 remained at a ET of 300°C and an overall DR of 1400 (same as previous UDDS high DR test).

The following analysis is based on the expectation that the dilution change will affect the MD19 3790, 3760A, and 3025A and have no affect on the MEL CPCs since its dilution was held constant. Also the high ET temperature experiment should only affect the MEL 3760A and 3025A and there should be no difference between the 1st and 2nd UDDS for the MD19 CPCs since they had similar MD19 PMP configurations. The second UDDS is actually a repeat of the first high dilution UDDS for the MD 19 CPCs, so one could confirm trends from the second MD19 results compared to previous low dilution configurations tests if necessary.

The data shown in Figure K-22 through Figure K-30 are the results from the high dilution and high temperature experiments. The measured absolute value of the MD-19 3790 dropped from ~5 #/cc to ~1 #/cc as expected for a DR change of five. Figure K-22 and Figure K-23 shows the integrated averaged #/mi data for the high dilution and high temperature (HD/HT) UDDS compared to other daily integrated averages. There are no apparent differences for the integrated averages for the high dilution or high ET temperature changes. It appears the PMP dilution is working reliably for the UDDS cycle, and higher dilutions or temperatures were not needed to eliminate particle breakthrough. One might see some effect due to dilution when there is a situation with very high concentrations of volatile particles in the CVS, although the PMP system is supposedly designed to provide adequate dilution even in situations with higher volatile concentrations. The concentrations found for the UDDS cycle are also relatively low compared to those found in other conditions such as the flow-of-traffic cycles.

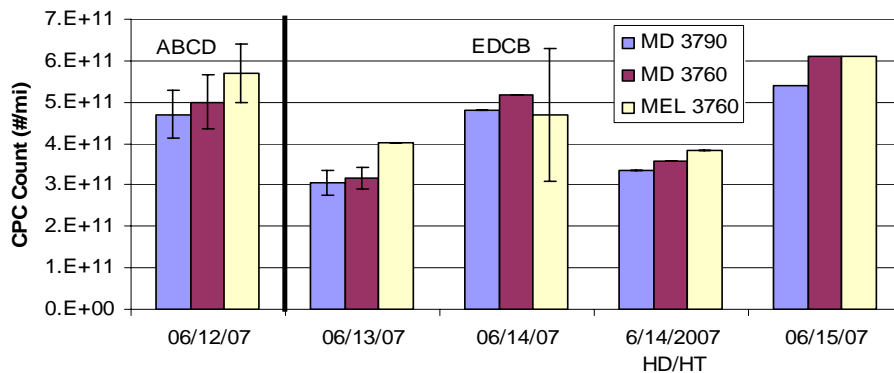


Figure K-22. High cut point CPC for the UDDS by day including the high dilution and high ET test

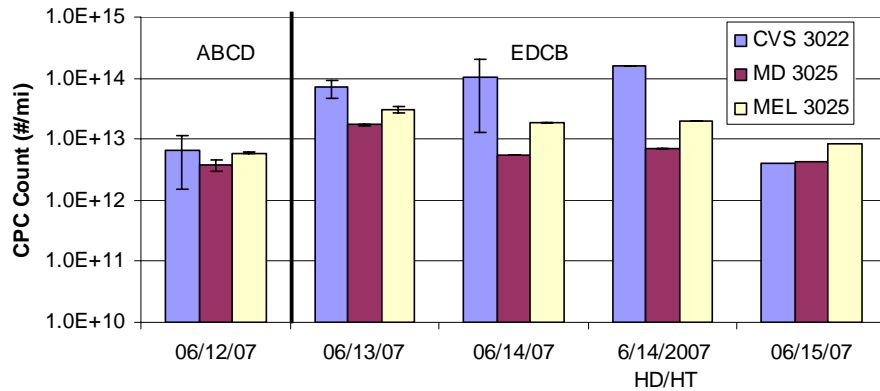


Figure K-23. Low cut point CPC for the UDDS by day including the high dilution and high ET test

The real time data should provide insight to see if there was a situation where a noticeable difference from dilution or temperature was discovered. This could occur if the event was short in duration and moderate in magnitude, which would suggest some partial break down of the original PMP configuration. The real time figures show CPC data normalized to a DR of 300 to show a relative trend between the high DR UDDS figures and the standard DR UDDS figures presented earlier. The high dilution and high ET real time analysis are considered separately. First, the dilution change is evaluated then the high temperature ET experiment is evaluated.

There are some differences between the previous UDDS cycles and the one performed for the comparison below. During the large UDDS hill there was a nucleation event as indicated by large CPC 3022 spike shown in Figure K-26 below. The same spike was also seen in the standard UDDS cycles, but the magnitude and duration were about half that seen during the high dilution and high temperature experiments. One other difference between the baseline and these tests are the exhaust temperatures were slightly higher for the standard dilution test compared to the high dilution, high temperature ET tests.

High Dilution Real-Time Analysis

The MD19 high cut point CPCs do not appear to show a significant difference between high dilution and standard dilution for the higher cut CPCs. Looking at the overall standard UDDS trace from the results section and Figure K-24 for the high dilution analysis you see about the same real-time trends. During the highest speed hill for the UDDS (Detail C), the peak measurement is around 25 #/cc at the beginning of the hill on all three CPCs, then drops as the speed is achieved, then goes to zero when decelerating. A closer look at detail C above for the standard dilution UDDS compared to detail C in Figure K-28 for the high dilution UDDS shows the same trend. In addition, all the CPCs, regardless of dilution ratio, track engine load even for the MEL CPCs, which are operated with the standard DR. It appears the high CPC 3022 spike during the large hill in detail C did not penetrate the PMP at either the higher or typical dilution ratios. If there was penetration, one would expect to see some noticeable difference. There could be some effect that was biased by the higher nucleation event during this single DR test. A second UDDS at this high dilution ratio was also performed when the MEL was operating at

high ET temperatures. No new information was found when looking at this data, so these data are not discussed further.

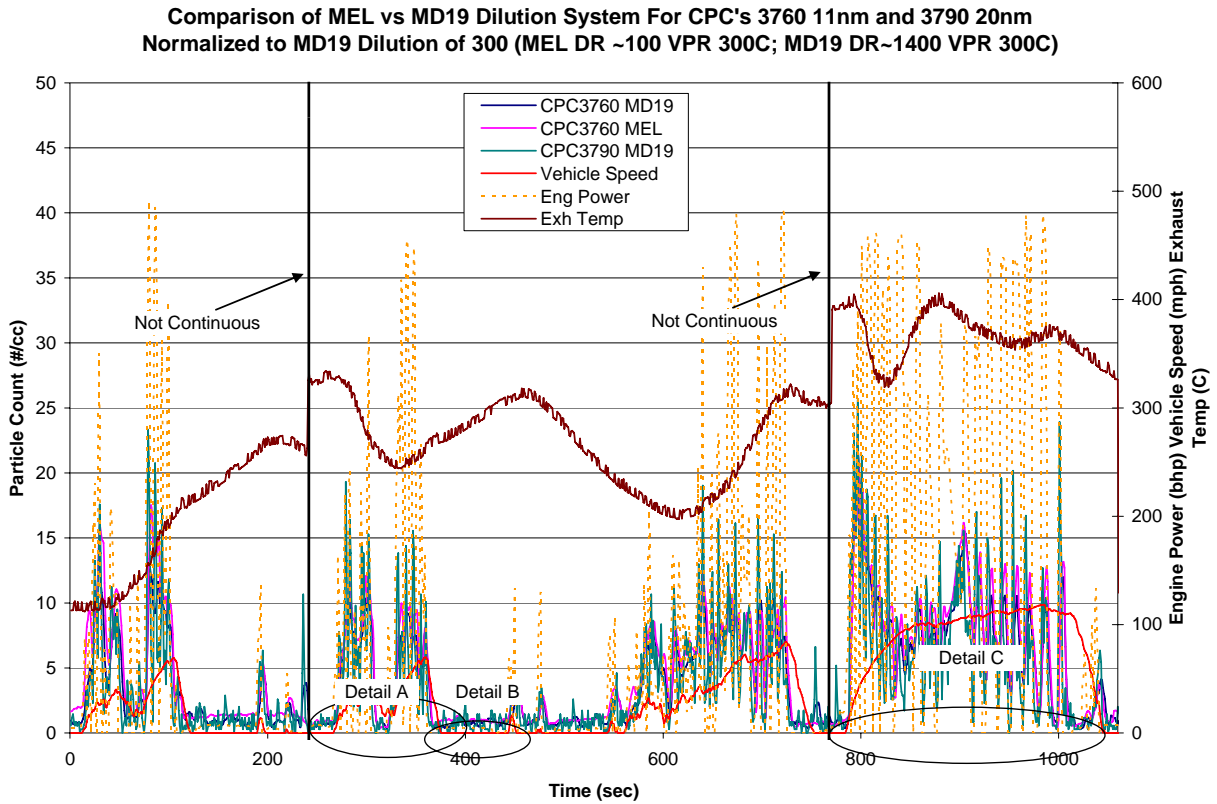


Figure K-24. Real-time particle rate (#/cc) MD-19 high dilution (~1400) MEL standard ET test for similar cuts point CPCs (3790 and 3760) on the UDDS cycle

The lower cut CPCs also do not show a significant difference between high and low dilution ratio. The comparison can be made between the standard dilution presented above and high dilution tests and looking for differences between the MD19 3025A's. The only observable difference is that there were more particles present for the high dilution test compared to the standard dilution test, as seen by the CPC3022 connected to the CVS. Since most of the relevant transient behavior is during detail C, a closer look at this detail in the standard dilution Figure and Figure K-28 high dilution is considered. Again, there is no observable difference between the MD19 3025A CPCs in both figures except for behavior that is most likely responding to the additional particles measured in the primary tunnel. The repeated high dilution test also showed no new information for the low cut MD19 CPC and is thus not presented.

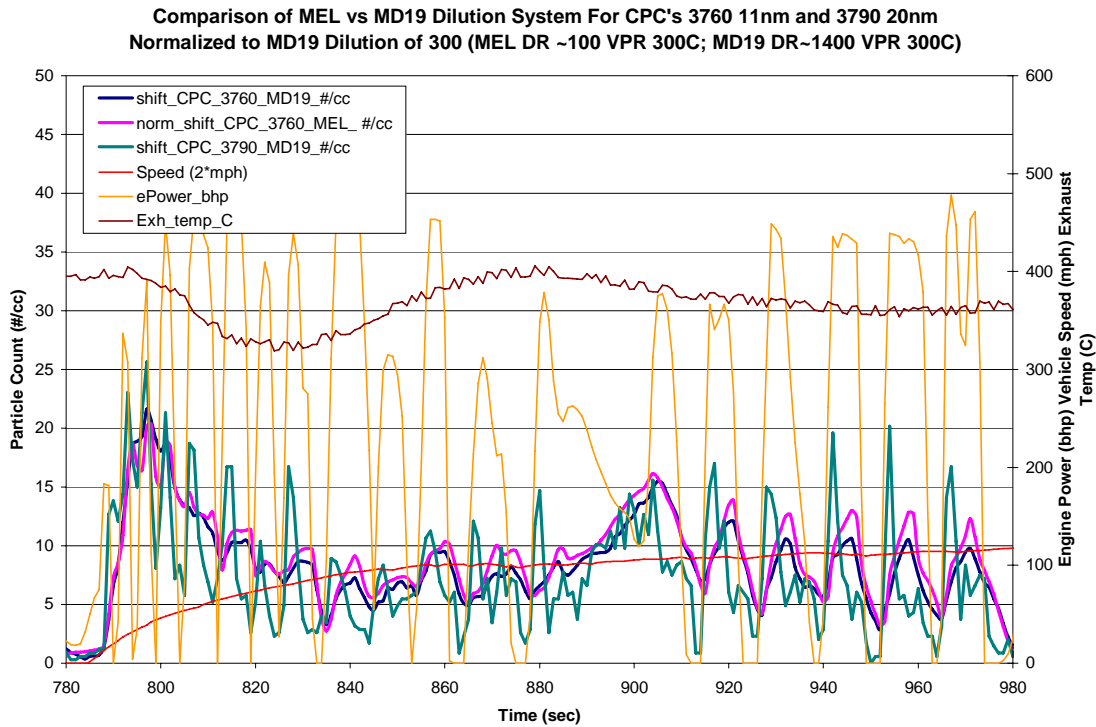


Figure K-25. Detail. Real-time particle rate (#/cc) MD-19 high dilution (~1400) MEL standard ET test for similar cuts point CPCs (3790 and 3760A) on the UDDS cycle

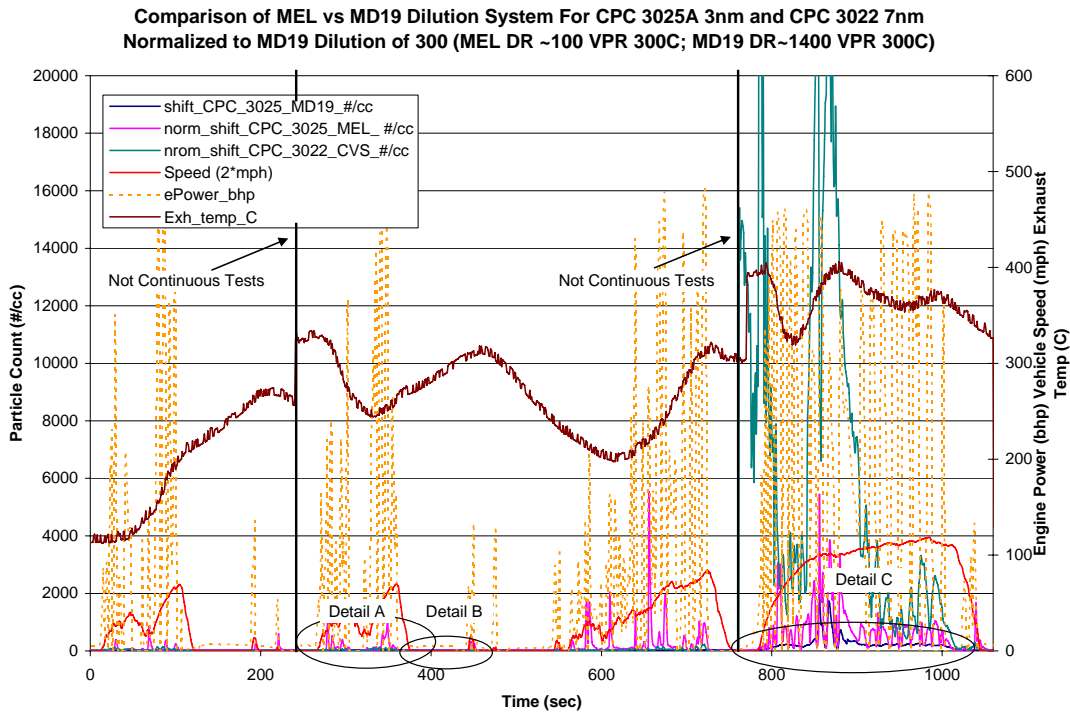


Figure K-26. Real-time particle rate (#/cc) MD-19 high dilution (~1400) MEL standard ET test for similar cuts point (3025A and 3022) on the UDDS cycle

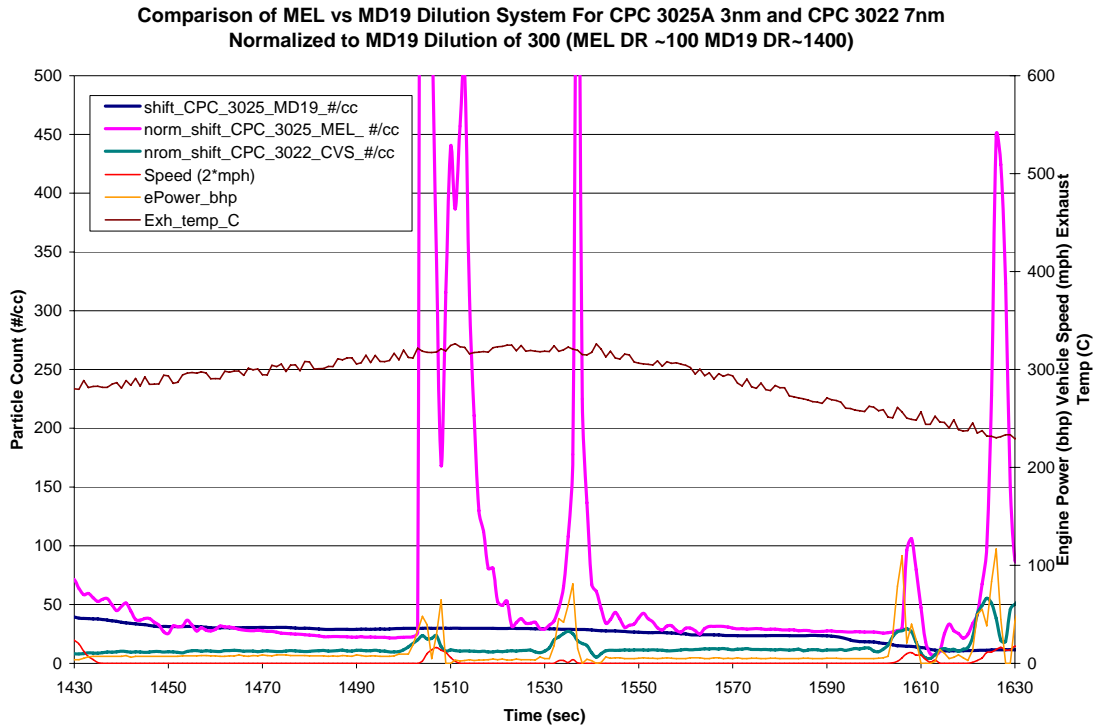


Figure K-27. Detail B. Real-time particle rate (#/cc) high dilution (~1400) MEL standard ET test for similar cuts point (3025A and 3022) on the UDDS cycle

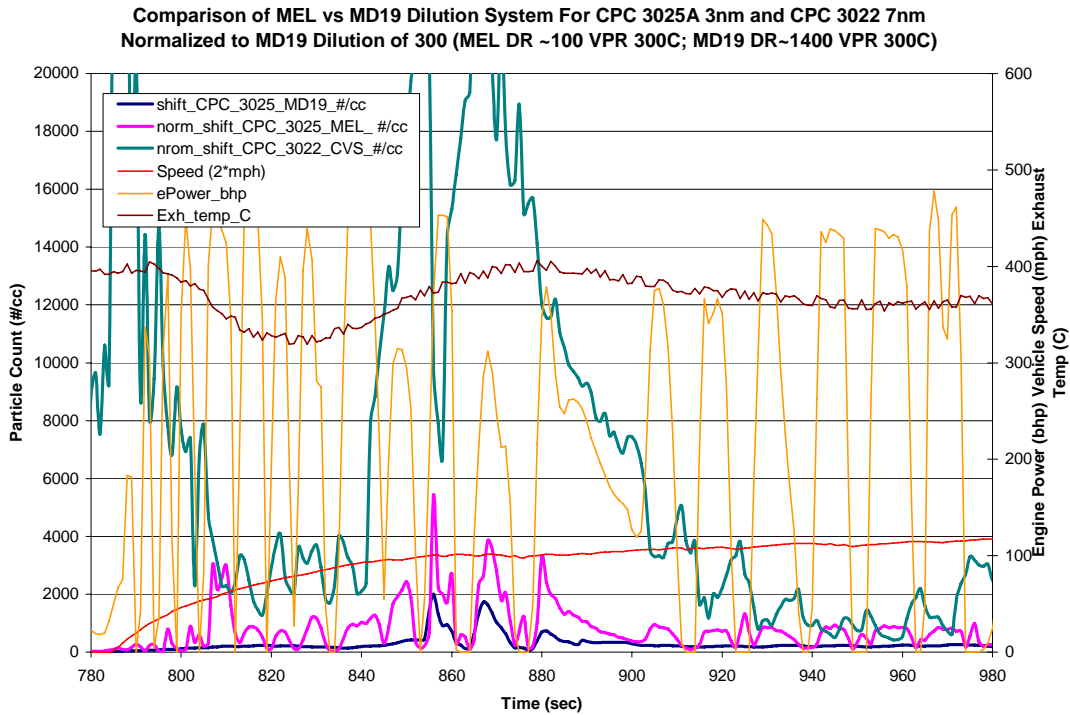


Figure K-28. Detail C. Real-time particle rate (#/cc) MD-19 high dilution (~1400) MEL standard ET test for similar cuts point CPCs (3025A and 3022) on the UDDS cycle

High Temperature ET Real-Time Analysis

Figure K-29 and Figure K-30 show the real time data for all the CPCs grouped by cut size for the high temperature MEL ET test and high DR MD19 repeat. Since most of the dynamic behavior is during detail C, the only analysis performed here is on detail C. The other data was evaluated and found to provide no additional information, and is thus not included. The 3760A did not show any noticeable difference between the MEL's high and standard ET temperatures. The 3760A measurements were very similar in magnitude and dynamics except for some possible response to the higher particle formation in the CVS as indicated by the 3022 CPC, as shown in Figure K-30. The low cut MEL 3205's also did not show any noticeable difference between the MEL's high and standard ET temperatures. A better comparison for the high temperature ET tests can be between made using the two back-to-back UDDS cycles since the first UDDS had the standard ET temperatures and the second UDDS had the high temperature ET. The back-to-back UDDS makes a better comparison because both UDDS tests had similar CVS nucleation events, as shown by the 3022 measurements in Figure K-28 and Figure K-30. Still, the MEL's 3025A comparisons for the high temperature ET and standard ET are very similar in magnitude and transient behavior thus the temperature change seems to have no measurable effect.

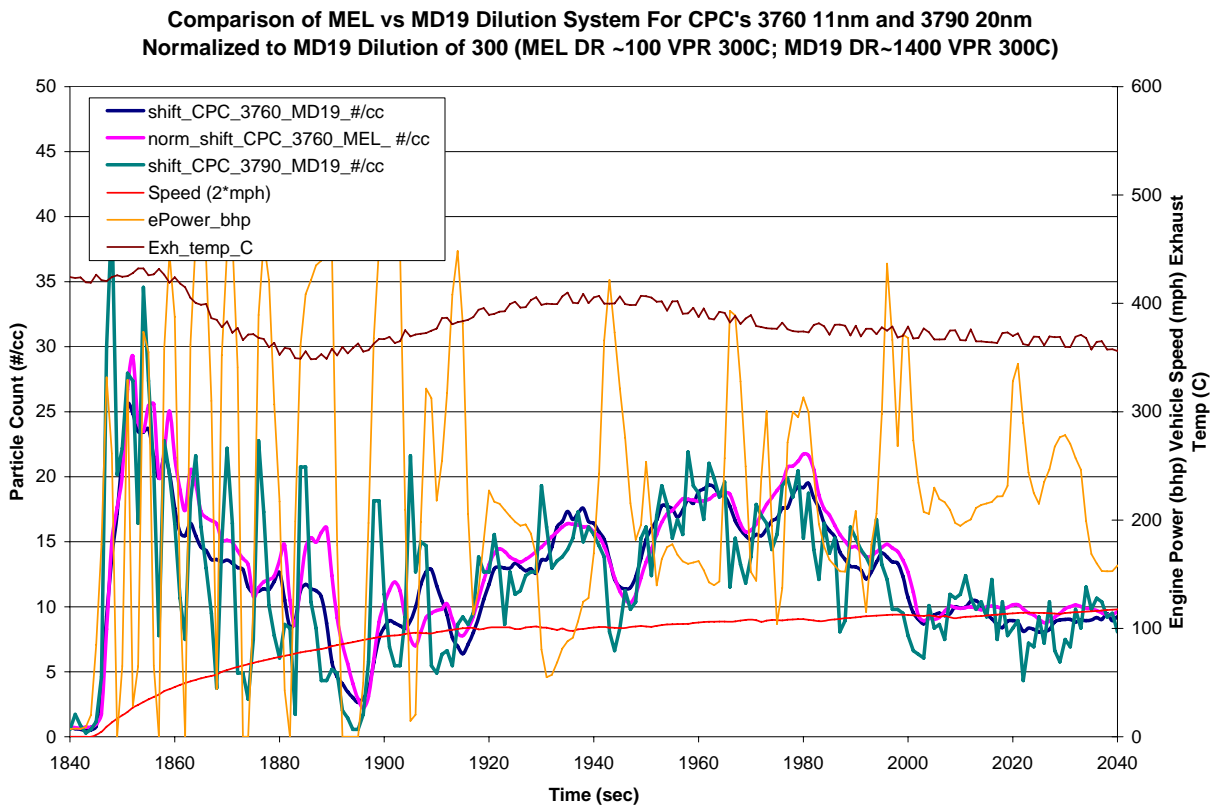


Figure K-29. Detail C. Real-time particle rate (#/cc) MD-19 high dilution (~1400) and high ET temperature for MEP PMP test for similar cuts point CPCs (3790 and 3760A) on the UDDS cycle

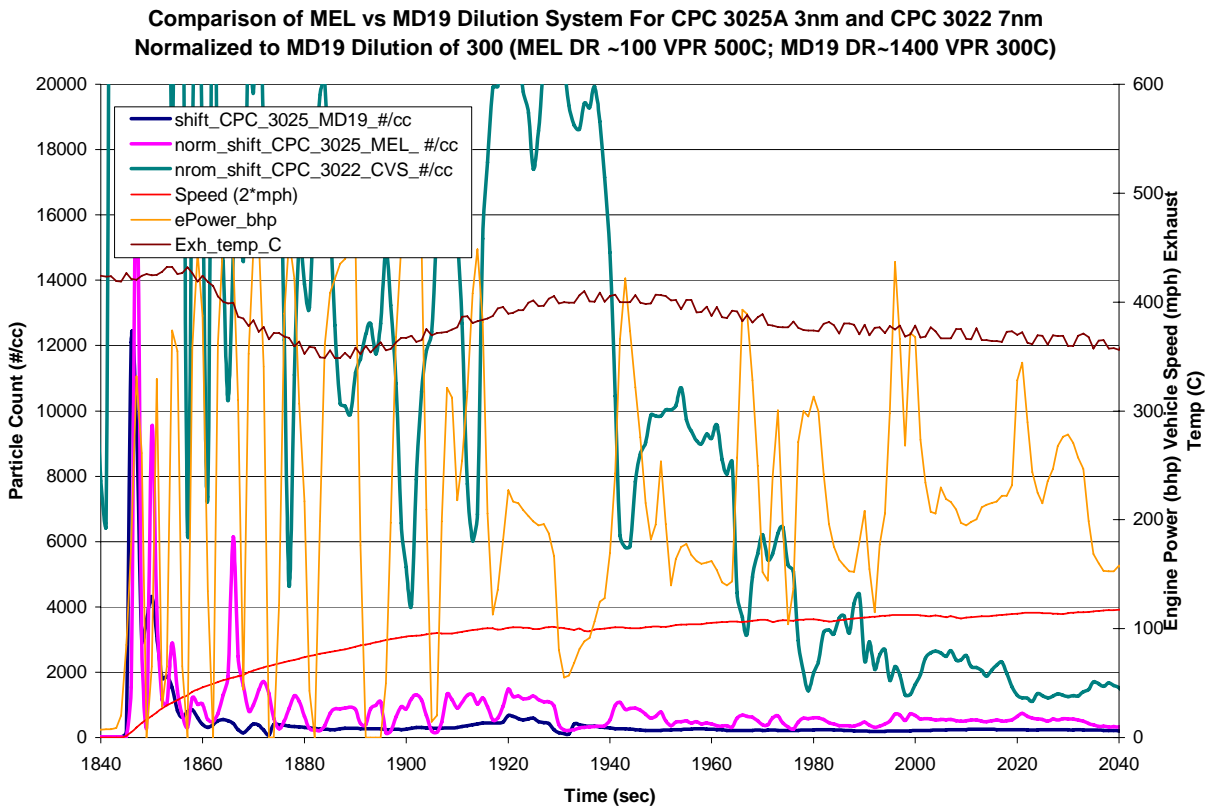


Figure K-30. Detail C. Real-time particle rate (#/cc) MD-19 high dilution (~1400) and high ET temperature for MEP PMP test for similar cuts point CPCs (3025A and 3022) on the UDDS cycle

Real-Time Correlation

The real-time second-by-second correlation analyses were performed to provide qualitative information on dynamic response (high or low spread), and possible issues at different magnitudes where correlations do not follow a linear relationship. Figure K-31 through Figure K-37 show the correlation of like CPCs for three different driving cycles: the ETC cruise, UDDS and flow-of-traffic test cycle. The ARB Creep and ETC urban correlation data was not included since both the creep and urban correlation results were very similar to the UDDS cycles. Similarities include data spread (scatter about the best fit line), R^2 and similar slopes. The only slight difference was the UDDS spanned larger axes compared to the creep and urban cycles. This is expected since the UDDS, ARB creep and ETC urban cycles are all transient in nature and relatively low power except on one segment of the UDDS where loads are higher and CPC measurements were larger. All the real time second-by-second correlation data is time aligned to engine load so that each figure represents the optimum correlation between CPCs. All CPC concentrations are normalized to the MD-19 dilution in order to identify a perfect correlation when the slope equals unity. Any spread in data would be a result of residence time and or response time of each CPC.

ETC Cruise Real-Time Correlation

The cruise correlation provides a comparison between CPCs where loads are fairly stable and the CPC measurements are fairly constant, see Figure K-31. The real time data above showed that there was some transient nature for the lower cut CPCs, but relative to the UDDS cycle, these transients were minor. The correlation between the 3790 and the 3760A on the same MD 19 diluter shows that each CPC is counting the same number of particles where the slope was 1.03 and the R^2 was 0.98. One would expect the slope of the two different CPC's (3760A and 3790) on the same PMP diluter to be close to unity assuming there are not more counts on one system over the other. The couple of points circled on the figure look like outliers, but when looking at the real time data above, these measurements are real where one CPC followed load and dropped to ~0 #/cc while the other CPCs did not. It is interesting to note the higher cut point CPC (3790) went to zero where the other CPC (3760A) measured a value around 10 #/cc. One explanation besides one CPC counting more particles than the other could be due to dynamic response differences between the CPCs. The CPC's dynamic responses were discussed above in the real time data and will be discussed again below with the UDDS evaluation. The background count rate of 10 #/cc for one of the 3760As could also indicate a small leak or a tail between 11 and 23 nm.

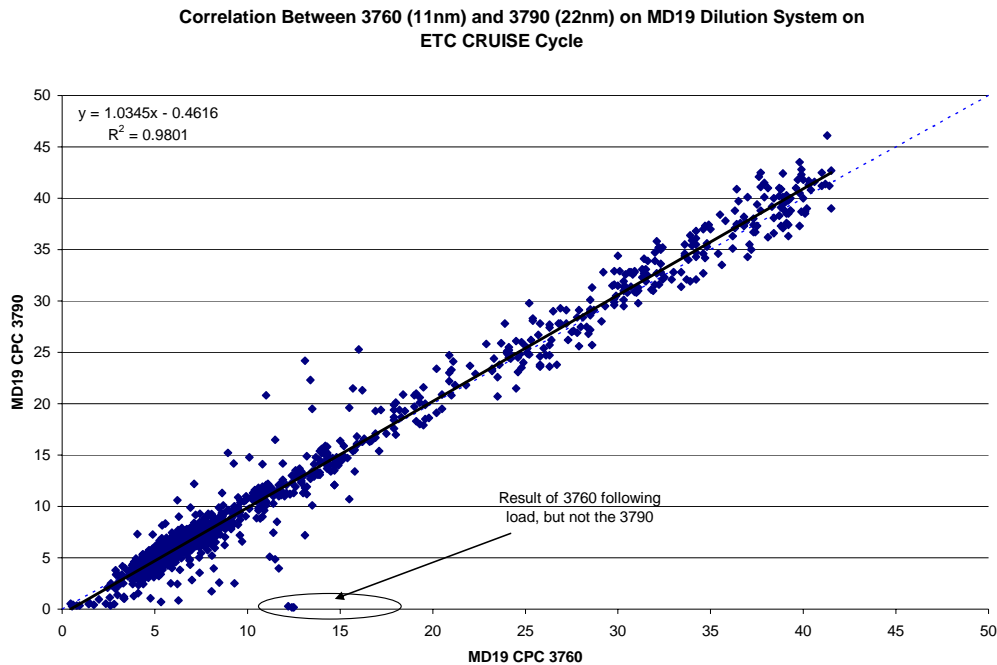


Figure K-31. Correlation between two similar CPCs (3790 and 3760) on a common MD-19 PMP diluter. CPC's are time aligned to engine power and include data from two ETC cruises one west bound and the other east bound

The 3760A correlation for different PMP systems is shown in Figure K-32 shows a good correlation between the high cut CPCs where the R^2 was 0.993 with a slope of close to unity at 1.04. The positive slope indicates the MEL is biased high by 4% or near unity for this data range of 0 to 50 #/cc. The 3760A's showed a tight spread indicating a more stable steady state

measurement compared to the other more transient cycles presented below for the same cut CPCs. The points highlighted in the figure appear to be outliers, but represent a real engine events where the MEL 3760A followed load (dropping to ~0 #/cc) and the MD19 3760A did not following load (stayed high at 12 #/cc). A description of these event differences between CPCs is described in the real time data analysis.

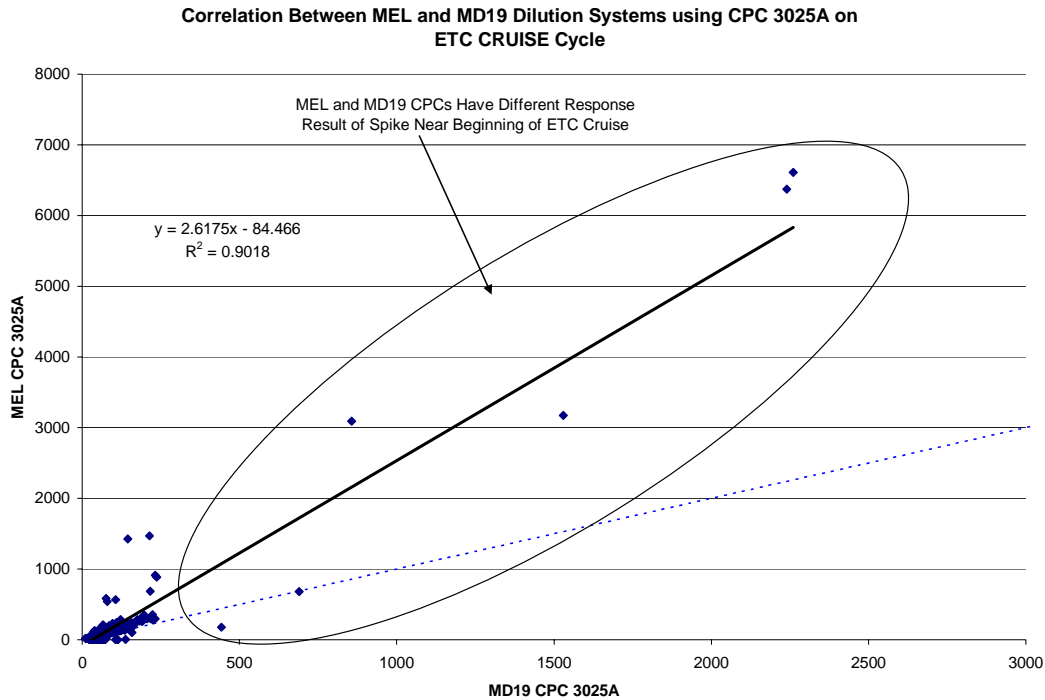


Figure K-32. Correlation between 3025A CPCs on two different PMP diluters. CPC's are time aligned to engine power and include data from two ETC Cruises one west bound and the other east bound

The poor correlation between 3025A's shows in Figure K-32 is a result, in part, of a few points that dominate the correlation. These highlighted points are from the initial spike where concentrations exceeded 350 #/cc. If points above 350/cc are filtered out for both CPC's, the slope drops from 2.6 to 1.3 and the R^2 stays about the same, as shown in Figure K-33. The small group of data that looks like outliers in Figure K-33 are real events where the MEL CPC follows load the MD19 does not. If those outliers are removed the slope and R^2 do not change significantly, but they do improve. The slope of 1.3 indicates the MEL is biased high relative to the MD19 CPC for this data set which agrees with the previous analysis of the cycle averaged data for the contrived driving cycles.

The significant change in CPC slopes between Figure K-32 and Figure K-33 is another indicator that large concentrations change biases between the PMP dilutions system. Since there are only a few points and time alignment is not perfect for large spikes, this data should not be considered representative to support the shift in biases with CPC measurement. There is more spread in the data as expected from the more transient nature of the MEL system compared to the MD19 system, as discussed in the real time analysis.

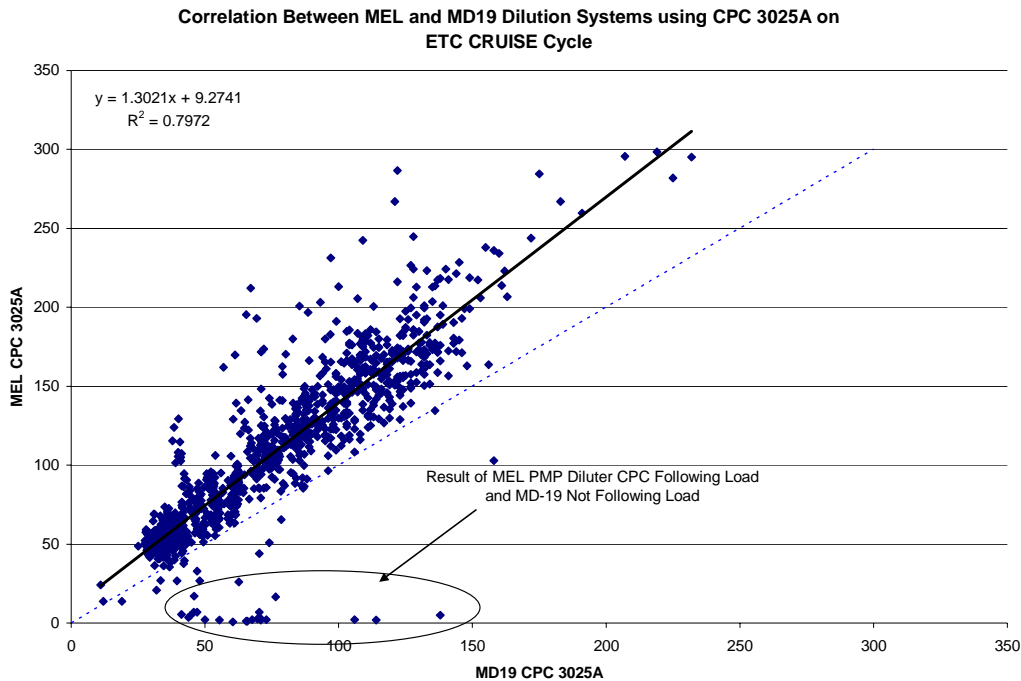


Figure K-33. Correlation between 3025A CPCs on two different PMP diluters. CPC's are time aligned to engine power and include data from two ETC Cruises one west bound and the other east bound (points over 500 #/cc removed)

UDDS Real-Time Correlation

Figure K-34 through Figure K-37 show the similar correlation charts as the cruise data above, but now for the transient UDDS. Figure K-34 shows the correlation between high cut CPCs on a common PMP dilution system. The slope is close to unity for the 3790 and 3760A correlation in Figure K-34, but the R^2 of 0.7 is much lower than the cruise R^2 . The good slope shows that the CPCs are counting about the same value and the R^2 indicated there is a different dynamic response between CPCs, as expected from the discussions earlier. Figure K-35 shows the correlation for the 3760s for the MEL and MD-19 PMP systems. The slope was close to unity at 1.13 and the R^2 was 0.96. The R^2 is slightly less than that for the cruise results most likely due to the more transient nature of the UDDS. Figure K-36 and Figure K-37 show that the correlation for the 3025A CPC's is not as good as the 3760. The R^2 when the points over 2000 #/cc are removed the R^2 drops from 0.86 to 0.64 and the slope changes from 1.2 to 1.6. The lower R^2 and higher slope again could be a result of the dynamics between the two dilution systems, particle penetration, or particle formation. At this time, the differences are not fully understood.

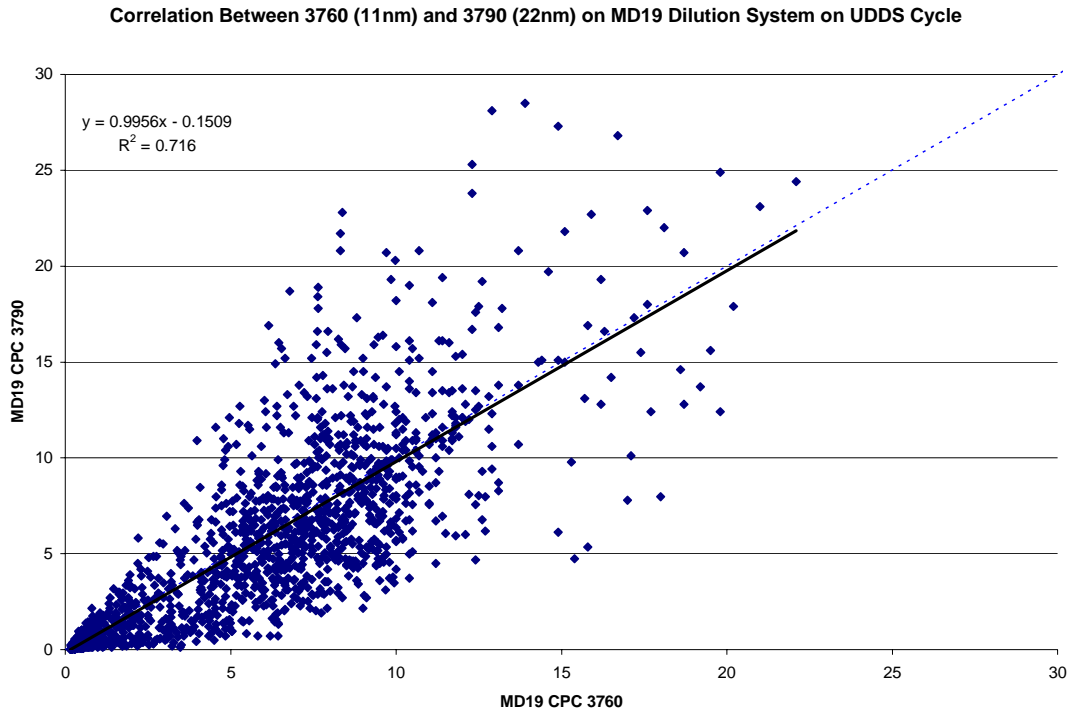


Figure K-34. Correlation between two similar CPCs (3790 and 3760) on a common MD-19 PMP diluter. CPC's are time aligned to engine power and include data from two UDDS cycles

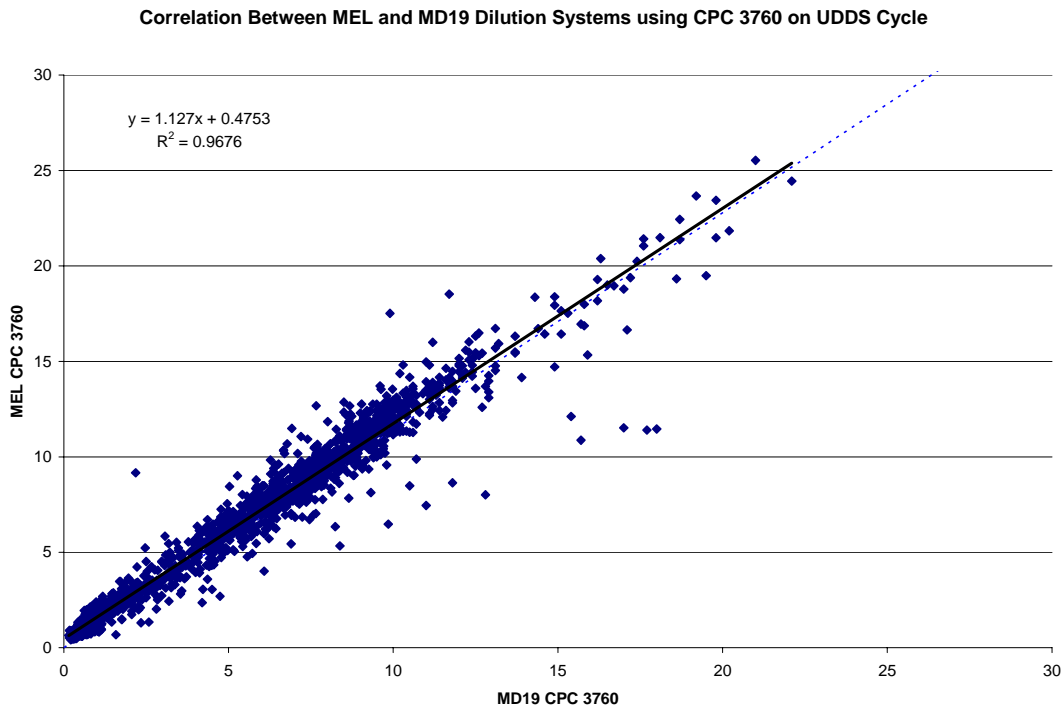


Figure K-35. Correlation between 3760A CPCs on two different PMP diluters. CPC's are time aligned to engine power and include data from two UDDS cycles

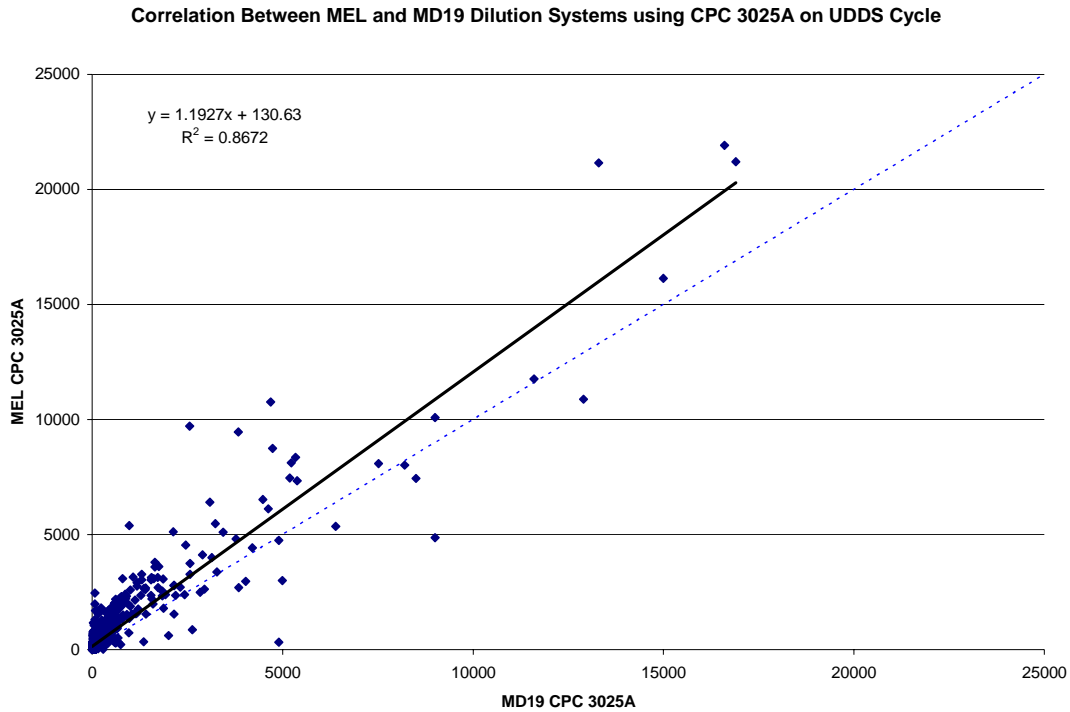


Figure K-36. Correlation between 3025A CPCs on two different PMP diluters. CPC's are time aligned to engine power and include data from two UDDS cycles

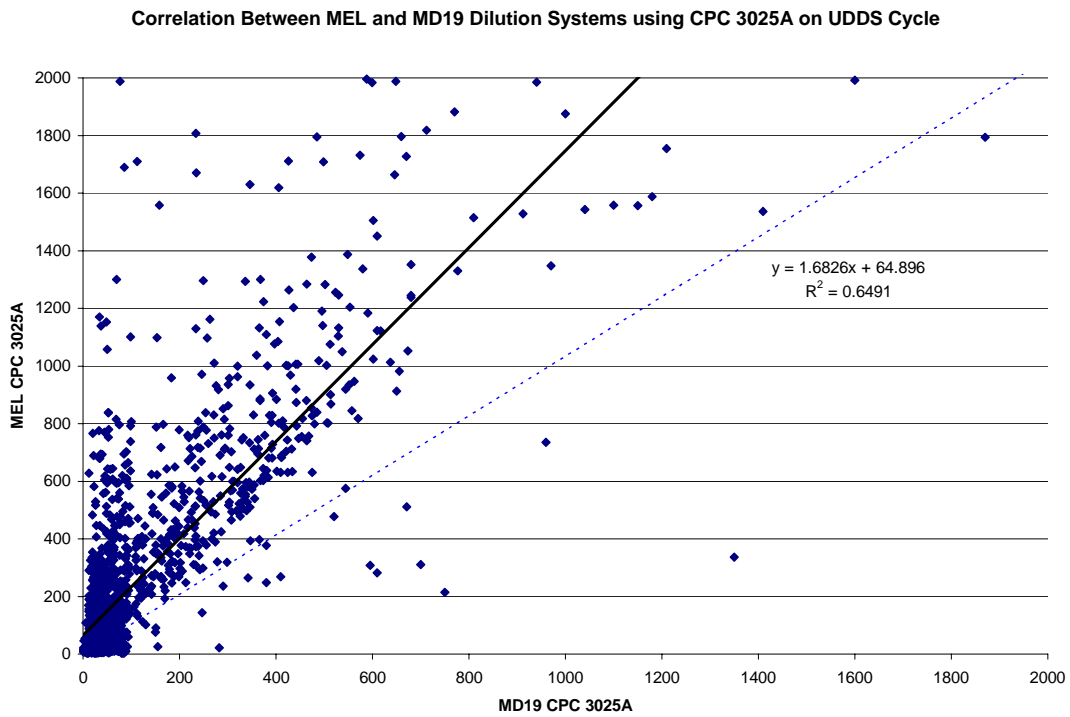


Figure K-37. Correlation between 3025A CPCs on two different PMP diluters. CPC's are time aligned to engine power and include data from two UDDS cycles (points over 2000 #/cc removed)

Flow-of-Traffic Real-Time Correlation

The flow-of-traffic correlations were very interesting because CPC counts reached levels near their maximum measurement capabilities. The flow-of-traffic correlations are shown in Figure K-38 through Figure K-41. The high cut point CPCs are compared on a common PMP diluter in Figure K-38. Notice the exponential trend between the two CPCs once the magnitude exceeds 10000 #/cc. The 3790 is a more sophisticated instrument that corrects for coincidence while the 3760A only provides an output relative to particle counting. The 3670A, as described in the experimental section, does not perform coincidence correction. In the real-time, flow of traffic data section, a discussion was presented on the magnitude of the coincidence correction at the measured levels between the CPCs.

The correlation between similar high cut CPCs, but on different PMP diluters had a good R^2 but showed that the MEL system is biased low relative to the MD19, which agrees with the integrated correlation results. The data spread appears low also when compared to the spread on the UDDS cycle for the high cut 3760A CPCs. One would expect the 3760A non-coincidence corrected CPCs to have some non linear trend in the data since each CPC was diluted differently and measuring different magnitudes. It appears the relative differences between dilutions are not enough to see the coincidence error. Another point to make is the MEL is biased low by a factor of two for the 3760A CPCs. This is opposite to the trend for the cycle averaged data and in the same direction as the integrated correlation analysis above.

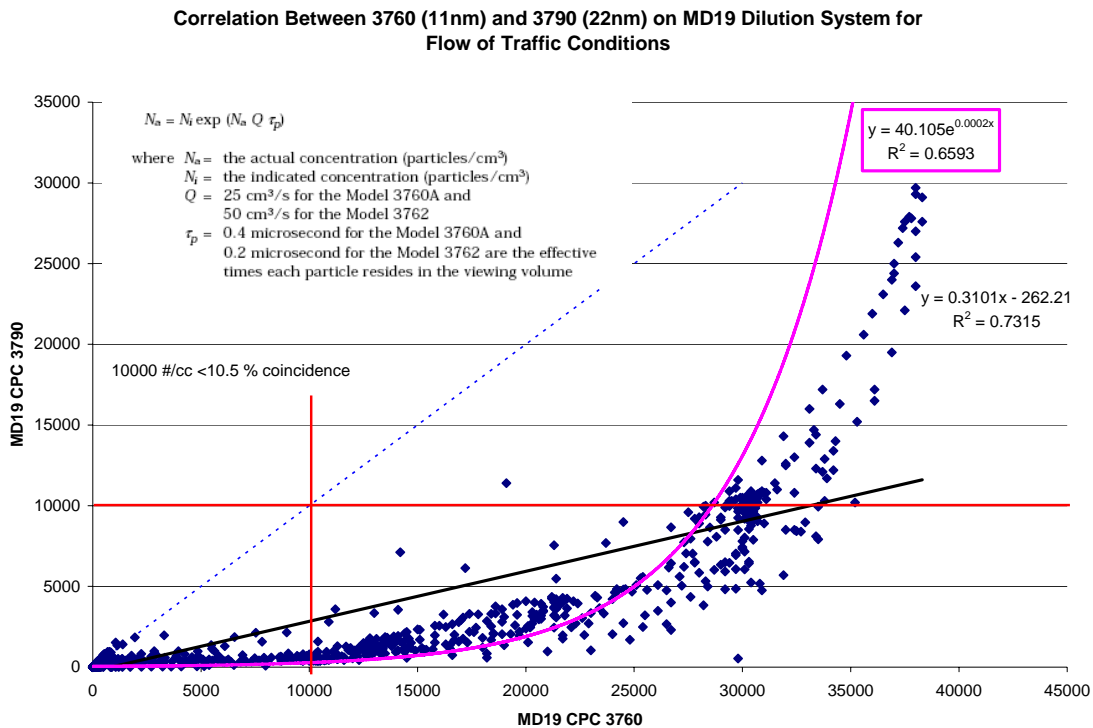


Figure K-38. High cut point CPCs on a common PMP diluter the MD-19 for the flow-of-traffic test

Correlation Between MEL and MD19 Dilution Systems using CPC 3760 for Flow of Traffic Conditions

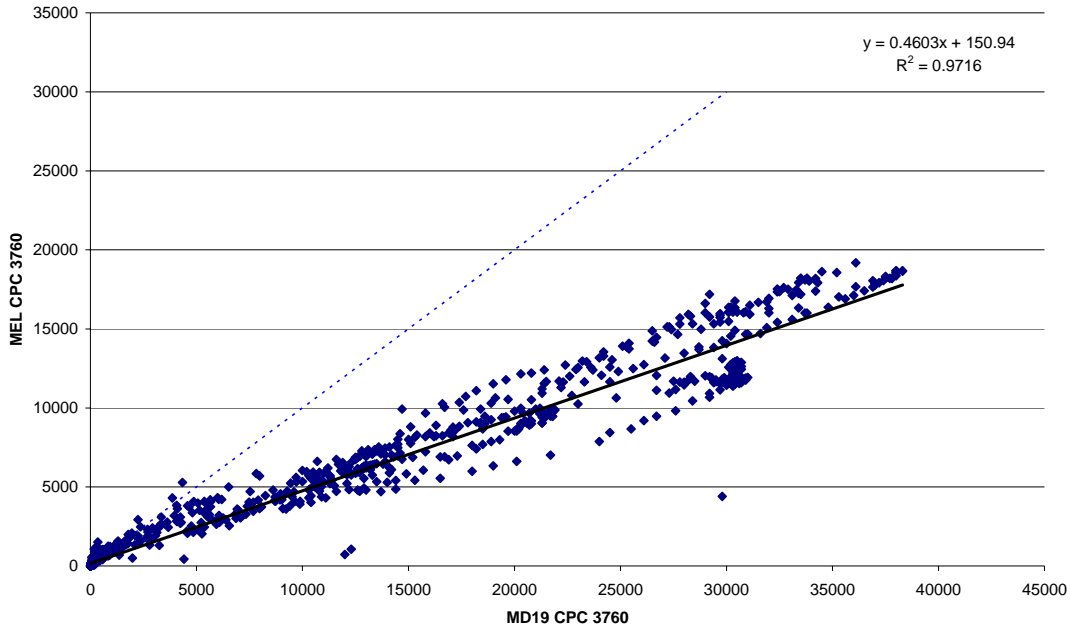


Figure K-39. High cut point CPCs on a common PMP diluter the MD-19 for the flow-of-traffic test

The lower cut CPC flow-of-traffic correlations are shown in Figure K-40 and Figure K-41 below. The low cut CPCs were saturated during many of the sustained loaded conditions, as described during the real-time analysis above. One can see the cluster of data at a constant count for the MEL at 40,000 #/cc and the MD19 at 100,000 #/cc in Figure K-40. When the saturated data is removed, a slope of 1.2 and R^2 of 0.9 is obtained. This says the MEL low cut CPC is biased higher than the MD19 system by about 20%, but only at concentrations below a MD19 3025A concentration of less than half its maximum range. The higher bias agrees with the cycle averaged data for the lightly loaded tests, but disagrees with the flow-of-traffic results and some of the discussion for the real time flow-of-traffic analysis. Most of this is probably a result of the filtering of the higher modes out of the data. It is interesting though that this bias is much closer to unity than the cycle averaged evaluation conclusions.

Correlation Between MEL and MD19 Dilution Systems using CPC 3025A for Flow of Traffic Conditions

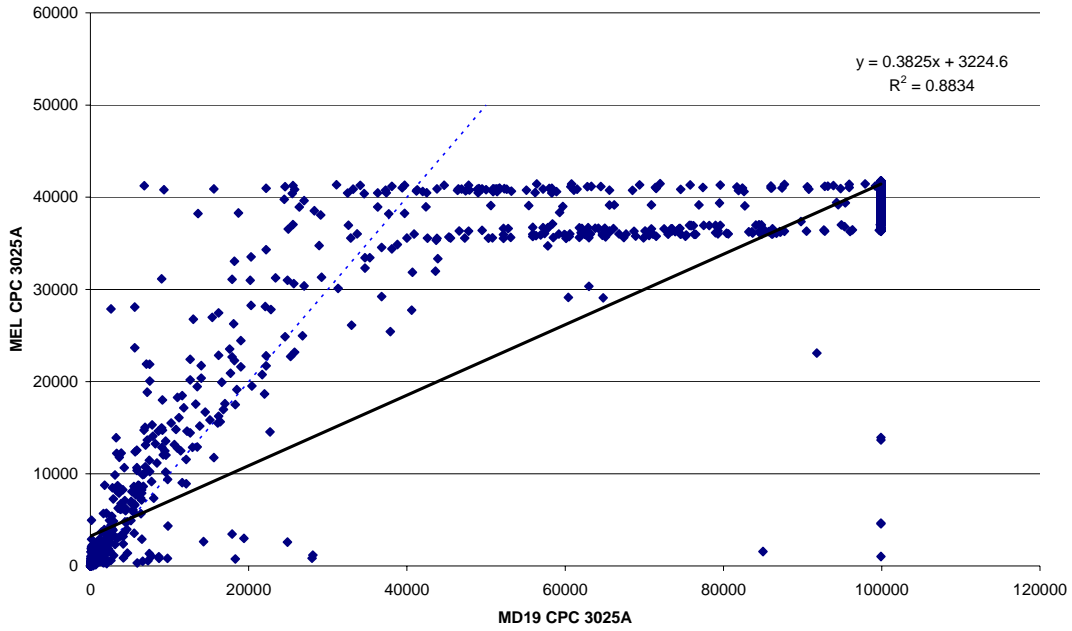


Figure K-40. High cut point CPCs on a common PMP diluter the MD-19 for the flow-of-traffic test

Correlation Between MEL and MD19 Dilution Systems using CPC 3025A for Flow of Traffic Conditions (filtered out saturated data)

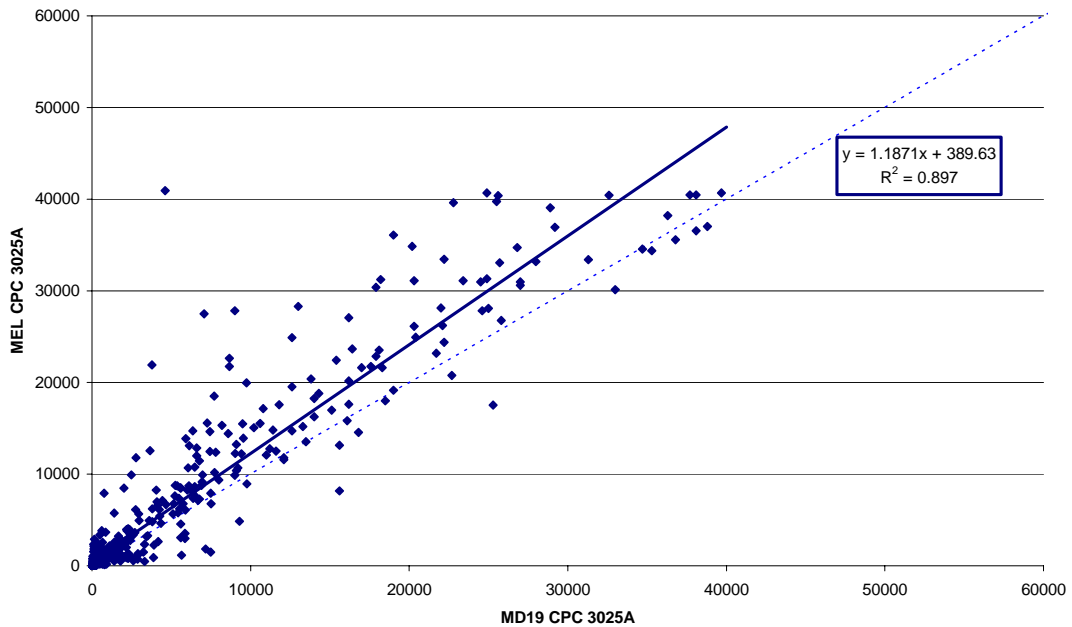


Figure K-41. High cut point CPCs on a common PMP diluter the MD-19 for the flow-of-traffic test